Dissertation zur Erlangung des Doktorgrades
der Fakultät für Chemie und Pharmazie
der Ludwig-Maximilians-Universität München

Involvement of chromatin modifying enzymes in the regulation of inflammatory genes by the Glucocorticoid Receptor

Aikaterini Mechtidou

aus

Thessaloniki,Greece

2022

Erklärung

Diese Dissertation wurde im Sinne von § 7 der Promotionsordnung vom 28. November 2011 von Frau Prof.Dr. Nina Henriette Uhlenhaut betreut.

Eidesstattliche Versicherung

Diese Dissertation wurde eigenständig und ohne unerlaubte Hilfe erarbeitet.

München, 11.01.2022

.....
Aikaterini Mechtidou

Dissertation eingereicht am	13.01.2022
1. Gutachterin / 1. Gutachter:	Prof. Dr. Nina Henriette Uhlenhaut
2. Gutachterin / 2. Gutachter:	Prof. Dr. Peter Becker
Mündliche Prüfung am	11.04.2022

Acknowledgements

First and foremost, I would like to thank my supervisor Prof. Dr. Nina Henriette Uhlenhaut for giving me the opportunity to pursue my PhD in her research group. I am grateful for your immense supervision, guidance, scientific input and encouragement throughout this period.

Additionally, I would like to thank my TAC members Prof. Dr. Peter Becker and Prof. Dr. Michaela Smolle for their annual feedback and scientific input on my project.

I would like to acknowledge the TRR205 and SFB1064 grants awarded to Prof. Dr. Nina Henriette Uhlenhaut. I am particularly grateful to the co-ordinator of the SFB1064 PhD program, Dr. Elizabeth Schroeder-Reiter, for her precious help during these years.

Among the MolEndo group, I would first like to thank Franziska Greulich for the scientific discussions, NGS analysis and most importantly for teaching me how to think as a researcher. Special thanks to Kostas Makris for all these nice memories and for really being by my side at every moment needed. I would like to thank Celine, Fabiana, Suhail, Ben, Afzal, Teresa, Ivonne and Sybille for their scientific and technical support and of course all the other members of the MolEndo group - Laura, Michael, Ken, Kinga, Lotte, Omar, Widad, Marika, Zanhua, Britta, Marion. This experience wouldn’t have been the same without you!

Additionally, I would like to thank Filippo Cernilogar for the successful collaboration with the establishment of the ATAC-sequencing in primary macrophages.

Τέλος, ένα πολύ μεγάλο ευχαριστώ στους γονείς μου και στην αδερφή μου που πάντα είναι δίπλα μου και με στηρίζουν σε κάθε βήμα μου. Επίσης θα ήθελα να ευχαριστήσω τους φίλους μου Βάσω και Γιάννη για την επιμονή τους να συνεχίσω τις σπουδές μου και να κάνω διδακτορικό. Μα περισσότερο απ’ όλους θα ήθελα να ευχαριστήσω τον σύντροφό μου Παναγιώτη, για την στήριξή του και την πνοή που μου έδινε για να ανταπεξέλθω σε κάθε δυσκολία.

Table of contents

Abstract

Glucocorticoids (GCs) are the gold standard treatment for numerous inflammatory conditions (including severe Covid-19), but their long-term use is limited due to severe adverse effects. Glucocorticoids bind to the Glucocorticoid Receptor (GR), a transcription factor that belongs to the family of nuclear hormone receptors. Upon ligand binding, GR translocates to the nucleus where it binds to DNA and induces or represses the expression of target genes. Transcriptional gene regulation is a complex procedure that requires interaction of transcription factors like GR with many co-regulatory partners such as histone modifiers, chromatin remodelers, the Mediator complex, etc. However, the exact mechanisms underlying GR-mediated positive versus negative regulation of inflammatory genes and possible co-regulators recruited at target regulatory loci are complex and not yet understood.

To discover novel partners of GR involved in the transcriptional regulation of inflammatory genes, we performed chromatin immunoprecipitation followed by mass spectrometry analysis (ChIP-MS) in macrophages in response to glucocorticoids. In addition to known co-regulators, we found that GR interacts with the SETD1A/COMPASS complex, a histone methyltransferase, as well as with the SWI/SNF ATPase chromatin remodeling complex. ChIP-sequencing revealed that BRG1, the catalytic subunit of SWI/SNF complex, and the core COMPASS component SETD1A are recruited by GR to a subset of cis-regulatory elements, in activated macrophages treated with glucocorticoids. BRG1 recruitment induced by GR correlated with chromatin accessibility as determined by ATAC sequencing, whereas GR-mediated SETD1A recruitment was associated with H3K4 dynamics only at specific loci. Loss of function studies revealed that both SETD1A and BRG1 are involved in the GR-mediated transcriptional regulation of inflammatory gene programs. SETD1A is an important partner of GR for the activation of anti-inflammatory genes, independently of its histone methyl transferase actions. Additionally, we found that BRG1 is required both for the transcriptional activation of GR targets genes by maintaining chromatin openness and recruitment of Mediator, and for the transcriptional repression of cytokines and chemokines by recruiting histone-deacetylases.

The data presented in this thesis demonstrate that both SETD1A and BRG1 synergize with GR to mediate its anti-inflammatory responses by regulating the transcription of distinct subset of genes, albeit by different mechanisms. These findings might be considered for the development of new immunomodulatory therapies.

Zusammenfassung

Der Einsatz von Glukokortikoiden bilden den Goldstandard bei der Behandlung zahlreicher entzündlicher Erkrankungen bis hin zu schweren Verläufen bei Covid-19. Leider ist die Langzeittherapie mit schweren Nebenwirkungen assoziiert, welches die Grenzen der Behandlungsmöglichkeiten aufzeigt. Auf zellulärer Ebene binden Glukokortikoide an den Glukokortikoidrezeptor (GR), einen Transkriptionsfaktor, der zur Familie der Liganden abhängigen nukleären Hormonrezeptoren gehört. Nach der Bindung des Liganden (Glukokortikoide) wandert der GR in den Zellkern, wo er an die DNA bindet und die Expression von Zielgenen entweder induziert oder unterdrückt. Die transkriptionelle Genregulation ist ein komplexer Vorgang, der die Interaktion von Transkriptionsfaktoren wie GR mit vielen co-regulatorischen Proteinen erfordert. Dazu zählen auch Modulatoren der Histon- und Chromatinkomplexe, wie der Mediator Komplex usw. Die genauen Mechanismen, die zur Aktivierung oder Unterdrückung von GR-abhängigen Entzündungsgenen führen, sowie die Interaktion mit Koregulatoren, die zu den Zielgenen rekrutiert werden, sind komplex und bisher unzureichend charakterisiert.

Um die an der Transkriptionsregulierung von Entzündungsgenen beteiligten Bindungspartner von GR zu identifizieren, wurden Chromatin-Immunpräzipitationen in Kombination mit Massenspektrometrie-Analyse (ChIP-MS) bei aktivierten Immunzellen (Makrophagen), die mit Glukokortikoiden behandelt wurden durchgeführt. Wir konnten zeigen, dass zusätzlich zu bereits bekannten Co-Regulatoren, GR auch mit dem SETD1A/COMPASS-Komplex, einer Histon-Methyl-Transferase, sowie mit dem SWI/SNF-ATPase-Chromatin-Remodeling-Komplex interagiert. Die ChIP-Sequenzierungen ergaben, dass in Glukokortikoid aktivierten Makrophagen, BRG1, die katalytische Untereinheit des SWI/SNF-Komplexes, sowie die COMPASS-Kernkomponente SETD1A von GR an eine Untergruppe von cis-regulierenden Elementen rekrutiert werden. Die durch GR induzierte BRG1-Rekrutierung korrelierte mit der durch ATAC-Sequenzierung ermittelten Chromatinöffnung, während die GR-vermittelte SETD1A-Mobilisierung nur an bestimmten Loci mit Veränderungen der H3K4-Methylierung in Verbindung gebracht werden konnte. Studien zum Funktionsverlust beider Komponenten zeigten dagegen, dass sowohl SETD1A als auch BRG1 an der GR-vermittelten Transkriptionsregulation von Entzündungsgenen beteiligt sind. SETD1A ist ein wichtiger Partner von GR für die Aktivierung entzündungshemmender Gene, unabhängig von seiner Histon-Methyltransferase-Aktivität. Des Weiteren konnten wir zeigen, dass BRG1 einerseits für die transkriptionelle Aktivierung von GR Zielgenen benötigt wird, indem es die Öffnung des Chromatins und die Rekrutierung des Mediatorkomplexes gewährleistet und andererseits durch die Rekrutierung von Histon Deacetylasen die Expression von Zytokin und Chemokingenen unterdrückt.

Die in dieser Arbeit vorgestellten Ergebnisse zeigen, dass SETD1A und BRG1 mit GR interagieren, um dessen entzündungshemmende Reaktionen zu unterstützen, indem sie mit verschiedenen, komplexen Mechanismen die Transkription einer bestimmten Untergruppe von Genen regulieren. Diese Erkenntnisse könnten bei der Entwicklung neuer Immuntherapien wegweisend sein.

Abbreviations

ATAC	assay for transposase-accessible chromatin
ATP	adenosine triphosphate
BMDM	bone marrow derived macrophages
ChIP	chromatin immunoprecipitation
COMPASS	complex proteins associated with Set1
CRISPR	clustered regularly interspace short palindromic repeats
Dex	dexamethasone
DNA	deoxyribonucleic acid
eRNA	enhancer RNA
etc.	etcetera
GBS	glucocorticoid receptor binding sites
GC	glucocorticoid
GR	glucocorticoid receptor
GRE	glucocorticoid response element
H3K27ac	acetylation at lysine 27 on histone 3
H3K4me	methylation at lysine 4 on histone3
HDAC	histone deacetylases
HMT	histone methyltransferase
HPA	hypothalamic-pituitary-adrenal
i.e.	id est, that is
IP	Immunoprecipitation
KD	knock down
KDM	lysine demethylase
KMT	lysine methyltransferase
LPS	lipopolysaccharide
MS	mass spectrometry
NGS	next generation sequencing
POMC	pro-opiomelanocortin
qPCR	quantitave polymerase chain reaction
RNA	ribonucleic acid
seq	sequencing
siRNA	small interfering RNA
SWI/SNF	switch/sucrose non-fermentable
TLR	toll like receptor

All gene names are written in *italics* and all proteins in regular font.

Index of tables

Index of figures

List of publications

Fighting the Fire: Mechanisms of Inflammatory Gene Regulation by the Glucocorticoid Receptor.

Laura Escoter-Torres*, Giorgio Caratti*, **Aikaterini Mechtidou***, Jan Tuckermann, Nina Henriette Uhlenhaut, Sabine Vettorazzi .2019. Front Immunol. 10:1859.

DOI: 10.3389/fimmu.2019.01859

Protocol for using heterologous spike-ins to normalize for technical variation in chromatin immunoprecipitation

Franziska Greulich*, **Aikaterini Mechtidou***, Teresa Horn, Nina HenrietteUhlenhaut. 2021. STAR protocols. 2(3):100609.

DOI: 10.1016/j.xpro.2021.100609

The glucocorticoid receptor recruits the COMPASS complex to regulate inflammatory transcription at macrophage enhancers

Franziska Greulich, Michael Wierer, **Aikaterini Mechtidou**, Omar Gonzalez-Garcia, N Henriette Uhlenhaut. 2021.Cell reports. 34(6):108742.

DOI: 10.1016/j.celrep.2021.108742

BRG1 defines a genomic subset of inflammatory genes transcriptionally controlled by the glucocorticoid receptor

Aikaterini Mechtidou*, Franziska Greulich*, Benjamin A. Strickland, Céline Jouffe, Filippo M. Cernilogar, Gunnar Schotta, N. Henriette Uhlenhaut. 2021.

Uploaded as pre-print in BioRxiv

DOI: https://doi.org/10.1101/2021.12.13.472398

* These authors contributed equally to this work

1. Introduction

1.1 Glucocorticoids and their action as immunomodulators

Glucocorticoids (GCs) are steroid hormones secreted from the adrenal gland through the hypothalamic-pituitary adrenal axis (HPA) in a diurnal and stress response manner (Biddie et al. 2012). GCs are involved in the regulation of many physiological processes. For example, they are important for lung maturation, muscle anabolism and catabolism and they can stimulate glucose production upon starvation through glycogenolysis and gluconeogenesis in the liver (Hanaoka et al. 2012; Silverman and Sternberg 2012; Kadmiel and Cidlowski 2013; Herman et al. 2016). Apart from the physiological effects, glucocorticoids play an important role in immune responses. Due to their anti-inflammatory effects, they are the most widely prescribed drugs for inflammatory diseases. Their use in the clinics dates back to 1949 when Phillip Hench administrated the compound E, which today is known as cortisone, to patients with rheumathoid arthritis (Hench et al. 1949). For this discovery Phillip Hench together with Edward Kendall and Tadeus Reichstein were nominated with the Nobel Prize in Physiology in 1950.

Nowadays GCs are used against a variety of acute and chronic inflammatory diseases like allergies, rheumatoid arthritis, multiple sclerosis, etc. (Figure 1). Their immunosuppressive role affects almost all immune cell types. For example, in neutrophils and dendritic cells glucocorticoids like dexamethasone regulate functions such as cell migration, maturation and apoptosis(Cao et al. 2013). Additionally, in macrophages GCs can inhibit an inflammatory response driven by an external stimulus (Ehrchen et al. 2019). GCs are also involved in adaptive immunity by reducing the production of antibodies in B cells, as well as inducing apoptosis in B cells and T cells (Alnemri et al. 1992; Wang et al. 2003; Goossens and Van Vlierberghe 2016). Furthermore, GCs are used for the treatment of respiratory conditions such as asthma and chronic obstructive pulmonary disease (COPD), they can improve skin disorders like psoriasis and eczema, and they are also used for the treatment of ocular inflammatory conditions (Niewoehner et al. 1999; Sevilla and Perez 2018; Holland et al. 2019). Additionally, GCs are prescribed for specific types of cancer such as some leukemias and lymphomas, and they are administrated to patients after organ transplantation to prevent graft vs. host disease (Ramamoorthy and Cidlowski 2016; De Lucena and Rangel 2018). Nowadays, glucocorticoids are also administrated to patients with severe Covid-19 symptoms (Group et al. 2021).

Intriguingly, GCs are used as drugs for 70 years to suppress inflammation despite several, in part devastating side effects, that were recognized soon after their first clinical use (Figure1) (Hench 1952). The most common of them are associated with metabolic dysregulation such as weight gain, insulin resistance and glucose intolerance. Exposure to GCs can also cause muscle and skin atrophy, glaucoma, hypertension, osteoporosis, adipocytes hypertrophy, impaired wound healing, insomnia and depression (Kadmiel and Cidlowski 2013; Hartmann et al. 2016).

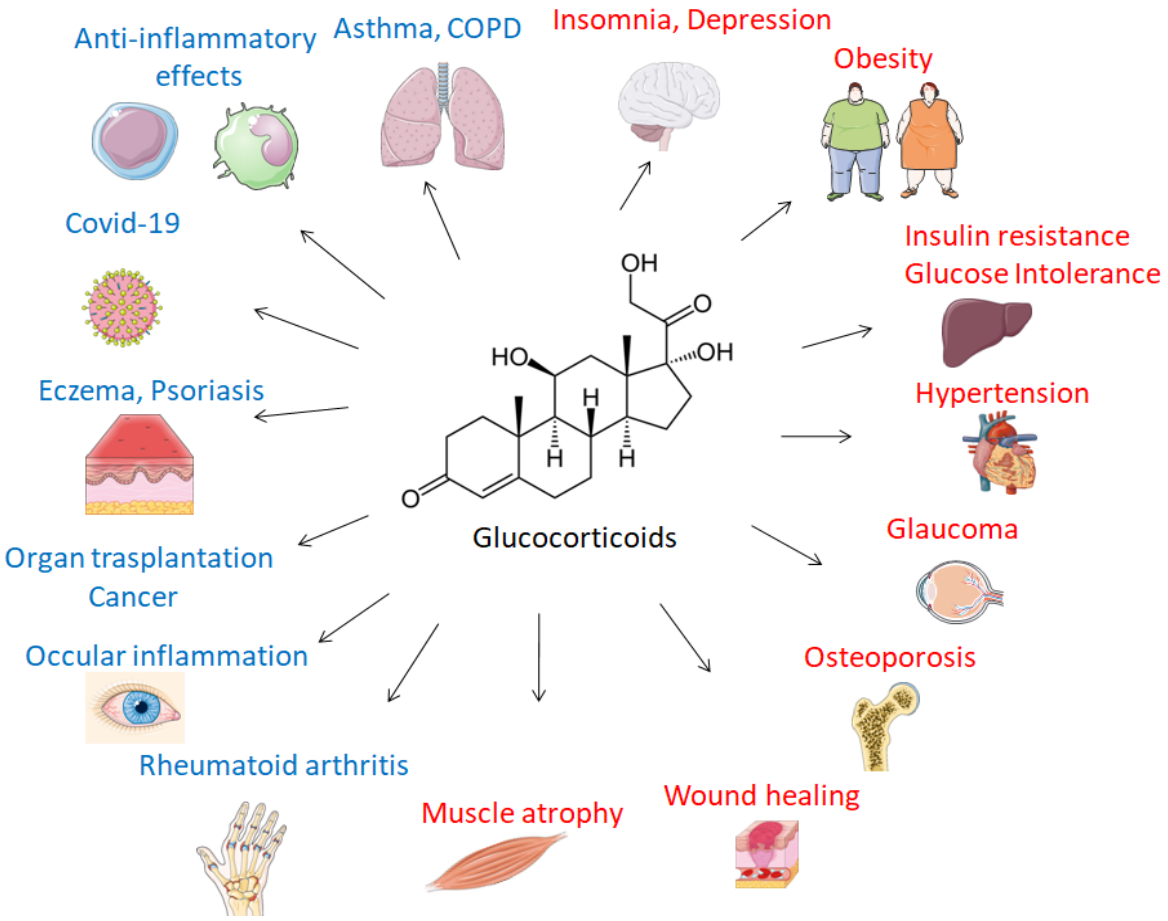

Figure 1.Beneficial (blue) and side effects (red) of Glucocorticoids. Image adapted from (Kadmiel and Cidlowski 2013). Individual pictures taken from Servier Medical Art (https://smart.servier.com/). The glucocorticoid molecule is cortisone taken from(Hardy et al. 2020).

Altered levels of GCs might lead to the development of pathological conditions. Elevated GCs, either endogenously produced, due to increased secretion of GCs from endocrine tumours or exogenous administrated, can result in the development of Cushing's syndrome (Raff and Carroll 2015). Some of the most common symptoms of patients with Cushing's disease are weight gain (abdominal and around the shoulders fat accumulation), muscle weakness and rounded face (Sharma et al. 2015). On the other hand, decreased levels of

GCs can lead to the development of Addison's disease. Addison's manifests as weight loss, fatigue, hypotension, loss of appetite and hyperpigmentation (Sarkar et al. 2012).

1.2 Glucocorticoid action in Macrophages

Macrophages are immune cells that infiltrate and reside in many tissues. They present an essential role in the defence response against foreign pathogenic organisms like bacteria, as well as in the removal of cell debris and cancer cells to regulate homeostasis through phagocytosis (Mosser and Edwards 2008). Apart from their phagocytic role, macrophages contribute to the initiation of an inflammatory response during an infection (Parihar et al. 2010). Based on the stimulus that activates them, macrophages can be categorized as M1 and M2.

The M1-like or classically activated macrophages were first characterized by Mackaness in 1960sand they are involved in the protection against viruses and other pathogens (Mackaness 1962). They can be stimulated by exposure to interferon γ (INF-γ), granulocyte-macrophage colony stimulation factor (GM-CSF) and many other pathogen or damage-associated molecular patterns (PAMPs and DAMPS respectively) (Martinez and Gordon 2014; Chen et al. 2018). M1 macrophages can also be activated by the lipopolysaccharide (LPS) which is a component of the cell wall of Gram-negative bacteria (Nijland et al. 2014; Kuzmich et al. 2017). LPS bind to Toll like receptors (TLRs), which leads to the activation of nuclear factor-κB (NF-κB) and Activator Protein 1 (AP-1) via the IKK and MAPK signalling pathways respectively (Zenz et al. 2008; Oeckinghaus and Ghosh 2009). All these stimuli can induce the expression of pro-inflammatory molecules like Interleukin (IL)-1, 6, 12, 23, the tumor necrosis factor (TNF) and various cytokines and chemokines via different signalling pathways(Martinez and Gordon 2014; Lee 2019). M1 macrophages are also characterized by production of nitric oxide (NO) and reactive oxygen intermediates (ROI) (Lee 2019).

On the other hand, the M2 or alternatively activated macrophages present anti-inflammatory properties. They are also involved in wound healing and tissue repair (Kim and Nair 2019). Based on their activation stimulus they are divided in three different groups. The M2a macrophages are activated by exposure to IL-4 and IL-13, the M2b by immune complexes and TLR ligands, and the M2c by IL10 and glucocorticoids (Gordon 2003; Mosser and Edwards 2008; Martinez and Gordon 2014). Unlike the M1 macrophages, all M2 macrophages are characterized by elevated IL10 and low IL12 production along with high levels of arginase-1 (Arg-1) (Mosser and Edwards 2008; Martinez and Gordon 2014).

Glucocorticoids can polarize macrophages to an anti-inflammatory phenotype in various ways (Martinez and Gordon 2014). They can suppress the expression of inflammatory mediators by disrupting signalling pathways, like the LPS/TLR pathway. GCs interfere with the transcription factors NF-κB and AP-1 downstream of the TLR pathway and repress the expression of pro-inflammatory genes like cytokines, chemokines matrix metalloproteinases and inducible nitric oxide syntase (iNOS) (Hayden and Ghosh 2004; Medzhitov and Horng 2009; Cain and Cidlowski 2017). In more details, GCs inhibit the production of cytokines like *Il1a, Il1b, Il6, Il8, Il12,TNF* and lead to the suppression of chemokine release such as *Ccl2, Ccl3, Cxcl9* and *Cxcl11*, which is important for the recruitment of immune cells to the site of inflammation (Zhang et al. 1997; Luecke and Yamamoto 2005; Flammer et al. 2010; Chinenov et al. 2012; Gupte et al. 2013; Uhlenhaut et al. 2013). Additionally, they can down-regulate the expression of the matrix metalloproteinase (Mmp) peptidases like *Mmp9, Mmp12* and *Mmp13*, which are involved in the degradation of the extracellular matrix and in chemotaxis (Rollins et al. 2017). Moreover, GCs inhibit the expression of E-selectin as well as the integrin ligands vascular cell adhesion molecule 1 (*Vcam1*) and intercellular adhesion molecule 1 (*Icam1*), that are adhesion molecules with an important role in chemotaxis (Cronstein et al. 1992; Atsuta et al. 1999; Cain and Cidlowski 2017).

Apart from the repression of pro-inflammatory genes, GCs mediate the expression of genes with an anti-inflammatory role. For example, they induce the dual-specificity protein phosphatase 1 (*Dusp1* or *Mkp1*) and the Il1 receptor associated kinase 3 (*Irak3*) by inhibiting the MAPK and IRAK1 respectively downstream of the TLR4 pathway (Lasa et al. 2002; Miyata et al. 2015). Additionally, GCs activate the expression of GC-induced leucine zipper (*Gilz* or *Tsc22d3*) which inhibits the transcription of pro-inflammatory genes by binding to NF-κb (Berrebi et al. 2003). Furthermore, they induce the expression I kappa B (*Ikb* a and b) that blocks NF-κB in the cytoplasm in an inactive form (Auphan et al. 1995; Scheinman et al. 1995). Finally, the Kruppel-like factors (*Klf2* and *Klf4*) are induced by GCs and have an important anti-inflammatory role, by competing and inhibiting NF-κB and AP-1 (Das et al. 2006; Liao et al. 2011; Das et al. 2012; Chinenov et al. 2014).

To summarize, GCs regulate inflammation in various ways which include both the repression of pro-inflammatory mediators but also the induction of anti-inflammatory proteins.

1.3 The Glucocorticoid Receptor

GCs, either endogenously produced from the adrenal glands or exogenously administrated, bind to the Glucocorticoid Receptor (GR). GR is a transcription factor and belongs to the family of ligand- activated nuclear hormone receptors (Hollenberg et al. 1985). It is encoded by the *NR3C1* gene, that in humans consists of 9 exons (Oakley and Cidlowski 2013). GR contains a trans-activation domain in the N-terminus (NTD), a central DNA binding domain (DBD) and a ligand binging domain (LBD) in the C-terminus (Figure 2). Between the DBD and the LBD lies a hinge region (H). Exon 2 encodes the NTD, exons 3 and 4 the DBD and exons 5-9 the LBD (Oakley and Cidlowski 2013). GR interacts with co-regulators and the transcriptional machinery through the activation function domain 1 (AF1) in the NTD, which contains sites for post-translational modifications (Kumar and Thompson 2005). The DBD is highly conserved among the nuclear receptors and is composed of two zinc fingers. The first one is needed for recognition and subsequent binding of GR to the DNA, and the second zinc finger is important for homodimerization of GR (Kumar and Thompson 2005). The LBD contains an activation function region (AF2) important for ligand- dependent interactions with the co-regulators (Kumar and Thompson 2005). The junction between the DBD and the hinge region as well as the LBD domain contain sequences involved in the nuclear localization of GR (Oakley and Cidlowski 2013).

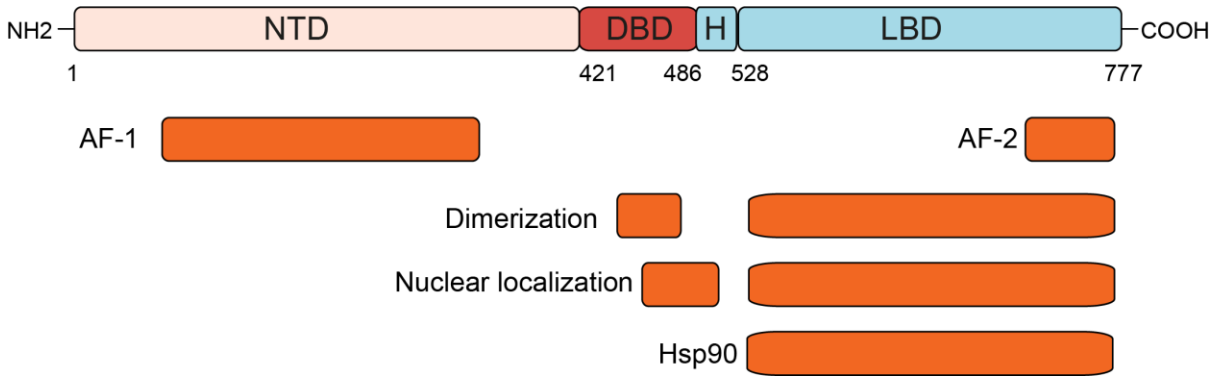

Figure 2. The structure of the glucocorticoid receptor protein. The glucocorticoid receptor consists of the N-terminal domain (NTD), the DNA binding domain (DBD), a hinge region (H) and the ligand binding domain (LBD). The AF1 and AF2 regions as well as regions involved in dimerization, nuclear localization and Hsp90 binding are indicated in orange. Image adapted from (Oakley and Cidlowski 2013).

Several isoforms are generated from the *NR3C1* gene through alternative splicing. In total five splice variants have been identified (GRα, GRβ, GRγ, GR-A and GR-P) (Zielinska et al. 2016). GRα is the most abundant isoform that can mediate the GCs effects (Oakley and Cidlowski 2013). GRα can undergo into alternative translation initiation, which leads to generation of 8 additional isoforms (Lu and Cidlowski 2005). GRβ is also a well described isoform but lacks the LBD domain, and therefore it is not able to bind to glucocorticoids. It is located constitutively to the nucleus and can inhibit the function of GRα (Lu and Cidlowski 2006; Oakley and Cidlowski 2013). The remaining isoforms are less characterized and differ from the GRα isoform by lacking the exons essential for the function of classical GR (Oakley and Cidlowski 2013).

1.4 Transcriptional regulation by the glucocorticoid receptor and co-regulators involved

In macrophages, LPS can trigger an inflammatory response by binding to TLR4 receptor. This leads to activation of inflammatory transcription factors like AP-1, NF-κB and subsequent expression of pro-inflammatory genes (Zenz et al. 2008; Oeckinghaus and Ghosh 2009). In the absence of GCs, GR is transcriptionally inactive and resides in the cytoplasm where it is bound by the heat shock proteins 70 and 90 (Hsp70, Hsp90), along with other chaperones and immunophilins (Pratt and Toft 1997). Upon binding of GCs to the LBD domain, GR is released from the heat shock proteins and translocates from the cytoplasm to the nucleus, where it can bind through the DBD domain to specific DNA sequences called GR response elements (GREs) located in promoters and enhancers. In this way, GR can regulate transcription by both activation of anti-inflammatory genes and repression of pro-inflammatory genes (Figure 3) (Glass and Saijo 2010; Lim et al. 2015). In line with other nuclear receptor, GR function also requires recruitment of co-regulators that are characterized as co-activators or co-repressors (Lonard and O'Malley B 2007).

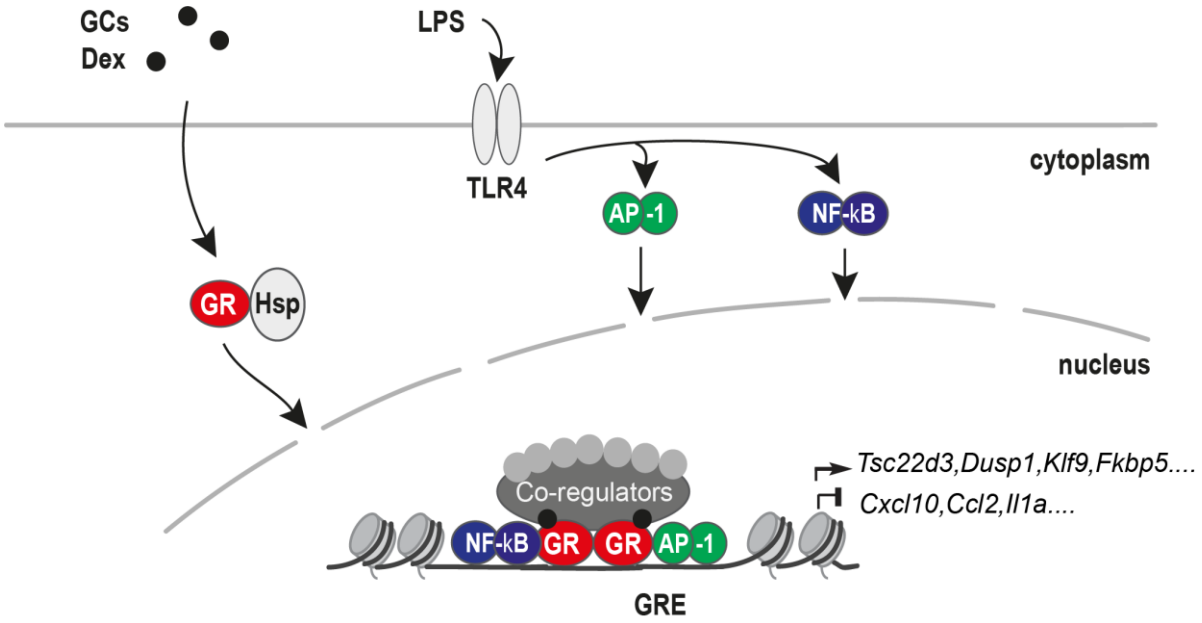

Figure 3. GR regulates the expression of inflammatory genes. In macrophages, inflammation can be triggered by binding of LPS to the TLR4 receptor which leads to activation of the transcription factors AP-1 and NF-κB. This results to the expression of pro- inflammatory genes like *Cxcl10, Ccl2* etc. Upon binding of GCs like Dex, GR is released from the heat shock proteins, can translocate to the nucleus where it binds to GREs and activate the expression of gene like *Tsc22d3, Klf9, Dusp1*, etc. and at the same time repress the expression of pro-inflammatory cytokines and chemokines. Image adapted from (Escoter-Torres et al. 2019).

The mechanisms of GR-mediated gene regulation, its known co-regulators, as well as some non-genomic actions of GR in immunomodulation are described in detail in the following review that I wrote together with my colleagues and in collaboration with Prof. Jan Tuckerman's lab from Ulm University.

frontiers in Immunology

REVIEW
published: 07 August 2019
doi: 10.3389/fimmu.2019.01859

Fighting the Fire: Mechanisms of Inflammatory Gene Regulation by the Glucocorticoid Receptor

Laura Escoter-Torres[1†], *Giorgio Caratti*[2†], *Aikaterini Mechtidou*[1†], *Jan Tuckermann*[2], *Nina Henriette Uhlenhaut*[1,3*] *and Sabine Vettorazzi*[2*]

[1] Molecular Endocrinology, Helmholtz Zentrum München (HMGU), German Center for Diabetes Research (DZD), Institute for Diabetes and Cancer IDC, Munich, Germany, [2] Department of Biology, Institute for Comparative Molecular Endocrinology, University of Ulm, Ulm, Germany, [3] Gene Center, Ludwig-Maximilians-Universität (LMU), Munich, Germany

For many decades, glucocorticoids have been widely used as the gold standard treatment for inflammatory conditions. Unfortunately, their clinical use is limited by severe adverse effects such as insulin resistance, cardiometabolic diseases, muscle and skin atrophies, osteoporosis, and depression. Glucocorticoids exert their effects by binding to the Glucocorticoid Receptor (GR), a ligand-activated transcription factor which both positively, and negatively regulates gene expression. Extensive research during the past several years has uncovered novel mechanisms by which the GR activates and represses its target genes. Genome-wide studies and mouse models have provided valuable insight into the molecular mechanisms of inflammatory gene regulation by GR. This review focusses on newly identified target genes and GR co-regulators that are important for its anti-inflammatory effects in innate immune cells, as well as mutations within the GR itself that shed light on its transcriptional activity. This research progress will hopefully serve as the basis for the development of safer immune suppressants with reduced side effect profiles.

Keywords: glucocorticoid receptor, inflammation, macrophages, mouse models, gene regulation

OPEN ACCESS

Edited by:
Claude Libert,
Flanders Institute for Biotechnology, Belgium

Reviewed by:
Zsuzsa Szondy,
University of Debrecen, Hungary
Marcel Schaaf,
Leiden University, Netherlands

***Correspondence:**
Nina Henriette Uhlenhaut
henriette.uhlenhaut@helmholtz-muenchen.de
Sabine Vettorazzi
sabine.vettorazzi@uni-ulm.de

[†]These authors have contributed equally to this work

Specialty section:
This article was submitted to Inflammation, a section of the journal Frontiers in Immunology

Received: *15 May 2019*
Accepted: *23 July 2019*
Published: *07 August 2019*

Citation:
Escoter-Torres L, Caratti G, Mechtidou A, Tuckermann J, Uhlenhaut NH and Vettorazzi S (2019) Fighting the Fire: Mechanisms of Inflammatory Gene Regulation by the Glucocorticoid Receptor. Front. Immunol. 10:1859. doi: 10.3389/fimmu.2019.01859

INTRODUCTION

Glucocorticoids as Immunomodulators

Glucocorticoids (GCs) are steroid hormones secreted in a diurnal and stress responsive manner, under the control of the hypothalamic-pituitary-adrenal (HPA) axis (1).GCs regulate numerous essential physiological and developmental processes, ranging from lung maturation to glucose metabolism and immune responses. This is clearly demonstrated in mice with abrogated GC signaling, which die perinatally due to pulmonary atelectasis (2). The effect on lung maturation is not merely limited to mice: in clinical practice, pre-term neonates are given GCs to accelerate pulmonary development (3). In adult mammals, endogenous GCs play important homeostatic roles. For instance, GCs increase glucose production through glycogenolysis and gluconeogenesis in the liver upon fasting, and as part of daily rhythmic energy mobilization (4, 5).

Pharmacologically, GCs are widely used to treat acute and chronic inflammatory diseases, such as asthma, allergies, rheumatoid arthritis, inflammatory bowel disease, multiple sclerosis etc., due to their potent anti-inflammatory actions. In addition, GCs are commonly prescribed to prevent graft-vs.-host immune responses after organ transplantation and for certain cancer types, such as lymphoma (6, 7). Currently, it is estimated that 1–3% of the adult Western population are receiving

GCs, demonstrating their broad applications (8). GCs have been used for over 70 years as anti-inflammatory drugs, despite their adverse effects on systemic metabolism, which were noted soon after their first clinical use (9). Long term exposure to GCs induces adipocyte hypertrophy, glucose intolerance and insulin resistance, hypertension, muscle and skin atrophy, osteoporosis, glaucoma, impaired wound healing and psychological effects such as mood changes, insomnia, and depression (4, 10). Long term GC exposure due to increased secretion from endocrine tumors or chronic exogenous administration, often causes a pathological condition known as Cushing's syndrome (11). Cushing's manifests as debilitating muscle wasting, fat accumulation, and susceptibility to infection and can be fatal if left untreated.

Separating beneficial therapeutic properties from detrimental side effects based on a molecular understanding of GC action is a long-term goal of biomedical research. Furthermore, the glucocorticoid receptor (GR) has been key to understanding the basic molecular concepts of GC action. There have been several paradigm shifts of the molecular understanding of GC/GR mechanisms since cloning of the receptor more than 30 years ago (12). The generation of GR mutants that interfere with specific functions of the receptor, the introduction of several mutants into preclinical models and the characterization of genome wide profiles all revolutionized our view of GC action. In this review, we summarize recent insights into the anti-inflammatory effects of GR, focusing on mechanisms of macrophage gene regulation, GR co-regulators, novel GR target genes, and mouse models of inflammation. We also summarize the current understanding of immune modulatory mechanism in the innate immune system based on mouse mutants. These might explain why, despite much progress, developing novel immune modulators that match the efficacy of GCs but avoid the adverse effects remains a major challenge for the field.

The Glucocorticoid Receptor

The endogenous GC, cortisol in humans and corticosterone in rodents, binds to the GR, encoded by the *NR3C1* gene. GR belongs to the nuclear receptor superfamily of ligand activated transcription factors. It consists of three major domains, the central DNA binding domain (DBD), the N-terminal transactivation domain (NTD), and the C-terminal ligand binding domain (LBD) [(12); **Figure 1**].

The *NR3C1* gene encodes several isoforms that are generated by alternative splicing and alternative initiation of translation (10, 13). The full-length isoform GRα-A is the focus of this review. GRβ, a second splice variant, and other GR isoforms, are known to modify GC sensitivity, but are discussed in detail elsewhere (14).

In the absence of ligand, GR resides in the cytoplasm, bound to heat shock proteins 70 and 90 (Hsp70 and Hsp90) together with other chaperones and immunophilins (15). Upon binding of GCs, GR translocates to the nucleus where it binds to DNA sequences. In this way, GR is recruited to target gene enhancers and promoters where it can both activate and repress transcription (16, 17). Canonical binding sites for the GR are called glucocorticoid response elements (GREs) and are composed of two 6bp palindromes (half sites) separated by a 3bp spacer, with the consensus AGAACAnnnTGTTCT. However, GR binding sites (GBS) in the genome vary to a certain degree of motif mismatch, expanding the number of possible target sequences. Furthermore, the context of neighboring transcription factor binding sites and the ensuing crosstalk is relevant for the regulation of inflammatory genes by the GR. The beauty of using GR as a model transcription factor is that its ability to regulate genes can be easily controlled *in vitro* and *in vivo* by the absence or presence of the GC ligand.

Chromatin Residence Time and Multimerization of the Glucocorticoid Receptor

GR, along with other transcription factors, was assumed to bind DNA in a relatively static manner, "sitting down" for long periods of time to regulate gene expression. However, visualization of the dynamics of fluorescent-tagged GR in living cells led to the insight that occupancy of dimeric GR molecules at GREs is rather in the order of seconds and less (18). Only a small portion of available molecules are specifically bound to chromatin at a given time, suggesting that transcription factors and co-factors have a transient rather than stable interaction at genomic response elements (19).

GR acts as a monomer (20), dimer (21, 22), and even tetramer (23–25) depending on the subcellular localization, presence of ligand, GREs, or artificial response elements such as the MMTV array. Interestingly, DNA binding was proposed to trigger allosteric regulation of GR, followed by a change in its oligomeric state (24). Ligand bound GR is mainly nuclear and dimeric. Interestingly, upon DNA binding, the structural LBD rearrangement promotes the formation of higher order oligomers, predominantly tetramers, through unstudied LBD surfaces (25). The physiological relevance and implications of a tetrameric GR, however, are still open for debate and further investigation.

In general, chromatin binding and gene regulation by GR appear to be much more dynamic than previously thought, and the residence time of GR on chromatin may have differential effects. The LBD seems to regulate the number of GR molecules bound at a specific genomic region, which may also affect the transcription of target genes.

Glucocorticoid Receptor Co-regulators

All nuclear receptors (NRs), including GR, require a host of co-activators and co-repressors to ultimately control the transcriptional apparatus.

Steroid receptor coactivator-1 (SRC-1, also known as nuclear receptor co-activator 1, NCOA1) was one of the first identified (26), followed by glucocorticoid receptor interacting protein (GRIP1, SRC-2, and NCOA2) (27). Originally found to be a co-activator of the progesterone receptor (PR), SRC-1, and GRIP1 were shown to directly interact with GR and other steroid receptors. This direct co-activator interaction with GR depends on the evolutionarily conserved LXXLL motif, or NR-box, and without this motif, GR loses transcriptional activity (28). SRC-1

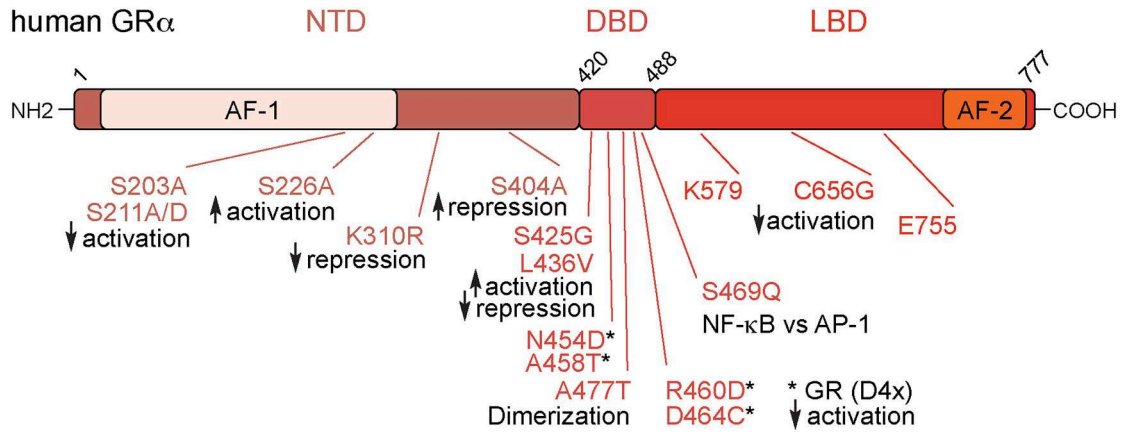

FIGURE 1 | Overview of the glucocorticoid receptor protein. The Glucocorticoid Receptor (GR) is organized into three main domains: the N-terminal Transactivation Domain (NTD), the DNA-Binding Domain (DBD), and the Ligand Binding Domain (LBD). In addition, there are the transactivation domains 1 and 2 (AF-1 and AF-2). These mutations numbered above are relevant for GR's immunomodulatory effects. Numbers are amino acids of the human protein.

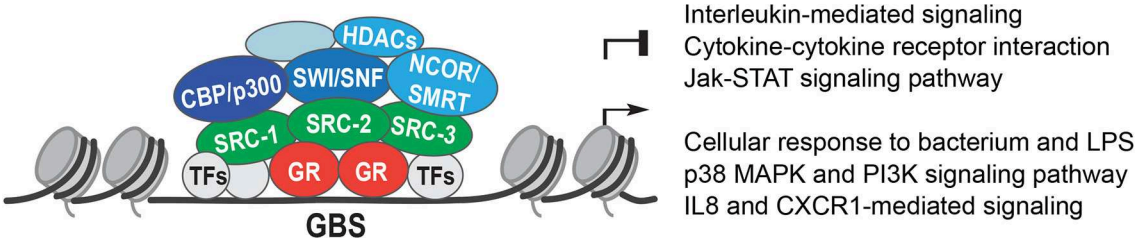

FIGURE 2 | Glucocorticoid receptor co-regulators. The Glucocorticoid Receptor (GR) binds to Glucocorticoid Receptor Binding Sites (GBS) in open chromatin. GR interacts with other transcription factors (TFs) and recruits co-activators or co-repressors, such as: the Steroid Receptor co-activators 1, 2, and 3 (SRC-1, SRC-2, and SRC-3); the histone acetyl transferases CREB binding protein (CBP) and p300; the Nuclear Receptor co-repressors NCOR1 and NCOR2 (NCOR, SMRT), which recruit histone deacetylases 1 and 3 (HDACs); and the SWItch/Sucrose-Non Fermentable (SWI/SNF) chromatin remodeling complex.

directly activates genes with its histone acetyltransferase (HAT) domain that decondenses chromatin [(29); **Figure 2**].

The strength of GR's interaction with SRC-1 and GRIP1 might determine the steroid responsiveness of cancer cells, suggesting that the loss of GC-induced apoptosis or growth arrest is due to, at least in part, co-activator recruitment (30). However, GR seems to preferably interact with GRIP1 over SRC-1, while the opposite is true for PR, which confers selectivity of GR activation and PR activation on chromatin modifications (31).

Importantly, the co-activator GRIP1 can also act as a co-repressor. Depending on the individual GR target gene, GRIP1 functions as either an activator or repressor by using its co-repressor domain. For example, GRIP1 was described to act as a co-repressor at the *osteocalcin* promoter (32). Moreover, the functionality of GRIP1 is modulated by post-translational modifications. CDK9 mediated phosphorylation of GRIP1 was shown to increase GR dependent activation, but had no effect on repression (33).

SRC-3 (NCOA3), another member of the SRC family, was originally identified through interaction with the estrogen receptor (ER) (34). Similar to SRC-1 and GRIP1, SRC-3 is recruited in a locus-specific manner (35).

In the mid-1990s, the discovery of two nuclear receptor co-repressors (NCOR)—NCOR1 (36), and NCOR2 (otherwise known as SMRT, silencing mediator co-repressor) drove further research into the field of NR co-regulators (37). The NCOR family interacts with nuclear receptors via the coRNR-box, consisting of the consensus sequence LXX I/H I XXX I/L, which contacts the AF-2 domain of NRs (38, 39). This is analogous to the LXXLL sequence in co-activators and occupies a similar location on the receptors.

While the NCOAs display intrinsic HAT activity, the co-repressors NCOR/SMRT were described to interact with the histone deacetylase HDAC3 (40). Both NCOR1 and SMRT were able to recruit HDAC3 to condense chromatin as part of their repressive mechanism (41).

SUMOylation of mouse GR at K310 was shown to be essential for repression, and in point mutant mice, neither NCOR1, SMRT nor the associated HDAC3 complex were recruited (42, 43). GCs down-regulate expression of GR itself, through a negative feedback loop. This occurs by recruitment of a GR-NCOR1-HDAC3 complex to an nGRE in exon 6 of the *NR3C1* gene (44). GC-mediated suppression of natural killer cells activity however, was described to be mediated by HDAC1 and SMRT specifically

(45). The differential control of GR action by recruitment of alternative co-activators and co-repressors, in tissue or signal specific contexts, is still an open area of investigation. Different GR ligands selectively recruit alternate co-factors (46), suggesting that ligand induced conformational changes might have discrete effects on GR target genes, adding another level of complexity to GR mediated gene regulation.

Two major proteins that are recruited by co-activators are CBP (CREB binding protein) and p300. Both CBP and p300 are histone acetyl transferases (HATs), and induce chromatin relaxation (47) (**Figure 2**). SRC-1 was shown to recruit p300 into a complex with nuclear receptors to activate transcription (48). Part of GR's repressive action might involve competition for CBP and p300, as GR repression of an AP-1 (Activator Protein 1) reporter was abolished by overexpression of CBP and p300 (49). Moreover, enhanced engraftment of hematopoietic stem cells in response to GCs was described to be controlled by SRC-1 and p300 recruitment to the *CXCR4* gene, with acetylation of histones H4K5 and H4K16 upregulating *CXCR4* (50).

GR and the tumor suppressor protein 53 (p53) were shown to interact in a ligand dependent manner via Hd2m (a transcription factor), which enhanced the GC-induced degradation of both GR and p53 (51). In fact, the interaction between GR and p53 is important for the repression of NF-κB (nuclear factor-κB) responsive genes. Without p53, GR did not repress inflammation in a mouse model of endotoxic shock (52).

Finally, GR interacts with components of the SWI/SNF complex (SWItch/Sucrose-Non Fermentable). These highly evolutionarily conserved ATP-dependent chromatin remodelers use energy from ATP hydrolysis to alter nucleosome positioning. GR was shown to directly interact with the Baf250, Baf57, and Baf60a subunits of SWI/SNF complexes, further demonstrating the ability of GR to modify the chromatin architecture [(53–56); **Figure 2**].

In summary, GR recruits co-activators such as SRC family members, which in turn assemble a transcriptional complex containing histone modifying enzymes and chromatin remodelers to control the transcriptional machinery and RNA Pol II activity. These interactions are crucial for its anti-inflammatory actions and might present novel therapeutic targets in the future.

Mechanistic Insights Into Immunomodulation From GR Point Mutations *in vitro*

Introducing point mutations into the *NR3C1* gene significantly contributed to our understanding of the molecular mechanisms of GR action. Here, we briefly address the insights gained from specific residues that revealed certain GR functions essential to suppress inflammation in cultured cells.

Besides promoter/enhancer occupancy, post-translational modifications of GR play a major role for transcriptional control. Three key phosphorylation sites were identified in the human GR: S203, S211, and S226 (57–59). All of them are located in the AF-1 domain, which is crucial for protein-protein interactions with TATA-box binding protein and others (60). By using phospho-deficient (S211A) or phospho-mimetic (S211D) mutations, it was shown that phosphorylation of GR at S211 increases association with the MED14 subunit of the mediator complex, a key bridge to the transcriptional machinery (59). In confirmation, the S211A mutant displays reduced expression of the GR targets *GILZ* and *IRF8*. S226A mutation however, had the opposite effect. The phosphorylation-deficient mutant S226A showed increased expression of *GILZ* and *IRF8*, suggesting an inhibitory role (59). In addition, S404, a site for GSK3β phosphorylation, regulates GR transcriptional activity. Mutation to S404A rewired the GR-regulated transcriptome, interestingly increasing its repressive capacity (61). Moreover, the SUMOylation-deficient murine GR K310R was shown to affect repression and the recruitment of co-regulators [(42, 43); **Figure 1**].

The AF-2 domain, located within the LBD (62), has additional sites modulating GR function. The mutation C656G within the AF-2 domain of the rat GR (C638 in human) reduced the ligand concentration required for activation of the *PEPCK* promoter (63). Mutations within the "charge-clamp"—that is the co-activator interaction site of K579 and E755—resulted in loss of transcriptional activation, but had no effect on repression (64).

Applying a random mutagenesis approach in yeast, Yamamoto and colleagues showed that multiple mutations within the zinc finger of the DBD impede GR binding to GREs *in vitro*, demonstrating the importance of this particular domain (65). Further mutagenesis studies in the 1990s identified a multitude of important amino acids involved in activation and repression. For example, the mutations S425G and L436V in the DBD could double the activation in a reporter assay, but almost completely abolished repression by GR (66).

Mutations in the dimer interface are also central for the understanding of GR biology. The GR^{dim} (human A458T), corresponding to rat A477T (67), and GR^{mon} (mouse A465T/I634A) (68) mutations disrupt the dimer interface. Further mutation of A458T outside the D-loop to the double N454D/A458T further increased the capacity of GR to repress a reporter *in vitro* (66). Generation of the GR(D4X), a quadruple mutant GR with the residues N454D, A458T, R460D, and D464C in the dimerization region of mouse GR provided deeper insight into the monomer/dimer action of GR. The GR (D4X) had equivalent repressive activity to wild type, while activation capacity as measured in reporter assays was near zero. This mutant demonstrated that opposition of TNF-α involved both activation of IKKB and repression, since mutant GR was unable to induce IKKB, but repressed the production of TNF-α (69). There is significant work on the GR^{dim} mutation *in vivo*, covered in the next section. Early *in vitro* work however, showed that the A477T mutation induced loss of the dimer interface and reduced DNA residence time, making target gene regulation by A477T rather difficult to interpret (70). Both wild type GR and GR^{mon} bound GRE half sites, but A447T was incapable of binding classic, full length GREs, which are occupied by receptor dimers [(67); **Figure 1**].

Another mutation in the second zinc finger of the DBD in rat GR R488Q (R469 in the human GR) was designed to discriminate between interactions with NF-κB and AP-1. Overexpressing GR R488Q in activated CV-1 cells under inflammatory conditions failed to suppress NF-κB reporter

activity, whereas AP-1 inhibition was preserved (71). Additional GR mutations with less impact on inflammation are reviewed in more detail elsewhere (72).

Taken together, these GR point mutants show the importance and complexity of GR interactions with transcription factors and chromatin modifiers. In fact, several discrete mutations within the GR AF-1, AF-2 domains and the dimer interface alter its activity in a gene-specific manner, indicating that different parts of the receptor are dispensable for certain gene regulatory events, but essential for others (32). Differentially interfering with GR function therefore affects multiple physiological processes, and distinct types of inflammatory responses.

Lessons Learned From Genome-Wide Studies

Chromatin as a key determinant of GR function has been highlighted in multiple genome-wide ChIP-sequencing studies since the early 2010s. For instance, GR gene regulation is determined by the chromatin architecture of the responsive cell. GR does not act as its own pioneer factor, but rather cell-type-specific gene regulation is dependent on pre-existing available binding sites, determined by chromatin accessibility (73). The pro-inflammatory transcription factor AP-1 governs a large subset of GR regulatory sites, making areas of DNA accessible to GR (74). As GR is largely dependent on pre-existing open chromatin for binding, it cemented the possibility that stimuli which are known for chromatin remodeling, for example inflammation, alters GR binding. Indeed, treatment with TNF-α amends the transcriptional response to GCs, as well as chromatin occupancy of GR, and surprisingly GR activation also transformed the occupancy of NF-κB (75). Recent data showed that GR could indeed act as a pioneer factor for other transcription factors, such as FOXA1, but only at a minority of genomic sites, and thus far this effect has not been demonstrated in immune cells (76).

When assessing GR activity in a more relevant cell-type, macrophages treated with LPS, GR, p65 (part of the NF-κB complex), and c-Jun (one of the members of the AP-1 dimer) binding overlapped significantly (see below). However, the directionality of the gene regulatory response did not correlate well with the type of interaction. That is, contrary to established models, GR binding to NF-κB loci did not only result in repression of target genes, but either repression or activation depending on the particular locus. The inverse is also true, that GR binding to canonical GREs did not only result in up-regulation of transcription at the assigned gene. Rather than the presence or absence of GR as the determining factor, the recruitment of different chromatin modifiers, such as GRIP1, were the prime measure of whether the particular gene would be activated or repressed (77).

Moreover, GR effects can be dependent on the timing of the inflammatory signal. Pre-treatment of macrophages with GCs before LPS stimulation resulted in differential gene regulation compared to treatment with GCs after LPS stimulation. In addition, a large part of GR's anti-inflammatory action can be accounted for by the induction of negative regulators of inflammation such as Mkp1, GILZ, and A20, see below (78). GR^{dim} macrophages treated with LPS and Dex also showed that the dimerization impaired GR preferentially occupied GR-half sites (16), a phenomenon also observed in cells overexpressing GR A477T (67).

Importantly, all these studies showed that GR not only binds to GREs, but occupies motifs near lineage determining factors, such as PU.1 in macrophages. Again this underscores the idea that GR requires open, pre-programmed chromatin for finding its genomic target sites (16, 74, 77–79). The chromatin landscape is cell-specific and depends on pioneer factors, cell lineage transcription factors and epigenetic marks that all predetermine GR binding. Only a minority of GR peaks are found in inaccessible chromatin and trigger chromatin remodeling upon hormone treatment (16, 73, 79–82). These findings strongly suggest that other DNA-binding proteins prime the chromatin landscape prior to GR arrival. The collaborative binding of lineage-determining transcription factors results in nucleosome remodeling, which generates open regions of chromatin. This provides access to signal-dependent transcription factors to bind open regions and modulate gene transcription in a cell-specific manner (83). In the context of macrophages, PU.1 and C/EBP are essential for the development of the myeloid lineage and have been shown to establish the monocyte-specific enhancer landscape (83, 84). PU.1 deletion results in loss of macrophages, neutrophils and B cells (85, 86). Importantly, PU.1 and C/EBP transcription factors often co-localize with GR in macrophages (16).

This new methodology has given deeper insights into the mechanisms by with GR regulates gene expression, identifying chromatin remodeling, and cooperation with other transcription factors, as a key determinants of GR activity. Importantly, GR's reliance on other factors to define its binding sites underscores the necessity of studying GC responses in a tissue-specific manner, rather than extrapolating effects from one cell-type to another.

Molecular Mechanisms of Immunomodulation by the Glucocorticoid Receptor

Non-genomic Actions of GR

Some therapeutic GC effects, such as bronchodilation, resolution of airway irritation or suppression of inflammation, occur almost too rapidly to result from transcription, raising the possibility of non-genomic GR actions (87, 88). These could be GR-unspecific interactions with cellular membranes, functions of membrane-bound GR or specific interactions with cytosolic GR, thereby altering posttranslational modifications like phosphorylation, or other mechanisms (89).

Membrane-bound GR was described in human monocytes and B cells (90, 91), and non-genomic functions have been found in macrophages (92), lung epithelial cells (93), and T-cells (94).

Downstream of inflammatory MAPK signaling, mitogen- and stress-activated protein kinase-1 (MSK1) is an essential kinase for NF-κB p65 S275 phosphorylation (95).Interestingly, GC-mediated repression of NF-κB targets involves loss of MSK1

kinase recruitment at inflammatory promoters and nuclear export of MSK1 via cytosolic GR (96). Putatively, GR can also crosstalk with AKT, GSK-3β, and mTOR signaling (93).

These non-genomic effects might be very interesting for the development of novel therapeutics, and will benefit from future studies, for example with novel cell lines or mouse models to dissect these complex interactions.

Genomic Actions of GR

Lipopolysaccharide (LPS) is a molecular component of the cell wall of Gram-negative bacteria commonly used to study inflammation (97, 98). On macrophages, LPS binds to Toll-Like Receptor 4 (TLR4) and activates a signaling cascade that results in NF-κB and AP-1 nuclear translocation. Together with other inflammatory transcription factors, these two protein complexes then activate pro-inflammatory gene expression (99, 100). TLR4 activates AP-1 via the MAPK signaling pathway and NF-κB via degradation of the cytosolic IKK complex that frees the NF-κB transcription factor (**Figure 3**).

GR can antagonize or synergize with pro-inflammatory signaling, depending on the context of promoters or enhancers. For antagonism of pro-inflammatory signaling, several mechanisms are proposed. These include the direct interference with MAPK or JNK signaling (101, 102), leading to repressive actions at the gene regulatory level. Conversely, repression of GR-target genes might be explained by tethering to other transcription factors or trans-repression, negative GREs (nGREs, with a different sequence), composite GREs, non-canonical novel GREs, DNA as a modulator of GR, and consensus classical GREs.

Most frequently, GR tethering to AP-1 or NF-κB via protein-protein interactions (trans-repression), instead of direct DNA binding, was suggested to underlie its repression of inflammatory responses (103, 104). In other words, GR has been shown to represses genes via protein-protein interactions with AP-1 (105), NF-κB (106), STAT3 (107), and other DNA-bound transcription factors (**Figure 3**). Interestingly, STAT3 tethering to GR resulted in synergistic gene regulation, and increased target gene expression in AtT-20 cells. On the other hand, GR tethering to DNA-bound STAT3 resulted in transcriptional repression (107).

Negative GREs (nGREs) were originally described as GREs motifs in the promoters of repressed target genes. nGREs can be found in very different cell types and genes involved in various processes, for example: HPA axis (*POMC* and *CRH*) (108, 109), lactation (*PRL3*) (110, 111), bone homeostasis (*osteocalcin*) (112), skin structure (*keratins*) (113), and inflammation (*IL-1β*) (114).

However, the definition of nGREs has not yet reached consensus in the literature, and subsequently, GBS with non-classical consensus sequences, near repressed targets, are also named nGREs. One study described a variation of nGREs, termed "inverted repeat (IR) nGRE." IR nGRE is a complex GBS with the following consensus motif: CTCC(n)$_{0-2}$GGAGA, which differs from the classical GRE (AGAACAnnnTGTTCT) or nGRE (115). These elements however, have not been identified by ChIP-seq, questioning how relevant they are to GR responses.

Similar to nGREs, composite elements, such as degenerate GREs overlapping with other transcription factor consensus motifs, may also affect the transcription of inflammatory targets. For example, a 25-base pair composite element (plfG element) in the promoter of the *proliferin* gene, is regulated by GR and AP-1 (116, 117). Furthermore, the GR DNA-binding domain (DBD) can bind a newly identified motif inside NF-κB consensus sequences. Crystal structures of the GR DBD demonstrated direct binding of GR to the AATTT nucleotides within the NF-κB motif from the promoter regions of *CCL2*, *IL-8*, *PLAU*, *RELB*, and *ICAM1*. This cryptic GR-binding site overlapping the NF-κB response element was named κBRE and was highly conserved between species (118).

An important aspect is the concept of DNA being an allosteric modulator of the GR. Here, the precise nucleotide sequence in a GBS is proposed to function as a shaping ligand that specifies GR's transcriptional activity. X-ray crystallography of GR DBD dimers bound to different GBSs showed that conformation of the lever arm in the DBD appeared to be influenced by the DNA sequence (24, 119). Furthermore, the addition of a single GR-binding site was sufficient to convert a gene, which was normally not regulated by GR, into a target gene, such as *IL-1β* and *IL1R2* in U2OS cells (120). The presence of classical GREs in GR-bound enhancers near both activated and repressed genes in murine bone marrow-derived macrophages (BMDM) stimulated with LPS and Dexamethasone (Dex) challenge these models. These findings suggest that first, direct GR:GRE binding is relevant for repression of inflammatory genes. Secondly, that the classical models described above are not sufficient for prediction of GR mediated activation or repression. Therefore, the presence of a different combination of cofactors in activated vs. repressed sites could explain or contribute to the up- or down-regulation of GR target genes (77, 118, 121, 122).

Taken together, how GR activates one set of target genes while repressing another is still an open question, and the molecular mechanisms specifying the repression of inflammatory genes remain unknown. Repression by GR is a complex process which likely involves different determinant factors. One factor is GR itself (phosphorylation, post-translational modifications and ligand-specific conformations), another factor is the DNA sequence, the cell type-specific chromatin landscape and the cooperation with co-regulators and other transcription factors. All of these, together with potentially unknown factors, ultimately determine which target genes are up- or down-regulated.

Mechanistic Insights Into Immunomodulation From GR Point Mutations *in vivo*

As described above, one particular class of point mutations, which interfere with GR dimerization, caught considerable attention. In tissue culture experiments expressing these GR^{dim} mutants (human GR A458T, mouse GR A465T, and rat A477T), the concept was developed that abrogation of dimerization could be beneficial to limit side effects of anti-inflammatory treatments. Therefore, pharmaceutical companies directed their research to develop dissociated ligands favoring GR monomer

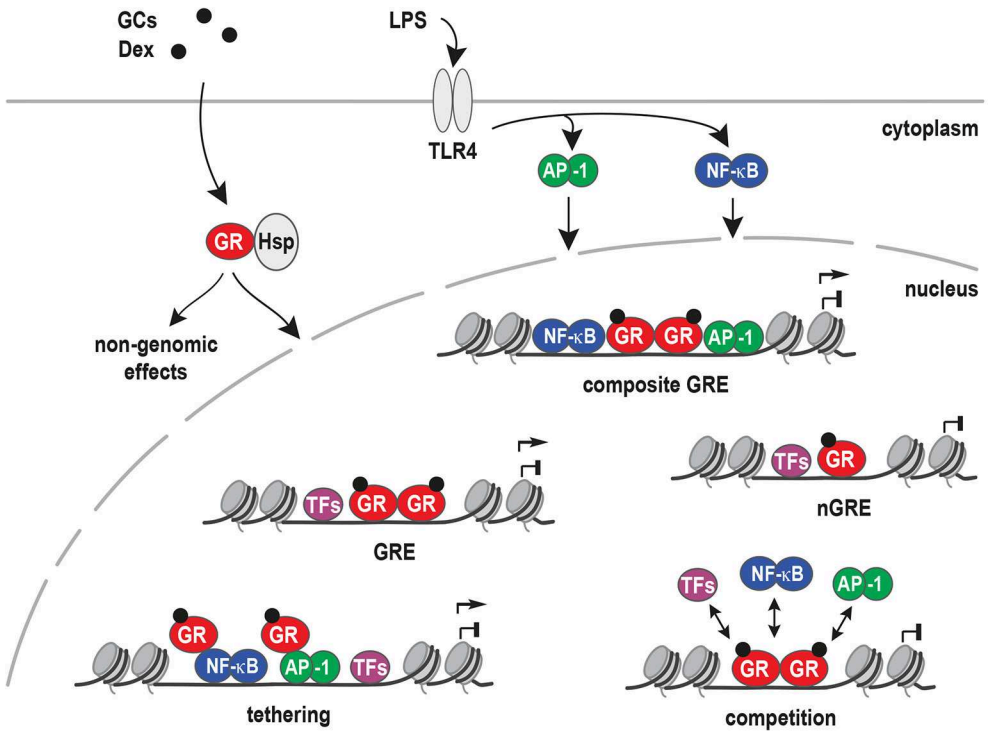

FIGURE 3 | Models for inflammatory gene regulation by the glucocorticoid receptor. Upon ligand binding (GCs), the glucocorticoid receptor (GR) is released from heat shock proteins (Hsp) and translocates to the nucleus. Inflammation can be activated by lipopolysaccharide (LPS) binding to Toll-like receptor 4 (TLR4). TLR4 signaling results in the activation of NF-κB, AP-1, and other inflammatory transcription factors that bind and regulate pro-inflammatory target genes. Different mechanisms have been proposed for GR's potent anti-inflammatory actions, i.e., binding to Glucocorticoid Response Elements (GREs), to composite GREs together with other transcription factors, to negative GREs (nGRE), by tethering to DNA-bound transcription factors, by competing with other factors for DNA binding sites or by non-genomic actions.

dependent favorable effects and reducing unwanted GR dimer action (123, 124).

Various selective GR agonists (SEGRAs), such as RU24858, RU24782, and non-steroidal ligands (LDG552, ZK216348, Compound A), were examined for desired anti-inflammatory effects with the hope that there would be minimal metabolic actions (124, 125). Only a few of these compounds, however, showed promise in preclinical trials (126). Their limited success arose from the generalized and oversimplified view that the GR monomer mediates trans-repression (anti-inflammatory) and the GR dimer regulates only unwanted effects (127). The disappointing conclusion of these programs for SEGRAs and non-steroidal ligands and their translation to the clinic called for new perspectives in the context of pathophysiology (10, 16, 104, 127–129). With knowledge gained from the GR^{dim} mouse and others, the development of selective monomerizing GRagonists or modulators (SEMOGRAMs) and selective dimerizing GRagonists or modulators (SEDIGRAMs) has begun to make progress (130). To find SEDIGRAMs, a screening identified Cortivazol and AZD2906 as compounds that increase GR dimerization and enhance the transactivation capacity. Both chemicals, however, still have GR monomer activity, indicating that these are not yet the ideal SEDIGRAMS (129). Efforts are still ongoing to identify perfect GR modulators separating dimer from monomer.

In 1998, the GR A465T mutation was introduced into mice (131, 132). Intriguingly, mice born with this mutation survived in certain backgrounds (131), and simple inflammatory models, such as phorbol ester induced skin irritation, responded to GC treatment in these animals. This indicated that GR monomer and thus transrepression by tethering might be sufficient to reduce inflammation. However, for most other inflammatory models, GCs failed to have an effect in these GR^{dim} mice (**Figure 4A**).

For instance, during LPS, CLP (cecal ligation and puncture), and TNF-α induced shock, GR^{dim} mice were highly susceptible to inflammation and cytokine production, impaired thermoregulation and metabolic alterations (133–135). Furthermore, macrophages from GR^{dim} mice were unable to efficiently repress cytokines in response to LPS (135). Moreover, GR^{dim} mice treated with exogenous GCs showed impairment of anti-inflammatory responses in models of acute lung injury (ALI), arthritis, contact allergy, and allergic airway inflammation (136–139). During ALI, this was partially due to diminished expression of the GR-dimer target gene *Sphk1* (138) (see above). In models of allergic airway inflammation, contact hypersensitivity, antigen-induced arthritis (AIA) or serum transfer-induced arthritis (STIA), GR^{dim} mice failed to repress

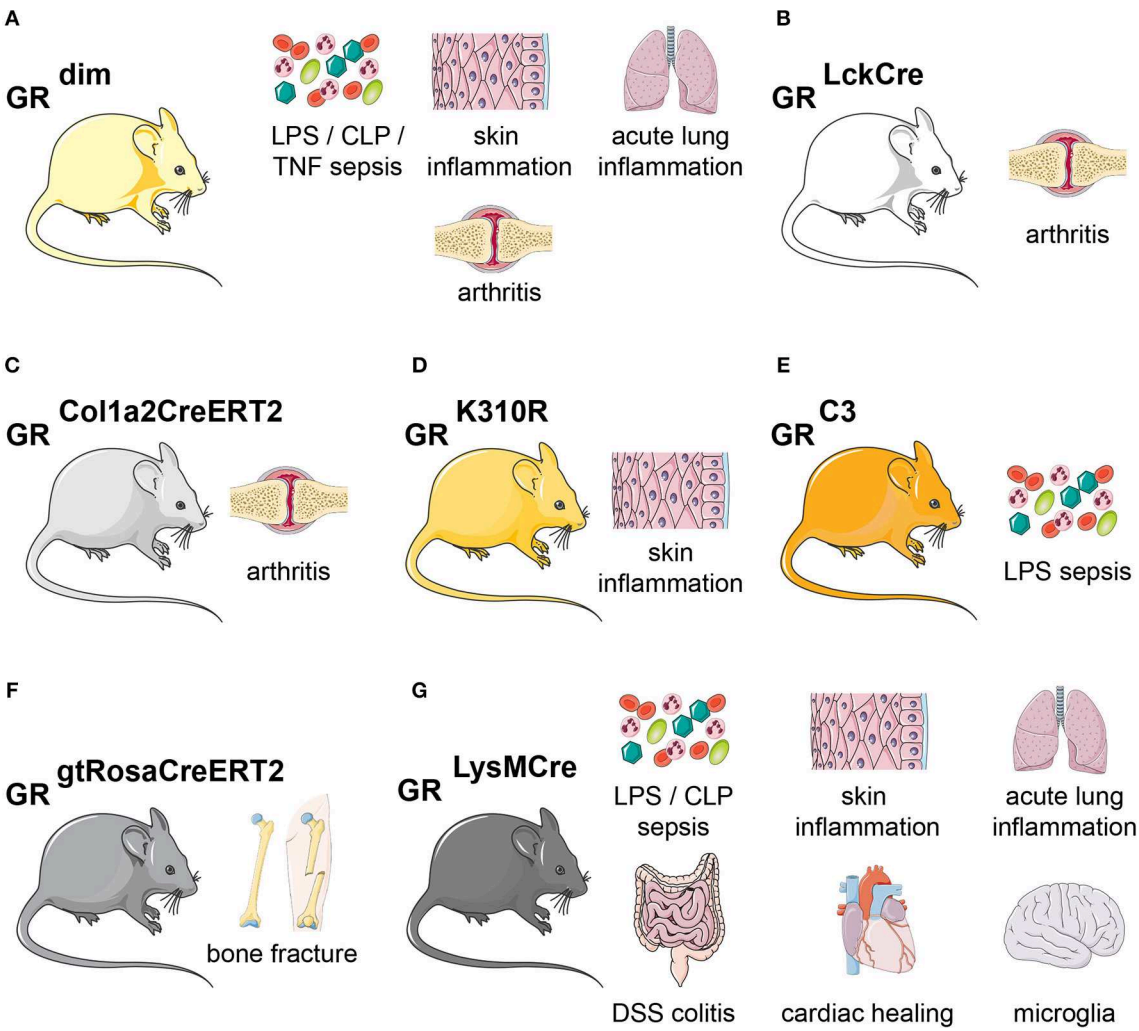

FIGURE 4 | Glucocorticoid receptor mutant mouse models of inflammation. Overview of the mouse lines discussed in this article. **(A)** GR^{dim} mice are more sensitive during LPS-, CLP-, or TNF inflammation. GR^{dim} mice are refractory to GC treatment in models of skin inflammation, acute lung injury and arthritis. **(B)** In GR^{LckCre} mice, GR is lacking in T-cells, making them refractory to GC treatment during arthritis. **(C)** $GR^{Col1a2CreERT2}$ (lacking GR in fibroblasts) show delayed GC-induced suppression in arthritis. **(D)** GR K310R mutant mice lack GR SUMOylation and show impaired control of skin inflammation. **(E)** GR-C3 mice, lacking the most active GR isoform C3, are more sensitive to LPS-induced endotoxic shock. **(F)** During fracture, GR is necessary in all cells, as shown by $GR^{gtRosaCreERT2}$ (tamoxifen-induced ubiquitous Cre-mediated recombination) for fracture healing. **(G)** $GR^{LysMCre}$ mice (GR is deleted in myeloid cells) show no proper healing in LPS- or CLP-sepsis, skin inflammation, acute lung injury, DSS colitis, cardiac healing, and Parkinson disease. The skin, lungs, bones, intestine, heart and brain cartoons were obtained from Servier Medical Art.

inflammation when given GC therapy (136, 137, 139, 140). In the model of AIA, GR dimerization was shown to be essential in T cells (GR^{LckCre} mice) to reduce inflammation [(137); **Figures 4A,B**]. More recently, GR^{dim} mice reconstituted with wild type hematopoietic stem cells failed to induce non-classical ($CD11b^{+}$, $F4/80^{+}$, $Ly6C^{-}$), non-activated ($CD11b^{+}$, $F4/80^{+}$ $MHCII^{-}$), anti-inflammatory (CD163, CD36, AnxA1, Axl, and MertK) macrophages during STIA, while cytokines were repressed normally (140). This strongly indicated that intact dimerization in stromal non-immune cells could contribute to the suppression of inflammation. More precise, the GR in fibroblast-like synoviocytes ($GR^{Col1a2CreERT2}$) was crucial to reduce STIA (140) (**Figure 4C**). GR^{dim} mice were also resistant to GC treatment during TNF-induced inflammation, and exhibited increased gut barrier leakiness, cell death of intestinal epithelial cells and cell death. An increased STAT1-responsive interferon-stimulated gene signature was observed in the gut of GR^{dim} mice (141).

Whereas, the GR^{dim} knock-in mice were intensively studied, less is known about other point mutations. The GRK310R mutation, which abrogates SUMOylation of the GR, failed to respond to GCs during skin inflammation. This was in part due to reduced SMRT/NCoR-co-repressor recruitment to GR/NF-κB/AP-1 repressive complexes [(42, 43); **Figure 4D**].

Finally, Cidlowski and colleagues published a knock-in mouse of the most active GR isoform C3. The lethality of these mice

could be overcome by antenatal GC administration, and adult mice were hypersensitive to LPS administration. This indicated that either the absence of other isoforms like the most abundant GR-A, or indeed the specific overexpression of GR-C3 might confer anti-inflammatory actions [(142); **Figure 4E**]. However, further studies are warranted to dissect these observations in more detail.

Taken together, GR point mutations introduced *in vivo*, namely the GR^{dim} mutation, but also the more recent mutations, have yield valuable insight into the molecular features of GR. With the emergence of CRISPR/Cas9 gene editing technology, more *in vivo* models for specific GR functions will help our understanding of GR in physiological processes in the future.

Glucocorticoid Action on Macrophages

GCs exert their immunosuppressive effects through many cells of the innate immune system, including dendritic cells, mast cells, neutrophils, and eosinophils (143, 144). GCs also play a major role in the regulation of adaptive immunity. For example, GCs decrease the proliferation of early B cell progenitors (145) and induce apoptosis in B cells and T cells (145–149). In this review, we will focus mainly on the effects of GCs in macrophages, since these innate immune cells are essential mediators of defense responses, beyond the mere removal of pathogens, and regulate tissue homeostasis in a myriad of ways (150).

Macrophages reside in many different tissues and are the first line of defense against pathogens (151). Depending on the activating stimulus, they can be categorized as M1-like and M2-like macrophages. The M1-like macrophages (classically activated macrophages) mediate pro-inflammatory actions. They are activated by exposure to LPS, INFγ, TNF-α, or pathogen- and danger-associated molecular patterns (PAMPs and DAMPs, respectively) (151–153). GCs suppress inflammatory responses downstream of TLRs, in part by interfering with the NF-κB- and AP-1-activated transcription of pro-inflammatory cytokines and chemokines (154, 155).

The M2-like macrophages on the other hand, are characterized by their anti-inflammatory potential and are activated by cytokines involved in inflammatory resolution, like IL-4, IL-10, and IL-13 (151, 153, 156). GCs can also polarize macrophages to an M2-like phenotype by regulating the expression of anti-inflammatory proteins (153, 156). A major, yet undervalued aspect of GC control of anti-inflammatory macrophage polarization is the regulation of efferocytosis. GCs enhance the clearance of apoptotic cells, which in itself can augment the development of an anti-inflammatory macrophage phenotype (157, 158).

In sum, GCs can modulate macrophage activity in a number of different and intricate ways, which include suppressing the production of pro-inflammatory proteins and inducing anti-inflammatory mediators.

Glucocorticoid Receptor Target Genes Mediating Immune Modulation

GC stimulated macrophages shift to an M2-like anti-inflammatory and inflammation-resolving phenotype (156). These effects are achieved by the repression of pro-inflammatory genes, the induction of gene products antagonizing pro-inflammatory signaling, and by synergism with pro-inflammatory signaling pathways to activate genes resolving inflammation.

While the mechanisms of gene repression have been extensively discussed [referring to interleukins, chemokines, matrix metalloproteinases, inducible nitric oxide synthase (iNOS), and other mediators], the activated anti-inflammatory genes have only recently received attention (**Table 1**).

Prominent examples are the induction of MAPK phosphatase 1 (Mkp1 or Dusp1), that interferes with the p38MAPK pathway; GC induced leucine zipper (GILZ/Tsc22d3), which binds to the NF-κB subunit p65; the induction of IκBα and β, which oppose NF-κB activity; the activation of kruppel like transcription factors (Klf), which are important for alternative macrophage polarization, and many others (**Table 1**). This upregulation of anti-inflammatory genes further emphasizes that both gene repression and activation are required for the immunomodulatory effects of GCs.

More recently, there were intriguing observations that GCs not only antagonize inflammatory signaling, but also synergize with pro-inflammatory signaling pathways (**Table 1**). GCs synergize with *Haemophilus influenzae* activated inflammatory pathways in macrophages, bronchial epithelial cells (BEAS-2B) and lung epithelial cells (A549) to induce IRAK-M, a negative regulator of TLR signaling (203). Mechanistically, this synergistic activation of *Irak-M/Irak-3* transcription is dependent on binding of both GR and p65 to its promoter, showing a cooperative induction by NF-κB and GR that limits inflammation (203). Similarly, GCs activate TLR2 expression synergistically with *H. influenza* signaling *in vitro* (194).

In ALI models, GR was shown to cooperate with LPS-induced p38MAPK-Msk1 to induce Sphingosine Kinase 1 (SphK1) expression in macrophages (138). SphK1 produces the active mediator Sphingosine-1-phosphate (S1P), that binds to the S1P receptor 1 (S1PR1) on endothelial cells to reduce vascular leakage and infiltration during lung inflammation (138, 204–208). In ALI, mice lacking SphK1 in macrophages were resistant to GC treatment and showed reduced S1P levels. Additional examples of synergistically regulated genes important for modulation of inflammation are acute phase proteins like Serpin A3 (α1-antichymotrypsin) (195) and Metallothioneins (Mt1 and Mt2) (196, 197).

The synergistic regulation of immune-modulating genes by GCs and pro-inflammatory pathways is an important component of their mechanism, but the underlying dynamics and time windows are still poorly understood.

Loss of Function Models of GC Signaling in Macrophages

Strong evidence for the role of GR during homeostasis and inflammation was derived from conditional loss-of-function studies in mice. Applying the Cre/LoxP system, GR tamoxifen-inducible mice ($GR^{gtROSACreERT2}$) could be used to determine the impact of GR deletion in adult animals, circumventing the lethality of global GR knockouts. For example, they have been useful to study GR during inflammation-dependent bone

TABLE 1 | GR target genes relevant for (anti-) inflammatory action.

GC-regulated genes	Targets	GC effect on immune responses	References
Cytokines	Il-1α, Il-1β, Il-6, Il-8, and Il-12	Repression of cytokine production	(114, 159, 160)
Chemokines	Ccl2, Ccl3, Ccl4, Cxcl9, and Cxcl11	Suppression of chemokine release	(77, 160–162)
Matrix metalloproteinases	Mmp12 and Mmp13	Reduction of extracellular matrix remodeling, proteolytic processing	(77, 161)
MAPK phosphatase 1	Induction of Mkp1	Suppression of Jnk and p38Mapk	(133, 163–169)
GC-induced leucine zipper (Tscd22d3)	Induction of Gilz	Inhibition of NF-κB	(170–177)
IκBα and IκBβ	Induction of IκBα and IκBβ	Trapping NF-κB in the cytoplasm, reduced NF-κB activity	(178, 179)
Kruppel-like factor 2	Induction of Klf2	Competition with AP-1 and NF-κB, reduction of inflammatory cytokines	(180–182)
Kruppel-like factor 4	Induction of Klf4	Inhibition of NF-κB	(180, 183)
A3 adenosine receptor	Upregulation of A3AR	Enhanced Erk1/2, anti-apoptotic and pro-survival	(184)
Annexin A1	Induction of Annexin A1	Induction of efferocytosis and monocyte recruitment	(185–189)
Pparγ	Upregulation of Pparγ	Reduced migration	(190)
Tristetraprolin	Induction of TTP	Destabilization of TNF-α	(191–193)
Irak-M	Irak-M induction through synergistic action of GC/GR and NF-κB	Suppression of pro-inflammatory mediators	(193, 194)
Sphingosine Kinase 1	Sphk1 induction through synergism of GC/GR and p38Mapk-Msk1	Reduced vascular leakage and infiltration during acute lung injury	(138)
Serpin A3	Serpin A3 induction through synergism GC/GR and TNFSR1	GR recruitment to Serpin A3 TSS by Dex and TNF-α treatment	(195)
Metallothioneins	Mt1 induction through synergism of Il-6 and GC/GR	Increased susceptibility in inflammatory model in the absence of Mts	(196–202)

repair after fracture (209). Overall, the mice displayed a mild increase in inflammation, with elevated serum IL-6 levels and increased IL-1β levels at the fracture hematoma, accompanied by increased $CD3^+$ and $CD8^+$ cells. Consequently, the lack of GR and potentially the elevated inflammation, caused a delayed endochondral regeneration and maturation of callus and a decreased healing response [(209); **Figure 4F**].

Since the publications of conditional GR alleles in 1999 (210), 2003 (211), and 2012 (212), many cell types have been targeted with specific Cre lines to characterize specific functions of the GR in numerous cell types in the brain, muscle, heart, T lymphocytes, and others.

Insights into the function of GR in macrophages *in vivo* mainly stems from Lysozyme 2 (LysM)–Cre mice crossed to GR floxed alleles, which causes deletion in the myeloid cell lineage (monocytes, mature macrophages, and granulocytes) [(135, 136, 163, 213); **Figure 4G**].

In both the LPS-induced endotoxic shock model and during CLP, myeloid GR is crucial for the repression of inflammatory cytokines and for survival (135, 163). Not only in LPS-induced inflammation, but also in dextran sodium sulfate (DSS)-induced colitis, the action of endogenous GCs in macrophages was essential to reduce intestinal inflammation (214). Mice deficient for macrophage GR had a higher disease score, with increased infiltration of neutrophils, T cells and macrophages in the colon, which was associated with enhanced serum IL-6 (214). Moreover, macrophages were shown to play an essential role for cardiac healing, tissue repair and hence survival in myocardial infarction (215). Deletion of GR in macrophages delayed cardiac healing 7 days after myocardial infarct, with impaired cardiac function, collagen scar formation and neovascularization, and larger myofibroblasts. Consequently, targeting macrophage GR during myocardial infarction might be a potential pharmacological intervention for tissue repair (215). In contrast, in a mouse model of atherosclerosis, macrophage GR deletion was beneficial and showed reduced levels of vascular calcification, due to reduced RANKL, BMP2, and Mx2 expression (216).

During skin inflammation in a model of contact hypersensitivity, the anti-inflammatory effects of GCs required GR in myeloid cells (136). Additionally, in a model of ALI, $GR^{LysMCre}$ mice were resistant to GC therapy, did not reduce cellular infiltration in the lung and did not induce the endothelial barrier stabilizing sphingosine-1-phosphate [(138); **Figure 4G**].

$GR^{LysMCre}$ mice were shown to efficiently express Cre in microglia, knocking out GR in brain resident macrophages. Studies on the function of microglial GR during acute inflammation demonstrated more cellular lesions, damage, demyelination in the corpus callosum, and increased neuronal degeneration. It also significantly increased pro-inflammatory cytokines after LPS injections (217). The activation of microglia induces secretion of pro-inflammatory proteins that contribute to dopaminergic neuronal death, a major a hallmark of Parkinson's disease. The absence of GR in microglia revealed that increased death of dopaminergic neurons in Parkinson's may contribute to neurodegenerative processes (218). Additionally, recent studies suggest that the absence of microglia GR facilitates TLR9 activation

of inflammatory processes and affects Parkinson's disease progression (219).

In summary, the genetic deletion of GR in myeloid cells in various inflammatory models demonstrated the pivotal role of this cell type for GC actions. However, one of the limitations of the LysMCre mouse is the recombination in other myeloid cells such as neutrophils, whose contribution cannot be excluded. Nonetheless, this wealth of data supports the concept that selective targeting of glucocorticoids to macrophages, while sparing other cell types, could be a promising approach to optimize therapy.

CONCLUSION

During the past decade, much has been learned about the immunomodulatory mechanisms employed by GR: analyzing various mouse models, creating distinct mutations, mapping GR target genes genome-wide, functionally characterizing individual proteins mediating GC responses, studying different inflammatory settings, identifying essential co-regulators, and applying novel molecular biology methods, have broadened our understanding of these steroids' intricate actions. Taken together, it becomes obvious how basic research is fundamental in enabling drug development. However, we now realize that GR's molecular mechanisms are very complex, cell-type, locus- and signal-specific, and much more sophisticated than we previously anticipated. Intra- and extra-cellular signals can control GR function on many levels, and these multi-layered machineries demand new interpretation of previous over-simplified models. In the future, the rapid advancement of high-throughput technologies such as machine learning, genomics, proteomics, genome engineering, etc. will be key to the development of safer immunomodulators or novel GR ligands.

AUTHOR CONTRIBUTIONS

LE-T, GC, AM, and SV wrote the manuscript with supervision of JT and NU. SV, JT, and NU secured funding.

FUNDING

This work was supported by funding from the DFG (SFB 1064 Chromatin Dynamics) & the ERC (ERC-StG-2014-StG 638573 SILENCE) to NU; and from the DFG (SFB1149, B07) & Start-Up Funding Program of the Medical Faculty University Ulm (Bausteinprogramm Universität Ulm) to SV; and from the DFG (SFB1149, C02) & AMPK ANR (DFG Tu220/13-1) to JT.

ACKNOWLEDGMENTS

We apologize to all authors who could not be cited due to space constraints. We sincerely thank Ivonne Guderian and Sybille Regn for assistance.

REFERENCES

1. Biddie SC, Conway-Campbell BL, Lightman SL. Dynamic regulation of glucocorticoid signalling in health and disease. *Rheumatology (Oxford)*. (2012) 51:403–12. doi: 10.1093/rheumatology/ker215
2. Cole TJ, Blendy JA, Monaghan AP, Krieglstein K, Schmid W, Aguzzi A, et al. Targeted disruption of the glucocorticoid receptor gene blocks adrenergic chromaffin cell development and severely retards lung maturation. *Genes Dev*. (1995) 9:1608–21. doi: 10.1101/gad.9.13.1608
3. Olaloko O, Mohammed R, Ojha U. Evaluating the use of corticosteroids in preventing and treating bronchopulmonary dysplasia in preterm neonates. *Int J Gen Med*. (2018) 11: 265–74. doi: 10.2147/IJGM.S158184
4. Kadmiel M, Cidlowski JA. Glucocorticoid receptor signaling in health and disease. *Trends Pharmacol Sci*. (2013) 34:518–30. doi: 10.1016/j.tips.2013.07.003
5. Herman JP, McKlveen JM, Ghosal S, Kopp B, Wulsin A, Makinson R, et al. Regulation of the hypothalamic-pituitary-adrenocortical stress response. *Compr Physiol*. (2016) 6:603–21. doi: 10.1002/cphy.c150015
6. Ramamoorthy S, Cidlowski JA. Corticosteroids: mechanisms of action in health and disease. *Rheum Dis Clin North Am*. (2016) 42:15–31; vii. doi: 10.1016/j.rdc.2015.08.002
7. De Lucena DD, Rangel EB. Glucocorticoids use in kidney transplant setting. *Expert Opin Drug Metab Toxicol*. (2018) 14:1023–41. doi: 10.1080/17425255.2018.1530214
8. McDonough AK, Curtis JR, Saag KG. The epidemiology of glucocorticoid-associated adverse events. *Curr Opin Rheumatol*. (2008) 20:131–7. doi: 10.1097/BOR.0b013e3282f51031
9. Hench PS. The reversibility of certain rheumatic and nonrheumatic conditions by the use of cortisone or of the pituitary adrenocotropic hormone. *Ann Intern Med*. (1952) 36:1–38. doi: 10.7326/0003-4819-36-1-1
10. Hartmann K, Koenen M, Schauer S, Wittig-Blaich S, Ahmad M, Baschant U, et al. Molecular actions of glucocorticoids in cartilage and bone during health, disease, and steroid therapy. *Physiol Rev*. (2016) 96:409–7. doi: 10.1152/physrev.00011.2015
11. Raff H, Carroll T. Cushing's syndrome: from physiological principles to diagnosis and clinical care. *J Physiol*. (2015) 593:493–506. doi: 10.1113/jphysiol.2014.282871
12. Giguere V, Hollenberg SM, Rosenfeld MG, Evans RM. Functional domains of the human glucocorticoid receptor. *Cell*. (1986) 46:645–52. doi: 10.1016/0092-8674(86)90339-9
13. Lu NZ, Cidlowski JA. Translational regulatory mechanisms generate N-terminal glucocorticoid receptor isoforms with unique transcriptional target genes. *Mol Cell*. (2005) 18:331–42. doi: 10.1016/j.molcel.2005.03.025
14. Cain DW, Cidlowski JA. Specificity and sensitivity of glucocorticoid signaling in health and disease. *Best Pract Res Clin Endocrinol Metab*. (2015) 29:545–6. doi: 10.1016/j.beem.2015.04.007
15. Pratt WB, Toft DO. Regulation of signaling protein function and trafficking by the hsp90/hsp70-based chaperone machinery. *Exp Biol Med (Maywood)*. (2003) 228:111–33. doi: 10.1177/153537020322800201
16. Lim HW, Uhlenhaut NH, Rauch A, Weiner J, Hubner S, Hubner N, et al. Genomic redistribution of GR monomers and dimers mediates transcriptional response to exogenous glucocorticoid *in vivo*. *Genome Res*. (2015) 25:836–44. doi: 10.1101/gr.188581.114
17. Glass CK, Saijo K. Nuclear receptor transrepression pathways that regulate inflammation in macrophages and T cells. *Nat Rev Immunol*. (2010) 10:365–76. doi: 10.1038/nri2748
18. Gebhardt JC, Suter DM, Roy R, Zhao ZW, Chapman AR, Basu S, et al. Single-molecule imaging of transcription factor binding to DNA in live mammalian cells. *Nat Methods*. (2013) 10:421–6. doi: 10.1038/nmeth.2411
19. Paakinaho V, Presman DM, Ball DA, Johnson TA, Schiltz RL, Levitt P, et al. Single-molecule analysis of steroid receptor and cofactor action in living cells. *Nat Commun*. (2017) 8: 15896. doi: 10.1038/ncomms15896

20. Wrange O, Carlstedt-Duke J, Gustafsson JA. Stoichiometric analysis of the specific interaction of the glucocorticoid receptor with DNA. *JBiol Chem*. (1986) 261:11770–8.
21. Tsai SY, Carlstedt-Duke J, Weigel NL, Dahlman K, Gustafsson JA, Tsai MJ, et al. Molecular interactions of steroid hormone receptor with its enhancer element: evidence for receptor dimer formation. *Cell*. (1988) 55:361–9. doi: 10.1016/0092-8674(88)90059-1
22. Wrange O, Eriksson P, Perlmann T. The purified activated glucocorticoid receptor is a homodimer. *J Biol Chem*. (1989) 264:5253–9.
23. Payvar F, DeFranco D, Firestone GL, Edgar B, Wrange O, Okret S, et al. Sequence-specific binding of glucocorticoid receptor to MTVDNA at sites within and upstream of the transcribed region. *Cell*. (1983) 35(2 Pt 1):381–92. doi: 10.1016/0092-8674(83)90171-X
24. Meijsing SH, Pufall MA, So AY, Bates DL, Chen L, Yamamoto KR. DNA binding site sequence directs glucocorticoid receptor structure and activity. *Science*. (2009) 324:407–10. doi: 10.1126/science.1164265
25. Presman DM, Ganguly S, Schiltz RL, Johnson TA, Karpova TS, Hager GL. DNA binding triggers tetramerization of the glucocorticoid receptor in live cells. *Proc Natl Acad Sci USA*. (2016) 113:8236–41. doi: 10.1073/pnas.1606774113
26. Onate SA, Tsai SY, Tsai MJ, O'Malley BW. Sequence and characterization of a coactivator for the steroid hormone receptor superfamily. *Science*. (1995) 270:1354–7. doi: 10.1126/science.270.5240.1354
27. Hong H, Kohli K, Trivedi A, Johnson DL, Stallcup MR. GRIP1, a novel mouse protein that serves as a transcriptional coactivator in yeast for the hormone binding domains of steroid receptors. *Proc Natl Acad Sci USA*. (1996) 93:4948–52. doi: 10.1073/pnas.93.10.4948
28. Ding XF, Anderson CM, Ma H, Hong H, Uht RM, Kushner PJ, et al. Nuclear receptor-binding sites of coactivators glucocorticoid receptor interacting protein 1 (GRIP1) and steroid receptor coactivator 1 (SRC-1): multiple motifs with different binding specificities. *Mol Endocrinol*. (1998) 12:302–13. doi: 10.1210/mend.12.2.0065
29. Spencer TE, Jenster G, Burcin MM, Allis CD, Zhou J, Mizzen CA, et al. Steroid receptor coactivator-1 is a histone acetyltransferase. *Nature*. (1997) 389:194–8. doi: 10.1038/38304
30. Clarisse D, Thommis J, Van Wesemael K, Houtman R, Ratman D, Tavernier J, et al. Coregulator profiling of the glucocorticoid receptor in lymphoid malignancies. *Oncotarget*. (2017) 8:109675–91. doi: 10.18632/oncotarget.22764
31. Li X, Wong J, Tsai SY, Tsai MJ, O'Malley BW. Progesterone and glucocorticoid receptors recruit distinct coactivator complexes and promote distinct patterns of local chromatin modification. *Mol Cell Biol*. (2003) 23:3763–73. doi: 10.1128/MCB.23.11.3763-3773.2003
32. Rogatsky I, Wang JC, Derynck MK, Nonaka DF, Khodabakhsh DB, Haqq CM, et al. Target-specific utilization of transcriptional regulatory surfaces by the glucocorticoid receptor. *Proc Natl Acad Sci USA*. (2003) 100:13845–50. doi: 10.1073/pnas.2336092100
33. Rollins DA, Kharlyngdoh JB, Coppo M, Tharmalingam B, Mimouna S, Guo Z, et al. Glucocorticoid-induced phosphorylation by CDK9 modulates the coactivator functions of transcriptional cofactor GRIP1 in macrophages. *Nat Commun*. (2017) 8:1739. doi: 10.1038/s41467-017-01569-2
34. Anzick SL, Kononen J, Walker RL, Azorsa DO, Tanner MM, Guan XY, et al. AIB1, a steroid receptor coactivator amplified in breast and ovarian cancer. *Science*. (1997) 277:965–8. doi: 10.1126/science.277.5328.965
35. Grenier J, Trousson A, Chauchereau A, Amazit L, Lamirand A, Leclerc P, et al. Selective recruitment of p160 coactivators on glucocorticoid-regulated promoters in Schwann cells. *Mol Endocrinol*. (2004) 18:2866–79. doi: 10.1210/me.2004-0241
36. Horlein AJ, Naar AM, Heinzel T, Torchia J, Gloss B, Kurokawa R, et al. Ligand-independent repression by the thyroid hormone receptor mediated by a nuclear receptor co-repressor. *Nature*. (1995) 377:397–404. doi: 10.1038/377397a0
37. Chen JD, Evans RM. A transcriptional co-repressor that interacts with nuclear hormone receptors. *Nature*. (1995) 377:454–7. doi: 10.1038/377454a0
38. Perissi V, Staszewski LM, McInerney EM, Kurokawa R, Krones A, Rose DW, et al. Molecular determinants of nuclear receptor-corepressor interaction. *Genes Dev*. (1999) 13:3198–208. doi: 10.1101/gad.13.24.3198
39. Webb P, Anderson CM, Valentine C, Nguyen P, Marimuthu A, West BL, et al. The nuclear receptor corepressor (N-CoR) contains three isoleucine motifs (I/LXXII) that serve as receptor interaction domains (IDs). *Mol Endocrinol*. (2000) 14:1976–85. doi: 10.1210/mend.14.12.0566
40. Watson PJ, Fairall L, Santos GM, Schwabe JW. Structure of HDAC3 bound to co-repressor and inositol tetraphosphate. *Nature*. (2012) 481:335–40. doi: 10.1038/nature10728
41. Guenther MG, Barak O, Lazar MA. The SMRT and N-CoR corepressors are activating cofactors for histone deacetylase 3. *Mol Cell Biol*. (2001) 21:6091–101. doi: 10.1128/MCB.21.18.6091-6101.2001
42. Hua G, Ganti KP, Chambon P. Glucocorticoid-induced tethered transrepression requires SUMOylation of GR and formation of a SUMO-SMRT/NCoR1-HDAC3 repressing complex. *Proc Natl Acad Sci USA*. (2016) 113:E635–43. doi: 10.1073/pnas.1522826113
43. Hua G, Paulen L, Chambon P. GRSUMOylation and formation of an SUMO-SMRT/NCoR1-HDAC3 repressing complex is mandatory for GC-induced IR nGRE-mediated transrepression. *Proc Natl Acad Sci USA*. (2016) 113:E626–34. doi: 10.1073/pnas.1522821113
44. Ramamoorthy S, Cidlowski JA. Ligand-induced repression of the glucocorticoid receptor gene is mediated by an NCoR1 repression complex formed by long-range chromatin interactions with intragenic glucocorticoid response elements. *Mol Cell Biol*. (2013) 33:1711–22. doi: 10.1128/MCB.01151-12
45. Bush KA, Krukowski K, Eddy JL, Janusek LW, Mathews HL. Glucocorticoid receptor mediated suppression of natural killer cell activity: identification of associated deacetylase and corepressor molecules. *Cell Immunol*. (2012) 275:80–9. doi: 10.1016/j.cellimm.2012.02.014
46. Ronacher K, Hadley K, Avenant C, Stubsrud E, Simons SS Jr, Louw A, et al. Ligand-selective transactivation and transrepression via the glucocorticoid receptor: role of cofactor interaction. *Mol Cell Endocrinol*. (2009) 299:219–31. doi: 10.1016/j.mce.2008.10.008
47. Turner BM. Histone acetylation and control of gene expression. *J Cell Sci*. (1991) 99 (Pt 1):13–20.
48. Yao TP, Ku G, Zhou N, Scully R, Livingston DM. The nuclear hormone receptor coactivator SRC-1 is a specific target of p300. *Proc Natl Acad Sci USA*. (1996) 93:10626–31. doi: 10.1073/pnas.93.20.10626
49. Kamei Y, Xu L, Heinzel T, Torchia J, Kurokawa R, Gloss B, et al. ACBP integrator complex mediates transcriptional activation and AP-1 inhibition by nuclear receptors. *Cell*. (1996) 85:403–14. doi: 10.1016/S0092-8674(00)81118-6
50. Guo B, Huang X, Cooper S, Broxmeyer HE. Glucocorticoid hormone-induced chromatin remodeling enhances human hematopoietic stem cell homing and engraftment. *Nat Med*. (2017) 23:424–8. doi: 10.1038/nm.4298
51. Sengupta S, Wasylyk B. Ligand-dependent interaction of the glucocorticoid receptor with p53 enhances their degradation by Hdm2. *Genes Dev*. (2001) 15:2367–80. doi: 10.1101/gad.202201
52. Murphy SH, Suzuki K, Downes M, Welch GL, De Jesus P, Miraglia LJ, et al. Tumor suppressor protein (p)53, is a regulator of NF-kappaB repression by the glucocorticoid receptor. *Proc Natl Acad Sci USA*. (2011) 108:17117–22. doi: 10.1073/pnas.1114420108
53. Fryer CJ, Archer TK. Chromatin remodelling by the glucocorticoid receptor requires the BRG1 complex. *Nature*. (1998) 393:88–91. doi: 10.1038/30032
54. Hsiao PW, Fryer CJ, Trotter KW, Wang W, Archer TK. BAF60a mediates critical interactions between nuclear receptors and the BRG1 chromatin-remodeling complex for transactivation. *Mol Cell Biol*. (2003) 23:6210–20. doi: 10.1128/MCB.23.17.6210-6220.2003
55. Nie Z, Xue Y, Yang D, Zhou S, Deroo BJ, Archer TK, et al. A specificity and targeting subunit of a human SWI/SNF family-related chromatin-remodeling complex. *Mol Cell Biol*. (2000) 20:8879–88. doi: 10.1128/MCB.20.23.8879-8888.2000
56. Hebbar PB, Archer TK. Chromatin remodeling by nuclear receptors. *Chromosoma*. (2003) 111:495–504. doi: 10.1007/s00412-003-0232-x
57. Bodwell JE, Orti E, Coull JM, Pappin DJ, Smith LI, Swift F. Identification of phosphorylated sites in the mouse glucocorticoid receptor. *J Biol Chem*. (1991) 266:7549–55.
58. Webster JC, Jewell CM, Bodwell JE, Munck A, Sar M, Cidlowski JA. Mouse glucocorticoid receptor phosphorylation status influences multiple

functions of the receptor protein. *J Biol Chem*. (1997) 272:9287–93. doi: 10.1074/jbc.272.14.9287
59. Chen W, Dang T, Blind RD, Wang Z, Cavasotto CN, Hittelman AB, et al. Glucocorticoid receptor phosphorylation differentially affects target gene expression. *Mol Endocrinol*. (2008) 22:1754–66. doi: 10.1210/me.2007-0219
60. Copik AJ, Webb MS, Miller AL, Wang Y, Kumar R, Thompson EB. Activation function 1 of glucocorticoid receptor binds TATA-binding protein *in vitro* and *in vivo*. *Mol Endocrinol*. (2006) 20:1218–30. doi: 10.1210/me.2005-0257
61. Galliher-Beckley AJ, Williams JG, Collins JB, Cidlowski JA. Glycogen synthase kinase 3beta-mediated serine phosphorylation of the human glucocorticoid receptor redirects gene expression profiles. *Mol Cell Biol*. (2008) 28:7309–22. doi: 10.1128/MCB.00808-08
62. Bledsoe RK, Montana VG, Stanley TB, Delves CJ, Apolito CJ, McKee DD, et al. Crystal structure of the glucocorticoid receptor ligand binding domain reveals a novel mode of receptor dimerization and coactivator recognition. *Cell*. (2002) 110:93–105. doi: 10.1016/S0092-8674(02)00817-6
63. Kucera T, Waltner-Law M, Scott DK, Prasad R, Granner DK. A point mutation of the AF2 transactivation domain of the glucocorticoid receptor disrupts its interaction with steroid receptor coactivator 1. *J Biol Chem*. (2002) 277:26098–102. doi: 10.1074/jbc.M204013200
64. Wu J, Li Y, Dietz J, Lala DS. Repression of p65 transcriptional activation by the glucocorticoid receptor in the absence of receptor-coactivator interactions. *Mol Endocrinol*. (2004) 18:53–62. doi: 10.1210/me.2002-0373
65. Schena M, Freedman LP, Yamamoto KR. Mutations in the glucocorticoid receptor zinc finger region that distinguish interdigitated DNA binding and transcriptional enhancement activities. *Genes Dev*. (1989) 3:1590–601. doi: 10.1101/gad.3.10.1590
66. Heck S, Kullmann M, Gast A, Ponta H, Rahmsdorf HJ, Herrlich P, et al. A distinct modulating domain in glucocorticoid receptor monomers in the repression of activity of the transcription factor AP-1. *EMBO J*. (1994) 13:4087–95. doi: 10.1002/j.1460-2075.1994.tb06726.x
67. Schiller BJ, Chodankar R, Watson LC, Stallcup MR, Yamamoto KR. Glucocorticoid receptor binds half sites as a monomer and regulates specific target genes. *Genome Biol*. (2014) 15:418. doi: 10.1186/s13059-014-0418-y
68. Presman DM, Ogara MF, Stortz M, Alvarez LD, Pooley JR, Schiltz RL, et al. Live cell imaging unveils multiple domain requirements for *in vivo* dimerization of the glucocorticoid receptor. *PLoS Biol*. (2014) 12:e1001813. doi: 10.1371/journal.pbio.1001813
69. Heck S, Bender K, Kullmann M, Gottlicher M, Herrlich P, Cato AC. I kappaB alpha-independent downregulation of NF-kappaB activity by glucocorticoid receptor. *EMBO J*. (1997) 16:4698–707. doi: 10.1093/emboj/16.15.4698
70. Watson LC, Kuchenbecker KM, Schiller BJ, Gross JD, Pufall MA, Yamamoto KR. The glucocorticoid receptor dimer interface allosterically transmits sequence-specific DNA signals. *Nat Struct Mol Biol*. (2013) 20:876–3. doi: 10.1038/nsmb.2595
71. Bladh LG, Liden J, Dahlman-Wright K, Reimers M, Nilsson S, Okret S. Identification of endogenous glucocorticoid repressed genes differentially regulated by a glucocorticoid receptor mutant able to separate between nuclear factor-kappaB and activator protein-1 repression. *Mol Pharmacol*. (2005) 67:815–26. doi: 10.1124/mol.104.005801
72. Beck IM, De Bosscher K, Haegeman G. Glucocorticoid receptor mutants: man-made tools for functional research. *Trends Endocrinol Metab*. (2011) 22:295–310. doi: 10.1016/j.tem.2011.03.009
73. John S, Sabo PJ, Thurman RE, Sung MH, Biddie SC, Johnson TA, et al. Chromatin accessibility pre-determines glucocorticoid receptor binding patterns. *Nat Genet*. (2011) 43:264–8. doi: 10.1038/ng.759
74. Biddie SC, John S, Sabo PJ, Thurman RE, Johnson TA, Schiltz RL, et al. Transcription factor AP1 potentiates chromatin accessibility and glucocorticoid receptor binding. *Mol Cell*. (2011) 43:145–55. doi: 10.1016/j.molcel.2011.06.016
75. Rao NA, McCalman MT, Moulos P, Francoijs KJ, Chatziioannou A, Kolisis FN, et al. Coactivation of GR and NFKB alters the repertoire of their binding sites and target genes. *Genome Res*. (2011) 21:1404–6. doi: 10.1101/gr.118042.110
76. Swinstead EE, Miranda TB, Paakinaho V, Baek S, Goldstein I, Hawkins M, et al. Steroid receptors reprogram FoxA1 occupancy through dynamic chromatin transitions. *Cell*. (2016) 165:593–605. doi: 10.1016/j.cell.2016.02.067
77. Uhlenhaut NH, Barish GD, Yu RT, Downes M, Karunasiri M, Liddle C, et al. Insights into negative regulation by the glucocorticoid receptor from genome-wide profiling of inflammatory cistromes. *Mol Cell*. (2013) 49:158–71. doi: 10.1016/j.molcel.2012.10.013
78. Oh KS, Patel H, Gottschalk RA, Lee WS, Baek S, Fraser ID C, et al. Anti-inflammatory chromatinscape suggests alternative mechanisms of glucocorticoid receptor action. *Immunity*. (2017) 47:298–309 e5. doi: 10.1016/j.immuni.2017.07.012
79. John S, Sabo PJ, Johnson TA, Sung MH, Biddie SC, Lightman SL, et al. Interaction of the glucocorticoid receptor with the chromatin landscape. *Mol Cell*. (2008) 29:611–24. doi: 10.1016/j.molcel.2008.02.010
80. So AY, Chaivorapol C, Bolton EC, Li H, Yamamoto KR. Determinants of cell- and gene-specific transcriptional regulation by the glucocorticoid receptor. *PLoS Genet*. (2007) 3:e94. doi: 10.1371/journal.pgen.0030094
81. Reddy TE, Pauli F, Sprouse RO, Neff NF, Newberry KM, Garabedian MJ, et al. Genomic determination of the glucocorticoid response reveals unexpected mechanisms of gene regulation. *Genome Res*. (2009) 19:2163–71. doi: 10.1101/gr.097022.109
82. Siersbaek R, Nielsen R, John S, Sung MH, Baek S, Loft A, et al. Extensive chromatin remodelling and establishment of transcription factor 'hotspots' during early adipogenesis. *EMBO J*. (2011) 30:1459–72. doi: 10.1038/emboj.2011.65
83. Heinz S, Benner C, Spann N, Bertolino E, Lin YC, Laslo P, et al. Simple combinations of lineage-determining transcription factors prime cis-regulatory elements required for macrophage and B cell identities. *Mol Cell*. (2010) 38:576–89. doi: 10.1016/j.molcel.2010.05.004
84. Jin F, Li Y, Ren B, Natarajan R. PU.1 and C/EBP(alpha) synergistically program distinct response to NF-kappaB activation through establishing monocyte specific enhancers. *Proc Natl Acad Sci USA*. (2011) 108:5290–5. doi: 10.1073/pnas.1017214108
85. Scott EW, Simon MC, Anastasi J, Singh H. Requirement of transcription factor PU.1 in the development of multiple hematopoietic lineages. *Science*. (1994) 265:1573–7. doi: 10.1126/science.8079170
86. Scott EW, Fisher RC, Olson MC, Kehrli EW, Simon MC, Singh H. PU.1 functions in a cell-autonomous manner to control the differentiation of multipotential lymphoid-myeloid progenitors. *Immunity*. (1997) 6:437–7. doi: 10.1016/S1074-7613(00)80287-3
87. Buttgereit F, Scheffold A. Rapid glucocorticoid effects on immune cells. *Steroids*. (2002) 67:529–34. doi: 10.1016/S0039-128X(01)00171-4
88. Panettieri RA, Schaafsma D, Amrani Y, Koziol-White C, Ostrom R, Tliba O. Non-genomic effects of glucocorticoids: an updated view. *Trends Pharmacol Sci*. (2019) 40:38–49. doi: 10.1016/j.tips.2018.11.002
89. Proven A, Gabriel SE, Orces C, O'Fallon WM, Hunder GG. Glucocorticoid therapy in giant cell arteritis: duration and adverse outcomes. *Arthritis Rheum*. (2003) 49:703–8. doi: 10.1002/art.11388
90. Bartholome B, Spies CM, Gaber T, Schuchmann S, Berki T, Kunkel D, et al. Membrane glucocorticoid receptors (mGCR) are expressed in normal human peripheral blood mononuclear cells and up-regulated after *in vitro* stimulation and in patients with rheumatoid arthritis. *FASEB J*. (2004) 18:70–80. doi: 10.1096/fj.03-0328com
91. Spies CM, Schaumann DH, Berki T, Mayer K, Jakstadt M, Huscher D, et al. Membrane glucocorticoid receptors are down regulated by glucocorticoids in patients with systemic lupus erythematosus and use a caveolin-1-independent expression pathway. *Ann Rheum Dis*. (2006) 65:1139–46. doi: 10.1136/ard.2005.048272
92. Long F, Wang YX, Liu L, Zhou J, Cui RY, Jiang CL. Rapid nongenomic inhibitory effects of glucocorticoids on phagocytosis and superoxide anion production by macrophages. *Steroids*. (2005) 70:55–61. doi: 10.1016/j.steroids.2004.10.004
93. Matthews L, Berry A, Ohanian V, Ohanian J, Garside H, Ray D. Caveolin mediates rapid glucocorticoid effects and couples glucocorticoid action to the antiproliferative program. *Mol Endocrinol*. (2008) 22:1320–30. doi: 10.1210/me.2007-0154

94. Lowenberg M, Verhaar AP, Bilderbeek J, Marle J, Buttgereit F, Peppelenbosch MP, et al. Glucocorticoids cause rapid dissociation of a T-cell-receptor-associated protein complex containing LCK and FYN. *EMBO Rep*. (2006) 7:1023–9. doi: 10.1038/sj.embor.7400775
95. Vermeulen L, De Wilde G, Van Damme P, Vanden Berghe W, Haegeman G. Transcriptional activation of the NF-kappaB p65 subunit by mitogen- and stress-activated protein kinase-1 (MSK1). *EMBO J*. (2003) 22:1313–24. doi: 10.1093/emboj/cdg139
96. Beck IM, Vanden Berghe W, Vermeulen L, Bougarne N, Vander Cruyssen B, Haegeman G, et al. Altered subcellular distribution of MSK1 induced by glucocorticoids contributes to NF-kappaB inhibition. *EMBO J*. (2008) 27:1682–93. doi: 10.1038/emboj.2008.95
97. Kuzmich NN, Sivak KV, Chubarev VN, Porozov YB, Savateeva-Lyubimova TN, Peri F. TLR4 Signaling pathway modulators as potential therapeutics in inflammation and sepsis. *Vaccines (Basel)*. (2017) 5:E34. doi: 10.3390/vaccines5040034
98. Nijland R, Hofland T, van Strijp JA. Recognition of LPS by TLR4: potential for anti-inflammatory therapies. *Mar Drugs*. (2014) 12:4260–73. doi: 10.3390/md12074260
99. Oeckinghaus A, Ghosh S. The NF-kappaB family of transcription factors and its regulation. *Cold Spring Harb Perspect Biol*. (2009) 1:a000034. doi: 10.1101/cshperspect.a000034
100. Zenz R, Eferl R, Scheinecker C, Redlich K, Smolen J, Schonthaler HB, et al. Activator protein 1 (Fos/Jun) functions in inflammatory bone and skin disease. *Arthritis Res Ther*. (2008) 10:201. doi: 10.1186/ar2338
101. Caelles C, Gonzalez-Sancho JM, Munoz A. Nuclear hormone receptor antagonism with AP-1 by inhibition of the JNK pathway. *Genes Dev*. (1997) 11:3351–64. doi: 10.1101/gad.11.24.3351
102. Limbourg FP, Huang Z, Plumier JC, Simoncini T, Fujioka M, Tuckermann J, et al. Rapid nontranscriptional activation of endothelial nitric oxide synthase mediates increased cerebral blood flow and stroke protection by corticosteroids. *J Clin Invest*. (2002) 110:1729–38. doi: 10.1172/JCI0215481
103. Scheschowitsch K, Leite JA, Assreuy J. New insights in glucocorticoid receptor signaling-more than just a ligand-binding receptor. *Front Endocrinol (Lausanne)*. (2017) 8:16. doi: 10.3389/fendo.2017.00016
104. Desmet SJ, De Bosscher K. Glucocorticoid receptors: finding the middle ground. *J Clin Invest*. (2017) 127:1136–45. doi: 10.1172/JCI88886
105. Yang-Yen HF, Chambard JC, Sun YL, Smeal T, Schmidt TJ, Drouin J, et al. Transcriptional interference between c-Jun and the glucocorticoid receptor: mutual inhibition of DNA binding due to direct protein-protein interaction. *Cell*. (1990) 62:1205–15. doi: 10.1016/0092-8674(90)90396-V
106. Ray A, Prefontaine KE. Physical association and functional antagonism between the p65 subunit of transcription factor NF-kappa B and the glucocorticoid receptor. *Proc Natl Acad Sci USA*. (1994) 91:752–6. doi: 10.1073/pnas.91.2.752
107. Langlais D, Couture C, Balsalobre A, Drouin J. The Stat3/GR interaction code: predictive value of direct/indirect DNA recruitment for transcription outcome. *Mol Cell*. (2012) 47:38–49. doi: 10.1016/j.molcel.2012.04.021
108. Drouin J, Trifiro MA, Plante RK, Nemer M, Eriksson P, Wrange O. Glucocorticoid receptor binding to a specific DNA sequence is required for hormone-dependent repression of pro-opiomelanocortin gene transcription. *Mol Cell Biol*. (1989) 9:5305–14. doi: 10.1128/MCB.9.12.5305
109. Malkoski SP, Dorin RI. Composite glucocorticoid regulation at a functionally defined negative glucocorticoid response element of the human corticotropin-releasing hormone gene. *Mol Endocrinol*. (1999) 13:1629–44. doi: 10.1210/mend.13.10.0351
110. Subramaniam N, Cairns W, Okret S. Studies on the mechanism of glucocorticoid-mediated repression from a negative glucocorticoid response element from the bovine prolactin gene. *DNA Cell Biol*. (1997) 16:153–63. doi: 10.1089/dna.1997.16.153
111. Sakai DD, Helms S, Carlstedt-Duke J, Gustafsson JA, Rottman FM, Yamamoto KR. Hormone-mediated repression: a negative glucocorticoid response element from the bovine prolactin gene. *Genes Dev*. (1988) 2:1144–54. doi: 10.1101/gad.2.9.1144
112. Aslam F, Shalhoub V, van Wijnen AJ, Banerjee C, Bortell R, Shakoori AR, et al. Contributions of distal and proximal promoter elements to glucocorticoid regulation of osteocalcin gene transcription. *Mol Endocrinol*. (1995) 9:679–90. doi: 10.1210/mend.9.6.8592514
113. Radoja N, Komine M, Jho SH, Blumenberg M, Tomic-Canic M. Novel mechanism of steroid action in skin through glucocorticoid receptor monomers. *Mol Cell Biol*. (2000) 20:4328–39. doi: 10.1128/MCB.20.12.4328-4339.2000
114. Zhang G, Zhang L, Duff GW. A negative regulatory region containing a glucocorticosteroid response element (nGRE) in the human interleukin-1beta gene. *DNA Cell Biol*. (1997) 16:145–52. doi: 10.1089/dna.1997.16.145
115. Surjit M, Ganti KP, Mukherji A, Ye T, Hua G, Metzger D, et al. Widespread negative response elements mediate direct repression by agonist-liganded glucocorticoid receptor. *Cell*. (2011) 145:224–41. doi: 10.1016/j.cell.2011.03.027
116. Mordacq JC, Linzer DI. Co-localization of elements required for phorbol ester stimulation and glucocorticoid repression of proliferin gene expression. *Genes Dev*. (1989) 3:760–9. doi: 10.1101/gad.3.6.760
117. Miner JN, Yamamoto KR. The basic region of AP-1 specifies glucocorticoid receptor activity at a composite response element. *Genes Dev*. (1992) 6:2491–501. doi: 10.1101/gad.6.12b.2491
118. Hudson WH, Vera IMS, Nwachukwu JC, Weikum ER, Herbst AG, Yang Q, et al. Cryptic glucocorticoid receptor-binding sites pervade genomic NF-kappaB response elements. *Nat Commun*. (2018) 9:1337. doi: 10.1038/s41467-018-03780-1
119. Schone S, Bothe M, Einfeldt E, Borschiwer M, Benner P, Vingron M, et al. Synthetic STARR-seq reveals how DNA shape and sequence modulate transcriptional output and noise. *PLoS Genet*. (2018) 14:e1007793. doi: 10.1371/journal.pgen.1007793
120. Thormann V, Glaser LV, Rothkegel MC, Borschiwer M, Bothe M, Fuchs A, et al. Expanding the repertoire of glucocorticoid receptor target genes by engineering genomic response elements. *Life Sci Alliance*. (2019) 2:e201800283. doi: 10.26508/lsa.201800283
121. Hoffman JA, Trotter KW, Ward JM, Archer TK. BRG1 governs glucocorticoid receptor interactions with chromatin and pioneer factors across the genome. *Elife*. (2018) 7:e35073. doi: 10.7554/eLife.35073
122. Hemmer MC, Wierer M, Schachtrup K, Downes M, Hubner N, Evans RM, et al. E47 modulates hepatic glucocorticoid action. *Nat Commun*. (2019) 10:306. doi: 10.1038/s41467-018-08196-5
123. Schacke H, Berger M, Rehwinkel H, Asadullah K. Selective glucocorticoid receptor agonists (SEGRAs): novel ligands with an improved therapeutic index. *Mol Cell Endocrinol*. (2007) 275:109–7. doi: 10.1016/j.mce.2007.05.014
124. De Bosscher K, Beck IM, Haegeman G. Classic glucocorticoids versus non-steroidal glucocorticoid receptor modulators: survival of the fittest regulator of the immune system? *Brain Behav Immun*. (2010) 24:1035–42. doi: 10.1016/j.bbi.2010.06.010
125. Hubner S, Dejager L, Libert C, Tuckermann JP. The glucocorticoid receptor in inflammatory processes: transrepression is not enough. *Biol Chem*. (2015) 396:1223–31. doi: 10.1515/hsz-2015-0106
126. Vandevyver S, Dejager L, Tuckermann J, Libert C. New insights into the anti-inflammatory mechanisms of glucocorticoids: an emerging role for glucocorticoid-receptor-mediated transactivation. *Endocrinology*. (2013) 154:993–1007. doi: 10.1210/en.2012-2045
127. Clark AR, Belvisi MG. Maps and legends: the quest for dissociated ligands of the glucocorticoid receptor. *Pharmacol Ther*. (2012) 134:54–67. doi: 10.1016/j.pharmthera.2011.12.004
128. Schone S, Jurk M, Helabad MB, Dror I, Lebars I, Kieffer B, et al. Sequences flanking the core-binding site modulate glucocorticoid receptor structure and activity. *Nat Commun*. (2016) 7:12621. doi: 10.1038/ncomms12621
129. Souffriau J, Eggermont M, Van Ryckeghem S, Van Looveren K, Van Wyngene L, Van Hamme E, et al. A screening assay for selective dimerizing glucocorticoid receptor agonists and modulators (SEDIGRAM) that are effective against acute inflammation. *Sci Rep*. (2018) 8:12894. doi: 10.1038/s41598-018-31150-w
130. De Bosscher K, Beck IM, Ratman D, Berghe WV, Libert C. Activation of the Glucocorticoid Receptor in Acute Inflammation: the SEDIGRAMConcept. *Trends Pharmacol Sci*. (2016) 37:4–16. doi: 10.1016/j.tips.2015.09.002
131. Reichardt HM, Kaestner KH, Tuckermann J, Kretz O, Wessely O, Bock R, et al. DNA binding of the glucocorticoid receptor is not essential for survival. *Cell*. (1998) 93:531–41. doi: 10.1016/S0092-8674(00)81183-6

132. Reichardt HM, Tuckermann JP, Gottlicher M, Vujic M, Weih F, Angel P, et al. Repression of inflammatory responses in the absence of DNA binding by the glucocorticoid receptor. *EMBO J*. (2001) 20:7168–3. doi: 10.1093/emboj/20.24.7168
133. Vandevyver S, Dejager L, Van Bogaert T, Kleyman A, Liu Y, Tuckermann J, et al. Glucocorticoid receptor dimerization induces MKP1 to protect against TNF-induced inflammation. *J Clin Invest*. (2012) 122:2130–40. doi: 10.1172/JCI60006
134. Silverman MN, Mukhopadhyay P, Belyavskaya E, Tonelli LH, Revenis BD, Doran JH, et al. Glucocorticoid receptor dimerization is required for proper recovery of LPS-induced inflammation, sickness behavior and metabolism in mice. *Mol Psychiatry*. (2013) 18:1006–7. doi: 10.1038/mp.2012.131
135. Kleiman A, Hubner S, Rodriguez Parkitna JM, Neumann A, Hofer S, Weigand MA, et al. Glucocorticoid receptor dimerization is required for survival in septic shock via suppression of interleukin-1 in macrophages. *FASEB J*. (2012) 26:722–9. doi: 10.1096/fj.11-192112
136. Tuckermann JP, Kleiman A, Moriggl R, Spanbroek R, Neumann A, Illing A, et al. Macrophages and neutrophils are the targets for immune suppression by glucocorticoids in contact allergy. *J Clin Invest*. (2007) 117:1381–90. doi: 10.1172/JCI28034
137. Baschant U, Frappart L, Rauchhaus U, Bruns L, Reichardt HM, Kamradt T, et al. Glucocorticoid therapy of antigen-induced arthritis depends on the dimerized glucocorticoid receptor in T cells. *Proc Natl Acad Sci USA*. (2011) 108:19317–22. doi: 10.1073/pnas.1105857108
138. Vettorazzi S, Bode C, Dejager L, Frappart L, Shelest E, Klassen C, et al. Glucocorticoids limit acute lung inflammation in concert with inflammatory stimuli by induction of SphK1. *Nat Commun*. (2015) 6:7796. doi: 10.1038/ncomms8796
139. Klassen C, Karabinskaya A, Dejager L, Vettorazzi S, Van Moorleghem J, Luhder F, et al. Airway epithelial cells are crucial targets of glucocorticoids in a mouse model of allergic asthma. *J Immunol*. (2017) 199:48–61. doi: 10.4049/jimmunol.1601691
140. Koenen M, Culemann S, Vettorazzi S, Caratti G, Frappart L, Baum W, et al. Glucocorticoid receptor in stromal cells is essential for glucocorticoid-mediated suppression of inflammation in arthritis. *Ann Rheum Dis*. (2018) 77:1610–8. doi: 10.1136/annrheumdis-2017-212762
141. Ballegeer M, Van Looveren K, Timmermans S, Eggermont M, Vandevyver S, Thery F, et al. Glucocorticoid receptor dimers control intestinal STAT1 and TNF-induced inflammation in mice. *J Clin Invest*. (2018) 128:3265–79. doi: 10.1172/JCI96636
142. Oakley RH, Ramamoorthy S, Foley JF, Busada JT, Lu NZ, Cidlowski JA. Glucocorticoid receptor isoform-specific regulation of development, circadian rhythm, and inflammation in mice. *FASEB J*. (2018) 32:5258–71. doi: 10.1096/fj.201701153R
143. Matyszak MK, Citterio S, Rescigno M, Ricciardi-Castagnoli P. Differential effects of corticosteroids during different stages of dendritic cell maturation. *Eur J Immunol*. (2000) 30:1233–42. doi: 10.1002/(SICI)1521-4141(200004)30:4<1233::AID-IMMU1233>3.0.CO;2-F
144. Tuckermann JP, Kleiman A, McPherson KG, Reichardt HM. Molecular mechanisms of glucocorticoids in the control of inflammation and lymphocyte apoptosis. *Crit Rev Clin Lab Sci*. (2005) 42:71–104. doi: 10.1080/10408360590888983
145. Alnemri ES, Fernandes TF, Haldar S, Croce CM, Litwack G. Involvement of BCL-2 in glucocorticoid-induced apoptosis of human pre-B-leukemias. *Cancer Res*. (1992) 52:491–5.
146. Goossens S, Van Vlierberghe P. Overcoming steroid resistance in T cell acute lymphoblastic leukemia. *PLoS Med*. (2016) 13:e1002208. doi: 10.1371/journal.pmed.1002208
147. Wang Z, Malone MH, He H, McColl KS, Distelhorst CW. Microarray analysis uncovers the induction of the proapoptotic BH3-only protein Bim in multiple models of glucocorticoid-induced apoptosis. *J Biol Chem*. (2003) 278:23861–7. doi: 10.1186/1475-4924-3-4
148. Gruver-Yates AL, Cidlowski JA. Tissue-specific actions of glucocorticoids on apoptosis: a double-edged sword. *Cells*. (2013) 2:202–23. doi: 10.3390/cells2020202
149. Cao Y, Bender IK, Konstantinidis AK, Shin SC, Jewell CM, Cidlowski JA, et al. Glucocorticoid receptor translational isoforms underlie maturational stage-specific glucocorticoid sensitivities of dendritic cells in mice and humans. *Blood*. (2013) 121:1553–62. doi: 10.1182/blood-2012-05-432336
150. Hirayama D, Iida T, Nakase H. The phagocytic function of macrophage-enforcing innate immunity and tissue homeostasis. *Int J Mol Sci*. (2017) 19:E92. doi: 10.3390/ijms19010092
151. Mosser DM, Edwards JP. Exploring the full spectrum of macrophage activation. *Nat Rev Immunol*. (2008) 8:958–69. doi: 10.1038/nri2448
152. Gordon S, Martinez FO. Alternative activation of macrophages: mechanism and functions. *Immunity*. (2010) 32:593–604. doi: 10.1016/j.immuni.2010.05.007
153. Gordon S. Alternative activation of macrophages. *Nat Rev Immunol*. (2003) 3:23–35. doi: 10.1038/nri978
154. Medzhitov R, Horng T. Transcriptional control of the inflammatory response. *Nat Rev Immunol*. (2009) 9:692–703. doi: 10.1038/nri2634
155. Hayden MS, Ghosh S. Signaling to NF-kappaB. *Genes Dev*. (2004) 18:2195–224. doi: 10.1101/gad.1228704
156. Martinez FO, Gordon S. The M1 and M2 paradigm of macrophage activation: time for reassessment. *F1000Prime Rep*. (2014) 6:13. doi: 10.12703/P6-13
157. McColl A, Bournazos S, Franz S, Perretti M, Morgan BP, Haslett C, et al. Glucocorticoids induce protein S-dependent phagocytosis of apoptotic neutrophils by human macrophages. *J Immunol*. (2009) 183:2167–75. doi: 10.4049/jimmunol.0803503
158. Lauber K, Keppeler H, Munoz LE, Koppe U, Schroder K, Yamaguchi H, et al. Milk fat globule-EGF factor 8 mediates the enhancement of apoptotic cell clearance by glucocorticoids. *Cell Death Differ*. (2013) 20:1230–40. doi: 10.1038/cdd.2013.82
159. Luecke HF, Yamamoto KR. The glucocorticoid receptor blocks P-TEFb recruitment by NFkappaB to effect promoter-specific transcriptional repression. *Genes Dev*. (2005) 19:1116–27. doi: 10.1101/gad.1297105
160. Flammer JR, Dobrovolna J, Kennedy MA, Chinenov Y, Glass CK, Ivashkiv LB, et al. The type I interferon signaling pathway is a target for glucocorticoid inhibition. *Mol Cell Biol*. (2010) 30:4564–74. doi: 10.1128/MCB.00146-10
161. Chinenov Y, Gupte R, Dobrovolna J, Flammer JR, Liu B, Michelassi FE, et al. Role of transcriptional coregulator GRIP1 in the anti-inflammatory actions of glucocorticoids. *Proc Natl Acad Sci USA*. (2012) 109:11776–81. doi: 10.1073/pnas.1206059109
162. Gupte R, Muse GW, Chinenov Y, Adelman K, Rogatsky I. Glucocorticoid receptor represses proinflammatory genes at distinct steps of the transcription cycle. *Proc Natl Acad Sci USA*. (2013) 110:14616–21. doi: 10.1073/pnas.1309898110
163. Bhattacharyya S, Brown DE, Brewer JA, Vogt SK, Muglia LJ. Macrophage glucocorticoid receptors regulate Toll-like receptor 4-mediated inflammatory responses by selective inhibition of p38 MAP kinase. *Blood*. (2007) 109:4313–9. doi: 10.1182/blood-2006-10-048215
164. Kassel O, Sancono A, Kratzschmar J, Kreft B, Stassen M, Cato AC. Glucocorticoids inhibit MAP kinase via increased expression and decreased degradation of MKP-1. *EMBOJ*. (2001) 20:7108–16. doi: 10.1093/emboj/20.24.7108
165. Lasa M, Abraham SM, Boucheron C, Saklatvala J, Clark AR. Dexamethasone causes sustained expression of mitogen-activated protein kinase (MAPK) phosphatase 1 and phosphatase-mediated inhibition of MAPK p38. *Mol Cell Biol*. (2002) 22:7802–11. doi: 10.1128/MCB.22.22.7802-7811.2002
166. Abraham SM, Lawrence T, Kleiman A, Warden P, Medghalchi M, Tuckermann J, et al. Antiinflammatory effects of dexamethasone are partly dependent on induction of dual specificity phosphatase 1. *J Exp Med*. (2006) 203:1883–9. doi: 10.1084/jem.20060336
167. Vattakuzhi Y, Abraham SM, Freidin A, Clark AR, Horwood NJ. Dual-specificity phosphatase 1-null mice exhibit spontaneous osteolytic disease and enhanced inflammatory osteolysis in experimental arthritis. *Arthritis Rheum*. (2012) 64:2201–10. doi: 10.1002/art.34403
168. Salojin KV, Owusu IB, Millerchip KA, Potter M, Platt KA, Oravecz T. Essential role of MAPK phosphatase-1 in the negative control of innate immune responses. *J Immunol*. (2006) 176:1899–907. doi: 10.4049/jimmunol.176.3.1899
169. Hammer M, Echtenachter B, Weighardt H, Jozefowski K, Rose-John S, Mannel DN, et al. Increased inflammation and lethality of Dusp1-/-

mice in polymicrobial peritonitis models. *Immunology*. (2010) 131:395–404. doi: 10.1111/j.1365-2567.2010.03313.x
170. Ayroldi E, Riccardi C. Glucocorticoid-induced leucine zipper (GILZ): a new important mediator of glucocorticoid action. *FASEB J*. (2009) 23:3649–58. doi: 10.1096/fj.09-134684
171. Riccardi C, Bruscoli S, Ayroldi E, Agostini M, Migliorati G. GILZ, a glucocorticoid hormone induced gene, modulates T lymphocytes activation and death through interaction with NF-κB. *Adv Exp Med Biol*. (2001) 495:31–9. doi: 10.1007/978-1-4615-0685-0_5
172. Pinheiro I, Dejager L, Petta I, Vandevyver S, Puimege L, Mahieu T, et al. LPS resistance of SPRET/Ei mice is mediated by Gilz, encoded by the Tsc22d3 gene on the X chromosome. *EMBO Mol Med*. (2013) 5:456–70. doi: 10.1002/emmm.201201683
173. Cannarile L, Cuzzocrea S, Santucci L, Agostini M, Mazzon E, Esposito E, et al. Glucocorticoid-induced leucine zipper is protective in Th1-mediated models of colitis. *Gastroenterology*. (2009) 136:530–41. doi: 10.1053/j.gastro.2008.09.024
174. Hahn RT, Hoppstadter J, Hirschfelder K, Hachenthal N, Diesel B, Kessler SM, et al. Downregulation of the glucocorticoid-induced leucine zipper (GILZ) promotes vascular inflammation. *Atherosclerosis*. (2014) 234:391–400. doi: 10.1016/j.atherosclerosis.2014.03.028
175. Beaulieu E, Ngo D, Santos L, Yang YH, Smith M, Jorgensen C, et al. Glucocorticoid-induced leucine zipper is an endogenous antiinflammatory mediator in arthritis. *Arthritis Rheum*. (2010) 62:2651–61. doi: 10.1002/art.27566
176. Ngo D, Beaulieu E, Gu R, Leaney A, Santos L, Fan H, et al. Divergent effects of endogenous and exogenous glucocorticoid-induced leucine zipper in animal models of inflammation and arthritis. *Arthritis Rheum*. (2013) 65:1203–12. doi: 10.1002/art.37858
177. Robert O, Boujedidi H, Bigorgne A, Ferrere G, Voican CS, Vettorazzi S, et al. Decreased expression of the glucocorticoid receptor-GILZ pathway in Kupffer cells promotes liver inflammation in obese mice. *J Hepatol*. (2016) 64:916–24. doi: 10.1016/j.jhep.2015.11.023
178. Auphan N, DiDonato JA, Rosette C, Helmberg A, Karin M. Immunosuppression by glucocorticoids: inhibition of NF-kappa B activity through induction of I kappa B synthesis. *Science*. (1995) 270:286–90. doi: 10.1126/science.270.5234.286
179. Scheinman RI, Cogswell PC, Lofquist AK, Baldwin AS Jr. Role of transcriptional activation of I kappa B alpha in mediation of immunosuppression by glucocorticoids. *Science*. (1995) 270:283–6. doi: 10.1126/science.270.5234.283
180. Chinenov Y, Coppo M, Gupte R, Sacta MA, Rogatsky I. Glucocorticoid receptor coordinates transcription factor-dominated regulatory network in macrophages. *BMC Genomics*. (2014) 15:656. doi: 10.1186/1471-2164-15-656
181. Das H, Kumar A, Lin Z, Patino WD, Hwang PM, Feinberg MW, et al. Kruppel-like factor 2 (KLF2) regulates proinflammatory activation of monocytes. *Proc Natl Acad Sci USA*. (2006) 103:6653–8. doi: 10.1073/pnas.0508235103
182. Das M, Lu J, Joseph M, Aggarwal R, Kanji S, McMichael BK, et al. Kruppel-like factor 2 (KLF2) regulates monocyte differentiation and functions in mBSA and IL-1beta-induced arthritis. *Curr Mol Med*. (2012) 12:113–25. doi: 10.2174/156652412798889090
183. Liao X, Sharma N, Kapadia F, Zhou G, Lu Y, Hong H, et al. Kruppel-like factor 4 regulates macrophage polarization. *J Clin Invest*. (2011) 121:2736–49. doi: 10.1172/JCI45444
184. Barczyk K, Ehrchen J, Tenbrock K, Ahlmann M, Kneidl J, Viemann D, et al. Glucocorticoids promote survival of anti-inflammatory macrophages via stimulation of adenosine receptor A3. *Blood*. (2010) 116:446–55. doi: 10.1182/blood-2009-10-247106
185. Perretti M, D'Acquisto F. Annexin A1 and glucocorticoids as effectors of the resolution of inflammation. *Nat Rev Immunol*. (2009) 9:62–70. doi: 10.1038/nri2470
186. Sugimoto MA, Vago JP, Teixeira MM, Sousa LP. Annexin A1 and the resolution of Inflammation: modulation of neutrophil recruitment, apoptosis, and clearance. *J Immunol Res*. (2016) 2016:8239258. doi: 10.1155/2016/8239258
187. Hannon R, Croxtall JD, Getting SJ, Roviezzo F, Yona S, Paul-Clark MJ, et al. Aberrant inflammation and resistance to glucocorticoids in annexin 1-/- mouse. *FASEB J*. (2003) 17:253–5. doi: 10.1096/fj.02-0239fje
188. Damazo AS, Yona S, Flower RJ, Perretti M, Oliani SM. Spatial and temporal profiles for anti-inflammatory gene expression in leukocytes during a resolving model of peritonitis. *J Immunol*. (2006) 176:4410–8. doi: 10.4049/jimmunol.176.7.4410
189. Patel HB, Kornerup KN, Sampaio AL, D'Acquisto F, Seed MP, Girol AP, et al. The impact of endogenous annexin A1 on glucocorticoid control of inflammatory arthritis. *Ann Rheum Dis*. (2012) 71:1872–80. doi: 10.1136/annrheumdis-2011-201180
190. Heming M, Gran S, Jauch SL, Fischer-Riepe L, Russo A, Klotz L, et al. Peroxisome proliferator-activated receptor-gamma modulates the response of macrophages to lipopolysaccharide and glucocorticoids. *Front Immunol*. (2018) 9:893. doi: 10.3389/fimmu.2018.00893
191. Smoak K, Cidlowski JA. Glucocorticoids regulate tristetraprolin synthesis and posttranscriptionally regulate tumor necrosis factor alpha inflammatory signaling. *Mol Cell Biol*. (2006) 26:9126–35. doi: 10.1128/MCB.00679-06
192. Ishmael FT, Fang X, Galdiero MR, Atasoy U, Rigby WF, Gorospe M, et al. Role of the RNA-binding protein tristetraprolin in glucocorticoid-mediated gene regulation. *J Immunol*. (2008) 180:8342–53. doi: 10.4049/jimmunol.180.12.8342
193. Qiu LQ, Stumpo DJ, Blackshear PJ. Myeloid-specific tristetraprolin deficiency in mice results in extreme lipopolysaccharide sensitivity in an otherwise minimal phenotype. *J Immunol*. (2012) 188:5150–9. doi: 10.4049/jimmunol.1103700
194. Shuto T, Imasato A, Jono H, Sakai A, Xu H, Watanabe T, et al. Glucocorticoids synergistically enhance nontypeable *Haemophilus influenzae*-induced Toll-like receptor 2 expression via a negative cross-talk with p38 MAP kinase. *J Biol Chem*. (2002) 277:17263–70. doi: 10.1074/jbc.M112190200
195. Lannan EA, Galliher-Beckley AJ, Scoltock AB, Cidlowski JA. Proinflammatory actions of glucocorticoids: glucocorticoids and TNFalpha coregulate gene expression *in vitro* and *in vivo*. *Endocrinology*. (2012) 153:3701–12. doi: 10.1210/en.2012-1020
196. Itoh N, Kasutani K, Muto N, Otaki N, Kimura M, Tanaka K. Blocking effect of anti-mouse interleukin-6 monoclonal antibody and glucocorticoid receptor antagonist, RU38486, on metallothionein-inducing activity of serum from lipopolysaccharide-treated mice. *Toxicology*. (1996) 112:29–36. doi: 10.1016/0300-483X(96)03345-8
197. Kasutani K, Itoh N, Kanekiyo M, Muto N, Tanaka K. Requirement for cooperative interaction of interleukin-6 responsive element type 2 and glucocorticoid responsive element in the synergistic activation of mouse metallothionein-I gene by interleukin-6 and glucocorticoid. *Toxicol Appl Pharmacol*. (1998) 151:143–51. doi: 10.1006/taap.1998.8452
198. Kelly EJ, Sandgren EP, Brinster RL, Palmiter RD. A pair of adjacent glucocorticoid response elements regulate expression of two mouse metallothionein genes. *Proc Natl Acad Sci USA*. (1997) 94:10045–50. doi: 10.1073/pnas.94.19.10045
199. Waelput W, Broekaert D, Vandekerckhove J, Brouckaert P, Tavernier J, Libert C. A mediator role for metallothionein in tumor necrosis factor-induced lethal shock. *J Exp Med*. (2001) 194:1617–24. doi: 10.1084/jem.194.11.1617
200. Takano H, Inoue K, Yanagisawa R, Sato M, Shimada A, Morita T, et al. Protective role of metallothionein in acute lung injury induced by bacterial endotoxin. *Thorax*. (2004) 59:1057–62. doi: 10.1136/thx.2004.024232
201. Inoue K, Takano H, Shimada A, Wada E, Yanagisawa R, Sakurai M, et al. Role of metallothionein in coagulatory disturbance and systemic inflammation induced by lipopolysaccharide in mice. *FASEB J*. (2006) 20:533–5. doi: 10.1096/fj.05-3864fje
202. Subramanian Vignesh K, Deepe GS Jr. Metallothioneins: emerging modulators in immunity and infection. *Int J Mol Sci*. (2017) 18:E2197. doi: 10.3390/ijms18102197
203. Miyata M, Lee JY, Susuki-Miyata S, Wang WY, Xu H, Kai H, et al. Glucocorticoids suppress inflammation via the upregulation of negative regulator IRAK-M. *Nat Commun*. (2015) 6:6062. doi: 10.1038/ncomms7062
204. Garcia JG, Liu F, Verin AD, Birukova A, Dechert MA, Gerthoffer WT, et al. Sphingosine 1-phosphate promotes endothelial cell barrier integrity

by Edg-dependent cytoskeletal rearrangement. *J Clin Invest*. (2001) 108:689–701. doi: 10.1172/JCI12450

205. McVerry BJ, Peng X, Hassoun PM, Sammani S, Simon BA, Garcia JG. Sphingosine 1-phosphate reduces vascular leak in murine and canine models of acute lung injury. *Am J Respir Crit Care Med*. (2004) 170:987–93. doi: 10.1164/rccm.200405-684OC
206. Peng X, Hassoun PM, Sammani S, McVerry BJ, Burne MJ, Rabb H, et al. Protective effects of sphingosine 1-phosphate in murine endotoxin-induced inflammatory lung injury. *Am J Respir Crit Care Med*. (2004) 169:1245–51. doi: 10.1164/rccm.200309-1258OC
207. Tauseef M, Kini V, Knezevic N, Brannan M, Ramchandaran R, Fyrst H, et al. Activation of sphingosine kinase-1 reverses the increase in lung vascular permeability through sphingosine-1-phosphate receptor signaling in endothelial cells. *Circ Res*. (2008) 103:1164–72. doi: 10.1161/01.RES.0000338501.84810.51
208. Camerer E, Regard JB, Cornelissen I, Srinivasan Y, Duong DN, Palmer D, et al. Sphingosine-1-phosphate in the plasma compartment regulates basal and inflammation-induced vascular leak in mice. *J Clin Invest*. (2009) 119:1871–9. doi: 10.1172/JCI38575
209. Rapp AE, Hachemi Y, Kemmler J, Koenen M, Tuckermann J, Ignatius A. Induced global deletion of glucocorticoid receptor impairs fracture healing. *FASEB J*. (2018) 32:2235–45. doi: 10.1096/fj.201700459RR
210. Tronche F, Kellendonk C, Kretz O, Gass P, Anlag K, Orban PC, et al. Disruption of the glucocorticoid receptor gene in the nervous system results in reduced anxiety. *Nat Genet*. (1999) 23:99–103. doi: 10.1038/12703
211. Brewer JA, Khor B, Vogt SK, Muglia LM, Fujiwara H, Haegele KE, et al. T-cell glucocorticoid receptor is required to suppress COX-2-mediated lethal immune activation. *Nat Med*. (2003) 9:1318–22. doi: 10.1038/nm895
212. Mittelstadt PR, Monteiro JP, Ashwell JD. Thymocyte responsiveness to endogenous glucocorticoids is required for immunological fitness. *J Clin Invest*. (2012) 122:2384–94. doi: 10.1172/JCI63067
213. Clausen BE, Burkhardt C, Reith W, Renkawitz R, Forster I. Conditional gene targeting in macrophages and granulocytes using LysMcre mice. *Transgenic Res*. (1999) 8:265–77. doi: 10.1023/A:1008942828960
214. Meers GK, Bohnenberger H, Reichardt HM, Luhder F, Reichardt SD. Impaired resolution of DSS-induced colitis in mice lacking the glucocorticoid receptor in myeloid cells. *PLoS ONE*. (2018) 13:e0190846. doi: 10.1371/journal.pone.0190846
215. Galuppo P, Vettorazzi S, Hovelmann J, Scholz CJ, Tuckermann JP, Bauersachs J, et al. The glucocorticoid receptor in monocyte-derived macrophages is critical for cardiac infarct repair and remodeling. *FASEB J*. (2017) 31:5122–32. doi: 10.1096/fj.201700317R
216. Preusch MR, Rattazzi M, Albrecht C, Merle U, Tuckermann J, Schutz G, et al. Critical role of macrophages in glucocorticoid driven vascular calcification in a mouse-model of atherosclerosis. *Arterioscler Thromb Vasc Biol*. (2008) 28:2158–64. doi: 10.1161/ATVBAHA.108.174128
217. Carrillo-de Sauvage MA, Maatouk L, Arnoux I, Pasco M, Sanz Diez A, Delahaye M, et al. Potent and multiple regulatory actions of microglial glucocorticoid receptors during CNS inflammation. *Cell Death Differ*. (2013) 20:1546–57. doi: 10.1038/cdd.2013.108
218. Ros-Bernal F, Hunot S, Herrero MT, Parnadeau S, Corvol JC, Lu L, et al. Microglial glucocorticoid receptors play a pivotal role in regulating dopaminergic neurodegeneration in parkinsonism. *Proc Natl Acad Sci USA*. (2011) 108:6632–7. doi: 10.1073/pnas.1017820108
219. Maatouk L, Compagnion AC, Sauvage MC, Bemelmans AP, Leclere-Turbant S, Cirotteau V, et al. Author correction: TLR9 activation via microglial glucocorticoid receptors contributes to degeneration of midbrain dopamine neurons. *Nat Commun*. (2018) 9:3109. doi: 10.1038/s41467-018-05680-w

Conflict of Interest Statement: The authors declare that the research was conducted in the absence of any commercial or financial relationships that could be construed as a potential conflict of interest.

The handling Editor declared a past co-authorship with one of the authors JT.

1.5 Epigenetic regulation of transcription

To gain insight into the interactome of Glucocorticoid receptor in inflammatory cells, Chromatin Immunoprecipitation followed by mass spectometry analysis (ChIP-MS) was performed in murine bone marrow derived macrophages (BMDMs) stimulated with LPS and treated with the GR ligand dexamethasone (Dex). Among other known co-regulators like EP300 and NCOA2 (or GRIP1), GR interacts also with epigenetic modifiers like histone methyltransferases (COMPASS complex) and chromatin remodelers (SWI/SNF complex) in LPS+Dex treated primary macrophages (Figure 4).

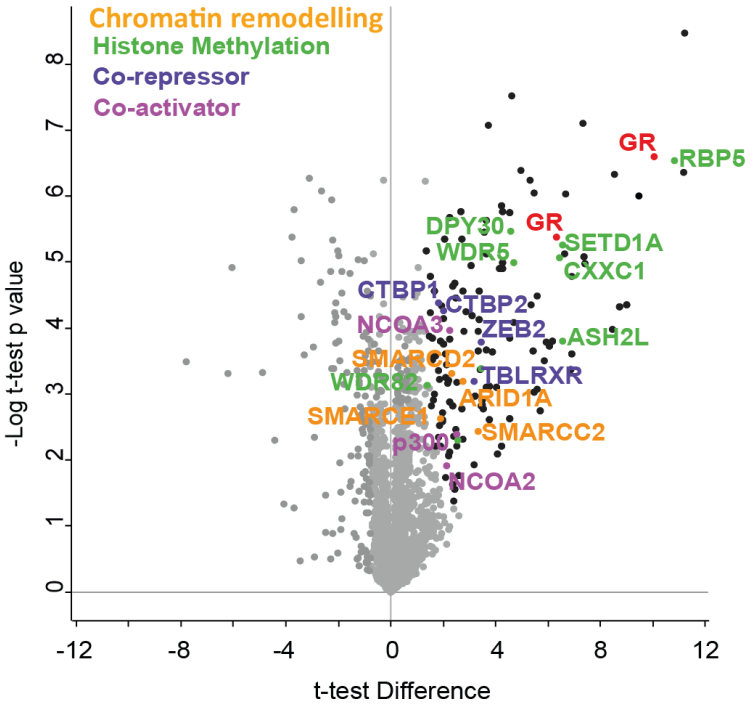

Figure 4.The GR interactome in LPS+Dex treated BMDMs. Volcano plot that shows the GR interactome in BMDMs treated with LPS and Dex (Greulich et al. 2021). The coloured dots indicate significantly enriched interaction partners in a GR IP over non-specific isotype-matched IgG IP (1.5fold, p<0.05).

In eukaryotes the DNA is packed into a chromatin state to fit into the nucleus. Nucleosomes are the basic structure units of the chromatin and consist of 146bp DNA wrapped around an octamer of four histones (2x H3, 2xH4, 2xH2A and 2xH2B) (Kornberg 1974). Nucleosomes are separated with a linker DNA. Apart from the core histones, a fifth linker histone protein 1 (H1) dynamically associates with each nucleosome core particle and facilitates the compaction of chromatin structures (Kornberg and Lorch 1999). Based on the order of packaging, chromatin can be stratified in heterochromatin and euchromatin. Heterochromatin represents most of the chromatin type in the nucleus. It was first characterized by Heitz as a darkly stained and condensed form of chromatin during the different stages of the cell cycle and displays low transcriptional activity (Heitz 1928). On the

other hand, euchromatin refers to a more relaxed state of chromatin. It can be packed and unpacked throughout the cell cycle and is generally associated with high transcriptional activity (Morrison and Thakur 2021).

The structural feature of the chromatin is a limiting factor for transcription. The rearrangement of nucleosomes and chromatin modifications facilitate binding of transcription factor such as GR to DNA and thus, regulate the transcription. These modifications (also known as epigenetic modifications) include methylation of cytokines, post translational modifications of histones, remodeling of the chromatin, RNA based methods and are catalysed by specific enzymes (Gibney and Nolan 2010).

1.5.1 Histone methylation

Histones can be post translationally modified in their N-terminal tails that overhang from the nucleosomes. There are 8 types of histone modifications; acetylation of lysines, ubiquitination, phosphorylation, methylation of lysines and arginines, deamination sumoylation ADP riobosylation and proline isomerisation (Kouzarides 2007). These modifications do not only affect the chromatin structure, but they can also recruit chromatin remodeling complexes like SWI/SNF to change the position of the nucleosomes and subsequent allow the binding of transcription factors to regulate gene expression (Swygert and Peterson 2014).

During histone methylation, methyl groups are transferred to lysine and arginine residues of the histones. Lysine methylation involves transfer of up to three methyl groups, whereas arginines may exist as either mono-methylated or di-methylated (Di Lorenzo and Bedford 2011; Han et al. 2019). The addition of the methyl groups does not alter the charge of the histones (Bannister and Kouzarides 2011). However, it is involved in the regulation of gene transcription. Methylation of lysine residues is correlated with both activation and repression of transcription based on their location and the number of methyl-groups added. Usually methylation of H3 at lysine 4 (H3K4), lysine 36 (H3K36) and lysine 79 (H3K79) is associated with transcriptional activation, whereas di- and tri-methylated H3K9, methylated H3K27 and H4K20 present important role in transcriptional repression (Hyun et al. 2017). Promoters of active genes are occupied by H3K4me2, H3K4me3 and H3K9me1, whereas promoters of repressed genes are enriched for H3K9me2, H3K9me3 H3K27me2 and H3K27me3 (Schneider and Grosschedl 2007). H3K4me3 and H3K27me3 can be present at the same time in promoters of bivalent genes (Vastenhouw and Schier 2012). Enhancers are marked by H3K4me1, which together with acetylation of lysine 27 in H3 (H3K27ac) are correlated

with transcriptional activation (Barski et al. 2007; Schneider and Grosschedl 2007; Gates et al. 2017).

Histone methylation is catalysed by enzymes named as histone methyltransferases (HMTs) and it is performed by the transfer of methyl groups from the S- Adenosyl methionine (SAM) donor (Smith and Denu 2009). Lysine methyltransferases (KMTs) are divided in two categories: the Su(var)3-9/Enhancer of zeste/trithorax (SET) domain and the non-SET domain KMTs (Smith and Denu 2009). Some examples of SET domain containing KMTs are the KMT2A-KMT2H proteins that belong to the COMPASS family of KMTs, the KMT6 which is part of the Ploycomb repressor complex, the KMT1C involved in heterochromatin formation and the KMT3C. The DOT1/KMT4 methyltransferase does not contain a SET domain and can methylate H3 at lysine 79 (Allis et al. 2007). On the contrary, histone demethylases (HDMs) can remove the methyl groups from the histone tails. Most lysine demethylases (KDMs) contain a Jumonji (Jmj) domain in the C-terminus and present different functions (Franci et al. 2014). Examples of Jumonji domain containing demethylases are the KDM2, KDM3, KDM4, KDM5 and KDM6 (Allis et al. 2007).The first protein member of the KDM family, KDM1 (or LSD1), does not contain a Jumonji domain and is involved both in transcriptional activation and repression (Allis et al. 2007; Smith and Denu 2009).

1.5.1.1 The COMPASS family of KMTs

The COMPASS (complex proteins associated with Set1) is a protein family of histone methyltransferases. It was first identified in *Saccharomyces cerevisiae* and contains the Set1 protein with a highly conserved catalytic SET domain (Miller et al. 2001). In yeast there is only one SET methyltransferase (the ySet1), whereas there are three in *Drosophila*; the dSet1, Trithorax (trx) and Trihorax-related (trr). Gene duplications have led to 6 SET methyltransferases in mammals; the SET1A (or SETD1A) and SET1B (or SETD1B), which are homologues of the *Drosophila* Set1, the Trithorax homologues mixed lineage leukemia 1 (MLL1 or KMT2A) and MLL2 (or KMT2B) and the Trithorax-related homologues MLL3 (or KMT2C) and MLL4 (or KMT2D) (Figure 5) (Shilatifard 2012).

Each methyltransferase can assemble a complete COMPASS complex by interacting with several other proteins that are necessary for its function (Figure 5). Some of the subunits are common and evolutionary conserved among all the COMPASS families, whereas others are specific to one or more families. The common core subunits are the proteins WDR5, ASH2L, RBBP5 and DPY30 which are also collectively known as WARD (Shilatifard 2012). WDR5 and RBBP5 are required for the assembly of the complex, whereas ASH2L and

DPY30 possess the methyltransferase activity (Shilatifard 2012; Schuettengruber et al. 2017; Cenik and Shilatifard 2021). The SETD1A/B complexes contain the WDR82, HCF1 and CXXC1 proteins and mediate bulk tri-methylation of H3K4 at promoter regions (Lee and Skalnik 2005; Lee et al. 2007; Wu et al. 2008). H3K4me3 requires di-methylation substrate, which is also deposited by SETD1A (Soares et al. 2017; Yang and Ernst 2017). MENIN and HCF1 are the supplementary subunits of the MLL1/2 complexes. The MLL1-COMPASS can tri-methylate H3K4 at promoters of genes involved in developmental processes and di-methylate H3K4 at CpG islands in HCT116 human colorectal cells (Wang et al. 2009; Rickels et al. 2016). The MLL2-COMPASS can deposit H3K4me3 at promoters of bivalent genes that are also occupied by H3K27me3 in mouse embryonic stem cells (Denissov et al. 2014). The MLL3/4 complexes have additionally four subunits; the NCOA6, PA1, PTIP and the histone demethylase UTX (or KDM6A). They can mediate mono-methylation of H3K4 at enhancers. The UTX subunit can catalyse demethylation of H3K27me3 from poised enhancers and switch them to their active state (Piunti and Shilatifard 2016).

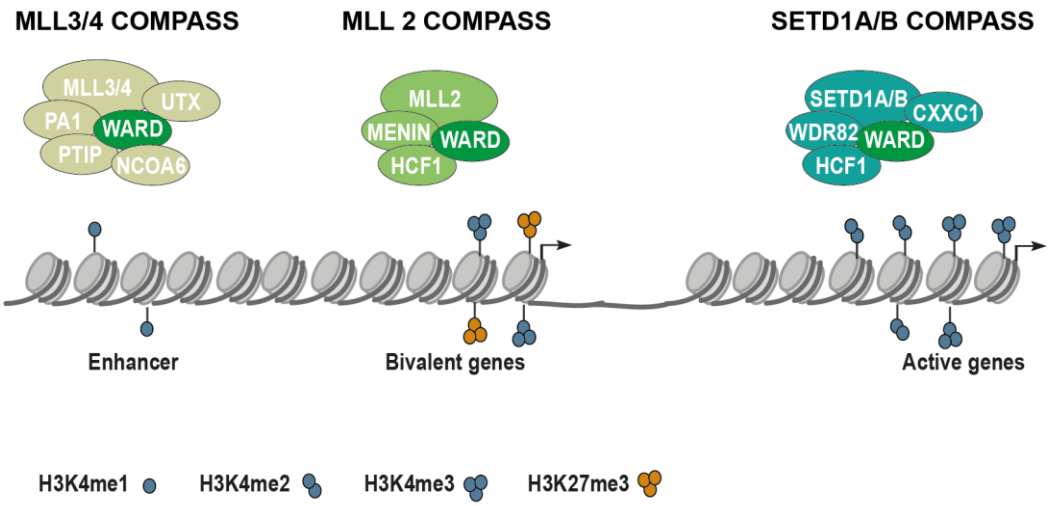

Figure 5.The COMPASS family of lysine methyltransferases. The MLL3/4 COMPASS complex can mono-methylate H3K4 at enhancers, the MLL2 COMPASS deposits H3K4me3 at bivalent regions whereas the SETD1A/B complex can catalyse di- and tri-methylation at promoters of active genes. Image adapted from (Schuettengruber et al. 2017).

COMPASS complexes can be recruited to chromatin in different ways. For example, binding of the COMPASS to chromatin can be mediated by transcription factors like OCT4 and the estrogen receptor alpha (Mo et al. 2006; Ang et al. 2011; Fang et al. 2016; Bochynska et al. 2018). Additionally, it has been reported that COMPASS complex can be recruited through interaction with RNA polymerase II, histone variants and histone modifications (Lee and

Skalnik 2008; Muntean et al. 2010; Bochynska et al. 2018; Cenik and Shilatifard 2021). Compass complexes can also bind directly to DNA at non-methylated CpG islands by the CxxC motifs (Long et al. 2013).

Even though COMPASS complexes are known histone methyltransferases, they also present some catalytic independent functions. For example, the catalytic activity of MLL1 is required for embryonic development in mice, but it is not involved in haematopoiesis (Hess et al. 1997; Terranova et al. 2006). Deletion of the catalytic SET domain of the SETD1A in mouse embryonic stem cells does not affect bulk H3K4me3 levels or their survival, but it can defect their differentiation (Cao et al. 2017; Sze et al. 2017). Additionally, in mouse embryonic stem cells the MLL3/4 complexes are crucial for enhancer activation and transcriptional expression independently of H3K4me1 deposition (Dorighi et al. 2017).

1.5.2 Chromatin remodeling

The process of changing the architecture of the chromatin is called chromatin remodeling. The re-organization of the chromatin is catalysed by ATP-dependent chromatin remodeling complexes that use the energy from ATP hydrolysis to assemble, remodel or edit nucleosomes (Voss and Hager 2014; Hasan and Ahuja 2019).
In eukaryotes, there are several chromatin remodelers. Based on differences in their catalytic activity, they can be categorized into four families: the switch/sucrose non-fermentable (SNI/SNF), chromodomain helicase DNA-binding (CHD), INO80 and imitation switch (ISWI). All four families contain an ATPase catalytic subunit which is involved in the translocation of the DNA along the histones (Clapier et al. 2017). The ATPase domain is surrounded by other subunits important for target recognition and remodeling function.

1.5.2.1 The SWI/SNF subfamily

SWI/SNF is a well-studied and evolutionary conserved chromatin remodeling complex. It was first discovered in yeast by two genetic screens for mutations in genes involved in the SWI and SNF pathways (Workman and Kingston 1998; Sudarsanam and Winston 2000). The SWI/SNF complex is composed of many subunits. Based on their function they are divided into different categories; the catalytic subunits with an ATPase activity (SMARCA2/BRM or SMARCA4/BRG1), the core subunits (SMARCB1/BAF47, SMARCC1/BAF155, SMARCC2/ BAF170), and accessory subunits (BAF45A-D, ACTL6A-B/BAF53A-B/, SMARCE1/BAF57, SMARCD1-3/BAF60A-C, PBRM1/BAF180, ARID2/BAF200, ARID1A-B/BAF250A-B, b-actin, BCL7A-C, BCL11A-B, BRD7, BRD9,

SS18/CREST, GLTSCR1/1L), that are important for binding of the complex to proteins or DNA (Weissman and Knudsen 2009; Hasan and Ahuja 2019) . In mammals there are three SWI/SNF complexes; the BAF (BRG1 associated factors), the pBAF (Polybromo associated BAF) and the ncBAF (noncanonical BAF).The three complexes share some subunits, but they also present some differences (Table 1) (Weissman and Knudsen 2009; Tang et al. 2010; Hohmann and Vakoc 2014; Michel et al. 2018; Hasan and Ahuja 2019; Sima et al. 2019; Centore et al. 2020).

Table 1. The three different mammalian SWI/SNF complexes.

<table>
<tr><th>pBAF</th><th>BAF</th><th>ncBAF</th></tr>
<tr><td>BRG1 or BRM</td><td>BRG1</td><td>BRG1 or BRM</td></tr>
<tr><td>BAF45A</td><td>BAF45B, C or D</td><td></td></tr>
<tr><td colspan="2">BAF47</td><td></td></tr>
<tr><td colspan="2">BAF57</td><td></td></tr>
<tr><td colspan="2">BAF60A, B or C</td><td>BAF60A</td></tr>
<tr><td colspan="2">BAF170</td><td></td></tr>
<tr><td>BAF180</td><td></td><td></td></tr>
<tr><td>BAF200</td><td>BAF250 A or B</td><td></td></tr>
<tr><td>BRD7</td><td></td><td>BRD9</td></tr>
<tr><td></td><td colspan="2">SS18 or CREST</td></tr>
<tr><td></td><td></td><td>GLTSCR1/1L</td></tr>
<tr><td></td><td>BCL11A or B</td><td></td></tr>
<tr><td colspan="3">BAF53A or B</td></tr>
<tr><td colspan="3">BAF155</td></tr>
<tr><td colspan="3">b-actin</td></tr>
<tr><td colspan="3">BCL7A, B or C</td></tr>
</table>

BRG1 and its homologue BRM have almost 75% identical amino acid sequence (Khavari et al. 1993). They are large proteins with many domains. They present a QLQ domain, an HSA domain, a BRK domain, an ATPase domain, a SnAC domain and a bromodomain. The N-terminal of the proteins contain the QLQ (Gln, Leu, Gln motif) domain, which mediates protein-protein interactions and the HSA (helicase/SANT-associated) domain, that is important for the binding to actin related proteins (Kim et al. 2003; Szerlong et al. 2008). The ATPase domain consists of a DExx box helicase and HELICc (helicase superfamily c-terminal) subdomains, that are separated by a linker amino acid sequence. The DExx subdomain includes an ATP binding region, and together with the HELICc subdomain can

unwrap the DNA (Trotter and Archer 2008; Tang et al. 2010). The C-terminal of BRG1 and BRM contain a SnAC (Snf2 ATP coupling) domain, which is a histone binding domain, and a bromodomain, that is involved in the binding to acetylated lysine residues (Haynes et al. 1992; Clapier et al. 2017).

The SWI/SNF complex can remodel the chromatin via nucleosome sliding, nucleosome ejection or histone dimer eviction (Figure 6). These functions occur via translocation of the DNA along the histones (Clapier et al. 2017). SWI/SNF binds to nucleosomes through the SnAC histone binding domain of BRG1 or BRM. Once bound, the ATPase domain can translocate the DNA by 1-2 bp using energy from one cycle of ATP-binding-hydrolysis-release (Harada et al. 2016; Clapier et al. 2017). Continued DNA translocation leads to sliding of nucleosomes (Clapier et al. 2017). The efficiency of the DNA translocation can be significantly improved by binding of the actin related proteins ARP7and ARP9 to the HSA domain of BRG1 or BRM which will result in disruption of histone-DNA contacts, histone dimer eviction and subsequently to octamer ejection (Lorch et al. 2006; Clapier et al. 2016). Alternatively, continued DNA translocation will bring the remodeler bound nucleosome closer to an adjacent one. This may result in the collision of two nucleosomes, which in turns leads to dimer or octamer ejection of the adjacent nucleosomes (Dechassa et al. 2010).

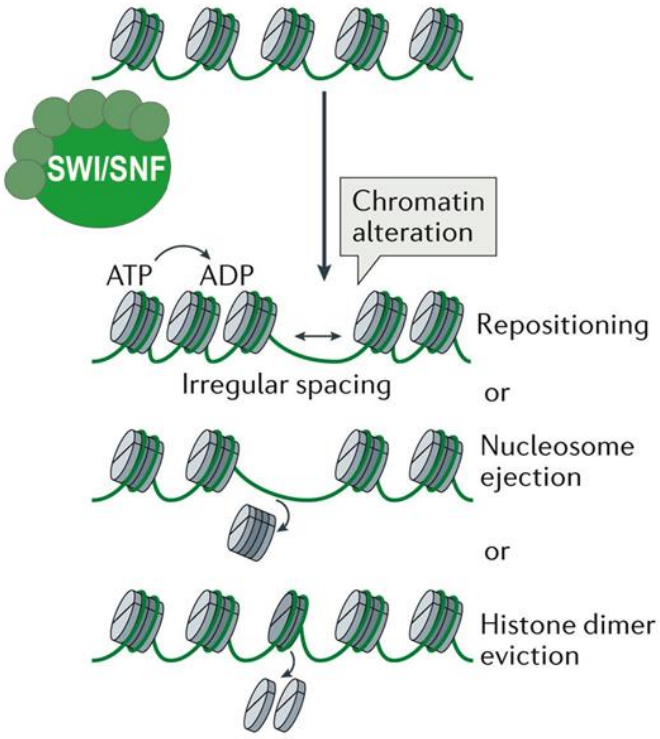

Figure 6. Mechanisms of action of the SWI/SNF chromatin remodeling complex. The SWI/SNF complex uses the energy from ATP hydrolysis to remodel chromatin via repositioning, ejection of nucleosomes and eviction of histone dimmers. Image adapted from (Clapier et al. 2017).

1.5.2.2 BRG1 as a transcriptional co-regulator

BRG1 is an important regulator of transcription. It interacts with proteins implicated in various processes like transcription factors and chromatin modifying enzymes. BRG1 is associated with proteins involved in transcriptional activation including nuclear receptors like androgen receptor (AR), estrogen receptor (ER), GR, progesterone receptor (PR) and peroxisome proliferator activated receptor γ (PPAR-γ) (Ichinose et al. 1997; Fryer and Archer 1998; Marshall et al. 2003; Debril et al. 2004; Vicent et al. 2006; Trotter and Archer 2008). Additionally, it interacts with the signal transducer and activator protein 1 (STAT1) and 2 (STAT2) and the transcriptional activator Mef2D (Trotter and Archer 2008). On the other hand, BRG1 can be involved in transcriptional repression due to its association with corepressors like the mSin3a/HDAC1/2 complex, the NCoR/SMRT complex and its components HDAC3 and HP1 as wells as the repressor element 1-silencing transcription factor (REST) complex (Trotter and Archer 2008).

The SWI/SNF complex is an essential coregulator of the glucocorticoid receptor. GR interacts directly with the SWI/SNF complex via the BAF57, BAF60A, BAF155 and BAF250 subunits (Hsiao et al. 2003; Muratcioglu et al. 2015). BRG1 is extensively reported to be implicated in gene activation by GR. It can pre-exist on GR binding sites (GBS), or it can be recruited by GR to remodel the chromatin and subsequently recruit RNA polymerase II as well as other factors to induce GR-regulated transcriptional activation (Fryer and Archer 1998; Trotter and Archer 2004; Johnson et al. 2008; Trotter et al. 2015; Hoffman et al. 2018). Even though BRG1 was mainly associated with transcriptional activation, there are some studies that indicate an involvement in transcriptional repression. Together with HDAC2 it is reported to play an important role in the repression of the negative GR target gene *POMC* (Bilodeau et al. 2006). Additionally, glucocorticoid-mediated gene repression was affected at a subset of genes in cell lines expressing a dominant negative BRG1, but it did not show any glucocorticoid-induced and/or BRG1-dependent changes in DNA accessibility (John et al. 2008).

1.6 Normalization strategies for Chromatin Immunoprecipitation experiments

ChIP is widely used to map the occupancy of histone modifications or transcription factors across the genome. It is a very complex procedure that can lead to technical variations. Therefore, it is difficult to compare the outcome between two different samples without internal controls.

Loci with constant occupancy of the protein of interest can be used for inter-tube normalization (Allhoff et al. 2016). However, this approach can be applied only if the occupancy of the protein of interest is similar between samples at particular loci. Recently Egan et al. described another one method to internally account for the technical variations of ChIP. In more details, they spiked-in chromatin from *Drosophila melanogaster* into the mouse chromatin and performed ChIP against H2Av, a *Drosophila* specific histone variant (Egan et al. 2016). However, this method is limited to the different IP efficiencies of the antibodies targeting the experimental and the spike-in chromatin. Even though the existing methods present some limitations, it is of great importance to normalize ChIP data in order to compare the occupancy of the protein of interest between different conditions. Therefore, the development of new normalization strategies might be useful.

2. Scope of the thesis

The hypothesis of this thesis was that the SETD1A/COMPASS complex and the SWI/SNF complex are involved in the GR-mediated transcription in murine LPS activated primary macrophages. The aims of this work are:

1. Develop a new normalization strategy for Chromatin Immunoprecipitation experiments against histone marks

A new spike-in normalization strategy for ChIP was applied to determine differences in the occupancy of histone marks at GBS between different treatment conditions.

2. Determine the role of SETD1A/COMPASS complex in the GR-mediated regulation of inflammatory genes

ChIP-sequencing was performed in LPS only and LPS+Dex treated macrophages against GR, SETD1A and CXXC1 to define the amount of GBS occupied by these co-regulators. In order to elucidate if H3K4 dynamics alter upon addition of the GR ligand, ChIP-sequencing against H3K4 marks was conducted in LPS and LPS+Dex treated macrophages. The CRISPR-Cas9 technology was applied in RAW 264.7 cells to generate a mutant cell line with an instable SETD1A (*Setd1a*$^{Del/+}$), and determine if SETD1A is involved in the regulation of the transcription of inflammatory genes by GR. Furthermore, changes in H3K4 levels at GBS were examined in *Setd1a*$^{Del/+}$ Raw 264.7 cells.

3. Determine the involvement of BRG1 in the transcriptional regulation of inflammatory genes regulated by GR

In order to determine if BRG1 is recruited at GBS in response to GR ligand, ChIP-sequencing against BRG1 was performed in LPS and LPS+Dex treated macrophages. To elucidate if there are changes in chromatin accessibility at the GBS upon addition of Dex, an assay for transposase-accessible chromatin followed by sequencing (ATAC-seq) was conducted. Loss of function experiments using siRNAs against BRG1 as well as pharmacological inhibition of BRG1 were performed in primary macrophages to characterize the GR-mediated transcriptional regulation upon loss of BRG1.To determine how BRG1 affects the expression of GR regulated genes, possible different recruitment of GR, MED1

and HDACs, as well as histone acetylation dynamics were investigated in LPS+Dex stimulated primary macrophages treated with a BRG1 catalytic inhibitor.

Mainly, the role of SETD1A and BRG1 in the GR-mediated inflammatory gene regulation was investigated. Elucidating the crosstalk between GR and transcriptional co-regulators like SETD1A and BRG1 might provide valuable insight into the different mechanism of transcriptional activation and repression mediated by GR in inflammatory cells. This ultimately can lead to the development of new anti-inflammatory drugs with less severe side effects.

3. Publications and summaries

3.1 Protocol for using heterologous spike-ins to normalize for technical variation in chromatin immunoprecipitation

Contribution

The article ‘Protocols for using heterologous spike-ins to normalize for technical variation in chromatin immunoprecipitation’’ was published in Star protocols in 2021. For this manuscript I developed, validated, optimized and performed the spike-in ChIP-qPCR. Additionally, I contributed to the writing and revision of the manuscript.

Summary

Chromatin immunoprecipitation is a very useful method for detecting transcription factor binding sites and histone modification occupancy profiles. However, the inherent technical variability of the method, for example in chromatin fragmentation, IP efficiency, etc. might lead to not accurate comparison between two different conditions. In this article a detailed protocol for a normalization method of ChIP followed either by qPCR (ChIP-qPCR) or sequencing (seq) is described to overcome the technical variations previously mentioned. In brief, heterologous spike-ins from *Drosophila* chromatin are added to the experimental mouse chromatin as internal control before shearing. The IP is performed with an antibody that detects the protein of interest in both experimental and spike-in chromatin. The results are normalized using a scaling factor derived from the ChIP on the spike-in chromatin. This method controls for inter-tube variation independent of the variability in IP efficiency of the antibodies, in case that a different antibody is used for IP in the spike-in chromatin. However, it is limited to proteins that are conserved between experimental and spike-in species.

STAR Protocols

CellPress
OPEN ACCESS

Protocol

Protocol for using heterologous spike-ins to normalize for technical variation in chromatin immunoprecipitation

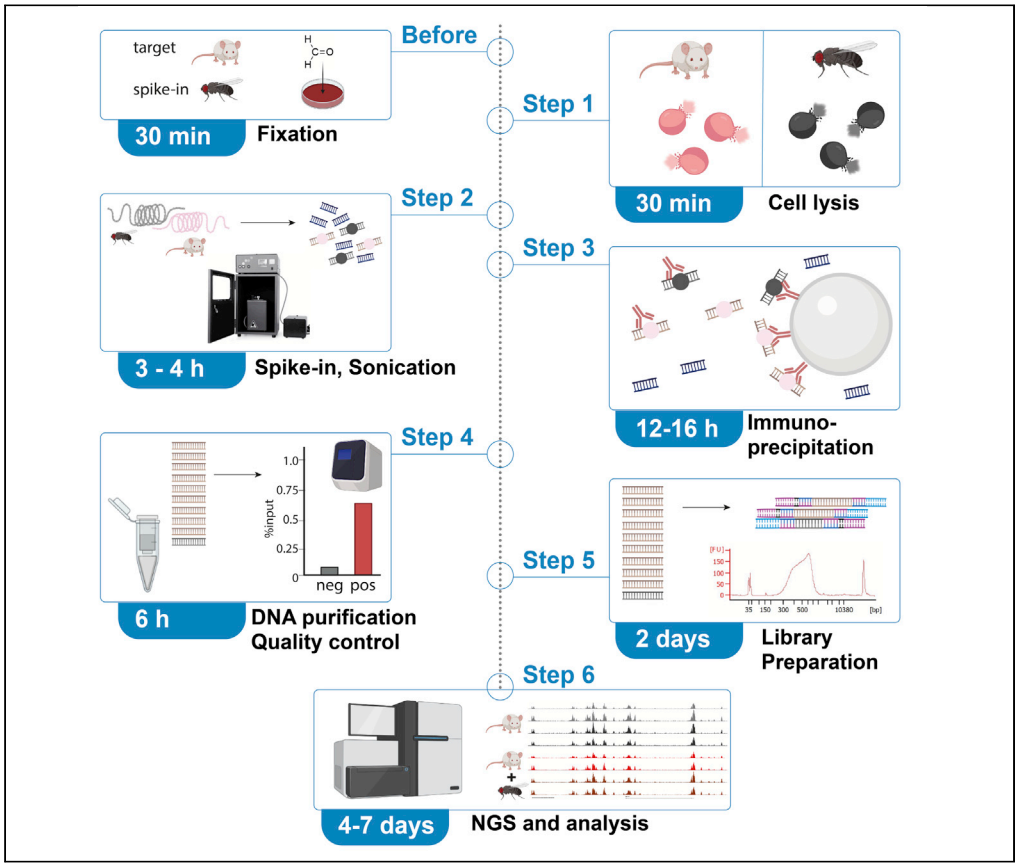

Quantifying differential genome occupancy by chromatin immunoprecipitation (ChIP) remains challenging due to variation in chromatin fragmentation, immunoprecipitation efficiencies, and intertube variability. In this protocol, we add heterologous spike-ins from *Drosophila* chromatin as an internal control to the mice chromatin before immunoprecipitation to normalize for technical variation in ChIP-qPCR or ChIP-seq. The choice of spike-in depends on the evolutionary conservation of the protein of interest and the antibody used.

Franziska Greulich, Aikaterini Mechtidou, Teresa Horn, Nina Henriette Uhlenhaut

franziska.greulich@tum.de

Highlights

Chromatin immunoprecipitation (ChIP) maps protein-binding sites in the genome

Heterologous spike-in ChIP reduces technical variation in ChIP experiments

Applicable to proteins with high interspecies conservation

Greulich et al., STAR Protocols *2*, 100609
September 17, 2021
https://doi.org/10.1016/j.xpro.2021.100609

STAR Protocols

CellPress
OPEN ACCESS

Protocol

Protocol for using heterologous spike-ins to normalize for technical variation in chromatin immunoprecipitation

Franziska Greulich,[1,3,4,5,*] Aikaterini Mechtidou,[2,3] Teresa Horn,[2] and Nina Henriette Uhlenhaut[1,2]

[1]Metabolic Programming, School of Life Sciences Weihenstephan, ZIEL-Institute for Food & Health, Technische Universitaet Muenchen (TUM), 85354 Freising, Germany

[2]Institute for Diabetes and Obesity (IDO) & Institute for Diabetes and Cancer (IDC), Helmholtz Center Munich (HMGU) and German Center for Diabetes Research (DZD), 85764 Neuherberg (Munich), Germany

[3]These authors contributed equally

[4]Lead contact

[5]Technical contact

*Correspondence: franziska.greulich@tum.de
https://doi.org/10.1016/j.xpro.2021.100609

SUMMARY

Quantifying differential genome occupancy by chromatin immunoprecipitation (ChIP) remains challenging due to variation in chromatin fragmentation, immunoprecipitation efficiencies, and intertube variability. In this protocol, we add heterologous spike-ins from *Drosophila* chromatin as an internal control to the mice chromatin before immunoprecipitation to normalize for technical variation in ChIP-qPCR or ChIP-seq. The choice of spike-in depends on the evolutionary conservation of the protein of interest and the antibody used.

For complete details on the use and execution of this protocol, please refer to Greulich et al. (2021).

BEFORE YOU BEGIN

Chromatin ImmunoPrecipitation (ChIP) profiles the occupancy of DNA-associated factors within cells by either quantitative PCR (ChIP-qPCR) or with next-generation sequencing (ChIP-seq). Cells or tissues are fixed with formaldehyde and target-specific antibodies are used to precipitate the protein of interest after cell, nuclear lysis and chromatin fragmentation. Due to the complex protocol design and the variability in chromatin fragmentation between samples, inter-tube comparability is difficult to achieve without internal controls. One method to address this issue is the use of loci that do not change occupancy between samples to perform inter-tube normalization (Allhoff et al., 2016). This resembles the "housekeeping" approach used to normalize mRNA expression in standard quantitative RT-PCR of cDNAs. Such approaches are the basis of software packages like Thor (Allhoff et al., 2016), DiffBind (Ross-Innes et al., 2012) or DESeq2 (Love et al., 2014) for ChIP-seq quantification. In ChIP-qPCR, the choice of a positive locus bound by the protein of interest that does not change across conditions can be very challenging. Often, the genomic targets of the protein of interest or the behavior in response to experimental perturbations are unknown. ChIP-seq approaches are slightly more robust, as long as the majority of binding events is unaffected by the experimental perturbation. In this case, several control regions can be picked for normalization, avoiding the bias of selecting one control region. Those regions might be promoter regions of well characterized housekeeping genes, as suggested by Allhoff et al. (Allhoff et al., 2016). However, those normalization approaches are limited by the assumption that the occupancy of the protein of interest remains unaltered at the majority of sites (ChIP-seq), or at a particular locus (ChIP-qPCR), under the various conditions studied.

One example, where this assumption is violated, was reported when profiling H3 lysine 27 trimethylation (H3K27me3) after inhibition of EZH2 (Enhancer of Zeste 2 Polycomb Repressive Complex 2 Subunit). The inhibition of EZH2, the major histone methyltransferase for H3K27, resulted in a global loss of H3K27me3. In order to quantify the observed genomic changes in H3K27me3, the authors developed "parallel ChIP". By spiking *Drosophila melanogaster* chromatin into the target samples (*Mus musculus*), they internally controlled for inter-tube variation by performing ChIP against the *Drosophila*-specific histone variant H2Av (Egan et al., 2016).

Here, we describe a very similar approach by using an antibody that specifically detects the protein of interest in the samples of target as well as the spike-in species. Our method is limited to the conservation of the protein of interest, but it is independent of the variability in IP efficiencies of the antibody. We successfully used this approach for profiling several histone modifications (H3K27ac, H3K4me1, H3K4me2 and H3K4me3) by ChIP-seq and ChIP-qPCR in murine macrophages with spike-ins from *Drosophila* S2 cells (Greulich et al., 2021). We also performed spike-in normalization for transcription factors with limited conservation in murine cells using human spike-in chromatin (HEK293 cells) by ChIP-qPCR.

Before you begin with the actual experiment, crosslink target and spike-in cells/tissues, establish the sonication conditions for each cell type, design species-specific negative and positive control primers and confirm the specificity of the antibody in both species (see the following sections for more details). We emphasize here that optimal sonication conditions and a thoroughly tested antibody are crucial for a successful ChIP experiment.

Crosslinking of target or spike-in cells

Timing: 30 min

1. Before starting:
   a. Plate 20 M cells in a 15 cm plate one day before fixation. Perform treatment of interest.
   b. Prepare 1% formaldehyde* (FA) solution and 1 M glycine solutions in DPBS. (see materials and equipment).

   ⚠ CRITICAL: Formaldehyde is toxic. Always use protective clothing and follow safety instructions when working with formaldehyde. Work in a fume hood and dispose of residuals according to local regulations for hazardous waste.
   c. Pre-cool DPBS.

2. Aspirate the medium, wash cells once with 10 mL DPBS. Aspirate again.
3. Add 1% FA (10 mL/plate) and incubate for 15 min at 18°C–24°C.

   Note: For proteins that are not contacting the DNA directly, a dual crosslinking with an additional protein-protein crosslinker like disuccinimidyl glutarate (DSG) might be required. In that case, start with a 30 min fixation with 2 mM DSG (in DPBS) at 4°C and proceed after aspiration of the DSG to the FA fixation without any wash step.

4. Add 1.5 mL 1 M glycine and incubate for 5 min at 18°C–24°C. Rock back and forth gently to mix.
5. Aspirate. Wash 2× with cold DPBS and harvest the cells by scraping off the dish.
6. Transfer the cell suspension to a tube and keep on ice.

   ⚠ CRITICAL: For the spike-in cells, split the cells into two tubes with 10 M cells each to avoid freeze and thaw cycles.

7. Spin the tubes for 5 min at 400 × *g* at 4°C. Aspirate Supernatant.

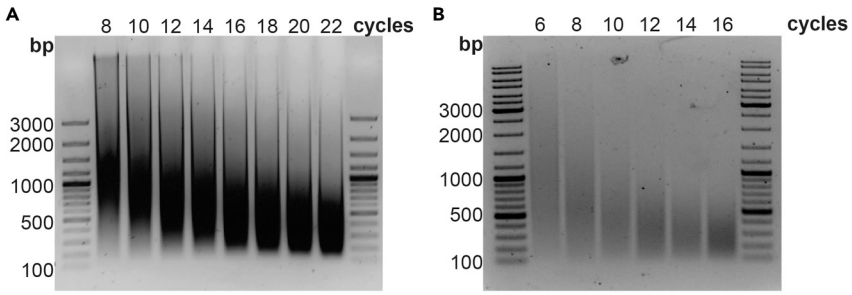

Figure 1. Optimization of sonication conditions

(A) Chromatin from murine bone marrow derived macrophages (male mice aged 6–12 weeks) was sheared for 8–22 cycles at high settings (30s on/off) using the Bioruptor 300 (Diagenode). Here, 12 cycles appear optimal.

(B) Chromatin from Drosophila melanogaster S2 cells was sonicated for 6–16 cycles at high settings (30s on/off) using the Bioruptor 300. The optimal shearing conditions appear to be 10 cycles. (A+B) 20 μl of chromatin aliquots were taken during sonication after the indicated number of cycles, reverse-crosslinked, purified (see steps 42–47), and loaded onto a 0.7% agarose gel stained with peqGreen DNA dye.

Pause point: Pellets might be stored at −80°C for up to one year.

Establish sonication conditions

Timing: 2 days

The number of sonication cycles and the amplitude of sonication needs to be optimized beforehand, for both the spike-in cells as well as the cells of interest (target). Ideally, chromatin is fragmented to 150 bp to 1.5 kb with as little energy added by sonication as possible. This step is very important, since "over-shearing" of the chromatin (bulk fragments below 200 bp) will reduce the IP efficiency by damaging the protein epitopes of interest. On the other hand, "under-shearing" (bulk fragments above 1 kb) will reduce the amount of purified DNA, due to loss of DNA during purification or size selection.

Test the sonication conditions by serial sonication of the same chromatin sample. For example, take a chromatin aliquot every two sonication cycles and perform reverse crosslinking overnight (see steps 42–47). The purified DNA is run on a 0.7% agarose gel. An example picture for a murine macrophage pellet sheared at 20 M cells/mL of shearing buffer, with the Bioruptor 300, is shown in Figure 1A and an example for *Drosophila* S2 cells in Figure 1B. In this case, the optimal number of cycles would be 12 for a mix of both cell types.

Design and order of qPCR primers

Timing: 1–2 h

In order to test the specificity of the ChIP, design at least one primer pair for a region bound by the protein of interest in each the target and spike-in species (positive locus). Additionally, design one primer pair for a region not bound by the protein of interest (negative locus). For histone marks, use publicly available data from ENCODE (https://www.encodeproject.org/ (Davis et al., 2018)), MOD-ENCODE data available for *Drosophila melanogaster* (http://gbrowse.modencode.org/fgb2/gbrowse/fly/), public track hubs on UCSC (https://www.genome.ucsc.edu/ (Kent et al., 2002)) or available data on the Gene Expression Omnibus (GEO) (Edgar et al., 2002). An example can be found in Figure 2A and 2B.

Note: If ChIP-Seq data for the mark or protein of interest is unavailable for the target or for the spike-in tissue, we recommend the generation of a ChIP-Seq data set before performing ChIP quantifications by qPCR.

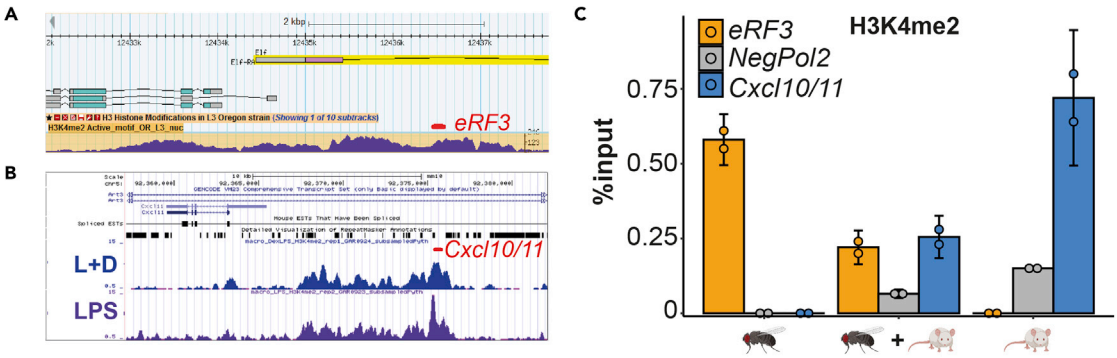

Figure 2. Selection and testing of species-specific PCR primers

(A) *Drosophila melanogaster* genome browser screen shot (http://gbrowse.modencode.org/fgb2/gbrowse/fly/) showing publicly available data for H3K4me2 ChIP-Seq at the *eRF3* (also known as *Elf*) locus.

(B) UCSC genome browser track for H3K4me2 ChIP-Seq in murine bone marrow derived macrophages after 3 h 100 ng/mL LPS (purple, lower track) or 16 h 1 μM dexamethasone and 3 h 100 ng/mL LPS treatment (L+D, blue, upper track) (Greulich et al., 2021).

(C) ChIP-qPCR against H3K4me2 in either pure S2 cells (indicated by the fly), 25% S2 cells mixed with 75% murine macrophages treated with 100 ng/mL LPS for 3 h (marked by the fly + mouse symbol) or pure murine macrophages treated with LPS (marked by the mouse symbol). The mean of two biological replicates is plotted. Dots represent single data points, and error bars reflect the standard deviation. The color indicates the locus. (A+B) The red lines indicate the fragments amplified by PCR in C. The DNA sequence of the regions covered by the H3K4me2 signal in both species was used as input for Primer-BLAST, in order to design the primers for C (https://www.ncbi.nlm.nih.gov/tools/primer-blast/, (Ye et al., 2012)).

Validate antibodies for specificity in target and spike-in species

Timing: 3 days

In order to confirm that the antibody indeed recognizes the protein of interest in both species and to validate the specificity of the PCR primer, perform ChIP-qPCR against the protein of interest (H3K4me2 in our case). Use the target species, the spike-in species and a mixture of target and spike-in species (10%–25% spike-in) as samples and follow the protocol below (steps 1–55). An example of the expected results are shown in Figure 2C. Here, we performed ChIP against H3K4me2 in *Drosophila* S2 cells, in murine bone marrow-derived macrophages treated with 100 ng/mL LPS for 3 h, and in a 1:4 mixture of *Drosophila* S2 cells with murine macrophages. The *Drosophila*-specific primers against H3K4me2 (*eRF3* locus) (Figure 2A) are only enriched in the samples containing chromatin from *Drosophila melanogaster*. On the other hand, the mouse-specific primers against a H3K4me2-positive (*Cxcl10/11*, Figure 2B) and H3K4me2-negative (NegPol2) locus give a specific signal in samples containing murine chromatin. In addition, we observe a higher enrichment at the positive (*Cxcl10/11*) over the negative (NegPol2) locus in murine macrophages, indicating specificity of the antibody (Figure 2C).

⚠ CRITICAL: The protein of interest needs to be conserved between target and spike-in species in order to be recognized by the antibody in both species (see limitations).

Material preparations

Timing: 30 min

8. Pre-cool centrifuges suitable for Eppendorf tubes to 4°C.
9. Turn on Bioruptor and pre-cool the water bath.
10. Prepare buffers (see materials and equipment) and aliquots of Fast IP, Shearing and Dilution, add EDTA-free proteinase inhibitors and store on ice.
11. Pre-heat thermomixers to 99°C, 37°C or 56°C.

KEY RESOURCES TABLE

REAGENT or RESOURCE	SOURCE	IDENTIFIER
Antibodies		
Rabbit polyclonal anti-H3K4me2	Abcam	Cat.#ab7766; RRID:AB_2560996
Rabbit normal IgG control	Cell Signaling	Cat.#2729 RRID:AB_1031062
Chemicals, peptides, and recombinant proteins		
cOmplete™, Mini, EDTA-free Protease Inhibitor Cocktail	Roche	Cat.#11836170001
cOmplete™ Ultra, EDTA-free Protease Inhibitor Cocktail	Roche	Cat.#5892953001
DPBS	Gibco	Cat.#14190144
16% Formaldehyde (w/v), Methanol-free	Thermo Fisher Scientific	Cat.#28906
Glycine, ReagentPlusTM, >= 99%	Sigma	Cat.#G7126
Dexamethasone	Sigma	Cat.#D4902
LPS E.COLI O111:B4	Sigma	Cat.#LPS25
5 M NaCl	Sigma	Cat.#71386
1 M Tris-HCl, pH 7.5	Invitrogen	Cat.#15567-027
1 M Tris-HCl, pH 8.0	Gibco	Cat.#15568-025
EDTA, 0.5 M sterile solution	VWR	Cat.#E177
NaOAc trihydrate, pure Ph. Eur.	AppliChem	Cat.#A1370
100× Tris-EDTA buffer solution	Sigma	Cat.#T9285
IGEPAL CA-630/NP40	Sigma	Cat.#I3021
Triton X-100	AppliChem	Cat.#A1388
SDS solution 20% (BioUltra for molecular biology)	Sigma	Cat.#05030
Tween 20	AppliChem	Cat.#A1389
$NaHCO_3$ Ph. Eur.	AppliChem	Cat.#A1353
BSA (molecular biology grade)	Sigma	Cat.#A3294
Nuclease-free water	Sigma	Cat.#W3513
RNase A (DNase free)	AppliChem	Cat.#A38320050
Proteinase K from Tritrachium album	Sigma	Cat.#P6556
Glycerol 86%	Roth	Cat.#4043.3
Dynabeads M-280 Sheep Anti-Rabbit IgG	Life Technologies	Cat.#11204D
peqGreen	PeqLab	Cat.#37-5010
peqGOLD Universal-Agarose	VWR	Cat.#732-2789
GeneRuler 100 bp DNA Ladder	Thermo Fisher Scientific	Cat.#SM0241
Acetic acid 100%	Merck Millipore	Cat.#818755
Sepharose Protein A/G beads	Rockland	Cat.#PAG50-00-0002
Power SYBR Green Master Mix	Thermo Fisher Scientific	Cat.#4367659
Agencourt AMPure XP beads	Beckman Coulter GmbH	Cat.#A63881
Ethanol absolute for molecular biology	AppliChem	Cat.# A3678
Critical commercial assays		
MinElute PCR Purification Kit	QIAGEN	Cat.#28006
Kapa HyperPrep Kit	Roche	Cat.#7962363001
KAPA Library Quantification Kit Illumina-Rox Low	Roche	Cat.#7960336001
High Sensitivity DNA Kit	Agilent	Cat.# 5067-4626
Qubit dsDNA HS Assay Kit	Life Technologies	Cat.#Q32854
Gel Cassettes, Pippin Prep, dye-free	Sage Science	Cat.#CDF2010
Deposited data		
ChIP-Seq in RAW264.7	Greulich et al 2021	GEO:GSE138017
Experimental models: Cell lines		
S2 cells (*Drosophila*)	Provided by Prof. P. Becker (LMU Munich, Germany)	RRID:CVCL_Z232
RAW264.7	ATCC	Cat.#TIB-71™ ; RRID:CVCL_0493
RAW264.7 *Setd1a*$^{Del/+}$	Greulich et al.2021	

(*Continued on next page*)

Continued

REAGENT or RESOURCE	SOURCE	IDENTIFIER
Experimental models: Organisms/strains		
Oligonucleotides		
*Fkbp5*_forward AGCGTAAGATCGCGAGAGTG	Eurofins	N/A
*Fkbp5*_reverse AACGTCGAGGGTGGAGAGTA	Eurofins	N/A
NegPol2_forward TAGCTTTCGACAGAGGTCCTAAG	Eurofins	N/A
NegPol2_reverse CCGAAGGTGGCCGGTTGT	Eurofins	N/A
*eRF3*_forward TGTTAACAATCACGGCGCAT	Eurofins	N/A
*eRF3*_reverse AAACGACACCACAAAGCGAA	Eurofins	N/A
*Cxcl10/11*_forward CCAGGCTATGCGATGGTTCA	Eurofins	N/A
*Cxcl10/11*_reverse GATAAGAGCTGACCCGGCAA	Eurofins	N/A
TruSeq Illumina universal adapter AATGATACGGCGACCACCGAGATCTACACT CTTTCCCTACACGACGCTCTTCCGATC*T	IDT	N/A
TruSeq Illumina index adapter Phos/GATCGGAAGAGCACACGTCTG AACTCCAGTCACNNNNNNATCTCGT ATGCCGTCTTCTGCTTG	IDT	N/A
Software and algorithms		
FastQC	http://www.bioinformatics.babraham.ac.uk/projects/fastqc/	RRID:SCR_014583
Trimmomatic	Bolger et al. 2014	RRID:SCR_011848; http://www.usadellab.org/cms/index.php?page=trimmomatic
BWA-MEM v0.7.13	Li et al. 2009	RRID:SCR_010910; https://sourceforge.net/projects/bio-bwa/files/
Picard Tools v2.0.1	http://picard.sourceforge.net/).	RRID:SCR_006525
Samtools v1.8	Li et al. 2009	RRID:SCR_002105; http://www.htslib.org/
Deeptools v3.0.2-1	Ramirez et al. 2014	RRID:SCR_016366; https://deeptools.readthedocs.io/en/develop/
Integrated genome browser v9.0.2	Freese et al. 2016	RRID:SCR_011792; https://www.bioviz.org/
MACS2 v2.1.1.20160309	Zhang et al. 2008	RRID:SCR_013291; https://github.com/macs3-project/MACS
BEDtools v2.25.0	Quinlan and Hall 2010	RRID:SCR_006646; https://bedtools.readthedocs.io/en/latest/#
DESeq2 v1.30.1	Love et al. 2014	RRID:SCR_015687; https://bioconductor.org/packages/release/bioc/html/DESeq2.html
GenomicRanges v1.42.0	Lawrence et al. 2013	RRID:SCR_000025; https://www.bioconductor.org/packages/2.13/bioc/html/GenomicRanges.html
R v3.6.1	Team 2017	RRID:SCR_001905; https://cran.r-project.org/
Other		
Bioruptor 300 with water cooler	Diagenode	Cat. # B01060001, B02010002, B02020004
QuantStudio 6 and 7	Applied Biosystems	N/A
DynaMag-2	Thermo Fisher Scientific	Cat. #12321D
DynaMag-PCR	Thermo Fisher Scientific	Cat. #492025
Qubit 2.0	Thermo Fisher Scientific	Cat. #Q32871
Pippin Prep	Sage Science	N/A
NovaSeq 6000	Illumina	N/A
Bioanalyzer 2010	Agilent	N/A

Alternatives: Any supplier may provide chemicals. Chemicals should be molecular-biology grade.

Alternatives: ChIP fragmentation with the Bioruptor might be other sonication devices like the Covaris systems (https://www.covaris.com/products-services/instruments) or probe sonicators. Alternatively, chromatin can be fragmented enzymatically using micrococcal nuclease (MNase). Either way, the optimal conditions have to be established before performing the actual ChIP experiment.

Alternatives: Any other equipment supplier may provide equivalent equipment.

MATERIALS AND EQUIPMENT

Buffers		
1% formaldehyde (FA)	Final concentration	Amount
Formaldehyde* (16%, MeOH-free)	1% vol/vol	1 mL
DPBS (1×)	1×	15 mL
Total		**16 mL**
1% formaldehyde can be stored at 4°C–8°C for up to 1 day.		

1 M glycine	Final concentration	Amount
Glycine	1 M	75.07 g
DPBS (1×)	1×	1 l
Total		**1 l**
Sterilize by filtering using a 0.22-μm filter. Store 1 M glycine at 18°C–24°C for up to 1 year. Always prepare aliquots.		

Fast IP buffer	Final concentration	Amount
NaCl (5 M)	150 mM	33.3 mL
Tris-HCl pH=7.5 (1 M)*	50 mM	50 mL
EDTA pH=7.5 (0.5 M)	5 mM	10 mL
NP-40/IGEPAL CA-630 (100%)	0.5% vol/vol	5 mL
Triton X-100 (100%)*	1% vol/vol	10 mL
ddH2O	N/A	891.7 mL
Total		**1 L**
Sterilize by filtering using a 0.22 μm filter. Store Fast IP Buffer at 4°C for up to 6 months. Always prepare aliquots.		

Shearing buffer	Final concentration	Amount
SDS (20%)*	1% vol/vol	50 mL
EDTA pH=8.0 (0.5 M)	10 mM	20 mL
Tris-HCl pH=8.0 (1 M)*	50 mM	50 mL
ddH2O	N/A	880 mL
Total		**1 l**
Sterilize by filtering using a 0.22 μm filter. Store Shearing Buffer at 18°C–24°C for up to 6 months. Always prepare aliquots.		

Alternatives: If the SDS concentration is too high for a particular antibody (Troubleshooting 7), low-SDS shearing buffers with SDS contents as low as 0.1% can be tried. **Note** that sonication conditions need to be re-established when changing the shearing buffer. We have observed prolonged sonication times (Bioruptor) to be required when reducing the SDS content.

Alternatives: Add 0.1% Triton X-100 to avoid SDS precipitation while shearing especially if longer sonication times are required.

Dilution buffer	Final concentration	Amount
SDS (20%)*	0.01% vol/vol	0.5 mL
Triton X-100 (100%)*	1.1% vol/vol	11 mL
EDTA pH=8.0 (0.5 M)	1.2 mM	2.4 mL
Tris-HCl pH=8.0 (1 M)*	16.7 mM	16.7 mL
NaCl (5 M)	167 mM	33.4 mL
ddH2O	N/A	936 mL
Total		**1 l**
Sterilize using a 0.22 μm filter. Store Dilution Buffer at 4°C for up to 6 months. Always prepare aliquots.		

Library elution buffer (LEB)	Final concentration	Amount
Tris-HCl pH=8.0 (1 M)*	10 mM	100 μL
Tween-20 (100%)	0.05% vol/vol	5 μL
Nuclease-free water	N/A	9.9 mL
Total		**10 mL**
Store LEB buffer at 18°C–24°C for up to 2 days.		

1× TE buffer	Final concentration	Amount
100× TE (0.2 μm-filtered, 1 M Tris and 100 mM EDTA)	1× (10 mM Tris and 1 mM EDTA)	100 μl
Nuclease-free water	N/A	9.9 mL
Total		**10 mL**
Store TE buffer at 18°C–24°C for up to 1 month.		

3 M NaOAc pH=5.2	Final concentration	Amount
NaOAc (molecular biology-grade, anhydrous)	3 M	82.03 g
Nuclease-free water	N/A	1 l
Total		**1 l**
Adjust pH to 5.2 with acetic acid* and filter with a 0.22 μm filter. Store NaOAc at 18°C–24°C for up to 1 year.		

10 mg/mL RNase A stock	Final concentration	Amount
RNase (DNase-free)	10 mg/mL	50 mg
1× TE buffer	1×	5 mL
Total		**5 mL**
Aliquot and store RNase A at −20°C for up to one year. Aliquots might be thawed for up to 5 times.		

10 mg/mL Proteinase K stock	Final concentration	Amount
Proteinase K	10 mg/mL	100 mg
Nuclease-free water	N/A	10 mL
Total		**10 mL**
Aliquot and store proteinase K at −20°C for up to one year. Aliquots might be thawed for up to 5 times.		

5% BSA	Final concentration	Amount
BSA	5% w/v	2.5 g
Nuclease-free water	N/A	50 mL
Total		**50 mL**
Filter the buffer with a 0.45 μm syringe filter. Aliquot and store 5% BSA at −20°C for up to one year. Aliquots might be thawed for up to 5 times.		

6× color-less loading dye	Final concentration	Amount
Glycerol (89%)	30% vol/vol	340 µl
Nuclease-free water	N/A	660 µl
Total		**1 mL**
The loading dye is stable at 8°C for 6 months.		

1 M $NaHCO_3$	Final concentration	Amount
$NaHCO_3$ (molecular biology-grade)	1 M	84 mg
Nuclease-free water	N/A	1 mL
Total		**1 mL**
1 M $NaHCO_3$ needs to be prepared freshly and only lasts for 2–3 h at 18°C–24°C.		

Bead elution buffer	Final concentration	Amount
fresh $NaHCO_3$ (1M)	100 mM	100 µl
SDS* (20%)	1% vol/vol	50 µl
Nuclease-free water		850 µl
Total		**1 mL**
Bead Elution Buffer needs to be prepared freshly and is stable at 18°C–24°C for 2–3 h.		

50× TAE buffer	Final concentration	Amount
Tris base	2 M	484.0 g
Acetic Acid* (100%)	1 M	114.2 mL
EDTA (di-sodium salt)	0.05 M	37.2 g
Deionized H_20	N/A	Fill to 2 l
Total		**2 l**
The pH of the buffer should be 8.3 and it can be stored at 18°C–24°C for 6 month.		

1× TAE buffer	Final concentration	Amount
50× TAE buffer	1×	100 mL
Deionized H_20	N/A	4.99 l
Total		**5 l**
The buffer can be stored at 18°C–24°C for 6 month.		

Note: For the Fast IP, Shearing and Dilution Buffers, prepare aliquots before starting the experiment and add EDTA-free proteinase inhibitors freshly. These solutions are stable for 1 day at 4°C.

⚠ CRITICAL: Harmful chemicals are indicated with an asterisk (*) here or in the following protocol.

Formaldehyde

Flammable liquid and vapor. Harmful if swallowed. Causes severe skin burns and eye damage. May cause an allergic skin reaction. Causes serious eye damage. Toxic if inhaled. May cause cancer (inhalation). Toxic to aquatic life. Only work with formaldehyde when specifically instructed. Keep away from heat sources and open flames. Take precautionary measures against static discharge. Do not eat, drink or smoke when using formaldehyde. Avoid environmental release. Wear protective

clothing, protective gloves, eye and face protection. Wash contaminated clothing before reuse. Store in well-ventilated cabinets and keep containers tightly closed. Dispose of content and containers to comply with local regulatory authorities.

Ethanol

Highly flammable liquid and vapor. Causes serious eye damage/irritation. Keep Ethanol away from heat sources, open flames. Do not smoke. Keep containers tightly closed. Large amounts should be stored in fireproof cabinets.

Acetic acid

Flammable liquid and vapor. Harmful if inhaled. Causes severe skin burns and eye damage. Causes serious eye damage. Harmful to aquatic life. Keep away from heat sources. Store in fireproof cabinets. Take precaution measures against static discharge. Wash exposed skin thoroughly after handling. Only work in well-ventilated areas or under the fume hood. Wear protective clothing, protective gloves, eye and face protection.

SDS

Flammable solid. Harmful if swallowed or inhaled, causes skin irritation or serious eye damage. May cause respiratory irritation. Harmful to aquatic life with long lasting effects. Keep away from heat sources. Avoid breathing dust by using pellets or masks. Wear protective clothing and eye protection.

Tris-HCl

May cause eye and skin irritation. Wear protective clothing.

Triton X-100

Harmful if swallowed. Causes serious eye damage. Toxic to aquatic life with long lasting effects. Do not eat, drink or smoke when using Triton X-100. Avoid environmental release. Wear protective gloves/eye protection.

RNase A

May cause allergy or asthma symptoms or breathing difficulties if inhaled. Avoid breathing dust/vapor.

Proteinase K

Causes skin irritation. May cause allergic skin reaction. Causes serious eye irritation. May cause allergy or asthma symptoms or breathing difficulties if inhaled. May cause respiratory irritation. Do not breathe dust. Wear protective gloves/eye protection.

STEP-BY-STEP METHOD DETAILS

Cell lysis

Timing: 30 min

In this step, the frozen, formaldehyde-fixed pellets from target and spike-in cells are processed for cell lysis. All steps are performed on ice.

Note: Target and spike-in cells are processed separately to allow for alternative cell lysis protocols e.g., when working with tissues instead of cell lines.

Alternatives: If the cell lysis and sonication conditions for target and spike-in cells are identical, both might already be mixed in step 2.

1. Thaw target and spike-in cell pellets on ice.

   Note: For one ChIP-seq experiment targeting a transcription factor, use 40 M cells, and for histone marks, use 20 M cells. For ChIP-qPCR, 2 M cells per IP are recommended. 5% of the experimental cell number is required for spike-in per ChIP-seq experiment, and 15%–25% should be used for ChIP-qPCR. Use spike-in pellets accordingly.

   ⚠ CRITICAL: The amount of spike-in chromatin must be adjusted depending on the genome size differences between the target and spike-in species and according to the genomic coverage of the protein of interest. The above-mentioned amount of spike-in chromatin is optimized for murine cells combined with *Drosophila* spike-in, and for performing ChIP-Seq against widely occurring histone marks such as H3K4me1/me2/me3 or H3K27ac. See Troubleshooting 5.

2. Resuspend 20 M cells in 1 mL ice-cold FastIP buffer. Let the chromatin sit on ice for 10 min. During this time, pull the cell suspension through an insulin syringe once for mechanical cell lysis.
3. Spin at 12,000 × *g* for 1 min at 4°C. Aspirate the supernatant using either vacuum or a pipette. Leave the pellet untouched. Some liquid may remain.
4. Repeat steps 2 and 3.

   ⚠ CRITICAL: Cell and tissue lysis needs to be optimized individually for each tissue or cell line. We refer to Mir at al. (Mir et al., 2019) for recommendations.

Spike-in and sonication

Timing: 30 min per 3 samples (depending on the Bioruptor tube holder)

In this step, 5% of spike-in chromatin is mixed with the target chromatin and fragmented by sonication.

5. Resuspend cell pellets completely in 1 mL ice-cold Shearing Buffer per 20 M cells.

   ⚠ CRITICAL: The Shearing Buffer needs to be cold but not "cloudy". In case of SDS precipitation, warm the sample briefly and vortex it to solubilize all precipitates.

6. Shortly before distributing the spike-in chromatin, mix spike-in nuclei very well and add 5% of spike-in per target chromatin per 1.5 mL Bioruptor TPP tube.

   Note: For sonication in 1.5 mL Bioruptor TPP tubes, do not fill the tube with more than 550 µl of chromatin, to ensure a complete immersion of the liquid-filled tube in the water bath. If 20 M target cells are resuspended in 1 mL Shearing Buffer and 10 M spike-in cells in 500 µl Shearing Buffer, aliquot 25 µl spike-in nuclei per 1.5 mL Bioruptor tube and add 500 µl of target chromatin. Two Bioruptor tubes per 20 M target cells are required during sonication.

Troubleshooting 1: Different sonication conditions for target and spike-in cells or tissues.

7. Continue with sonication using a Bioruptor 300 or similar model (Diagenode).

   Note: If the Bioruptor tube holder cannot fit all the tubes in one round, distribute aliquots from the same sample across different rounds to avoid sonication biases introduced by the samples being in different sonication rounds.

8. Unite the sheared chromatin from each sample aliquot inside a 2 mL low binding Eppendorf tube and store on ice until proper sonication is confirmed by fast-reverse cross-linking.

Fast reverse cross-linking

Timing: 2–3 h

Here, the appropriate size of the chromatin fragments is validated before proceeding with immunoprecipitation.

9. Take 20 µL of sheared chromatin from each sample (e.g., experimental condition) and adjust the volume to 100 µL with 1×TE buffer.
10. Add 4 µL 5 M NaCl and incubate at 99°C for 15 min mixing at 1,000 rpm in a thermomixer.
11. Remove samples from the thermomixer and wait for them to cool down to 18°C–24°C.
12. Add 0.5 µL RNase A* (10 mg/mL stock). Incubate for 15 min at 37°C and 300 rpm.
13. Add 4 µL 1 M Tris-HCl* pH=7.5, 2 µL 0.5 M EDTA pH=8 and 1 µL Proteinase K* (10 mg/mL stock). Incubate at 56°C for 1 h, while mixing at 300 rpm.
14. Purify the samples with the MinElute PCR purification kit (QIAGEN) following the manufacturer's instructions. Elute the samples in 15 µL elution buffer.

Note: Adjust the pH of the PB buffer if the color is not yellow, by adding 1 µl 3 M NaOAc pH=5.2.

15. Mix each sample with 4 µl of 6× colorless DNA loading dye and load onto a 0.7% agarose gel containing peqGreen or similar.

Note: Dyes in the sample loading buffer might lower the fluorescence intensity of the sample DNA at the front of the dye and thereby affect the visibility of the fragmented chromatin.

16. If required, add additional sonication cycles and repeat the fast reverse crosslink.

⚠ CRITICAL: The fragment size of the chromatin should be comparable between all samples under study. See Figure 3 for an example.

Immunoprecipitation

Timing: 2 days

In this step, the chromatin fraction bound by the factor of interest is purified using immunoprecipitation (IP).

17. Leave the fragmented chromatin at 18°C–24°C until all SDS precipitates are dissolved. Occasionally vortex samples gently. (1–2 min)
18. Centrifuge at 12,000 × *g* for 10 min at 4°C.
19. Take the top 90% of each sample's supernatant (900 µl for one 20 M cell pellet) into a 15 mL conical tube. Do not touch the pellet (cell debris).
20. Transfer 9 µl of supernatant from each sample to a 1.5 mL tube as an input control (1% input) and freeze at −20°C until de-crosslinking in step 41. Discard the remaining volume and the pellet.

Note: The amount of input material might be increased to 10%, if an independent input sample is required for sequencing. Adjust the percentage input calculations accordingly.

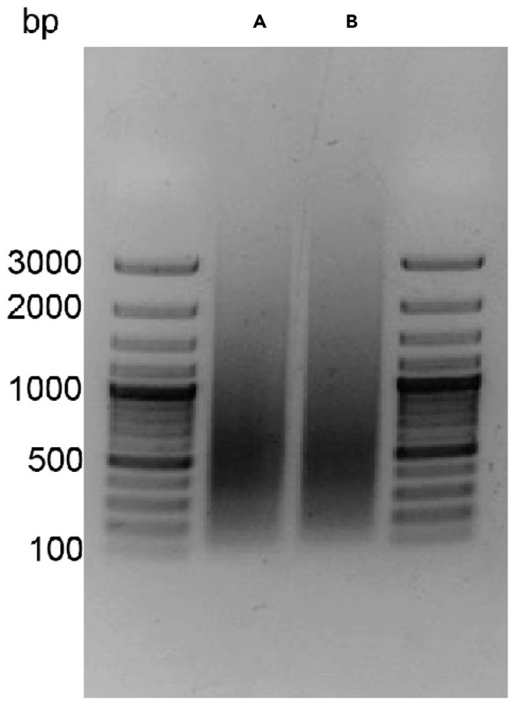

Figure 3. DNA fragment size verification
Purified DNA form macrophages treated with LPS (A) or LPS plus Dexamethasone (B) was loaded onto a 0.7% agarose gel stained with peqGreen DNA dye. Each sample contains 5% spike-in chromatin from *Drosophila* S2 cells

21. Add 8.1 mL Dilution Buffer to the 15 mL conical tube containing the sample (1:10 dilution of the sheared chromatin).

Note: For ChIP-qPCR, take 10% input (9 µl) and 90 µl of chromatin per IP. Dilute the chromatin with 810 µl of dilution buffer and perform IPs in 1.5 mL low binding Eppendorf tubes. Adjust the percentage input calculations accordingly.

Alternatives: If the epitope of interest is expressed at low levels or if the antibody affinity is low, reducing the dilution of the sheared chromatin might be advantageous. In this case, reduce the amount of SDS in the shearing buffer (see Troubleshooting 7).

Alternatives: An additional pre-clearing step might be included, in the event that high background signal is detected (see Troubleshooting 7).

22. Add 4 µg of antibody to each 15 mL conical tube containing the diluted sample.

Note: For ChIP-qPCR, use 1 µg of antibody for each IP.

Note: Antibody concentrations need optimization and depend on the antibody affinity and the amount of epitope present within the sample.

Note: Antibodies must be tested for specificity. See Troubleshooting 2.

23. Rotate tubes 12–16 h at 4°C.

24. Block Dynabeads.

Note: The type of beads depends on the isotype and species of the ChIP antibody. For polyclonal antibodies raised in rabbit, we recommend sheep anti-rabbit IgG Dynabeads (Life Technologies).

a. Transfer 60 μL of well suspended Dynabeads/IP from the stock bottle into a 1.5 mL low binding tube and place the tube into a magnetic rack.
b. Add 1 mL Dilution Buffer. Remove the tube from the rack and resuspend the beads by inverting and flicking the tube.
c. Place the tube back into the magnetic rack and wait for 30 s until the liquid is cleared from the beads.
d. Aspirate the supernatant without disturbing the beads.
e. Repeat b-d twice more.
f. Add 1 mL Dilution Buffer supplemented with 0.5% BSA (molecular biology-grade), completely resuspend the beads by flicking the tube and incubate 12–16 h at 4°C while rotating slowly.

Note: For ChIP-qPCR, use 20 μL of sepharose protein A/G beads per IP. Instead of the magnetic rack, spin the beads 30 s at 300 × *g* for washing. Take care to **never** vortex sepharose beads.

Alternatives: Dynabeads perform equally well in ChIP-qPCR.

25. The next day, spin the 15 mL conical tubes containing the IP for 20 min at 3,600 × *g* at 4°C.

Note: For ChIP-qPCR, spin IPs at 12,000 × *g* for 10 min at 4°C (1.5 mL Eppendorf tubes).

26. During the centrifugation, wash the blocked beads 3 times in Dilution Buffer.
    a. Place the Dynabeads in the magnetic rack. Wait 30 s until all beads are collected and the liquid is cleared.
    b. Aspirate the supernatant carefully without losing beads.
    c. Add 1 mL Dilution Buffer, remove the tube from the magnetic rack and resuspend the beads by flicking the tube.
    d. Place the Dynabeads inside the magnetic rack. Wait 30 s until all the beads are collected and the liquid cleared, and aspirate the supernatant carefully.
    e. Repeat c-d twice more.
    f. Resuspend beads in 65 μl Dilution buffer/IP.

Note: For sepharose beads, spin the beads 30 s at 300 × *g* and 4°C instead of using the magnetic rack.

27. Aliquot 15 μL Dynabeads into fresh 2 mL low binding Eppendorf tubes (4 tubes for one 20 M cell pellet).
28. After centrifugation, take the top 90% (approx. 8 mL) of chromatin. On ice, aliquot 2 mL per 2 mL low binding Eppendorf tube containing Dynabeads beads (from step 27).

Note: For ChIP-qPCR, transfer the top 90% of the chromatin (800 μl) into a new 1.5 mL low binding tube that contains 20 μL of sepharose beads in Dilution Buffer.

29. Incubate for 6 h at 4°C while slowly rotating the tubes.
30. *Note:* For ChIP-qPCR, incubate for 3 h at 4°C while rotating. On ice, wash the beads with the immobilized chromatin of interest with FAST IP Buffer. Place magnetic racks on ice.
    a. Place the 2 mL Eppendorf tubes inside the magnetic rack. Wait for 30 s until the liquid is cleared.
    b. Aspirate the supernatant and add 1 mL ice-cold Fast IP buffer.
    c. Take the tubes from the magnetic rack and mix by inverting and flicking the tubes. Let the samples sit on ice for 2 min.
    d. Repeat a-c four more times.

Note: For sepharose beads, spin beads 30 s at 300 × *g* and 4°C instead of using the magnetic rack.

31. During the washes, prepare the Bead Elution Buffer.

Note: Steps 32 and 33 are only required for ChIP-seq samples

32. After the fifth wash, add 100 µL ice-cold 1 × TE buffer to each tube. Unite the beads from the four 2 mL tubes (for one 20 M cell pellet) by removing the tubes from the magnetic rack and resuspending the beads with the P200. Collect all beads from one sample in one tube. Afterward, one tube with 400 µl bead suspension per sample remains.
33. Add another 50 µL ice-cold 1 × TE buffer to each one of the empty tubes, resuspend any remaining beads and unite with the beads from step 32 (650 µl beads in 1 ×TE).
34. Place the tubes into the magnetic rack, wait 1 min until the solution is cleared, and carefully remove the supernatant with a pipette. Be careful, the beads will only be loosely attached in TE buffer.

Note: For ChIP-qPCR, the steps 32 and 33 are not required, since every tube is a separate IP.

35. Add 1 mL 1 × ice-cold TE buffer, resuspend the beads by inversion and by flicking the tubes, and place them back into the magnetic rack. Wait 1 min until the solution is cleared.
36. Carefully pipet the TE buffer off using a pipette. Shortly spin the beads and transfer the tube back to the magnetic rack. Remove any remaining supernatant.

Note: For sepharose beads, spin beads 30 s at 300 × *g* and 18°C–24°C instead of using the magnetic rack.

37. Add 100 µL Bead Elution Buffer per tube, vortex and incubate 15 min at 18°C–24°C and 1,000 rpm in a thermomixer.

Note: For ChIP-qPCR, add 50 µL Bead Elution Buffer to each IP.

38. Place the tubes into the magnetic rack and collect the supernatant into fresh 1.5 mL low binding Eppendorf tubes.
39. Add another 100 µL Bead Elution Buffer to the beads, vortex and incubate again inside the thermomixer for 15 min at 18°C–24°C and 1,000 rpm.

Note: For ChIP-qPCR, add 50 µL bead elution buffer and spin beads 30 s at 300 × *g* and 18°C–24°C instead of using the magnetic rack.

40. Shortly spin the tubes in a bench top centrifuge. Place the tubes into the magnetic rack and collect the supernatant into the 1.5 mL tubes from step 38. The final volume of the eluted chromatin is 200 µL.

Note: For ChIP-qPCR, the final volume should be 100 µL.

41. Thaw the input sample and adjust the volume of the input sample to 200 µL using 1 × TE buffer.
42. Add 8 µL of 5 M NaCl to the 200 µL eluted chromatin and input, vortex and heat at 65°C for 12–16 h. Do not shake.

Note: For ChIP-qPCR, adjust the volume of the input sample to 100 µL and add 4 µL of 5 M NaCl.

DNA purification

Timing: 3 h

In this step, the chromatin is de-crosslinked and the DNA is purified.

43. Add 1 μL of RNase A* (10 mg/mL stock) to the eluted DNA and input samples.
44. Incubate for 30 min at 37°C and 300 rpm in a thermomixer.
45. Add 4 μL 0.5 M EDTA pH=8, 8 μL 1 M Tris-HCl* pH=7.5 and 1 μL Proteinase K* (10 mg/mL stock).
46. Incubate in a thermomixer for 2 h at 56°C and 300 rpm.

47. Purify the de-crosslinked chromatin using the MinElute PCR purification kit from QIAGEN.
    a. Add 1,110 μL PB buffer and 50 μL 3M NaOAc pH=5.2. The color of the pH indicator should be yellow.

Note: For ChIP-qPCR, add 500 μL PB buffer and 20 μL 3M NaOAc pH 5.2.

    b. Mix with a pipette and load 700 μl de-crosslinked chromatin in PB buffer onto the spin column and spin at 20,000 × *g* for 30 s at 18°C–24°C.
    c. Discard the flow-through.
    d. Repeat step b with the remaining chromatin.
    e. Wash with 750 μL PE buffer (containing EtOH*) to the spin column.
    f. Spin at 20,000 × *g* for 30 s and discard the flow- through.
    g. Spin the empty column at 20,000 × *g* for 1 min to remove residual PE buffer.
    h. Add 16 μL EB buffer and spin at 20,000 × *g* for 1 min.

Pause point: For ChIP-seq, the purified ChIP DNA might be stored at −20°C until libraries can be prepared. Before freezing the samples, take a 2 μl aliquot for qPCR (see steps 48–55)) and another 1–2 μl aliquot to measure the DNA concentration with Qubit. Avoid freeze and thaw cycles.

⚠ CRITICAL: Purified DNA for ChIP-qPCR is very unstable due to its low concentration. ChIP samples with lowly concentrated DNA tend to lose a higher fraction of DNA to adsorption by the tube walls and subsequent denaturation of smaller fragments (Gaillard, 1998; Zhong et al., 2017). Low-concentrated ChIP DNA (as from ChIP-qPCR) should be processed immediately. The maximal storage time is 12–16 h at −20°C.

Quantitative PCR (qPCR)

Timing: 3 h

In this step, the enrichment is quantified. It serves as a quality control of ChIP samples designated for sequencing.

48. Thaw SYBR Green PCR master mix and prepare 10-μM dilutions of the primers for at least one negative and positive locus.
49. Take 2 μl from the eluted ChIP or input DNA, and add 118 μl of nuclease-free water (1:60 dilution). This is sufficient for 8 qPCRs in a 384-well format when performing triplicates.

Note: For ChIP-qPCR experiments, only dilute the eluted DNA (ChIP or input) 1:15 at the highest, depending on how many qPCRs will be performed. Further dilution will make the spike-ins undetectable.

50. Create five standards by making serial dilutions of the input samples, as indicated in the following table:

Standard	Dilution
Std1	1:2 from **all** diluted inputs (step 49)
Std2	1:10 from Std1
Std3	1:10 from Std2
Std4	1:10 from Std3
Std5	1:10 from Sdt4

51. Further dilute the input 1:5.
52. Add 4.5 µl of each standard, water (as non-template control), input and ChIP samples to 3 of the 384 wells each (triplicates).
53. Prepare the qPCR master mix based on the following table. Replace n by the number of ChIP samples (including all input samples).

qPCR master mix			
Reagent	Final concentration	Amount per reaction	Amount
SYBR Green PCR master mix (2×)	1×	5 µL	5 × 3 × (n + 6)
Forward primer (10 µM)	0.25 µM	0.25 µL	0.25 × 3 × (n + 6)
Reverse primer (10 µM)	0.25 µM	0.25 µL	0.25 × 3 × (n + 6)
Total		5.5 µL	5.5 × 3 × (n + 6)

54. Run the following protocol on the qPCR machine:

qPCR cycling conditions			
Steps	Temperature	Time	Cycles
Initial activation/denaturation	95°C	10 min	1
Denaturation	95°C	15 sec	45×
Annealing/extension/data acquisition	60°C	1 min	

Optional: Run a melt curve analysis.

55. Confirm that the reaction efficiency is between 90%–110% by analyzing the standard curve.

Quality control

Before proceeding to library preparation, the following two quality control standards must be met.

56. Specific enrichment for the factor of interest, as determined by ChIP-qPCR.

Test the enriched chromatin for a positive locus occupied by the factor of interest **and** for a negative locus that should not be bound by the factor of interest (see Figure 6).

Note: The negative control is of utmost importance, as ChIP-seq experiments are not usually compared to IgG controls to test whether an antibody is specific.

57. The majority of the input chromatin should be fragmented between 200 and 1500 bp as determined by agarose gel electrophoresis (see Figures 1 and 3).

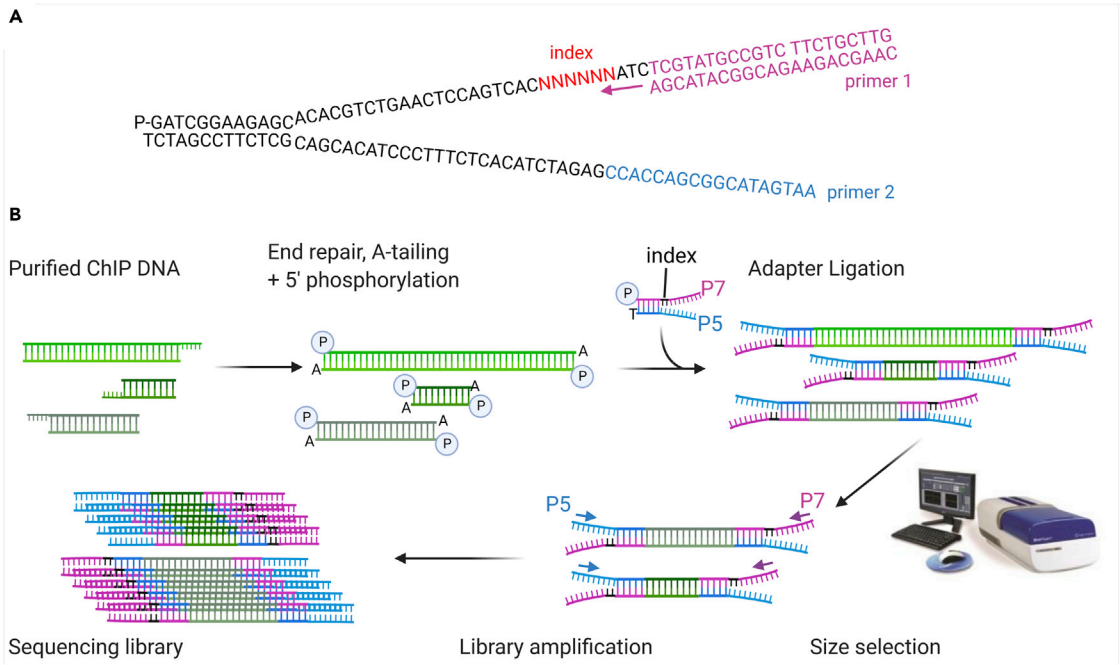

Figure 4. Library preparation

(A) Sequence of adapters (single index) used in our protocol. Red nucleotides mark the barcode/index sequence, purple and blue colors show the primer and the primer-binding site for each of the primers used during library amplification (step 69). Those lie within the universal part of the adapter.

(B) Schematic view of the four major steps of library preparation, including end-repair, A-tailing, adapter ligation, size selection and library amplification.

Library preparation

Timing: 2 days for 1 to 20 libraries

Timing: 3 h until next pause point per five libraries for steps 66 and 67

Timing: approx. 3–16 h for step 68

Timing: 2 h depending on the cycle number for steps 69 and 70

Timing: 3 h for 1–10 libraries for step 71

In this part, the ChIP DNA is prepared for sequencing on an Illumina NGS machine using a ligation-based approach (see Figure 4).

58. Bring AMPure XP beads to 18°C–24°C.
59. Prepare fresh 80% EtOH* (molecular biology-grade) with nuclease-free water.
60. Prepare fresh Library Elution Buffer (LEB).
61. Quantify the ChIP and input DNA using Qubit.

Note: Input DNA has to be diluted at least 1:100 for Qubit quantification.

62. Dilute up to 5 ng of ChIP DNA in 50 µl nuclease-free water.

Note: If the ChIP DNA is undetectable, it might still be processed for library preparation (see Troubleshooting 3).

63. Perform end repair and A-tailing
    a. Prepare one end repair reaction per sample in a PCR tube as follows:

End repair reaction	
Reagent	Amount
Diluted ChIP DNA	50 µL
End Repair & A-Tailing Buffer	7 µL
End Repair & A-Tailing Enzyme Mix	3 µL
Total	**60 µL**

    Buffers and enzymes are from the KAPA HyperPrep Kit.
    b. Mix thoroughly and spin samples using a benchtop centrifuge.
    c. Incubate the samples in a thermocycler with the following program, and proceed to the next step immediately:

PCR cycling conditions			
Steps	Temperature	Time	Cycles
End repair, A-tailing, 5′ phosphorylation	20°C	30 min	1
Heat inactivation	65°C	30 min	1
Hold	4°C	max. 2 h	

64. Adapter ligation (single index)
    a. Add the following reagents to the end-repaired and A-tailed ChIP DNA:

Ligation reaction		
Reagent	Amount	Note
End repair & A-tailing reaction product	60 µL	
Nuclease-free water	5 µL	Prepare Master mix
Ligation buffer	30 µL	
DNA ligase	10 µL	
3 µM Adapters	5 µL	
Total	**110 µl**	

    Buffers and enzymes are from the KAPA HyperPrep Kit.
    b. Mix thoroughly and spin samples shortly in a benchtop centrifuge.
    c. Incubate at 20°C for 15 min in a thermocycler and proceed to the next step immediately.

Note: The adapter identifies each sample. Accordingly, use different adapters for each sample and record the adapters used, to enable computational demultiplexing after sequencing. An adapter contains the primer binding sequence for the universal amplification primers in step 69, and a unique barcode (index) on one (single index) or both strands (dual index), which are required for the identification of each sample (see Figure 4). Adapters might be ordered from any oligonucleotide vendor.

We are using single index adapters here. However, dual indices are recommended for sequencing on Illumina NovaSeq 6000 machines to avoid index hopping.

65. Post-ligation Clean-up (0.8× AMPure XP bead clean-up)

⚠ CRITICAL: AMPure XP beads should be equilibrated to 18°C–24°C.

Note: Timing during AMPure XP bead clean-up is important, we therefore recommend to process at most 10 libraries at the same time. Multiple rounds of 10 purifications are possible.

a. Mix AMPure XP beads well and add 88 µl per 110 µl ligation reaction using a pipette. Mix reaction by pipetting up and down for 10×.
b. Incubate 5 min at 18°C–24°C.
c. Place PCR tubes in magnetic tube holder (8-stripe) and wait until the liquid is clear (1–3 min).
d. Remove 175 µl of the supernatant with a pipette and discard it.

⚠ CRITICAL: Do not disturb the beads.

e. Add 200 µl of freshly prepared 80% EtOH* without disturbing the beads. Incubate 1 min.
f. Remove all EtOH* with a pipet without disturbing the beads.
g. Dry beads at 18°C–24°C (2–5 min).

⚠ CRITICAL: Check each tube individually. Do not overdry beads. Overdried beads will show cracks.

h. Add 25 µl Library Elution Buffer to the beads, take the PCR tubes from the magnetic rack and pipet up and down for 10× times. Incubate 2 min at 18°C–24°C.
i. Place PCR tubes into the magnetic tube holder and wait until the liquid is cleared (1–5 min).
j. Transfer 22 µl of the supernatant to a fresh PCR tube.

Pause point: Adapter-ligated DNA can be stored at 4°C for one week or at −20°C for one month.

66. Size Selection with the Pippin Prep

Alternatives: Double-sided size selection with AMPure XP beads might be performed, but does not yield size ranges as accurately as the Pippin Prep. For a target range of 200–660 bp, 0.5× AMPure XP beads are added to the sample in the first step. Larger fragments are bound to the beads, while the desired fragments remain in the supernatant. New beads are added to the supernatant according to the following formula, using a left-sided ratio of 0.8×:

$$V(SPRIbeads) = V(sample) \times (left\ sided\ ratio - rigth\ sided\ ratio) = V(sample) \times 0.3$$

The desired fragments are bound by the beads and small fragments are discarded together with the supernatant. The procedure is the same as described in point 65 after adjusting for the AMPure XP bead ratio.

Note: With one Pippin Gel Cassette, size selection of up to five libraries can be performed. For more libraries, consecutive runs of Size Selection might be performed.

a. Turn the Pippin Prep on and create the following protocol:
   i. Select the correct cassette from the drop-down menu: "2% Marker E"
   ii. Select Range (turns orange).
   iii. Enter 200 into the "BP Start" and 600 in the "BP End" field.
   iv. Enter the sample ID.
   v. Press "Use Internal Standards", which will auto-fill the Reference Lane box.
   vi. "End Run when Elution is Completed"
   vii. Save the protocol.
b. Calibrate the Pippin Prep
   i. Press "Calibrate" on the control panel.
   ii. Put the calibration fixture onto the optical nest (dark-side down).
   iii. Close the lid and press "Calibrate".

iv. After calibration, press "EXIT" to return to the main menu.

c. Bring loading solution/marker mix to 18°C–24°C.

d. Add 8 μl of library elution buffer and 10 μl of loading solution/marker mix to each sample.

e. Mix thoroughly by vortexing and spin tubes in a benchtop centrifuge.

f. Unpack one 2% Dye-free Pippin Gel Cassette from the box and inspect it for cracks in the gel or for missing buffer (e.g., dried wells).

Note: Do not use cassettes with cracks or dried wells.

g. Check for air bubbles in the detection regions and behind the elution wells. Dislodge them by slightly tapping against the cassette.

Note: If an air bubble is visible between the plastic and the agarose, do not use this well.

h. Place the cassette into the optical nest of the Pippin Prep and remove the adhesive strips.

i. Refill buffer wells with less than 50% buffer.

j. Remove all buffer (approx. 50 μl) from the elution wells and replace with 40 μl fresh Electrophoresis Buffer.

Note: Carefully place the pipet tip at the bottom of the elution well for refill and move upwards with the buffer level to avoid the introduction of air bubbles.

k. Seal elution wells with the provided adhesive tape strips.

l. Fill sample wells with Electrophoresis Buffer (approx. 70 μl in total).

m. Run the Continuity test by pressing "TEST".

Note: If a separation lane fails the continuity test, check the sample well's buffer level. If the buffer is sufficient but the lane still fails, do not use this lane. If the elution channel failed, replace the elution buffer and rerun the continuity test. If it fails again, do not use this lane for any sample.

n. Fill up sample wells with Electrophoresis Buffer if required.

o. Remove 40 μl of Electrophoresis Buffer from each sample well that will be used.

p. Load 40 μl of sample into each well.

Note: Place the pipet tip just below the buffer level and follow the liquid level while loading the sample to avoid air bubbles.

q. Select the prepared protocol and press "START". One run takes approx. 2.5 h.

r. After the run, collect the samples by removing the adhesive tape from the top of the elution wells and carefully pipet 40 μl of eluted DNA into a fresh PCR tube using a pipette.

67. Concentrate the size-selected library with AMPure XP beads

a. Combine 72 μl of well-mixed AMPure XP beads with 40 μl of size-selected ChIP DNA and mix with a pipet (10 times).

b. Proceed with the AMPure XP bead purification as described in points 66b-g.

c. Add 26 μl Library Elution Buffer to the beads, take the PCR tubes from the magnetic rack and pipet up and down 10 times. Incubate for 2 min at 18°C–24°C.

d. Place PCR tubes into the magnetic tube holder and wait until the liquid is cleared (1–5 min).

e. Transfer 24 μl of the supernatant to a fresh PCR tube.

Pause point: ChIP DNA can be stored at 4°C for up to 24 h after size selection. Do not freeze.

68. Kapa Library Quantification

Library quantification estimates the amount of adapter-ligated ChIP DNA and is required to estimate the number of amplification cycles for the library.

a. Prepare serial dilutions of the ChIP DNA in Library Elution Buffer (LEB) as follows:

Serial dilution of ChIP DNA		
Dilution	Volume	Volume LEB
1:500	1 µl ChIP DNA	499 µl
1:1000	100 µl 1:500 dilution	100 µl
1:2000	100 µl 1:1000 dilution	100 µl

b. Load 4 µl of each standard (provided by the KAPA Library Quantification Kit) and sample into a 384-well plate. Perform assay in triplicates.

Note: The standard concentrations are as follows: Std 1: 20 pM; Std2: 2 pM; Std 3: 0.2 pM; Std 4: 0.02 pM; Std 5: 0.002 pM; Std 6: 0.0002 pM

c. Add 6 µl of Kapa SYBR Green master mix per well.

Note: Premix 5 mL KAPA SYBR Fast qPCR Master Mix with 1 mL of 10× Primer before the first use and prepare aliquots. All reagents are provided by the KAPA Library Quantification Kit. Store in the dark at −20°C. Do not freeze and thaw more than twice.

d. Run the following protocol on the qPCR machine: approx. 2.5 h

qPCR cycling conditions			
Steps	Temperature	Time	Cycles
Initial activation/denaturation	95°C	5 min	1
Denaturation	95°C	30 s	35×
Annealing/Extension/Data acquisition	60°C	45 s	

Optional: Run a melt curve analysis.

e. Confirm that the reaction efficiency is between 90%–110% by analyzing the standard curve.

f. Calculate the library concentration as follows:

Library concentration as determined by qPCR					
	Library concentration by qPCR in pM				
Library dilution	Rep1	Rep2	Rep3	Mean concentration in pM	Dilution factor
1:500	x1	x2	x3	X	d1 = 500
1:1000	y1	y2	y3	Y	d2 = 1000
1:2000	z1	z2	z3	Z	d3 = 2000

$$c(\text{undiluted library in pM}) = \frac{d1 \times \left(\frac{f_{Std}}{f_{Lib}} \times x\right) + d2 \times \left(\frac{f_{Std}}{f_{Lib}} \times y\right) + d3 \times \left(\frac{f_{Std}}{f_{Lib}} \times z\right)}{3}$$

$$m(\textit{undiluted library in ng}) = c(\text{undiluted library in pM}) \times 10^9 \times f_{Lib} \times M_{bp} \times V_{Lib}$$

The average standard fragment length f_{Std} (standards from the KAPA Library Quantification Kit) is 452 bp. The average size-selected library fragment length f_{Lib} (Pippin Prep) is 350 bp. The molecular weight of one base pair (M_{bp}) is approximated with 660 g/mol. The ChIP library volume (V_{Lib}) is 20 µl (see point 67e).

g. Determine the number of amplification cycles required from the amount of ChIP DNA (ng) with the help of the following table from the KAPA Library Quantification Kit (Roche):

PCR amplification cycles	
m(undiluted library in ng)	Number of cycles
<0.002	18
0.002–0.007	17
0.007–0.01	16–15
0.015–0.03	14
0.03–0.07	13
0.07–0.09	12
0.1–0.2	11
0.2–0.3	10
0.3–0.5	9
0.5–1	8
1–2	7
2–3	6
3–5	5

⚠ CRITICAL: Take care to avoid too many rounds of amplification in order to prevent PCR duplicates from making up most of your sequencing reads. See Troubleshooting 6.

69. Library amplification
    a. For each sample, prepare the following PCR reaction on ice:

Library amplification reaction	
Reagent	Amount
Adapter-ligated library	20 µL
2× KAPA HiFi HotStart ReadyMix	25 µL
10× Library Amplification Mix	5 µL
Total	**50 µl**
All reagents are from the KAPA HyperPrep Kit.	

    b. Run the following PCR program:

PCR cycling conditions			
Steps	Temperature	Time	Cycles
Initial activation/denaturation	98°C	45 s	1
Denaturation	98°C	15 s	X
Annealing	60°C	30 s	
Extension	72°C	30 s	
Final extension	72°C	60 s	1
Hold	4°C	Max 2 h	

Note: The number of cycles X has to be adapted according to the amplification cycles determined in 68g.

70. Post-amplification Clean-up with AMPure XP beads (1× AMPure XP bead clean-up)
    a. Mix 50 µl of the amplified ChIP library with 50 µl of well mixed AMPure XP beads with a pipet by pipetting up and down for 10 times.
    b. Proceed with the AMPure XP bead purification as described in 66b-g.
    c. Add 16 µl Library Elution Buffer to the beads, remove the PCR tubes from the magnetic rack and pipet up and down for 10 times. Incubate for 2 min at 18°C–24°C.

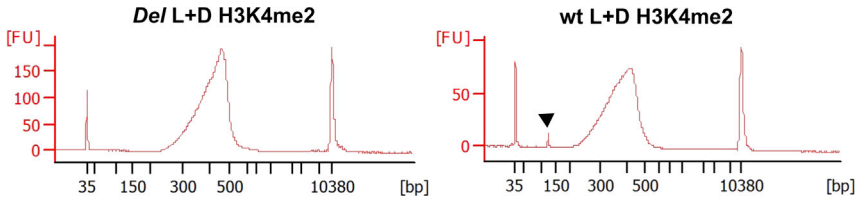

Figure 5. Profiles of libraries from H3K4me2 ChIP-seq in RAW264.7 cells on an Agilent Bioanalyzer 2010
Left: Setd1a$^{Del/+}$ cells (Del). Right: Wild type cells (wt). The arrowhead points at contaminating adapters that need to be removed by another round of AMPure XP bead selection (see Troubleshooting 4).

d. Place PCR tubes into the magnetic tube holder and wait until the liquid is cleared (1–5 min).
e. Transfer 14 µl of the supernatant to a fresh PCR tube. This is the final library.

Pause point: The final library can be stored at −20°C for up to 1 year. Take aliquots for Bioanalyzer and Qubit concentration measurement before freezing. Avoid freeze and thaw cycles.

71. Perform quality control with the Agilent Bioanalyzer.

The Bioanalyzer profile on the left in Figure 5 shows an ideal library with a size distribution between 200 and 600 bp and no adapter or primer dimer contaminations:

In case of adapter contamination, see Troubleshooting 4.

72. Pooling of libraries for sequencing
    a. Measure the library concentrations by Qubit.
    b. Calculate the volume of each library to be pooled for sequencing as follows:

$$V_{Lib} = \frac{N_{lanes} \times c_{pool} \times V_{pool} \times M_{bp} \times f_{Lib}}{N_{samples\ per\ lane} \times c_{Lib} \times 10^3}$$

V_{Lib} – volume to pool for the individual library in µlN_{lanes} – number of lanesc_{pool} – concentration of the final pool in µMV_{pool} – volume of the final pool in µlM_{bp} – molecular weight of one base pair (approx. 660 g/mol)f_{Lib} – average library size as determined by the Bioanalyzer$N_{samples\ per\ lane}$ – number of samples to pool per lane (see notes)c_{Lib} – concentration of individual library in ng/µl as measured by Qubit

    c. Fill to the V_{pool} with nuclease-free water and store the pool of ChIP libraries at −20°C until sequencing.

Note: Flow cells and pooling strategy need to be adapted according to the number of libraries, the sequencer available and the desired sequencing depth. We recommend contacting the sequencing facility or provider before pooling. The number of samples to pool in one lane is determined by the total number of reads given by a flow cell (e.g., 800 M reads for one lane on the SP flow cell for the NovaSeq 6000) and the desired sequencing depth. Sequencing depth recommendations for the mouse genome are as follows:

Sequencing depth	
ChIPed factor	Desired sequencing depth
Transcription factor	30–40 M
Narrow histone modifications, RNA Polymerase II	60 M
Broad histone modification s	80 M
Input	200 M

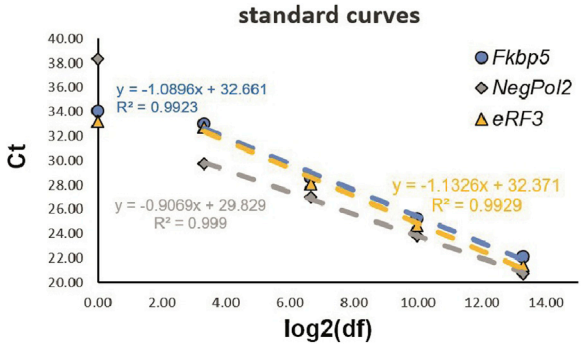

Figure 6. Standard curve for Fkbp5 (circle, blue), NegPol2 (rectangle, gray) and eRF3 (triangle, orange) for ChIP-qPCR in murine macrophages with Drosophila S2 cell spike-in

The mean Ct values of three technical replicates are plotted as data points, and the linear regression for S1-S4 is presented as dashed line. The linear regression formulas and regression coefficients R^2 are given.

EXPECTED OUTCOMES

ChIP-seq libraries with 1–5 ng/µl size-selected DNA can be expected. If a library meets the following quality control standards, it can be processed for pooling and sequencing.

First, the ChIP-qPCR shows a significant enrichment at a positive locus when compared to a negative region, for both the target and the spike-in genome (see Figure 6).

Secondly, the bulk of the fragmented chromatin used for library preparation is between 200 and 1,500 bp in size. The size-selected library therefore resembles the majority of the fragmented chromatin.

Third, the fragment length distribution of the library resembles a shape similar to the library visualized in the Bioanalyzer profiles in Figure 5 left or broader. A homogeneous distribution of fragments from 200 to 600 bps is expected. No adapter dimers are detected.

QUANTIFICATION AND STATISTICAL ANALYSIS

Normalization of ChIP-qPCR results

Analyze ChIP-qPCR data by calculating the percentage input (%input) for each IP and for each locus (target and spike-in) as described in the following section. Here, we present an example of ChIP-qPCR against H3K4me2 in murine macrophages stimulated with LPS (L) or LPS plus Dexamethasone (L+D). 25% of spike-in chromatin from *Drosophila* S2 cells was used. In this example, the %input was calculated separately for each replicate. *Fkbp5* represents the positive locus of the target genome and *eRF3* denotes the positive locus of the spike-in genome. NegPol2 is a negative locus in the target genome.

1. First, determine the performance of the primers used, by calculating the PCR efficiency from the standard curve.

Find the mean Ct values (technical replicates) of each standard in Table 1. Standards were prepared as described in step 50.

We plot the standard curve as linear regression of the mean Ct values (technical replicates) over the log2-transformed dilution factor (Figure 6) and determine the PCR efficiency from the slope of the standard curve as follows.

Table 1. Ct values for standard (S) curve and non-template control (NTC). df – dilution factor

		Ct values	*Fkbp5*	NegPol2	*eRF3*
log2(df)	Df	NTC	36.21	33.56	36.19
13.29	10000	S1	22.09	20.73	21.36
9.97	1000	S2	25.23	23.81	24.68
6.64	100	S3	28.55	26.98	28.11
3.32	10	S4	33.05	29.71	32.76
0.00	1	S5	34.06	33.24	38.34
PCR efficiency in %			94.0	91.2	106.7

$$PCR\ efficiency\ = 100 \times 2^{(1-slope)}$$

The linear range of the standard curve is defined as the Ct value range, with the standard curve being linear. In our example, all the primers have a linear range from S1 (22 for *Fkbp5*) to S4 (33 for *Fkbp5*). S5 was excluded, as it was either outside the linear range or within one Ct value of the non-template control (Tab. 1).

2. Adjust the input to 100% using the following formula:

$$inp_{adj} = \overline{Ct_{inp}} - log_2 df$$

inp_{adj} – adjusted inputdf – dilution factor (500 for 1% input diluted 1:5 during qPCR)$\overline{Ct_{inp}}$ – mean Ct value of the qPCR replicates from the input sample

3. Calculate the percentage input using the following formula:

$$\%inp = 100 \times 2^{-\left(\overline{Ct_{IP}} - inp_{adj}\right)}$$

$\overline{Ct_{IP}}$ – mean Ct value of the qPCR replicates for the ChIP sample

Table 2 shows the example data from the ChIP-qPCR against H3K4me2 in murine macrophages.

4. Continue to spike-in normalization using the following formula:

$\%inp_{norm} = \%inp_{target}/\%inp_{spike-in}$

$\%inp_{target}$ - %input of a locus occupied by the protein of interest in the target genome (positive)

$\%inp_{spike-in}$ - %input of a locus occupied by the protein of interest in the spike-in genome (positive)

Table 3 illustrates the example data for a H3K4me2 ChIP-qPCR experiment in murine macrophages.

Figure 7 shows the enrichment of H3K4me2 in LPS (L) and LPS plus Dexamethasone (L+D) treated macrophages at a positive (*Fkbp5*) and a negative locus (Negpol2) before (Figure 7A) and after spike-in normalization (Figure 7B). Before spike-in normalization, the results from both replicates are highly variable, both in LPS and LPS plus Dexamethasone stimulated macrophages. A similar variation is observed for the *Drosophila* spike-in locus *eRF3* pointing towards a technical bias between the different test tubes (Figure 7A). By normalization to the positive spike-in locus (*eRF3*), we are able to account for this variation (Figure 7B).

Table 2. Spike in normalization for H3K4me2 in murine macrophages after LPS (L) or LPS+ Dexamethasone (L+D) treatment

	Raw Ct value			%input		
	Fkbp5	NegPol2	*eRF3*	*Fkbp5*	NegPol2	*eRF3*
IgG1 L+D_1	32.32	30.17	32.00	0.047	0.080	0.042
IgG1 L+D_2	33.55	29.66	32.27	0.020	0.115	0.035
IgG1 L+D_3	32.37	29.51	31.20	0.045	0.127	0.074
IgG2 L+D_1	34.88	29.76	32.23	0.008	0.107	0.036
IgG2 L+D_2	33.26	30.92	32.01	0.024	0.048	0.042
IgG2 L+D_3	33.31	29.70	32.4	0.023	0.112	0.032
H3K4me2_1 L+D_1	23.10	27.66	23.41	28.087	0.459	16.429
H3K4me2_2 L+D_2	22.78	27.25	23.51	35.062	0.610	15.273
H3K4me2_3 L+D_3	23.17	27.24	23.54	26.850	0.617	14.950
H3K4me2_1 L+D_1	25.25	28.79	25.31	6.324	0.210	4.407
H3K4me2_2 L+D_2	24.57	28.39	25.11	10.146	0.277	5.028
H3K4me2_3 L+D_3	24.48	29.28	25.05	10.829	0.150	5.256
Input L+D 50%_1	22.35	20.93	21.78			
Input L+D 50%_2	22.33	20.85	21.78			
Input L+D 50%_3	22.13	20.92	21.85			
IgG1 L_1	33.37	29.59	37.74	0.015	0.082	0.000
IgG1 L_2	33.33	29.24	43.52	0.015	0.105	0.000
IgG1 L_3	32.53	29.46	31.86	0.027	0.090	0.042
IgG2 L_1	34.91	32.30	32.41	0.005	0.012	0.029
IgG2 L_2	32.79	30.84	33.37	0.022	0.034	0.014
IgG2 L_3	33.62	30.47	32.93	0.012	0.045	0.020
H3K4me2_1 L_1	24.20	27.85	25.01	8.847	0.277	4.907
H3K4me2_2 L_2	24.23	28.13	25.07	8.628	0.229	4.702
H3K4me2_3 L_3	24.17	27.51	24.83	9.026	0.352	5.553
H3K4me2_1 L_1	22.92	26.54	23.62	21.409	0.686	12.888
H3K4me2_2 L_2	22.88	27.49	23.71	22.057	0.356	12.138
H3K4me2_3 L_3	22.84	27.20	23.69	22.646	0.436	12.263
Input L_1 50%	21.64	20.22	21.34			
Input L_2 50%	21.66	20.30	21.43			
Input L_3 50%	21.79	20.56	22.22			
Mean of Input Samples						
	Fkbp5	NegPol2	*eRF3*			
Input L+D	22.270	20.897	21.801			
Input L	21.698	20.359	21.664			
Adjusted Input to 100%						
	Fkbp5	NegPol2	*eRF3*			
Input L+D	21.270	19.897	20.801			
Input L	20.698	19.359	20.664			

Raw Ct values and %input.

⚠ CRITICAL: The spike-in ratio must be sufficiently high to measure reliable Ct values by qPCR (see Troubleshooting 5).

Normalization of ChIP-seq results

The quality of the sequencing reads can be evaluated by FASTQC (https://www.bioinformatics.babraham.ac.uk/projects/fastqc/). Samples not yielding at least 50% of the required sequencing depth (see 72c) should be submitted for re-sequencing. The "per base quality score" should be above 28 for all read positions. Low quality reads are filtered out during sample processing with Samtools (Li et al., 2009). Adapter sequences are removed with Trimmomatic (Bolger et al., 2014).

Table 3. Spike in normalization for H3K4me2 in murine macrophages after LPS (L) or LPS+ Dexamethasone (L+D) treatment

Mean %input				Spike-in Norm %inp	
	Fkbp5	NegPol2	*eRF3*		*Fkbp5*
IgG1 L+D	0.037	0.107	0.050	H3K4me2_1 L+D_1	1.71
IgG2 L+D	0.018	0.089	0.036	H3K4me2_2 L+D_2	2.30
H3K4me2_1 L+D	30.000	0.562	15.550	H3K4me2_3 L+D_3	1.80
H3K4me2_1 L+D	9.099	0.212	4.897	H3K4me2_1 L+D_1	1.43
IgG1 L	0.019	0.093	0.014	H3K4me2_2 L+D_2	2.02
IgG2 L	0.013	0.030	0.021	H3K4me2_3 L+D_3	2.06
H3K4me2_1 L	8.834	0.286	5.054	H3K4me2_1 L_1	1.80
H3K4me2_1 L	22.037	0.493	12.430	H3K4me2_2 L_2	1.83
				H3K4me2_3 L_3	1.63
SD %input				H3K4me2_1 L_1	1.66
	Fkbp5	NegPol2	*eRF3*	H3K4me2_2 L_2	1.82
IgG1 L+D	0.015	0.024	0.020	H3K4me2_3 L_3	1.85
IgG2 L+D	0.009	0.035	0.004		
H3K4me2_1 L+D	4.427	0.089	0.777	Mean spike-in Norm	
H3K4me2_1 L+D	2.427	0.063	0.439		*Fkbp5*
IgG1 L	0.006	0.011	0.024	H3K4me2_1 L+D	1.93
IgG2 L	0.008	0.016	0.007	H3K4me2_1 L+D	1.84
H3K4me2_1 L	0.199	0.062	0.444	H3K4me2_1 L	1.75
H3K4me2_1 L	0.618	0.172	0.402	H3K4me2_1 L	1.77
				SD Spike-in Norm	
					Fkbp5
				H3K4me2_1 L+D	0.32
				H3K4me2_1 L+D	0.35
				H3K4me2_1 L	0.11
				H3K4me2_1 L	0.10

SD - standard deviation, Norm-normalized.

Samples are processed via a standard ChIP-seq pipeline (Figure 8 left). Each sample is mapped against the target genome (*Mus musculus* Ensembl genome build GRCm38.p6 (mm10)) (Cunningham et al., 2019) and against the spike-in genome (*Drosophila melanogaster* Ensembl BDGP6 release 78 (dm6)) in this example (Cunningham et al., 2019)) using BWA-MEM (Li, 2013). Peaks

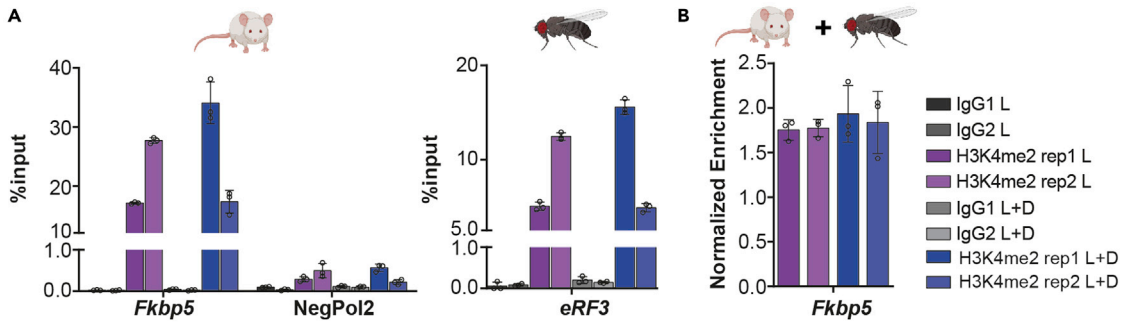

Figure 7. Spike-in ChIP-qPCR of H3K4me2 in murine macrophages stimulated with LPS (L) and LPS plus Dexamethasone (L+D)

(A) Non-normalized ChIP-qPCR results showing the percentage input for the Fkbp5 (positive) and NegPol2 (negative) loci in the murine genome and the percentage input for the eRF3 locus (positive for the spike-in genome). A ChIP against IgG is included as additional negative control.

(B) Spike-in normalized enrichment of the Fkbp5 locus. The experiment was performed in duplicates. Error bars represent the standard deviation of the qPCR triplicates.

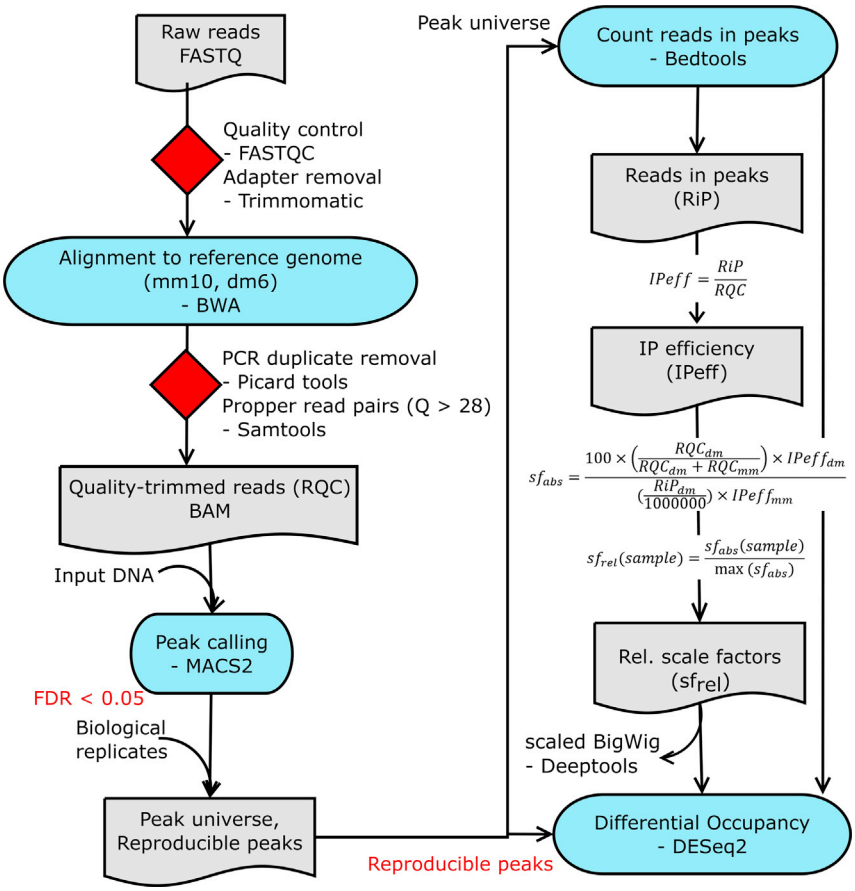

Figure 8. ChIP-seq pipeline and scaling by spike-in chromatin for differential occupancy analysis

Left: Standard ChIP-seq pipeline, run separately against the mm10 (target) and the dm6 (spike-in) reference genomes. Filters are indicated in red, tasks in blue. Right: Spike-in normalization. RQC – number of quality-filtered reads; RiP – number of reads overlapping peaks; IPeff – IP efficiency; dm – Drosphila melanogaster (spike-in genome); mm – Mus musculus (target genome); sf – scale factor; abs – absolute; rel – relative, max - maximum

are called using MACS2 (Zhang et al., 2008). For more details, see Mir et al. (Mir et al., 2019) and the ENCODE pipeline (https://www.encodeproject.org/data-standards/chip-seq/ (Landt et al., 2012)).

Samples with fewer than 80% of reads mapping to the target genome or more than 80% of PCR duplicates (see Troubleshooting 6) should be excluded from analysis. Furthermore, ChIP-seq samples of transcription factors with <1% of reads overlapping peaks (RiP), or histone marks with <10% RiP in either target genome or spike-in genome should be removed as well (see Troubleshooting 7). Samples with a recovery of <1% spike-in DNA (of all non-duplicated and aligned reads) were removed, too. Note that the proportion of recovered spike-in reads will depend on the target and the spike-in genome size ratio and the genomic coverage of the protein of interest (see Troubleshooting 5).

The peak union of all replicates (peak universe) can be generated in R (https://www.R-project.org/

(Team, 2017)) using the GenomicRanges package (Lawrence et al., 2013), and blacklisted regions can be removed using the following script:

```
library('GenomicRanges')


#Generate a function converting data frame into a GRange object.

bed2GRanges <-function(peaks)

{

  myrange <- GRanges(seqnames = peaks[,1], range = IRanges(start = peaks[,2], end = peaks[,3], names = paste(peaks[,1], peaks[,2],sep = '_')), strand = '*')

  return(myrange)

}


#Load blacklisted regions for the target (mm10) and spike-in species (dm6).

blacklist_mm <- read.table('mm10.blacklist.bed', header = FALSE, sep = '\t', stringsAsFactors = FALSE)

blacklist_mm <- bed2GRanges(blacklist_mm)

blacklist_dm <- read.table('dm6.blacklist.bed', header = FALSE, sep = '\t', stringsAsFactors = FALSE)

blacklist_dm <- bed2GRanges(blacklist_dm)


#Load chromosome names of nuclear chromosomes. If chromosome names are preceded by "chr" depends on the used reference genome. Make sure to filter using the correct chromosome annotation.

Chr_mm <- c('chr1', 'chr2', 'chr3', 'chr4', 'chrs5', 'chr6', 'chr7', 'chr8', 'chr9', 'chr10', 'chr11', 'chr12', 'chr13', 'chr14',' chr15', 'chrl6', 'chr17', 'chr18', 'chr19', 'chrX', 'chrY')

chr_dm <- c('2L', '2R', '3L', '3R', '4', 'chrX', 'chrY')


#The following part needs to be done for either target or spike-in peaks. Replace *chr* and *blacklist* according to the used species.

#Read narrowPeak files from MACS2 output and remove non-nuclear chromosomes.

rep1 <- read.table('rep1.narrowPeak', header = FALSE, sep = '\t', stringsAsFactors = FALSE)

rep1 <- rep1[rep1$V1%in%chr,]

rep2 <- read.table('rep2.narrowPeak', header = FALSE, sep = '\t', stringsAsFactors = FALSE)

rep2 <- rep2[rep2$V1%in%chr,]

rep3 <- read.table('rep3.narrowPeak', header = FALSE, sep = '\t', stringsAsFactors = FALSE)

rep3 <- rep3[rep3$V1%in%chr,]

union <- rbind(rep1[,c(1:3)], rep2[,c(1:3)], rep3[,c(1:3)])

union <- bed2GRanges(union)

#Remove duplicated ranges.

union <- reduce(union)

#Remove regions overlapping blacklisted regions.

union <- subsetByOverlaps(union, blacklist, invert = TRUE, minoverlap = 1, ignore.strand = TRUE)

#Export as BED file.

write.table(as.data.frame(union)[,c(1:3)],file = "peakUniverse.bed', sep = '\t', col.names = FALSE, row.names = FALSE, quote = FALSE)
```

Note: At the time of publications, BED files of the updated blacklisted regions could be found at https://github.com/Boyle-Lab/Blacklist/tree/master/lists.

The number of reads covering peaks (RiP) is determined using BEDTools (Quinlan and Hall, 2010)

```
bedtools multicov -bams Cond1_rep1.bam Cond1_rep2.bam Cond1_rep3.bam Cond2_rep1.bam
Cond2_rep2.bam Cond2_rep3.bam -bed peakUniverse.bed > output.txt
```

and the R script below:

```
rip <- read.table('output.txt', sep = '\t', header = FALSE, stringsAsFactors = FALSE)

colnames(rip) <-c('chr', 'start', 'end', 'Cond1_rep1', 'Cond1_rep2', 'Cond1_rep3',
'Cond2_rep1', 'Cond2_rep2', 'Cond2_rep3')

colSums(rip[,c(4:9)])
```

The immunoprecipitation efficiency (IPeff) is calculated from the reads covering peaks (RiP) divided by all quality-filtered reads (RQC) for each reference genome. The absolute scale factor (sf_{abs}) for each sample is calculated from the percentage of spike-in chromatin (100*spike-in reads (R_{dm})/(spike-in reads (R_{dm}) + target reads (R_{mm}))) divided by the RiP for the spike-in genome and normalized by the IP efficiency ratio between spike-in and target genome ($IPeff_{dm}/IPeff_{mm}$) (see Figure 8 right).

The absolute scale factors of all samples are set into relation (sf_{rel}) by normalizing to the highest occurring absolute scale factor among all samples. Those relative scale factors are used for scaling BigWig files with deepTools (Ramirez et al., 2014):

```
bamCoverage -b .bam -o .bw -scaleFactor sfrel -bs 10
```

The inverse of the relative scale factors replaces the sizeFactors in DESeq2 (Love et al., 2014) for differential occupancy analysis in R.

```
#Read count data from BEDtools output.

counts <- read.table('output.txt', header = FALSE, sep = '\t', stringsAsFactors = FALSE)

colnames(counts) <- c('chr', 'start', 'end', 'Cond1_rep1', 'Cond1_rep2', 'Cond1_rep3', 'Cond2_rep1', 'Cond2_rep2',
'Cond2_rep3')

counts$id <- paste(counts$chr, counts$start, counts$end, sep = "_")

counts <- counts[!duplicated(counts$id),]


#Perform DESeq analysis.

library('DESeq2')

rownames(counts) <- counts$id

counts <- counts[,c(4:9)]

counts <- counts[unique(rownames(counts)),]

#Define experimental design.

condition <- c('Cond1', 'Cond1', 'Cond1', 'Cond2', 'Cond2', 'Cond2')

pdata <- cbind(colnames(counts),condition)
```

```
dds <- DESeqDataSetFromMatrix(counts, pdata, design = ~condition)

#set the reference level of the experimental condition.

dds$condition <- factor(dds$condition,level = c("Cond1","Cond2"))

dds <- DESeq(dds)

#Use the precalculated relative scale factors here for normalization.

sizeFactors(dds) <- c(1/sf(Cond1_rep1), 1/sf(Cond1_rep2), 1/sf(Cond1_rep3), 1/sf(cond2_rep1), 1/sf(cond2_rep 2),
1/sf(Cond2_rep3))

#Compute differential binding results.

res <- data.frame(results(dds, name = "condition_cond2_vs_cond1", pAdjustMethod = "BH" ), stringsAsFactors = FALSE)

res$id<-rownames(res)


#The resulting data frame contains the log2Foldchange between cond2 over Cond1 as well as the Benjamini-Hochbe rg-
adjusted p-value. The data can be used for the generation of volcano plots or heatmaps, peak annotation, functional enrich-
ment and subsequent filtering on differential occupancy.
```

Alternatives: Diffbind (Ross-Innes et al., 2012) also offers spike-in normalization and differential occupancy analyses for simple designs.

Note: DESeq2 allows the usage of complex experimental designs.

Table 4 includes the mapping statistics (%map), the calculated IP efficiencies (IPeff), the absolute (abs.) and the relative (rel.) scale factors (sf) of an example data set (Greulich et al., 2021). FASTQ files are deposited on GEO with the accession number GEO: GSE138017.

The effect of spike-in normalization on the read counts across all H3K4me2 peaks (peak universe) between replicates, and examples of normalized versus non-normalized genome browser tracks, are shown in Figure 9.

LIMITATIONS

ChIP depends on the specificity and availability of the antibody. Any antibody used in ChIP experiments needs to be extensively tested by ChIP-qPCR in the cell type or tissue of interest, ideally by comparing wild type and knockout cells. A pre-screen by Western blot is possible. If knockout

Table 4. Scale factor calculations and mapping statistics for H3K4me2 in wild type (wt) and *Setd1a*$^{Del/+}$ (*Del*) RAW264.7 cells after LPS (L) or LPS plus Dexamethasone (L+D) treatment

Sample ID	Genotreat	#Reads	%map mm10	%map dm6	RQC mm10	%Dupl. mm10	RQC dm6	%Dupl. dm6	RiP mm10	IPeff mm10	IPeff RiP dm6	IPeff dm6	Abs. Sf	Rel. Sf
GSM4096676Wt	LPS	15059415	298.0	1.1	55647040	62.3	750324	53.1	9015482	0.16	217412	0.29	10.94	1.000
GSM4096677Wt	L+D	27364876	698.3	1.5	13270691	451.1	1979352	52.3	41604331	0.31	610549	0.31	2.37	0.216
GSM4096678Wt	L+D	17879981	298.3	2.0	10687421	439.2	2281740	41.6	31827833	0.30	552688	0.24	3.08	0.281
GSM4096679Del	LPS	20395842	698.3	2.4	15634839	222.1	3315942	30.8	19587761	0.13	629492	0.19	5.00	0.457
GSM4096680Del	LPS	21020809	498.2	1.7	75365880	63.5	1758958	52.2	18737752	0.25	482824	0.27	5.22	0.477
GSM4096681Del	L+D	24371825	098.3	1.7	69405402	71.0	1826934	55.8	23061949	0.33	509125	0.28	4.22	0.386
GSM4096683Wt	L+D	11442080	295.8	3.2	46958500	57.2	1949396	46.6	12314423	0.26	550129	0.28	7.80	0.712
GSM4096684Wt	LPS	11333114	896.7	2.6	45138652	59.5	1388290	53.2	13706729	0.30	469364	0.34	7.08	0.647
GSM4096685Del	L+D	77635734	96.4	3.6	36757906	50.9	1207134	56.8	12829586	0.35	539918	0.45	7.55	0.690
GSM4096686Del	LPS	14315966	694.8	3.2	64833572	52.3	2469554	45.9	23516324	0.36	1077635	0.44	4.10	0.374

treat – treatment; geno – genotype, Dupl. - duplicates

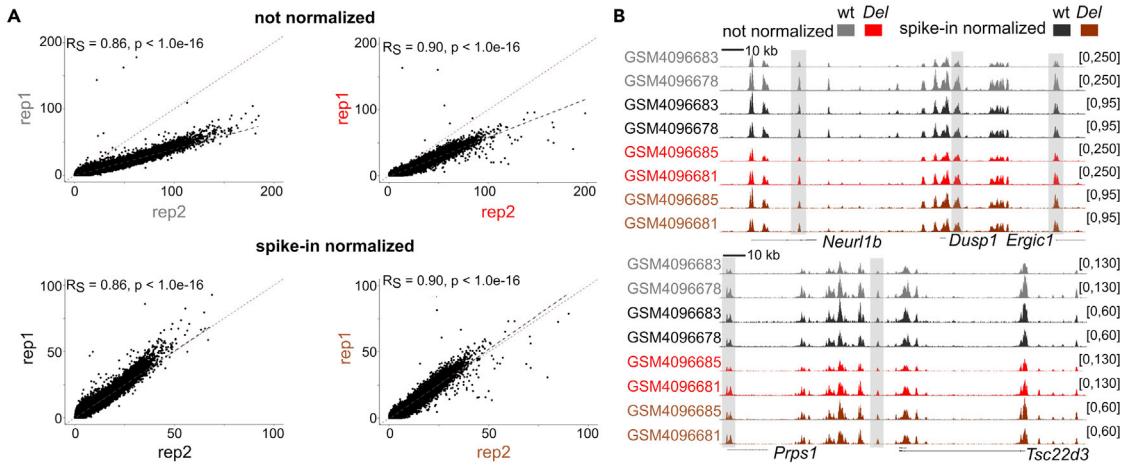

Figure 9. Spike-in normalization of ChIP-seq data

(A) Tag counts per peak (resized to 1 kb) for the H3K4me2 peak union from two biological replicates of H3K4me2 ChIP-seq in LPS plus Dexamethasone treated wild type (left, gray) and Setd1a$^{Del/+}$ (Del, right, red) RAW264.7 cells. The upper plots show raw tag counts, whereas the lower plots show the tag counts after spike-in normalization. Dashed lines indicate the linear regression (gray) and ideal regression lines (red), if both samples were identical. R_S – Spearman correlation coefficient. p – Significance of the correlation. Rep – replicate.

(B) Example genome browser tracks of the Dusp1 (up) and Tsc22d3 (down) loci for the same samples as in A. Visualization with Integrative Genome Browser (Freese et al., 2016). Gray shadows indicate peaks with reduced inter-replicate variation after spike-in normalization. Colors as in A.

cells/tissues are not available, specific blocking peptides might be purchased and included as controls. The latter is recommended when profiling closely related histone modifications to ensure that the ChIP antibodies do not cross-react. Additionally, ChIP experiments require a certain amount of starting material. For low amounts of input material, Cut&Run or Cut&Tag techniques are an alternative, but come with their own limitations (Kaya-Okur et al., 2019; Skene and Henikoff, 2017). ChIP-seq experiments in particular are limited to the availability of genome sequences for the target species.

Heterologous spike-in ChIP experiments have several additional technical limitations. For heterologous spike-in ChIP, the protein of interest needs to be conserved between the target and the spike-in species. Closely related species can be used for ChIP-qPCR, given that the primers were tested for cross-reactivity, but are not recommended for ChIP-seq experiments. To test for cross-mappability of the spike-in species, obtain the reference genome for the spike-in species, bin it into fragments matching the sequencing read length (e.g., 50 or 101 bp) and map it against the target species, and vice versa. Less than 10% cross-mappability are acceptable for heterologous spike-in experiments. On top of the target protein conservation, the antibody of interest needs to react with the protein epitope of interest across species. The reactivity of the ChIP antibody needs to be tested in cross-linked tissue or cell material form the target species as well as for the spike-in cells or tissues. For this purpose, one can design primers against positive and negative regions in both genomes and test several antibodies against the protein of interest for specificity by ChIP-qPCR.

Note: Polyclonal antibodies are more likely to react with the protein of interest across species.

TROUBLESHOOTING

Problem 1

Target and spike-in cells have different sonication conditions (step 6).

Potential solution

Sonication conditions have to be optimal for each of the tissues/cells used as target or spike-in. Therefore, optimal sonication conditions need to be established before the start of the experiment.

In the case of murine macrophages and *Drosophila* S2 cells, sonication conditions are very similar (12 cycles for macrophages and 10 cycles for S2 cells at high settings, see Figure 1). Thus, both cell types can be mixed at the desired spike-in ratio before sonication. This might not always be the case.

If the sonication conditions differ substantially between target and spike-in species, lyse and shear both cell types separately with the optimal conditions for each sample. Mix the fragmented chromatin at the desired spike-in ratio, after removing insoluble chromatin (step 18).

Problem 2

Find a ChIP-grade antibody (Before you begin, step 22).

Potential solution

A key success factor for ChIP experiments is a specific antibody. Find below some recommendations on how to select a good ChIP antibody.

- Acquire ChIP-validated antibodies, but still confirm the specificity of those antibodies by performing ChIP-qPCR against a positive and negative locus in the specific experimental system (e.g., cell type or tissue) as described in the "Before you begin" section.
- Try antibodies suitable for immunohistochemistry or immunofluorescence of formaldehyde-fixed tissues.
- Try polyclonal antibodies, as they may have a higher probability of recognizing an unmasked epitope and as they may exhibit cross-species specificity.
- Test each antibody against a knockout or knockdown cell line if available, or use blocking peptides to confirm antibody specificity.
- Include more than one negative (not bound by the protein of interest) and positive locus, as well as an IgG control, to test for specificity in Chip-qPCR.

Problem 3

Undetectable ChIP DNA (step 62).

Potential solution

The sensitivity of the Qubit dsDNA HS kit lies between 0.2–100 ng of DNA. A ChIP sample might be undetectable by Qubit.

- Repeat the ChIP and combine the eluted DNA samples from two ChIP experiments.
- If the input material is limiting a repetition of the experiment, process the complete ChIP DNA for library preparation. After library quantification, do not add more than 14 PCR cycles to avoid over amplification of the library. A specific enrichment for the factor of interest must have been observed by ChIP-qPCR (see Figure 7), and the majority of the chromatin fragments must lie between 150 and 1500 bp, as determined by agarose gel electrophoresis or Bioanalyzer of the input DNA (see Figures 1 and 3).

Problem 4

Adapter contamination of the final library.

Potential solution

The Bioanalyzer profiles might reveal an additional peak at approx. 120 bp similar to Figure 5. Those are adapter dimers contaminating the library. In contrast to the remaining PCR primers at around 35 bp, adapter dimers need to be removed before sequencing, as they contain the adapter sequence able to bind to the flow cell.

Repeat post amplification clean-up step 70.

Note that any additional clean-up step will result in the loss of approximately half the concentration of the final library.

Problem 5

Low amount of spike-in DNA after ChIP (step 6).

Potential solution

If the spike-in qPCR yields very high Ct values or N/As in the ChIP samples, or if they fall below 1% of all non-duplicated and properly aligned reads for ChIP-Seq samples, the concentration of the spike-in chromatin is too low to allow for proper estimation of technical bias.

- Make sure the spike-in primers are optimal, by determining at the PCR efficiency and the melt curve. The melt curve should only show one prominent peak. The PCR efficiency should lie between 90 - 100% for a Ct value range, recapitulating the Ct values of the ChIP samples.
- If the spike-in primers are optimized and show significant enrichment for the input sample, the chosen positive locus might not be positive.
- If the input sample also shows a high Ct value for the spike-in chromatin, or if < 1% spike-in reads are detected in ChIP-Seq, consider increasing the spike-in ratio up to 25% in ChIP-qPCR or up to 10% in ChiP-Seq experiments.

Problem 6

High number of PCR duplicates (step 69).

Potential solution

PCR duplication rates >50% are not only expensive, but they also bias the occupied chromatin fraction towards smaller fragments. A true PCR duplicate has the same start and end of the sequencing read. In order to differentiate PCR duplicates from naturally occurring duplicates, paired-end sequencing is recommended. PCR duplicates mostly arise from library amplification (step 69), when more than 7 amplification cycles were performed.

- Limit PCR cycles to maximum 7 cycles.
- If sufficient ChIP DNA is available, consider combining two library preparations of the same sample, with low numbers of amplification cycles each.
- If sufficient ChIP DNA was obtained, insufficient adapter annealing might cause a requirement for extra PCR cycles during library amplification. Amplification primers only bind adapters and therefore, only adapter-ligated chromatin fragments will be amplified. To ensure optimal adapter ligation, avoid freeze and thaw cycles of adapter dilutions and make sure that the T4 ligase is stored properly. If the problem persists, reorder adapter stocks or prepare fresh adapter dilutions.

Problem 7

High background signal (steps 5, 7, 22, and 26).

Potential solution

The fraction of reads mapping into peaks reflects the efficiency of the ChIP (IP efficiency) and serves as quality readout that reports on how many reads were specifically purified. IP efficiencies below 10% indicate an unspecific recovery of chromatin fragments, due to various reasons. Similarly, a low enrichment for a positive locus over the negative locus in ChIP-qPCR might indicate unspecific binding, even if the IgG control was not affected.

There are several reasons for a high background signal.

If the antibody causes an unspecific signal (see Troubleshooting 2), the enrichment for a positive locus over the negative locus (region not bound by the protein of interest) will be low, and both signals will be significantly higher than the signal observed in the IgG control.

Besides an unspecific antibody, the antibody-epitope interaction may be inhibited by the SDS content of the shearing buffer. Try a low-SDS shearing buffer (step 5) and add Triton X-100 up to 1%, to sequester the SDS during immunoprecipitation (step 21).

Low-SDS shearing buffer	Final concentration	Amount
SDS (20%)*	0.1% vol/vol	5 mL
Sodium deoxycholate (10%)*	0.1% vol/vol	10 mL
EDTA pH=8.0 (0.5 M)	1 mM	2 mL
Tris-HCl pH=8.0 (1 M)*	50 mM	50 mL
Triton X-100	1% vol/vol	10 mL
ddH2O	N/A	880 mL
Total		1 l

Low-SDS Shearing Buffer is stable at 18°C–24°C for up to 6 month.

*Sodium deoxycholate is harmful when swallowed and may cause respiratory irritation. Avoid breathing dust/fume/vapors or sprays. Do not eat/drink or smoke while using Sodium Deoxycholate. Wash hands after handling. Wear protective clothing. Work in a well-ventilated area. Dispose according to regional/national regulations.

Note: When changing the shearing buffer, sonication conditions have to be re-established.

"Over-sheared" chromatin displays unspecific binding to the beads or interactions of the ChIP antibody with alternative epitopes. Confirm fragment sizes after sonication, and do not proceed with ChIP if most of the chromatin fragments are below 500 bp after fast-reverse cross-link.

Unspecific binding of chromatin and DNA to the beads may cause increased background signal. Try to reduce the incubation time with the beads. Otherwise, pre-clearing of chromatin with pre-blocked Dynabeads or sepharose beads might remove proteins and DNA that binds unspecifically to the beads. Add 20 µl of pre-blocked beads to each sample and incubate for 1 h at 4°C while rotating slowly. After 1 h, place tubes in a magnetic rack (Dynabeads) or spin for 30 s at 300 × *g* at 4°C (sepharose beads). Transfer the supernatant to a fresh tube and proceed with the immunoprecipitation (step 22).

Rarely, batch effects in the Dynabeads or sepharose beads might cause higher background signal and are resolved after purchase of a new batch.

RESOURCE AVAILABILITY

Lead contact

Further information and requests for resources and reagents should be directed to and will be fulfilled by the lead contact, Franziska Greulich (franziska.greulich@tum.de).

Material availability

This study did not generate any unique reagents. All reagents used are commercially available and listed in the Key Resource table.

Data and code availability

The example data used in this study is available from GEO (https://www.ncbi.nlm.nih.gov/geo/ (Edgar et al., 2002)) under the accession number GEO: GSE138017. All unique code is reported in this study.

ACKNOWLEDGMENTS

We sincerely thank E. Graf, S. Loesecke, T. Schwarzmayr, and I. de la Rosa (HMGU genomics core) for their contribution to the NGS studies. We are grateful to I. Guderian and S. Regn for administrative assistance. This work received funding from the DFG (UH 275/1-1, SFB 1064 Chromatin Dynamics and TRR205 Adrenal Research to NHU and Entzuendungsprozesse GR 5179/1-1 to FG) and from the ERC (ERC-2014-StG 638573 SILENCE to NHU). Figures were partially created using BioRender.

AUTHOR CONTRIBUTIONS

F.G. designed, performed, and analyzed the NGS experiments. F.G. and A.M. developed, validated, and optimized the spike-in ChIP protocol. A.M. performed the spike-in ChIP-qPCR. T.H. optimized the library preparation protocol. F.G. and N.H.U. supervised the work and secured funding. A.M. and F.G. wrote the manuscript together with N.H.U. All authors read and approved the final manuscript.

DECLARATION OF INTERESTS

The authors declare no competing interests.

REFERENCES

Allhoff, M., Sere, K., J, F.P., Zenke, M., and I, G.C. (2016). Differential peak calling of ChIP-seq signals with replicates with THOR. Nucleic Acids Res. *44*, e153.

Bolger, A.M., Lohse, M., and Usadel, B. (2014). Trimmomatic: a flexible trimmer for Illumina sequence data. Bioinformatics *30*, 2114–2120.

Cunningham, F., Achuthan, P., Akanni, W., Allen, J., Amode, M.R., Armean, I.M., Bennett, R., Bhai, J., Billis, K., Boddu, S., et al. (2019). Ensembl 2019. Nucleic Acids Res. *47*, D745–D751.

Davis, C.A., Hitz, B.C., Sloan, C.A., Chan, E.T., Davidson, J.M., Gabdank, I., Hilton, J.A., Jain, K., Baymuradov, U.K., Narayanan, A.K., et al. (2018). The Encyclopedia of DNA elements (ENCODE): data portal update. Nucleic Acids Res. *46*, D794–D801.

Edgar, R., Domrachev, M., and Lash, A.E. (2002). Gene Expression Omnibus: NCBI gene expression and hybridization array data repository. Nucleic Acids Res. *30*, 207–210.

Egan, B., Yuan, C.C., Craske, M.L., Labhart, P., Guler, G.D., Arnott, D., Maile, T.M., Busby, J., Henry, C., Kelly, T.K., et al. (2016). An alternative approach to ChIP-seq normalization enables detection of genome-wide changes in histone H3 lysine 27 trimethylation upon EZH2 inhibition. PLoS One *11*, e0166438.

Freese, N.H., Norris, D.C., and Loraine, A.E. (2016). Integrated genome browser: visual analytics platform for genomics. Bioinformatics *32*, 2089–2095.

Gaillard, C.S.F. (1998). Avoiding adsorption of dna to polypropylene tubes and denaturation of short dna fragments. Technical Tips Online.

Greulich, F., Wierer, M., Mechtidou, A., Gonzalez-Garcia, O., and Uhlenhaut, N.H. (2021). The glucocorticoid receptor recruits the COMPASS complex to regulate inflammatory transcription at macrophage enhancers. Cell Rep. *34*, 108742.

Kaya-Okur, H.S., Wu, S.J., Codomo, C.A., Pledger, E.S., Bryson, T.D., Henikoff, J.G., Ahmad, K., and Henikoff, S. (2019). CUT&Tag for efficient epigenomic profiling of small samples and single cells. Nat. Commun. *10*, 1930.

Kent, W.J., Sugnet, C.W., Furey, T.S., Roskin, K.M., Pringle, T.H., Zahler, A.M., and Haussler, D. (2002). The human genome browser at UCSC. Genome Res. *12*, 996–1006.

Landt, S.G., Marinov, G.K., Kundaje, A., Kheradpour, P., Pauli, F., Batzoglou, S., Bernstein, B.E., Bickel, P., Brown, J.B., Cayting, P., et al. (2012). ChIP-seq guidelines and practices of the ENCODE and modENCODE consortia. Genome Res. *22*, 1813–1831.

Lawrence, M., Huber, W., Pages, H., Aboyoun, P., Carlson, M., Gentleman, R., Morgan, M.T., and Carey, V.J. (2013). Software for computing and annotating genomic ranges. PLoS Comput Biol *9*, e1003118.

Li, H. (2013). Aligning sequence reads, clone sequences and assembly contigs with BWA-MEM. arXiv.

Li, H., Handsaker, B., Wysoker, A., Fennell, T., Ruan, J., Homer, N., Marth, G., Abecasis, G., and Durbin, R.; Genome Project Data Processing, S. (2009). The Sequence Alignment/Map format and SAMtools. Bioinformatics *25*, 2078–2079.

Love, M.I., Huber, W., and Anders, S. (2014). Moderated estimation of fold change and dispersion for RNA-seq data with DESeq2. Genome Biol *15*, 550.

Mir, A.A., Dyar, K.A., Greulich, F., Quagliarini, F., Jouffe, C., Hubert, M.J., Hemmer, M.C., and Uhlenhaut, N.H. (2019). In vivo ChIP-seq of nuclear receptors: a rough guide to transform frozen tissues into high-confidence genome-wide binding profiles. Methods Mol Biol *1966*, 39–70.

Quinlan, A.R., and Hall, I.M. (2010). BEDTools: a flexible suite of utilities for comparing genomic features. Bioinformatics *26*, 841–842.

Ramirez, F., Dundar, F., Diehl, S., Gruning, B.A., and Manke, T. (2014). deepTools: a flexible platform for exploring deep-sequencing data. Nucleic Acids Res. *42*, W187–W191.

Ross-Innes, C.S., Stark, R., Teschendorff, A.E., Holmes, K.A., Ali, H.R., Dunning, M.J., Brown, G.D., Gojis, O., Ellis, I.O., Green, A.R., et al. (2012). Differential oestrogen receptor binding is associated with clinical outcome in breast cancer. Nature *481*, 389–393.

Skene, P.J., and Henikoff, S. (2017). An efficient targeted nuclease strategy for high-resolution mapping of DNA binding sites. Elife *6*.

Team, R.C. (2017). R: A Language and Environment for Statistical Computing.

Ye, J., Coulouris, G., Zaretskaya, I., Cutcutache, I., Rozen, S., and Madden, T.L. (2012). Primer-BLAST: a tool to design target-specific primers for polymerase chain reaction. BMC Bioinformatics *13*, 134.

Zhang, Y., Liu, T., Meyer, C.A., Eeckhoute, J., Johnson, D.S., Bernstein, B.E., Nusbaum, C., Myers, R.M., Brown, M., Li, W., et al. (2008). Model-based analysis of ChIP-Seq (MACS). Genome Biol *9*, R137.

Zhong, J., Ye, Z., Lenz, S.W., Clark, C.R., Bharucha, A., Farrugia, G., Robertson, K.D., Zhang, Z., Ordog, T., and Lee, J.H. (2017). Purification of nanogram-range immunoprecipitated DNA in ChIP-seq application. BMC Genomics *18*, 985.

3.2 The glucocorticoid receptor recruits the COMPASS complex to regulate inflammatory transcription at macrophage enhancers

Contribution

The article ‘’The glucocorticoid receptor recruits the Compass complex to regulate inflammatory transcription at macrophage enhancers’’ was published in Cell reports in 2021. For this manuscript I performed harvesting and differentiation of primary macrophages, ChIP-seq against H3K4me1 in primary macrophages and the ChIP-qPCRs, where I applied the spike-in strategy described in the previous section.

Summary

In this article a ChIP-MS experiment was performed against glucocorticoid receptor in bone marrow derived macrophages stimulated with LPS and Dex. This experiment revealed that components of the SETD1A/COMPASS complex were direct or indirect interacting with GR in LPS+Dex treated macrophages. ChIP-Seq against GR, SETD1A and CXXC1 (a specific subunit of the SETD1A/COMPASS complex) demonstrated that they co-occupy some genomic loci which are mostly intergenic, indicating that the SETD1A/COMPASS can also bind to mammalian enhancers *in vivo*. Comparison of the ChIP-seq datasets in LPS stimulated macrophages with and without the addition of the GR ligand showed that there is a subset of GR/SETD1A co-bound sites that gain SETD1A recruitment upon Dex. These sites are related to GR targets genes with an anti-inflammatory role like *Tsc22d3* and *Dusp1*, whereas there was no difference in SETD1A occupancy on GR binding sites of cytokines and chemokines that are suppressed by GCs, like *Cxcl10* and *Ccl2*. ChIP-seq against H3K4 methylation marks revealed that there were no global alterations in H3K4 levels, rather than locus specific changes at some enhancers with GR-mediated SETD1A recruitment. Deletion of the catalytic SET domain of the SETD1A in RAW264.7 cells (a murine mouse macrophage cell line) didn’t show changes in H3K4 methylation around GR bound sites suggesting an alternative function of SETD1A at these sites. RNA-sequencing in control and *Setd1a*$^{Del/+}$ cells revealed that SETD1A is required for the activation of anti-inflammatory genes like *Tsc22d3*, *Dusp1* as well as for the induction of pro-inflammatory GR targets genes by LPS. Altogether, these data suggest that GR interacts with the SETD1A/COMPASS complex to regulate the transcription of a distinct subset of anti-inflammatory genes in LPS stimulated macrophages.

Cell Reports

Resource

The glucocorticoid receptor recruits the COMPASS complex to regulate inflammatory transcription at macrophage enhancers

Graphical Abstract

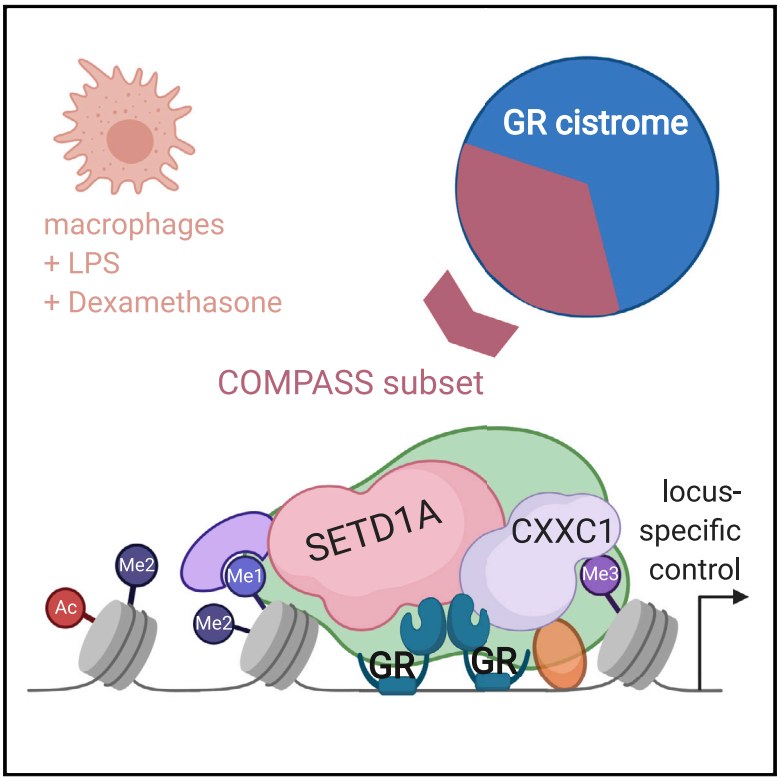

Authors

Franziska Greulich, Michael Wierer, Aikaterini Mechtidou, Omar Gonzalez-Garcia, N. Henriette Uhlenhaut

Correspondence

henriette.uhlenhaut@tum.de

In Brief

Glucocorticoids such as dexamethasone are widely used immunomodulators. Combining proteomics, ChIP-seq, RNA-seq, and genetic loss-of-function studies in murine macrophages, Greulich et al. show that recruitment of the SETD1A/COMPASS complex to *cis*-regulatory elements by the glucocorticoid receptor mediates some of their anti-inflammatory actions.

Highlights

- GR's transcriptional complex in macrophages includes COMPASS proteins
- GR ligand changes SETD1A chromatin occupancy in activated macrophages
- Subsets of GR target sites show COMPASS binding and H3K4 methylation dynamics
- SETD1A is required for some of GR's anti-inflammatory actions

Greulich et al., 2021, Cell Reports *34*, 108742
February 9, 2021
https://doi.org/10.1016/j.celrep.2021.108742

CellPress

Cell Reports

CellPress
OPEN ACCESS

Resource

The glucocorticoid receptor recruits the COMPASS complex to regulate inflammatory transcription at macrophage enhancers

Franziska Greulich,[1,2] Michael Wierer,[3] Aikaterini Mechtidou,[1] Omar Gonzalez-Garcia,[1] and N. Henriette Uhlenhaut[1,2,4,5,6,*]

[1]Institute for Diabetes and Obesity (IDO) & Institute for Diabetes and Cancer (IDC), Helmholtz Center Munich (HMGU) and German Center for Diabetes Research (DZD), 85764 Neuherberg (Munich), Germany
[2]Metabolic Programming, School of Life Sciences Weihenstephan, ZIEL - Institute for Food & Health, Technische Universitaet Muenchen (TUM), 85354 Freising, Germany
[3]Department of Proteomics and Signal Transduction, Max Planck Institute of Biochemistry, 82152 Martinsried, Germany
[4]Metabolic Biochemistry and Genetics, Gene Center, Ludwig-Maximilians-Universitaet LMU, 81377 Munich, Germany
[5]Twitter: @uhlenhautlab
[6]Lead contact
*Correspondence: henriette.uhlenhaut@tum.de
https://doi.org/10.1016/j.celrep.2021.108742

SUMMARY

Glucocorticoids (GCs) are effective anti-inflammatory drugs; yet, their mechanisms of action are poorly understood. GCs bind to the glucocorticoid receptor (GR), a ligand-gated transcription factor controlling gene expression in numerous cell types. Here, we characterize GR's protein interactome and find the SETD1A (SET domain containing 1A)/COMPASS (complex of proteins associated with Set1) histone H3 lysine 4 (H3K4) methyltransferase complex highly enriched in activated mouse macrophages. We show that SETD1A/COMPASS is recruited by GR to specific *cis*-regulatory elements, coinciding with H3K4 methylation dynamics at subsets of sites, upon treatment with lipopolysaccharide (LPS) and GCs. By chromatin immunoprecipitation sequencing (ChIP-seq) and RNA-seq, we identify subsets of GR target loci that display SETD1A occupancy, H3K4 mono-, di-, or tri-methylation patterns, and transcriptional changes. However, our data on methylation status and COMPASS recruitment suggest that SETD1A has additional transcriptional functions. *Setd1a* loss-of-function studies reveal that SETD1A/COMPASS is required for GR-controlled transcription of subsets of macrophage target genes. We demonstrate that the SETD1A/COMPASS complex cooperates with GR to mediate anti-inflammatory effects.

INTRODUCTION

Inflammation is a cellular response to injury or infection, characterized by the secretion of cytokines, chemokines, and other signaling molecules to limit infection, attract immune cells to the site of injury, and orchestrate damage repair (Turvey and Broide, 2010). Excessive activation or impaired silencing of these initially beneficial reactions contributes to a variety of severe human disorders, such as sepsis, arthritis, asthma, etc. (Nathan and Ding, 2010). Therefore, understanding the mechanisms controlling inflammation may enable the development of immunomodulatory therapies.

Glucocorticoids (GCs), such as cortisone or dexamethasone (Dex), are widely prescribed anti-inflammatory drugs that activate the nuclear receptor glucocorticoid receptor (GR) (Oakley and Cidlowski, 2013). Ligand-bound GR translocates to the nucleus to control target gene expression through GC response elements (GREs) or other binding sites present in promoters or enhancers. GR recruits transcriptional coregulators and enzymes, such as histone acetyltransferases (HATs) or histone deacetylases (HDACs), chromatin remodelers, p160 proteins, histone lysine methyltransferases (KMTs), and demethylases (KDMs), etc., to regulate transcription either positively or negatively (Ito et al., 2000; Chen and Roeder, 2007; Chinenov et al., 2008; Uhlenhaut et al., 2013; Hua et al., 2016; Sacta et al., 2018; Clark et al., 2019). In fact, the details of how GR functions are inherently complex, and its presence in many cells and tissues makes selective pharmacological targeting difficult.

GR binds to distinct *cis*-regulatory elements in a tissue-specific manner (Gross and Cidlowski, 2008). These cistromes arise from the pre-defined accessibility of certain chromatin loci, established by lineage-specific pioneer transcription factors (John et al., 2011; Grøntved et al., 2013; Greulich et al., 2016). Within the same cell type, GR may also regulate target genes in a locus- or signal-specific manner (Rollins et al., 2017; Sacta et al., 2018; Hemmer et al., 2019). GR uses discrete molecular mechanisms and varying coregulators in conjunction with local chromatin contexts for gene-specific transcriptional control (Sacta et al., 2018).

To identify the components mediating GR's immunomodulatory functions, we performed interactome mapping by proteomics, identifying the COMPASS (complex of proteins associated with Set1) complex as a major GR interactor. This conserved protein family catalyzes different stages of histone H3 lysine 4 methylation (H3K4me), a histone mark associated with gene and enhancer activation (Briggs et al., 2001; Nagy et al., 2002). COMPASS complexes are generally composed of multiple subunits including WDR5, ASH2L, DPY30, and RBBP5 (Shilatifard, 2012; Couture and Skiniotis, 2013). Subunits specific to the SETD1A (SET domain containing 1A)/COMPASS complex are WDR82 and CXXC1 (Lee and Skalnik, 2005, 2008; Wu et al., 2008). SETD1A/COMPASS has been associated with global H3K4me3, mostly, but not exclusively, of promoter regions (Wu et al., 2008; Clouaire et al., 2012; Bledau et al., 2014).

In general, H3K4me3 is deposited at the transcriptional start site (TSS) of highly expressed genes (Santos-Rosa et al., 2002; Shilatifard, 2012). Tri-methylation of H3K4 requires a H3K4me2 substrate, which is also established by SETD1A, and expands downstream into the gene body (Soares et al., 2017; Yang and Ernst, 2017). However, a causal relationship between H3K4me3 and transcription has not been definitely established. H3K4me3 has also been proposed to recruit chromatin remodelers, HAT and HDAC complexes, histone demethylases, and the transcription factor II D (TFIID) complex (Briggs et al., 2001; Li et al., 2006; Wysocka et al., 2006; Sims et al., 2007; Vermeulen et al., 2007; Bian et al., 2011; Beurton et al., 2019).

H3K4me1 and H3K4me2 mainly mark enhancers that are MLL3/4 dependent, occasionally with low levels of H3K4me3 (Vermeulen et al., 2007; Pekowska et al., 2011; Kaikkonen et al., 2013). A function for SETD1A/COMPASS in enhancer methylation has not been shown, but studies in yeast, in *Drosophila*, and in mice demonstrate its crucial role in global H3K4me (Ardehali et al., 2011; Bledau et al., 2014; Soares et al., 2014). However, yeast SET1 is dispensable for cellular survival under steady-state conditions (Briggs et al., 2001; Boa et al., 2003).

Here, we identified the SETD1A/COMPASS complex as a coregulator in GR-mediated inflammatory gene regulation. We observed that GR recruits the SETD1A/COMPASS complex to control a subset of enhancers in activated macrophages. SETD1A/COMPASS recruitment to chromatin coincided with binding-site specific changes, but not with global changes, in H3K4me. *Setd1a* depletion in macrophages confirmed its requirement for locus-dependent, GR-mediated gene regulation, without loss of H3K4me status. We therefore suggest that SETD1A contributes to GR's anti-inflammatory actions, independently of H3K4me, in a gene-specific manner.

RESULTS

SETD1A/COMPASS interacts with the GR in macrophages

In order to identify the GR nuclear interactome under inflammatory conditions, we performed chromatin immunoprecipitation coupled to mass spectrometry (ChIP-MS) in primary murine bone-marrow-derived macrophages (BMDMs). Cells were treated with the GR ligand Dex and the Toll-like receptor 4 (TLR4) stimulus lipopolysaccharide (LPS), which activates nuclear AP-1, nuclear factor κB (NF-κB), and interferon (IFN) regulatory factors (IRFs). Significantly enriched proteins are shown in Figure 1A ($p < 0.05$, >1.5-fold enrichment over immunoglobulin G [IgG] controls; Table S1).

We confirmed known interactions with NCOA2/GRIP1, CBP/P300, and the NF-κB subunits c-Rel (REL) and p65 (RELA) (Ray and Prefontaine, 1994; Kino et al., 1999; Wang et al., 2012; Uhlenhaut et al., 2013; Rollins et al., 2017). We detected all the components of the SETD1A/COMPASS complex, namely SETD1A, SETD1B, WDR5, ASH2L1, RBBP5, DPY30, CXXC1, and WDR82, among GR's direct or indirect physical partners in the presence of LPS + Dex (Figure 1A). Gene Ontology (GO) analysis revealed H3K4me among the main functionalities of the GR interacting proteins (Figure 1B).

These data were confirmed by co-immunoprecipitation (coIP) in the macrophage cell line RAW264.7 (Figure 1C; Figures S1A and S1B). coIP with a GR-specific antibody co-enriched the catalytic subunit SETD1A, CXXC1, and WDR82. Using a SETD1A-specific antibody, we validated the interaction of SETD1A, CXXC1, and WDR82 with GR. Conversely, CXXC1 and WDR82 coIPs also enriched GR (Figure 1C).

We also found SETD1A, CXXC1, and COMPASS subunits co-enriched in our ChIP-MS interactome from mouse livers, suggesting that these interactions occur *in vivo* and are not only macrophage specific (Figure S1C) (Hemmer et al., 2019).

To characterize the functional relationships between SETD1A, SETD1B, and GR, we generated conditional *Setd1b* knockouts (Bledau et al., 2014). (We could not obtain viable *Setd1a* null macrophages, suggesting that *Setd1a* is essential for cell survival.) *Setd1b* knockout macrophages were differentiated, treated with either LPS or Dex + LPS, and processed for RNA-seq (Figure S1D). We did not detect major differences in GR target gene regulation between wild-type and *Setd1b* knockout macrophages in response to GR ligand (Figure S1E). Thus, SETD1B may not be critical for GC-induced transcriptional responses. We therefore focused on SETD1A for further functional analyses.

GR and SETD1A/COMPASS co-occupy genomic regions in macrophages

To understand the function of the protein-protein interactions between GR and SETD1A/COMPASS in macrophages under inflammatory conditions, we tested whether SETD1A, CXXC1, and GR co-occupy genomic loci in murine BMDMs using ChIP-seq. In macrophages treated with LPS + Dex, 42% of the GR binding sites (GBSs) were co-occupied by SETD1A, of which 60% additionally bound CXXC1 (Figure 2A).

Bioinformatic motif analyses confirmed the central enrichment of various GRE motifs in all genomic regions bound by GR. In addition to palindromic GREs (NGNACA(N)$_3$TGTNCN) with three spacer nucleotides (Strähle et al., 1987), the subset of regions binding GR, SETD1A, and CXXC1 was enriched for GRE sequences with only one spacer nucleotide (GNNACA(N)$_1$TGTNNC, log(p value) of $2.7e^{-4}$) (Figure 2B). These results suggest that co-recruitment of CXXC1 with SETD1A by GR may involve specific GRE sequences.

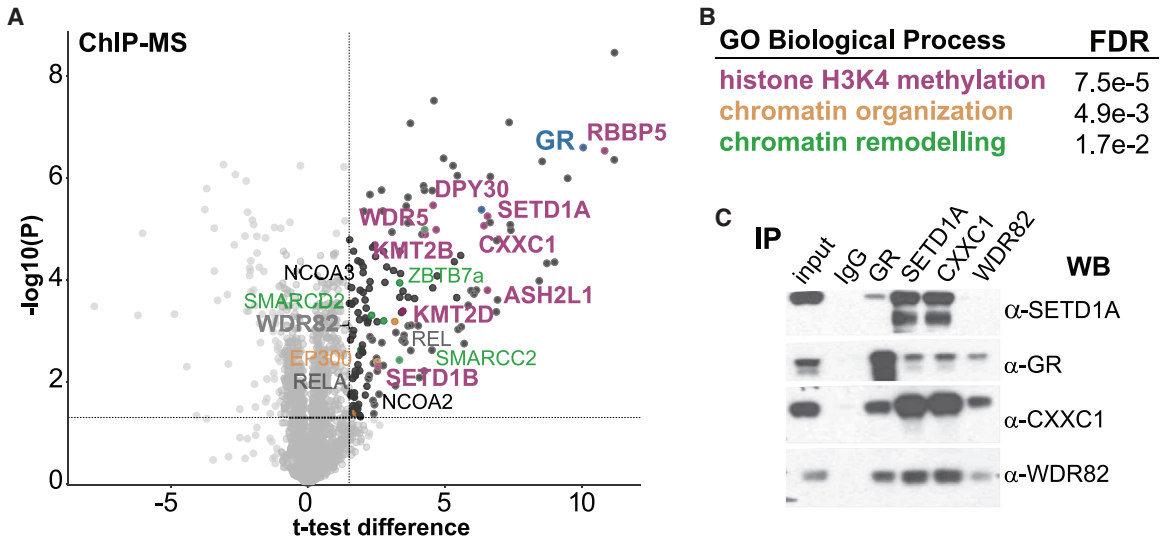

Figure 1. SETD1A/COMPASS interacts with the glucocorticoid receptor (GR)

(A) ChIP-MS proteomics. Volcano plot shows proteins enriched in the GR coIP. Each dot is a detected protein. Dashed lines and darker colors delineate the threshold of 1.5-fold enrichment and $p < 0.05$ significance ($n = 3$). Selected proteins belonging to over-represented Gene Ontology (GO) categories (B) are labeled in color.

(B) GO functional annotation of significantly co-enriched proteins ($p < 0.05$, fold change [FC] > 1.5).

(C) Western blots of endogenous coIPs for GR, SETD1A, CXXC1, and WDR82 in RAW264.7 cells treated with Dex + LPS.

Genomic regions bound by SETD1A without co-occupancy of CXXC1 or GR were enriched for ETS motifs, and SETD1A-CXXC1 co-occupied regions were enriched for YY1 motifs (Figure 2B). Both ETS and YY1 motifs are usually associated with promoters, consistent with these SETD1A-binding regions mapping close to TSSs (Figure 2C). Most GR-bound subsets, including those without co-binding COMPASS proteins, mapped to intergenic locations (Figure 2C), agreeing with previous results showing GR mainly binds distant enhancers in macrophages (Uhlenhaut et al., 2013).

Other motifs co-enriched among all GR-occupied sites, within 100 bp of the peak center, included the pioneer factor PU.1 (Figure S2E), a lineage-determining pioneer factor known to shape the myeloid chromatin landscape (Heinz et al., 2010). Furthermore, regions co-bound by GR-SETD1A-CXXC1 also featured AP-1 motifs, a known interaction partner of GR (Jonat et al., 1990; Yang-Yen et al., 1990). By contrast, GR-SETD1A co-bound sites were enriched for C/EBP and RBPJ motifs, suggesting there may be different modes of transcription factor crosstalk for distinct subsets of enhancers. In the absence of GR, SETD1A- or SETD1A-CXXC1-bound sequences mostly localized to promoters and thus were enriched for SP1 motifs, as was shown for CG-rich promoter elements (Dynan and Tjian, 1983). Common SETD1A-CXXC1-bound sites found in macrophages treated only with LPS contained NF-κB and AP-1 motifs and mapped to inflammatory signaling pathways, indicating that the COMPASS complex might be involved in the LPS response itself (Figures S2A–S2D).

Having identified different groups of genomic loci involved in the combinatorial recruitment of GR, SETD1A, and CXXC1 in BMDMs under Dex + LPS conditions, we assigned biological functions to these regions by KEGG (Kyoto Encyclopedia of Genes and Genomes) pathway over-representation analysis. All the sites co-occupied by GR-SETD1A-CXXC1 were associated with inflammatory pathways (Figure 2D), consistent with GR's immunomodulatory activity (Uhlenhaut et al., 2013; Escoter-Torres et al., 2019). Sites bound by GR alone were associated with Ca^{2+} signaling, endocytosis, and cell cycle, and sites bound by SETD1A alone were enriched for protein degradation and processing pathways (Figure 2D). Thus, SETD1A/COMPASS proteins are associated with the anti-inflammatory properties of GCs.

Altogether, GR, SETD1A, and, to a lesser extent, CXXC1 co-occupy genomic loci in macrophages treated with Dex + LPS. These common *cis*-regulatory regions were mostly intergenic, demonstrating that the SETD1A/COMPASS complex is bound to mammalian enhancers *in vivo* (van de Lagemaat et al., 2018; Mukai et al., 2019). However, this co-occupancy only represents a fraction of the GR cistrome, indicating that diverse functional classes or categories of regulatory sites likely exist.

GR recruits SETD1A/COMPASS to chromatin in response to ligand

To determine whether genomic SETD1A/COMPASS binding was influenced by GC treatment, we compared the SETD1A and CXXC1 ChIP-seq signals in macrophages treated either with LPS alone or with Dex + LPS. (As we were most interested in the regulation of inflammatory genes by GR, we did not investigate quiescent macrophages without LPS stimulation [vehicle or Dex only].) We found that the addition of GR ligand substantially increased the genomic occupancy of both SETD1A and CXXC1, in a manner similar to known GR coregulators, such

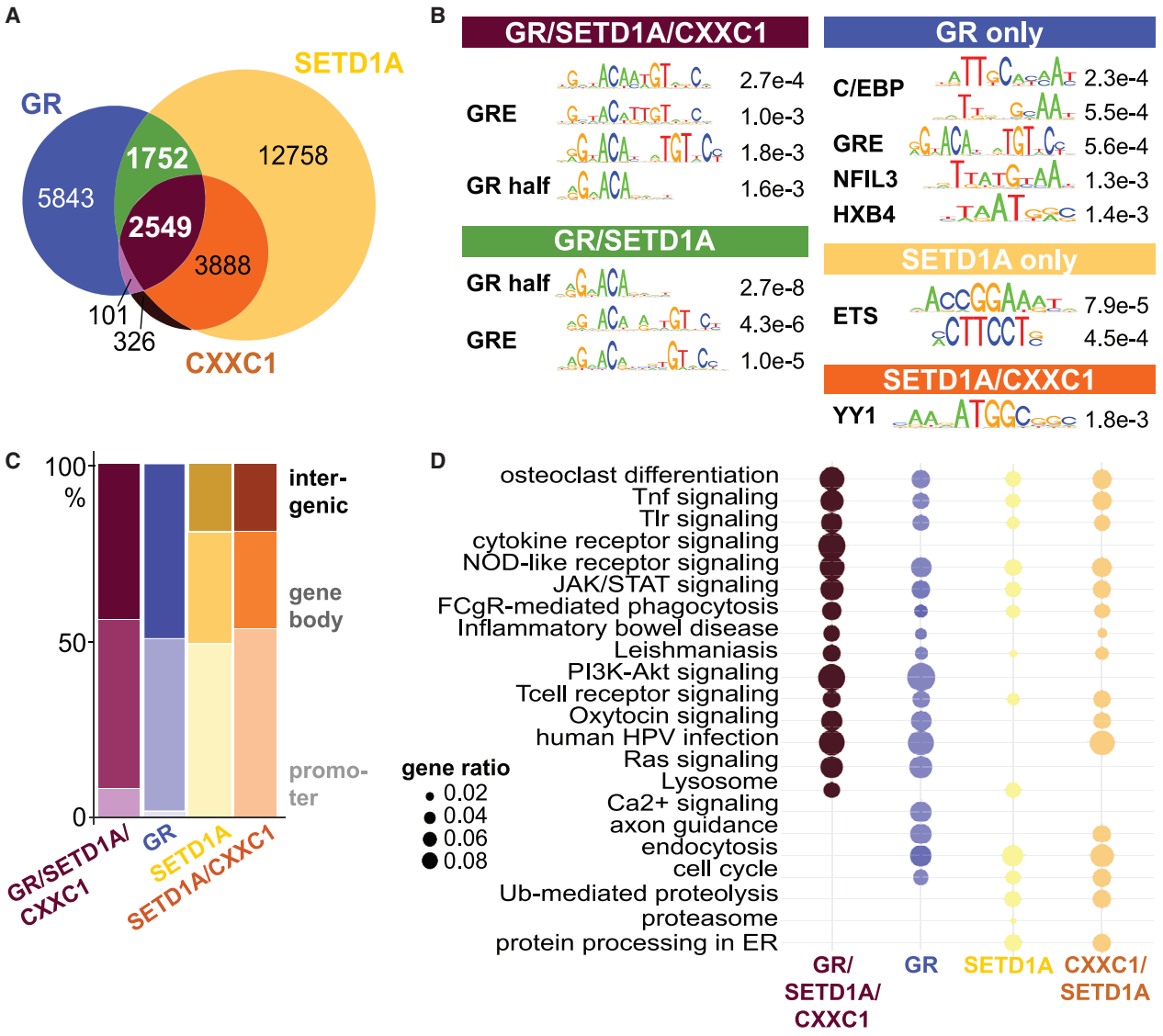

Figure 2. GR and SETD1A/COMPASS co-occupy genomic regions in macrophages

(A) Venn diagram of GR (blue, n = 3), SETD1A (yellow, n = 2), and CXXC1 (brown, n = 2) ChIP-seq peak overlap in macrophages treated with Dex + LPS.

(B) Differential Centrimo motif enrichment of indicated subsets over the total called 27,127 GR, SETD1A, and CXXC1 peaks, with Bonferroni-adjusted (adj) binomial p values (right).

(C) Feature distribution over genomic locations of the different peak subsets (promoters defined as <1 kb from the TSS, intergenic defined as >1 kb from any gene).

(D) KEGG pathway over-representation analysis for peak subsets (Benjamini-Hochberg adj hypergeometrical p value). Circle sizes represent gene ratios.

as NCOA2/GRIP1 (Figure 3A; Figures S3A and S3B) (Uhlenhaut et al., 2013). We then analyzed 1,765 intergenic regions (>1 kb from any gene) bound by both GR and SETD1A in response to Dex, as revealed by ChIP-seq. We plotted the SETD1A and CXXC1 occupancy at the GR target sites in descending order of GR-dependent SETD1A recruitment. Numerous sites gained SETD1A centrally at the GBS, while most other signals appeared peripherally near the GBS (Figure 3A). Similar results were obtained for CXXC1, suggesting that SETD1A and CXXC1 are recruited to chromatin by GR in response to ligand (Figure 3A).

GC-induced SETD1A/CXXC1 recruitment was seen at the anti-inflammatory GR target genes *Tsc22d3* (*Gilz*) and *Dusp1* (Figure 3B; Figure S3C). Cytokines or chemokines, such as the GR targets *Cxcl10* or *Il1a*, which are suppressed by GCs, however, did not show altered SETD1A or CXXC1 occupancy at their GR-bound enhancers after Dex stimulation. The binding of SETD1A and CXXC1 over the gene body of *Cxcl10* was reduced by Dex (Figure 3B; Figure S3C), in line with previous characterizations of SETD1A promoter binding and with known correlations between active transcription and H3K4me3 levels (Nagy et al., 2002; Santos-Rosa et al., 2002; Sims et al., 2007; Shilatifard 2012).

CellPress
OPEN ACCESS

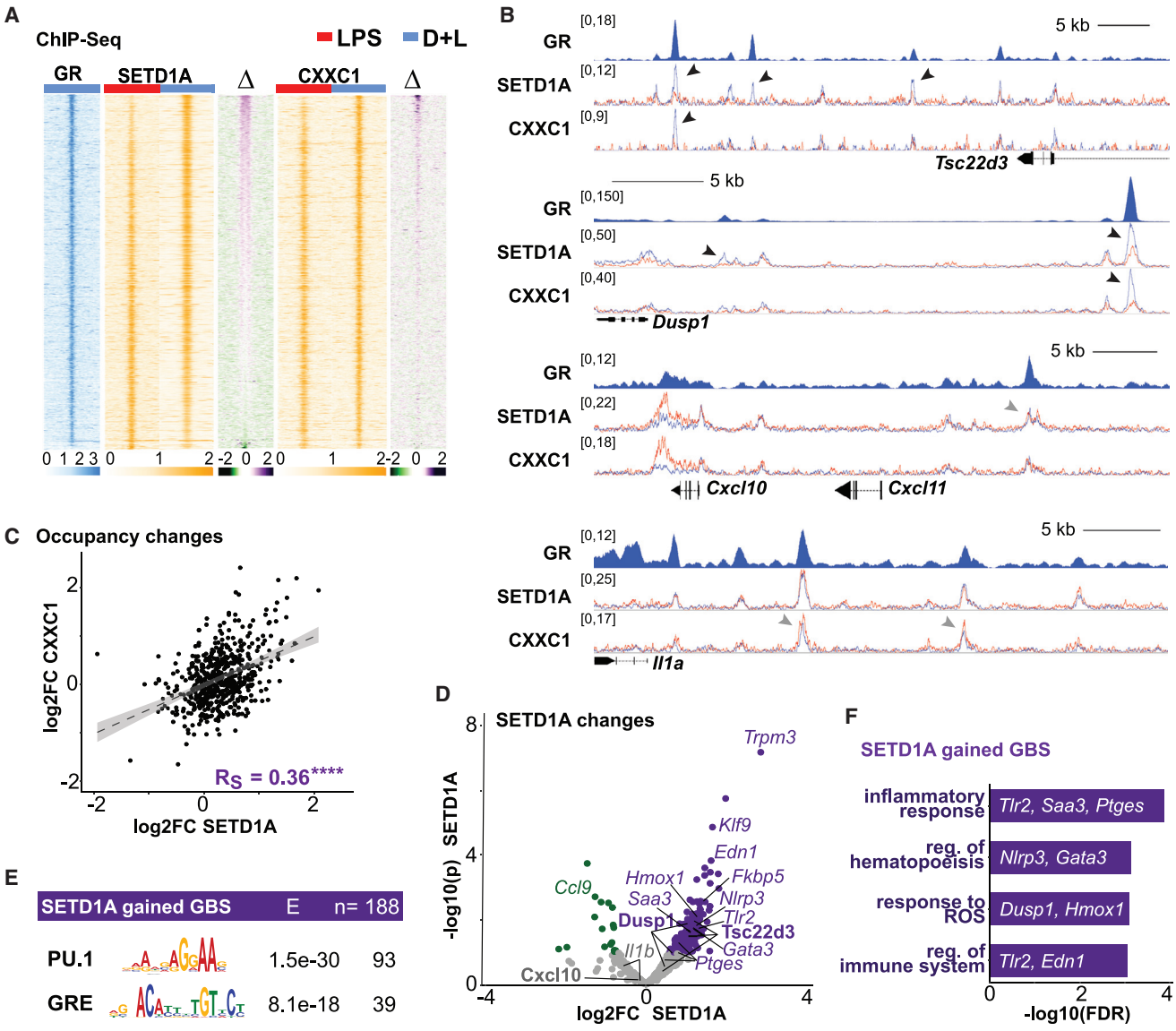

Figure 3. GR recruits SETD1A/COMPASS to chromatin in response to ligand

(A) Heatmap of mean GR, SETD1A, and CXXC1 ChIP-seq coverage in Dex + LPS- and LPS-treated macrophages (n = 2). Each line is one GR-bound site ±2 kb. Binding sites are sorted by log2FC of SETD1A occupancy between Dex + LPS and LPS. Δ represents the difference in normalized coverage between Dex + LPS and LPS.

(B) Example genome browser tracks of ChIP-seq for GR, SETD1A, and CXXC1 in macrophages treated with LPS or Dex + LPS. GR occupancy is the filled area under the curve (blue) (n = 1). Lines are medians of two replicates. Arrows point toward signal changes.

(C) Correlation of SETD1A and CXXC1 occupancy at GR-SETD1A-CXXC1 co-bound enhancers; scatterplot of log2FC of CXXC1 and SETD1A. The dashed regression line includes the 95% confidence interval (gray shadow). ****$p < 0.0001$. R_S, Spearman correlation coefficient.

(D) Changes in SETD1A occupancy ($log2FC_{SETD1A}$) in response to Dex + LPS over LPS. GBSs with increased SETD1A occupancy (FC > 1.5, $p < 0.1$) are purple; GBSs with reduced SETD1A binding (FC < −1.5) are green. Selected enhancers are labeled.

(E) MEME motif enrichment of sites recruiting SETD1A ($p < 0.1$, FC > 1.5), with E-values and numbers of positive sites.

(F) GO analysis for biological processes of the closest genes, with examples and the −log10 of the hypergeometric false discovery rate (FDR).

Overall, the changes in SETD1A and CXXC1 recruitment to intergenic regions co-bound by GR-SETD1A-CXXC1 correlated well for the recruitment of both factors (Spearman correlation coefficient of 0.36) (Figure 3C). We classified the GR-SETD1A sites into those significantly gaining SETD1A (>1.5-fold, $p < 0.1$), those with unchanged occupancy ($p < 0.1$, fold change [FC] < 1.5×), and those losing SETD1A ($p < 0.1$, FC < −1.5×). CXXC1 occupancy was similar to SETD1A, with enhancers gaining SETD1A also gaining CXXC1 and enhancers losing SETD1A also losing CXXC1 binding (Figure S3D). This co-dependency of SETD1A and CXXC1 recruitment is consistent with their known function within the same complex and with the observation that CXXC1

is required for SETD1A recruitment at promoters (Brown et al., 2017; van de Lagemaat et al., 2018).

Analysis of SETD1A enrichment at GR enhancers by differential binding analysis revealed that those loci gaining SETD1A correspond to GR target genes, such as *Tsc22d3*, *Dusp1*, *Fkbp5*, and *Klf9* (Figure 3D). These are known GR-dependent genes in macrophages and are enriched for the palindromic GRE and PU.1 motifs (Figure 3E) (Uhlenhaut et al., 2013; Rollins et al., 2017; Escoter-Torres et al., 2019). These enhancers were significantly enriched for the biological processes "inflammatory response" (*Tlr2*, *Ptges*), "response to reactive oxygen species" (*Dusp1*, *Hmox1*), "positive regulation of the immune system" (*Nlrp3*), and "regulation of hematopoiesis" (*Gata3*) (Figure 3E; Table S3). The small number of sites that lost SETD1A upon GR binding did not show any enrichment for specific motifs or GO terms.

Since we had also detected COMPASS components in our liver ChIP-MS interactome, we tested whether the occupancy of SETD1A and CXXC1 was dependent on GR *in vivo*. Indeed, we found reduced binding of both SETD1A and CXXC1 to GR target sites in livers from hepatocyte-specific GR knockout mice (Figure S3E).

In sum, we found that ligand-induced GR chromatin occupancy leads to the recruitment of the SETD1A/COMPASS H3K4 methyltransferase complex to a subset of GR-bound *cis*-regulatory elements. These GC-activated enhancers control inflammatory responses and represent a distinct subset of the GR cistrome.

GR-mediated SETD1A/COMPASS recruitment to enhancers shows locus-specific histone methylation

To assess whether ligand-dependent recruitment of SETD1A/COMPASS to GR target sites changed mono-, di-, and trimethylation patterns in activated cells, we used ChIP-seq in primary macrophages treated either with LPS or with Dex + LPS. H3K27ac was measured as a modification associated with active enhancers, and RNA-seq was used to determine target gene transcription (Creyghton et al., 2010). We performed model-based clustering of log2 FCs in SETD1A, CXXC1, H3K4me1/me2/me3, and H3K27ac ChIP-seq signals for GBSs with significantly altered SETD1A binding (absolute [abs](FC) > 1.5, $p < 0.1$) in Dex + LPS- versus LPS-treated BMDMs. We assumed heterogeneity among the GR enhancers with differential SETD1A binding and therefore chose generalized mixed models. The appropriate model was selected by maximizing the Bayesian information criterion (Scrucca et al., 2016). A model with three components and ellipsoidal distribution with variable volume and equal shape fitted the data best and was used to classify target sites (Figure S4A).

This analysis revealed three clusters of epigenetic changes, correlating with the recruitment of SETD1A to GR enhancers. Two clusters gained SETD1A occupancy, and the smallest cluster lost SETD1A upon Dex + LPS treatment (Figures 4A–4D). Consistent with our previous results, GR enhancers significantly gaining SETD1A ($p < 0.0001$) also acquired CXXC1 and H3K27ac and were associated with nearby genes that mainly increased mRNA expression upon Dex stimulation (Figures 4B and 4E). Note that one cluster (22 loci, red) additionally gained H3K4me2 in response to ligand (Figure 4B, Figure S4C). These loci represent the fraction of sites that recruited SETD1A *de novo*, such as *Tsc22d3* (Figures 3B, 4C, and 4D; Figures S4B and S4C). Those enhancers with reduced SETD1A binding upon Dex treatment lost CXXC1, H3K4me3, and H3K27ac (21 sites, blue) (Figures 4A and 4B). Similar results were obtained by model-based clustering and correlation analysis of these differential target sites, with increased gene expression corresponding to gaining SETD1A and H3K27ac, independent of H3K4me2 or H3K4me3 (Figures 4E and 4F; Figures S4C and S4D).

These data highlight the existence of locus- and factor-specific modes of regulation. For instance, the *Tsc22d3* enhancer showed increased H3K4me1/me2/me3 and H3K27ac, while the *Dusp1* enhancer showed almost no significant changes in H3K4me (with the exception of H3K4me3) or H3K27ac. The *Cxcl10/11* and *Il1a* enhancers, with constant SETD1A occupancy unaffected by ligand, only showed reductions in H3K27ac and H3K4 monomethylation, and no changes in di- or tri-methylation (Figure 4C; Figure S4B). The ChIP-seq results were confirmed by spike-in ChIP-qPCR for selected sites. The changes in H3K4me1 at the *Tsc22d3* enhancer were less prominent in ChIP-qPCR, which was normalized to total H3, suggesting that they might result from nucleosome repositioning rather than increased monomethylation at this particular site (Figure 4D).

H3K4me dynamics upon SETD1A depletion

Investigation of the function of the mammalian SETD1A/COMPASS complex has been complicated by the early lethality of *Setd1a* knockout mice (Bledau et al., 2014). Hematopoietic-cell-specific deletion of *Setd1a* causes loss of hematopoietic differentiation, indicating a requirement of *Setd1a* for cellular identity and development (Tusi et al., 2015). However, its function in fully differentiated cells in response to signaling stimuli has not been explored. To elucidate the functional impact of SETD1A on gene regulation by GR, we generated a *Setd1a* hypomorph using CRISPR-Cas9 in RAW264.7 cells. We truncated SETD1A by introducing a premature stop codon before the essential SET domain, which lowers COMPASS family protein stability (Soares et al., 2014; Dorighi et al., 2017; Jang et al., 2017). Western blots confirmed the reduced SETD1A protein expression in $Setd1a^{Del/+}$ (*Del*) heterozygous clones (Figures S5A and S5B). We were unable to generate homozygous *Setd1a* deletion mutants, presumably because *Setd1a* null macrophages are not viable, as seen with the floxed BMDMs. The suitability of RAW264.7 cells was confirmed by comparing GR cistromes and target gene expression in primary and RAW264.7 macrophages (Figure S5C). GR binding to the *Tsc22d3* and *Dusp1* enhancers was not affected in *Del* cells (Figure S5D).

To investigate whether *Setd1a* depletion reduced H3K4me1, H3K4me2, or H3K4me3 near common macrophage GR/SETD1A binding sites, we profiled H3K4me1/me2/me3 by ChIP-seq in wild-type and *Del* RAW264.7 cells after either LPS or Dex + LPS stimulation. We excluded global loss of H3K4me1/me2/me3 due to *Setd1a* deletion (Figure S5B) and performed spike-in normalizations for our ChIP-seq samples. The cumulative and median H3K4me1/me2/me3 signals around the GBSs were unaltered by *Setd1a* mutation (Figures 5A and 5C; Figures S5E–S5G).

CellPress
OPEN ACCESS

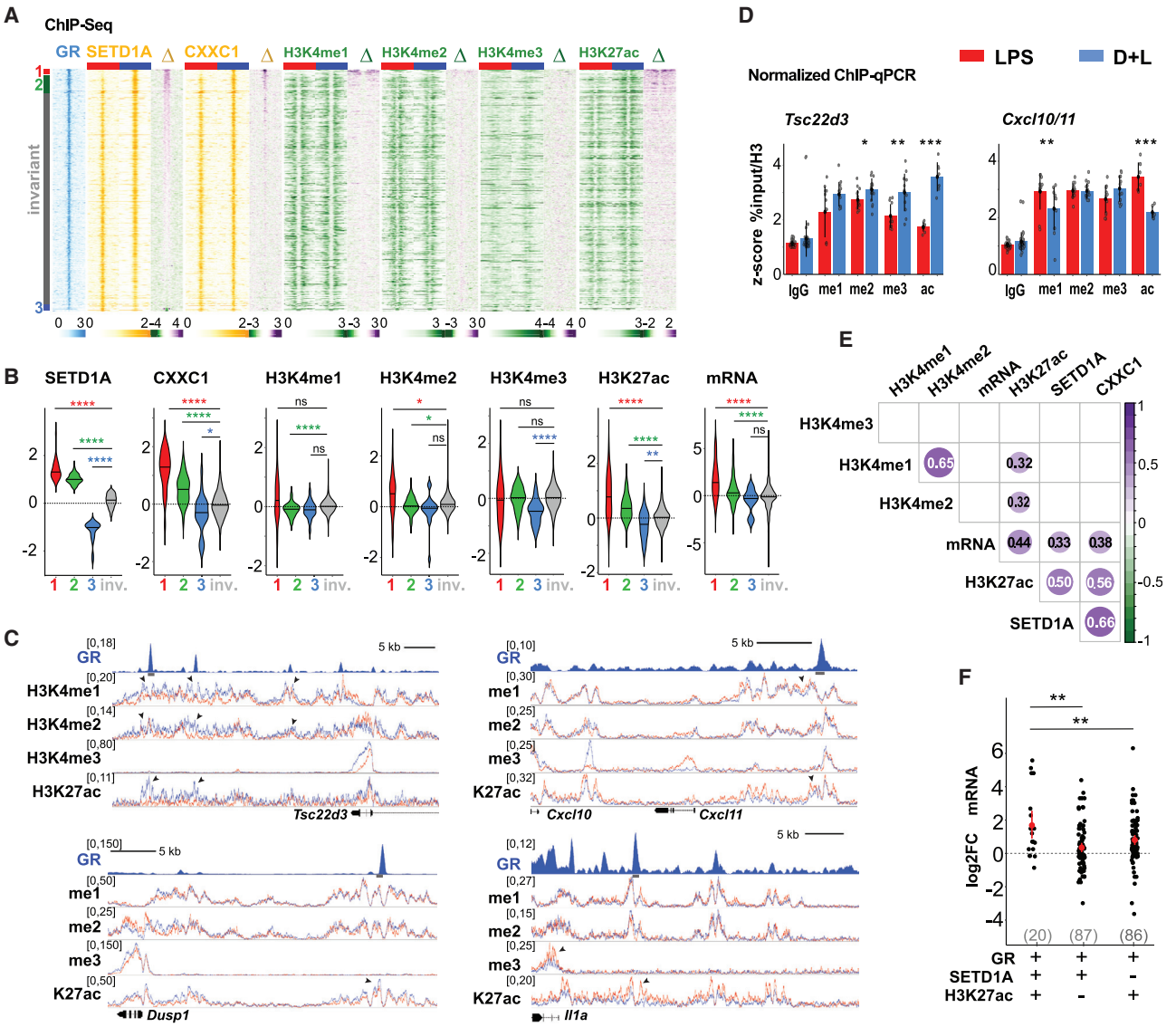

Figure 4. GR-mediated SETD1A/COMPASS recruitment to enhancers shows locus-specific histone methylation

(A) Normalized SETD1A, CXXC1, H3K4me1/me2/me3, and H3K27 acetylation (H3K27ac) ChIP-seq signals in LPS- and Dex + LPS-treated macrophages, ±2 kb around the GBS. Loci are sorted by clusters identified in Figure S4C. Invariant: GBSs with unchanged SETD1A ($p > 0.1$, $-1.5 < FC < 1.5$) occupancy, 588 bp around the GBS. Δ represents the coverage difference between Dex + LPS and LPS treatments.

(B) Log2FC in SETD1A, CXXC1, H3K4me1/me2/me3, and H3K27ac ChIP-seq signals at intergenic regions. mRNA expression of the genes closest to the enhancers from cluster 1, cluster 2, and cluster 3 is displayed together with those showing invariant SETD1A occupancy (inv., $p > 0.1$, $-1.5 < FC < 1.5$; gray). Black lines indicate the distribution mean. (ChIP-seq: Kruskal-Wallis test with post hoc Dunn's test; RNA-seq: one-way ANOVA with post hoc pairwise two-sided t test, Benjamini-Hochberg adj). n = 2.

(C) Normalized median genome browser tracks for H3K4me1/me2/me3 and H3K27ac ChIP-seq ($n \geq 2$, LPS- (red) versus Dex + LPS-treated (blue) BMDMs) plus GR. Arrowheads point at treatment-dependent changes; lines below GR peaks indicate primer locations for (D).

(D) Normalized spike-in ChIP-qPCR for selected loci; mean *Z* scores of total H3 normalized % inputs. Error bars represent standard deviation (n = 3, two-sided Wilcoxon-Mann-Whitney test).

(E) Correlation plot of log2FC in SETD1A, CXXC1, H3K4me1/me2/me3, and H3K27ac at intergenic GBSs with differential SETD1A occupancy ($-1.5 > FC > 1.5$, $p < 0.1$) and the mRNA expression of the closest gene. Pearson correlation coefficients with $p < 0.001$ are displayed as numbers.

(F) Log2FC in mRNA expression of genes with nearby GBS over changes in SETD1A occupancy and/or H3K27ac levels (+, gain; −, invariant or lost). Each dot reflects one enhancer. Red: mean and 95% confidence intervals (Kruskal-Wallis test with post hoc Dunn's test, Benjamini-Hochberg adj). Enhancer numbers are in parentheses.

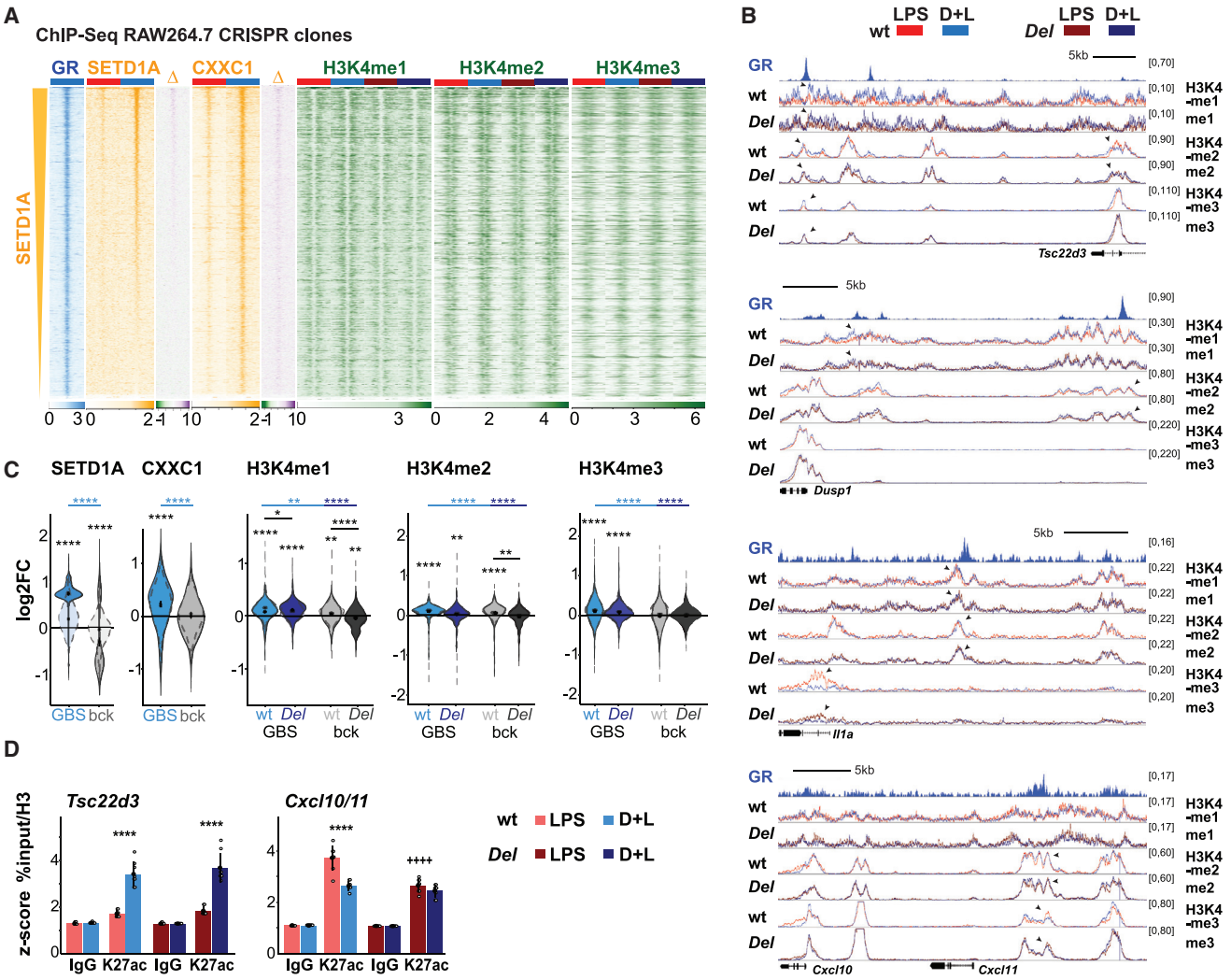

Figure 5. H3K4 methylation dynamics upon SETD1A depletion

(A) Heatmaps for mean SETD1A, CXXC1, and H3K4me1/me2/me3 ChIP-seq at ±2 kb around GR-SETD1A common sites in wild-type (WT) and *Setd1a*$^{Del/+}$ (*Del*) RAW264.7 cells treated with LPS or Dex + LPS. GBSs are sorted by descending SETD1A ChIP signal strength (n = 2–3). See legend (B).

(B) Example genome browser tracks with median ChIP-seq signals for GR, H3K4me1/me2/me3 in WT and mutant RAW264.7 cells. Arrows point towards GR binding sites or changes observed at the TSS.

(C) Violin plots for log2FC in SETD1A, CXXC1, and H3K4me1/me2/me3 ChIP-Seq signals at intergenic regions, comparing Dex + LPS to LPS. GBSs bind GR and SETD1A, while background (bck) sites show H3K4me1/me2/me3, but no GR, SETD1A, or CXXC1 peaks. Signal distributions for constant (light blue, dashed outline) and for GR-SETD1A sites with changed SETD1A binding (full blue, solid outline) are shown (LPS + Dex versus LPS, $p < 0.05$). Treatment effect was determined by one-sample Wilcoxon-Mann-Whitney test, genotype differences by two-sided Wilcoxon-Mann-Whitney test, and group differences by paired two-sample Wilcoxon-Mann-Whitney test.

(D) Spike-in normalized H3K27ac ChIP qPCR in LPS- or Dex + LPS-treated RAW264.7 cells. Mean *Z* scores of total H3 normalized % inputs are plotted (n = 3). Error bars represent standard deviations. Kruskal-Wallis with post hoc Dunn's test, with Benjamini-Hochberg adj p values (adj ps). For all graphs, *$p < 0.05$, **$p < 0.01$, ***$p < 0.001$, ****$p < 0.0001$.

Similar to primary macrophages, H3K4me1/me2/me3 ChIP signals were increased at the *Tsc22d3* enhancer in response to Dex in both wild-type and *Del* cells. We did not observe reductions in H3K4me1/me2/me3 in *Setd1a* mutants at the *Dusp1*, *Tsc22d3*, *Il1a*, or *Cxcl10* loci (Figure 5B; Figures S5H and S5I). H3K27ac was not affected at the *Tsc22d3* or *Cxcl10* enhancers in *Setd1a*$^{Del/+}$ mutants either (Zhang et al., 2020) (Figure 5D).

In summary, we show that GR occupancy, SETD1A recruitment, and increased H3K27ac at a subset of GBSs confer a robust activation potential onto the nearest target gene. However, we did not identify a significant correlation between H3K4me1, H3K4me2, or H3K4m3 and GR-mediated transcriptional control of inflammatory response genes. We conclude that ligand-mediated H3K4me1/me2/me3 dynamics at distant GR-bound sites do not depend on *Setd1a* function. SETD1A depletion did not reduce H3K4 methylation levels, suggesting that the role of SETD1A/COMPASS at enhancers may be distinct from its promoter function and histone methyltransferase activity.

SETD1A mediates regulation of specific myeloid GR targets

To test the hypothesis that SETD1A recruitment by GR plays a role in target gene regulation, we determined the transcriptional effect of *Setd1a* reduction using RNA-seq. The Dex-induced or -repressed mRNA FCs in wild-type and *Setd1a*$^{Del/+}$ RAW264.7 cells stimulated with LPS were compared at two time points (6 and 16 h). We identified 312 ligand-dependent genes that showed an altered Dex response in *Setd1a*$^{Del/+}$ mutants. Four differential response clusters were identified by weighted gene network correlation analysis (Figures 6A and 6B; Figures S6A and S6B).

Cluster 1 contained inflammatory mediators that were repressed by GR in both wild-type and *Del* mutants, albeit with different FCs (Figures 6A–6C). Many of them displayed constant, GC-independent SETD1A occupancy of GBSs in wild-type macrophages, similar to *Cxcl10*, and showed diminished induction by LPS in *Del* mutants. We confirmed the diminished LPS response by qRT-PCR time-series expression analysis of *Cxcl10*, *Irf7*, and *Infb1* in wild-type and *Del* cells (Figure 6D; Figures S6A and S6C). Since *Cxcl10* was expressed at much lower levels in *Del* mutants, it is difficult to interpret GR repression in this case (Figure 6D). However, IFN-β1 treatment rescued the diminished LPS response and induced high levels of *Cxcl10* and *Irf7* expression (Figures S6D–S6F). These observations imply that the genes in cluster 1 may have failed to respond to LPS as a consequence of lost *Infb1* induction in *Del* mutants. Furthermore, when we profiled the mRNA levels of SET domain containing of methyltransferase-encoding genes in LPS and in LPS + IFN-β1-treated control and *Del* cells, we observed differential expression of several enzymes, such as *Setdb2* or *Nsd3*, for example (Figure S6G). These might potentially compensate for SETD1A loss of function and could explain the rescue effect as well.

Similarly, cluster 3 is comprised of inflammatory genes activated by LPS and repressed by Dex and involved in "cytokine production," "response to lipids," "apoptotic signaling," and "response to LPS" (Figure 6C; Table S2). In contrast to cluster 1, the induction of these genes by LPS and their repression by GR were unaltered in *Del* mutants at 6 h, for example, *Tnfa* (Figures 6A and 6B; Figures S6B and S6C).

Clusters 2 and 4 represent genes activated by Dex either early (cluster 2, 6 h) or late (cluster 4, 16 h), among them the anti-inflammatory GR targets *Dusp1* and *Tsc22d3* (Figures 6A–6D). Cluster 4 was enriched for pathways such as "response to bacteria" (Figure 6C; Table S4), and both clusters had a high percentage of genes featuring nearby GR ChIP peaks (Figure S6A). The early induction and the severely diminished or delayed responses of *Dusp1*, *Tsc22d3*, and *Lcn2* to ligand in *Setd1a*$^{Del/+}$ mutants were validated by qRT-PCR at different time points (Figure 6D; Figure S6C). This reduced transcriptional activation was accompanied by a decrease of the Dex-induced H3K4me3 ChIP signals at the TSSs of those targets in *Del* clones (Figures 5B and 6E). However, the genes displaying prominent H3K4me3 signals around their TSSs again only represent a fraction of GR targets. For a global correlation between H3K4me dynamics, transcriptional changes, and SETD1A dependence, we analyzed GR-SETD1A co-bound sites with detectable H3K4me changes in response to Dex. For these targets, we determined the fraction which either displayed altered H3K4me1/me2/me3 patterns or differential transcript expression of the nearest gene in *Del* mutants (Figure 6E). These results again only show subsets of sites with differential H3K4me and a larger subset of target genes whose transcription is affected by SETD1A depletion.

On the other hand, when studying our defined GR subsets with SETD1A recruitment and H3K4me dynamics (Figure 4B), we found that a significant number of them are associated with nearby genes whose expression was affected by *Setd1a* mutation (Figure 6F).

Taken together, Dex-dependent transcriptional activation was disturbed in *Setd1a*$^{Del/+}$ macrophages. Most of the affected genes had a nearby GBS, suggesting that SETD1A mediates a significant part of GR's immunomodulatory actions.

We validated the specificity of our findings by reintroducing *Setd1a* into *Del* cells and were able to rescue *Dusp1* and *Tsc22d3* activation by overexpression of *Setd1a* (Figure 6G; Figure S6H). As the GR occupancy at those enhancers was not affected in *Del* cells (Figure S5D), the observed gene expression changes indeed resulted from impaired SETD1A function and not simply from loss of GR expression or binding.

In summary, we show that *Setd1a* is required for transcriptional control of specific innate immune responses mediated by GR and for activation of the interferon response downstream of TLR4 signaling in RAW264.7 cells.

GR-SETD1A target gene regulation in the absence of TLR4 signaling

Since our observations likely hint at a role for SETD1A downstream of TLR4 activation, which we did not fully investigate, we performed an RNA-seq experiment in RAW264.7 controls and mutants treated only with Dex, in the absence of LPS stimulation. Under these conditions, GR regulates a significantly different set of target genes (Figures 7A and 7B). While *Tsc22d3* and *Dusp1* are still induced, there is very little repression of inflammatory genes (such as *Cxcl10*, *Tnfa*, or *Il1a*, etc.) in macrophages treated only with Dex (compared with vehicle).

When comparing this response to ligand between control and *Setd1a* mutants, we found that several GR targets, such as *Dusp1* or *Il7r*, also showed differential expression upon SETD1A depletion in quiescent cells (Figure 7C). While GR target gene regulation was clearly affected in *Setd1a* mutants treated with Dex, the effect appears less pronounced and does not include as many inflammatory mediators (enriched GO terms "ossification" and "mononuclear cell migration") (Figures S7A and S7B).

Altogether, our data indicate that SETD1A is required for the transcriptional regulation of a subset of macrophage targets by GR, which is most prominent under inflammatory conditions.

DISCUSSION

Our genome-wide studies in LPS-activated macrophages revealed that GR interacts with the SETD1A/COMPASS complex to control the transcription of distinct subsets of

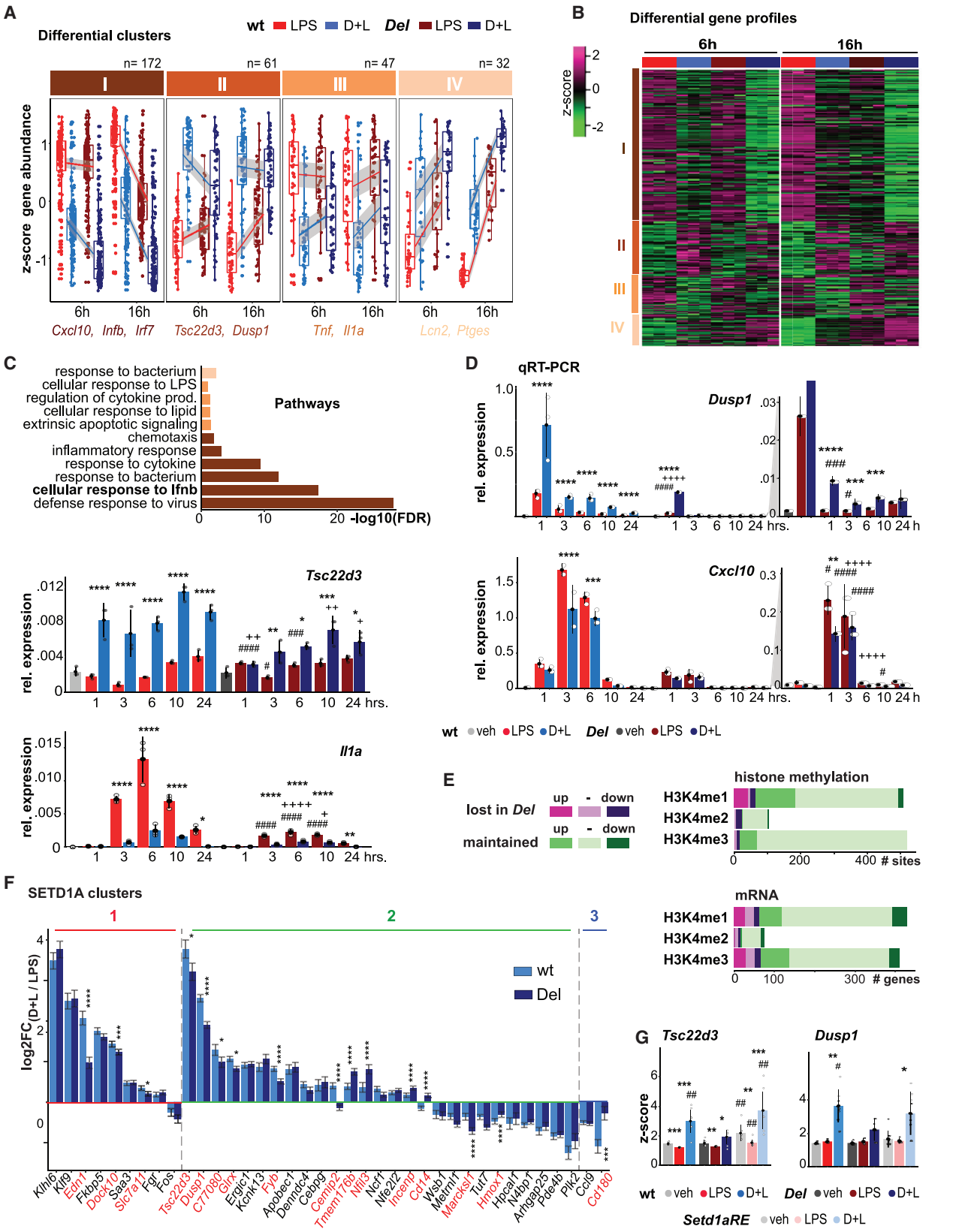

(legend on next page)

inflammatory gene networks. This interaction coincided with changes in H3K4me only at a limited number of specific loci, suggesting distinct *cis*-regulatory mechanisms exist at different enhancers. We characterized a mutant with unstable SETD1A protein and showed that *Setd1a* is required for a subset of GR-dependent gene regulation, but not for enhancer H3K4me.

Our observations of SETD1A/COMPASS enhancer occupancy agree with recent studies on accessible regions in erythrocytes and on MEF2-marked neuronal enhancers (van de Lagemaat et al., 2018; Mukai et al., 2019). These results challenge earlier views that SETD1A/COMPASS is exclusively recruited to promoters, as described in yeast and *Drosophila* (Ng et al., 2003; Ardehali et al., 2011). Conceivably, mammalian COMPASS family members acquired additional functions during their diversification, in line with increased genomic complexity. In addition to H3K4me, our data suggest SETD1A may exert additional transcriptional regulatory functions at distant sites, possibly independent of its H3K4 methyltransferase activity. Enhancer or promoter-specific factors might control the activity of SETD1A (Lee and Skalnik, 2008; Clouaire et al., 2012; Kim et al., 2013; Ebmeier et al., 2017; Hsu et al., 2019), for example, directing it to methylate non-histone proteins, as proposed for other SET-domain-containing complexes (Carlson and Gozani, 2016).

Recently, enhancer H3K4me2 was reported to inhibit GR binding in A549 cells (Clark et al., 2019). We did not detect a correlation between H3K4me2 and GR occupancy at the *Tsc22d3* and *Dusp1* enhancers, but we did observe reduced transcriptional activation of these genes in our *Setd1a* mutant (Figure 6; Figures S6D, 6G, 4C and 5B). Our results are consistent with the idea that H3K4me2 marks active transcription factor-binding regions in the genome (Wang et al., 2014). Nevertheless, locus- and cell-type-specific differences in H3K4me2 function may exist, as we observed that a certain fraction of GBSs gain H3K4me2 in response to Dex in macrophages. For instance, SETD1A recruitment co-occurs with increased H3K4me2 at the *Tsc22d3* locus, but not at other sites, emphasizing context-specific mechanisms for GR action.

For one of these subsets, we found that recruitment of SETD1A/COMPASS was linked to increased H3K27ac upon Dex + LPS stimulation in macrophages, indicating additive effects of SETD1A/COMPASS and HATs. A similar dependency of histone methyltransferases (HMTs) and P300 was previously seen for MLL4 and for GR-dependent G9a recruitment (Bittencourt et al., 2012; Wang et al., 2017). However, our ChIP experiments do not imply that SETD1A/COMPASS is required for HAT activity. On the contrary, P300 might potentially be required by GR to recruit SETD1A/COMPASS in response to ligand (Tang et al., 2013).

Unlike *set1* loss-of-function studies in *S. cerevisiae* (Schneider et al., 2005; Dehé et al., 2006; Kim et al., 2013), global H3K4me2/me3 was not abolished in our *Setd1a*$^{Del/+}$ cells. This suggests there may be redundancy between mammalian COMPASS complex family members. Also, the residual SETD1A or SETD1B proteins present in our *Del* cells could be sufficient to maintain di- and tri-methylation. Other HMTs could be compensating for depositing essential H3K4me3 at promoters (MLL1/2) and H3K4me2 at enhancers (MLL3/4) (Shilatifard, 2012; Meeks and Shilatifard, 2017). Nevertheless, we identified a number of differentially marked H3K4me1/me2/me3 sites, as well as thousands of differentially expressed *Setd1a*-dependent genes. These results suggest that distinct regulatory circuits are controlled by SETD1A/COMPASS, which differentially affect transcription dynamics and H3K4me patterns.

Moreover, we found COMPASS components co-enriched together with GR at hepatic *cis*-regulatory elements in mouse livers, and we measured transcriptional effects of SETD1A depletion in quiescent, Dex-treated macrophages without LPS stimulation. Conceivably, these findings might point toward additional roles for SETD1A as a GR coregulator in other conditions.

Taken together, we propose a model in which SETD1A is essential for the transcriptional control of GR-mediated inflammatory responses in a locus-specific manner, but which do not necessarily correlate with H3K4me or with H3K27ac. Our study shows that GR functions in a context- and locus-specific manner. For any given cell type or condition, different pioneer factors, cellular signals, neighboring transcription factors, epigenetic environments, and coregulators may shape the GC response. In order to develop novel immunomodulatory therapies and to reduce the adverse effects of anti-inflammatory GC treatment, all of these different mechanisms may need to be considered (Sacta et al., 2018; Clark et al., 2019).

Figure 6. SETD1A is required for the transcriptional regulation of certain myeloid GR targets

(A) Clustering of Dex-dependent genes affected by *Setd1a* deletion (weighted gene co-expression network analysis). The *Z*-standardized gene abundance of all genes per cluster is shown, with individual genes as single data points. The distribution median is the vertical line within the boxplot. Regression lines display transcriptional changes between WT and *Del* cells after LPS or Dex + LPS treatment (including a 95% confidence interval, gray shadow). n = cluster size, with example genes.

(B) *Setd1a*-dependent, Dex-regulated genes sorted by the log2FC in WT plus cluster membership (see A).

(C) GO biological process enrichment. Bar plots show −log10 of the FDR for each term (colors as in A).

(D) Time-series qRT-PCR, with mean relative expression as bars and standard deviation as error bars. n = 3, ANOVA with post hoc pairwise t test, Benjamini-Hochberg adj. *, treatment effect Dex + LPS over LPS; #, genotype effect compared with WT (LPS); +, genotype effect compared with WT (Dex + LPS).

(E) Bar plots classifying GR-SETD1A sites by significantly changed H3K4me1/me2/me3 (in response to ligand) and showing the number of sites with altered H3K4me1/me2/me3 (top, pink) or altered nearby transcripts in *Setd1a*$^{Del/+}$ cells (bottom, pink) ($p < 0.05$). Maintained regulation is shown in green, referring to Dex + LPS over LPS. −, invariant, unchanged.

(F) Log2FC of transcripts associated with GR-SETD1A sites classified in Figure 4B. Dex + LPS-treated WT and mutant cells were compared with LPS-treated samples. Error bars are log2 standard errors (n = 3, Wald test, Benjamini-Hochberg adj).

(G) qRT-PCR for GR targets in RAW264.7 cells re-expressing (RE) *Setd1a* in *Del* clones. Bars represent the means, and error bars represent the standard deviation. (n = 3, Kruskal-Wallis with post hoc pairwise Wilcoxon-Mann-Whitney test, Benjamini-Hochberg adj. *, treatment effect; #, genotype effect compared with *Del* cells). *$p < 0.05$, **$p < 0.01$, ***$p < 0.001$, ****$p < 0.0001$.

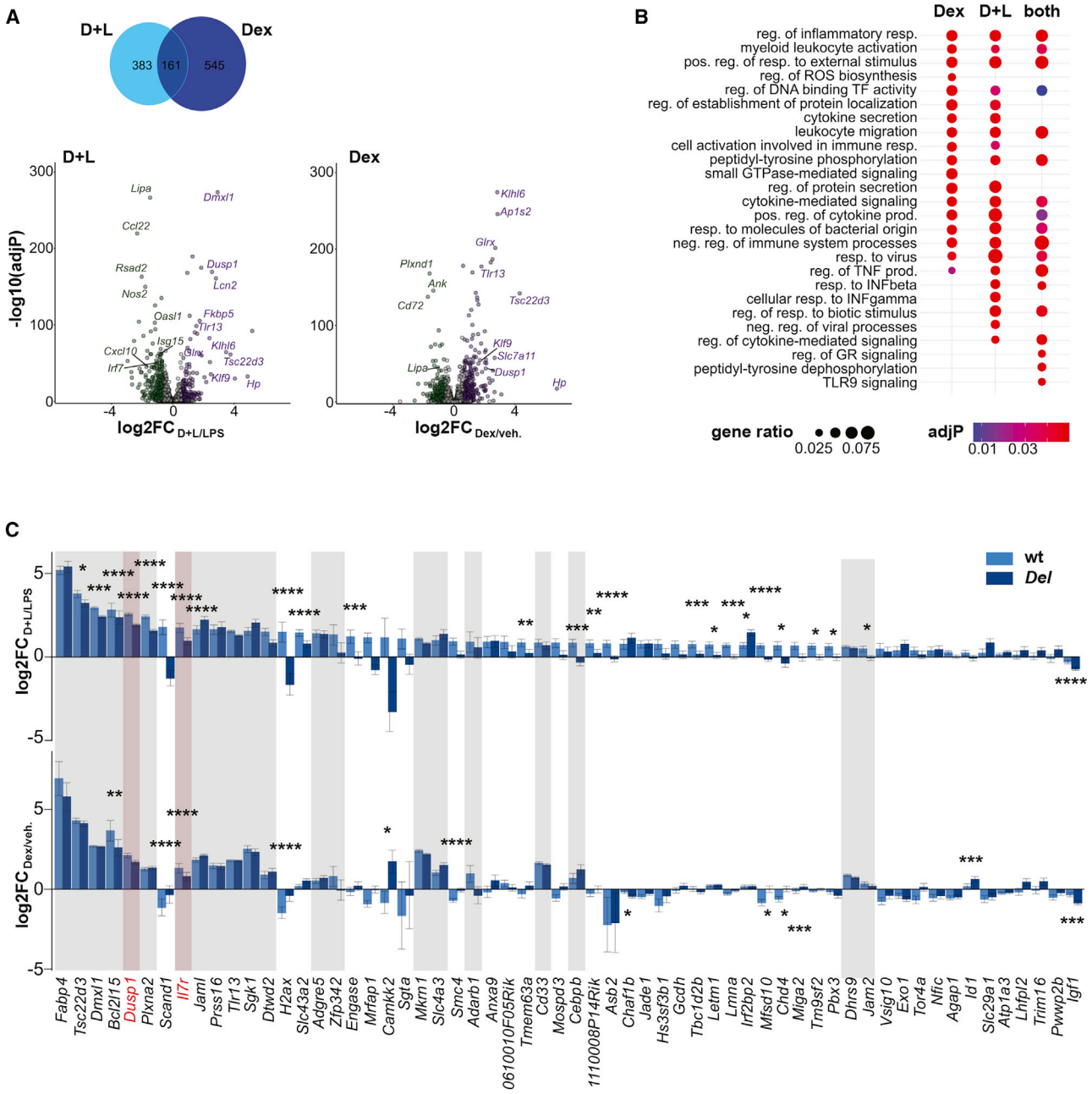

Figure 7. GR-SETD1A target gene regulation in the absence of TLR4 signaling

(A) Numbers of differentially expressed genes (Benjamini-Hochberg adj $p < 0.05$, FC > 1.5) in resting (Dex versus vehicle [veh]) and inflamed (Dex + LPS versus LPS) WT RAW264.7 cells (top). Volcano plots of transcriptional changes in Dex + LPS (over LPS)- and Dex (over veh)-treated cells (adj ps over log2 FCs). Purple, upregulated (adj $p < 0.05$, FC > 1.5); green, downregulated (adj $p < 0.05$, FC > 1.5) genes.

(B) Enrichment of GO biological pathways for genes exclusively regulated by Dex in resting (Dex) or in activated (D + L) macrophages, or in both.

(C) Comparison of the Dex response of cluster 2 (Figure 6A) in LPS-stimulated (D + L over LPS) and in untreated (Dex over veh) RAW264.7 cells. Bars, log2FC for WT and *Setd1aDel*/+ mutant cells; error bars, log2 standard error (Wald test, Benjamini-Hochberg-adjusted). Genes are sorted by their log2FC in WT LPS-treated cells. Gray shades: genes with similar responses to Dex in WT cells. Red shades: genes with impaired regulation in *Del* cells under both conditions. Benjamini-Hochberg adj p-values signify the genotype contribution to the Dex response (~genotype+treatment+treatment:genotype).

STAR★METHODS

Detailed methods are provided in the online version of this paper and include the following:

- KEY RESOURCES TABLE
- RESOURCE AVAILABILITY
  - Lead contact
  - Materials availability

SUPPLEMENTAL INFORMATION

Supplemental information can be found online at https://doi.org/10.1016/j.celrep.2021.108742.

ACKNOWLEDGMENTS

We sincerely thank E. Graf, S. Loesecke, T. Schwarzmayr, and I.A. de la Rosa-Velazquez (HMGU genomics core) for their contribution to the next generation sequencing (NGS) studies and K. Anastassiadis (TU Dresden) for the *Setd1a*$^{fl/fl}$ and *Setd1b*$^{fl/fl}$ bone marrow. We are grateful to M.M. Stephen, A. Sabir, and L. Dinkel for their help with macrophage experiments and I. Burtscher (Helmholtz Diabetes Center, Munich) for the CRISPR-Cas9 plasmids. We thank S. Regn, I. Guderian, and T. Horn for assistance and G. Riddihough (LSE) for editing support. This work received funding from the DFG (UH 275/1-1, SFB 1064 *Chromatin Dynamics*, and TRR 205 *Adrenal Research* to N.H.U. and Entzuendungsprozesse GR 5179/1-1 to F.G.) and from the ERC (ERC-2014-StG 638573 SILENCE to N.H.U.).

AUTHOR CONTRIBUTIONS

F.G. designed and performed the majority of experiments and analyzed the NGS datasets. M.W. carried out the ChIP-MS proteomics, A.M. performed ChIP-qPCRs, and O.G.-G. did coIPs. F.G. and N.H.U. secured funding and wrote the manuscript together. N.H.U. supervised the work. All authors read and approved the final manuscript.

DECLARATION OF INTERESTS

The authors declare no competing interests.

Received: July 13, 2020
Revised: December 9, 2020
Accepted: January 20, 2021
Published: February 9, 2021

REFERENCES

Ardehali, M.B., Mei, A., Zobeck, K.L., Caron, M., Lis, J.T., and Kusch, T. (2011). Drosophila Set1 is the major histone H3 lysine 4 trimethyltransferase with role in transcription. EMBO J. *30*, 2817–2828.

Bembom, O. (2019). seqLogo: Sequence logos for DNA sequence alignments. R package version R package version 1.34.0.

Beurton, F., Stempor, P., Caron, M., Appert, A., Dong, Y., Chen, R.A., Cluet, D., Couté, Y., Herbette, M., Huang, N., et al. (2019). Physical and functional interaction between SET1/COMPASS complex component CFP-1 and a Sin3S HDAC complex in C. elegans. Nucleic Acids Res. *47*, 11164–11180.

Bian, C., Xu, C., Ruan, J., Lee, K.K., Burke, T.L., Tempel, W., Barsyte, D., Li, J., Wu, M., Zhou, B.O., et al. (2011). Sgf29 binds histone H3K4me2/3 and is required for SAGA complex recruitment and histone H3 acetylation. EMBO J. *30*, 2829–2842.

Bittencourt, D., Wu, D.Y., Jeong, K.W., Gerke, D.S., Herviou, L., Ianculescu, I., Chodankar, R., Siegmund, K.D., and Stallcup, M.R. (2012). G9a functions as a molecular scaffold for assembly of transcriptional coactivators on a subset of glucocorticoid receptor target genes. Proc. Natl. Acad. Sci. USA *109*, 19673–19678.

Bledau, A.S., Schmidt, K., Neumann, K., Hill, U., Ciotta, G., Gupta, A., Torres, D.C., Fu, J., Kranz, A., Stewart, A.F., and Anastassiadis, K. (2014). The H3K4 methyltransferase Setd1a is first required at the epiblast stage, whereas Setd1b becomes essential after gastrulation. Development *141*, 1022–1035.

Boa, S., Coert, C., and Patterton, H.G. (2003). Saccharomyces cerevisiae Set1p is a methyltransferase specific for lysine 4 of histone H3 and is required for efficient gene expression. Yeast *20*, 827–835.

Briggs, S.D., Bryk, M., Strahl, B.D., Cheung, W.L., Davie, J.K., Dent, S.Y., Winston, F., and Allis, C.D. (2001). Histone H3 lysine 4 methylation is mediated by Set1 and required for cell growth and rDNA silencing in Saccharomyces cerevisiae. Genes Dev. *15*, 3286–3295.

Brown, D.A., Di Cerbo, V., Feldmann, A., Ahn, J., Ito, S., Blackledge, N.P., Nakayama, M., McClellan, M., Dimitrova, E., Turberfield, A.H., et al. (2017). The SET1 Complex Selects Actively Transcribed Target Genes via Multivalent Interaction with CpG Island Chromatin. Cell Rep. *20*, 2313–2327.

Carlson, S.M., and Gozani, O. (2016). Nonhistone Lysine Methylation in the Regulation of Cancer Pathways. Cold Spring Harb. Perspect. Med. *6*, a026435.

Chen, W., and Roeder, R.G. (2007). The Mediator subunit MED1/TRAP220 is required for optimal glucocorticoid receptor-mediated transcription activation. Nucleic Acids Res. *35*, 6161–6169.

Chinenov, Y., Sacta, M.A., Cruz, A.R., and Rogatsky, I. (2008). GRIP1-associated SET-domain methyltransferase in glucocorticoid receptor target gene expression. Proc. Natl. Acad. Sci. USA *105*, 20185–20190.

Clark, E.A., Wu, F., Chen, Y., Kang, P., Kaiser, U.B., Fang, R., and Shi, Y.G. (2019). GR and LSD1/KDM1A-Targeted Gene Activation Requires Selective H3K4me2 Demethylation at Enhancers. Cell Rep. *27*, 3522–3532.e3.

Clouaire, T., Webb, S., Skene, P., Illingworth, R., Kerr, A., Andrews, R., Lee, J.H., Skalnik, D., and Bird, A. (2012). Cfp1 integrates both CpG content and gene activity for accurate H3K4me3 deposition in embryonic stem cells. Genes Dev. *26*, 1714–1728.

Couture, J.F., and Skiniotis, G. (2013). Assembling a COMPASS. Epigenetics *8*, 349–354.

Cox, J., and Mann, M. (2008). MaxQuant enables high peptide identification rates, individualized p.p.b.-range mass accuracies and proteome-wide protein quantification. Nat. Biotechnol. *26*, 1367–1372.

Creyghton, M.P., Cheng, A.W., Welstead, G.G., Kooistra, T., Carey, B.W., Steine, E.J., Hanna, J., Lodato, M.A., Frampton, G.M., Sharp, P.A., et al. (2010). Histone H3K27ac separates active from poised enhancers and predicts developmental state. Proc. Natl. Acad. Sci. USA *107*, 21931–21936.

Cunningham, F., Achuthan, P., Akanni, W., Allen, J., Amode, M.R., Armean, I.M., Bennett, R., Bhai, J., Billis, K., Boddu, S., et al. (2019). Ensembl 2019. Nucleic Acids Res. *47* (*D1*), D745–D751.

Dehé, P.M., Dichtl, B., Schaft, D., Roguev, A., Pamblanco, M., Lebrun, R., Rodríguez-Gil, A., Mkandawire, M., Landsberg, K., Shevchenko, A., et al. (2006). Protein interactions within the Set1 complex and their roles in the regulation of histone 3 lysine 4 methylation. J. Biol. Chem. *281*, 35404–35412.

Dorighi, K.M., Swigut, T., Henriques, T., Bhanu, N.V., Scruggs, B.S., Nady, N., Still, C.D., 2nd, Garcia, B.A., Adelman, K., and Wysocka, J. (2017). Mll3 and Mll4 Facilitate Enhancer RNA Synthesis and Transcription from Promoters Independently of H3K4 Monomethylation. Mol. Cell *66*, 568–576.e4.

Durinck, S., Spellman, P.T., Birney, E., and Huber, W. (2009). Mapping identifiers for the integration of genomic datasets with the R/Bioconductor package biomaRt. Nat. Protoc. *4*, 1184–1191.

Dynan, W.S., and Tjian, R. (1983). The promoter-specific transcription factor Sp1 binds to upstream sequences in the SV40 early promoter. Cell *35*, 79–87.

Ebmeier, C.C., Erickson, B., Allen, B.L., Allen, M.A., Kim, H., Fong, N., Jacobsen, J.R., Liang, K., Shilatifard, A., Dowell, R.D., et al. (2017). Human TFIIH Kinase CDK7 Regulates Transcription-Associated Chromatin Modifications. Cell Rep. *20*, 1173–1186.

Eden, E., Navon, R., Steinfeld, I., Lipson, D., and Yakhini, Z. (2009). GOrilla: a tool for discovery and visualization of enriched GO terms in ranked gene lists. BMC Bioinformatics *10*, 48.

Egan, B., Yuan, C.C., Craske, M.L., Labhart, P., Guler, G.D., Arnott, D., Maile, T.M., Busby, J., Henry, C., Kelly, T.K., et al. (2016). An Alternative Approach to ChIP-Seq Normalization Enables Detection of Genome-Wide Changes in Histone H3 Lysine 27 Trimethylation upon EZH2 Inhibition. PLoS ONE *11*, e0166438.

Escoter-Torres, L., Caratti, G., Mechtidou, A., Tuckermann, J., Uhlenhaut, N.H., and Vettorazzi, S. (2019). Fighting the Fire: Mechanisms of Inflammatory Gene Regulation by the Glucocorticoid Receptor. Front. Immunol. *10*, 1859.

Freese, N.H., Norris, D.C., and Loraine, A.E. (2016). Integrated genome browser: visual analytics platform for genomics. Bioinformatics *32*, 2089–2095.

Greulich, F., Hemmer, M.C., Rollins, D.A., Rogatsky, I., and Uhlenhaut, N.H. (2016). There goes the neighborhood: Assembly of transcriptional complexes during the regulation of metabolism and inflammation by the glucocorticoid receptor. Steroids *114*, 7–15.

Grøntved, L., John, S., Baek, S., Liu, Y., Buckley, J.R., Vinson, C., Aguilera, G., and Hager, G.L. (2013). C/EBP maintains chromatin accessibility in liver and facilitates glucocorticoid receptor recruitment to steroid response elements. EMBO J. *32*, 1568–1583.

Gross, K.L., and Cidlowski, J.A. (2008). Tissue-specific glucocorticoid action: a family affair. Trends Endocrinol. Metab. *19*, 331–339.

Heigwer, F., Kerr, G., and Boutros, M. (2014). E-CRISP: fast CRISPR target site identification. Nat. Methods *11*, 122–123.

Heinz, S., Benner, C., Spann, N., Bertolino, E., Lin, Y.C., Laslo, P., Cheng, J.X., Murre, C., Singh, H., and Glass, C.K. (2010). Simple combinations of lineage-determining transcription factors prime cis-regulatory elements required for macrophage and B cell identities. Mol. Cell *38*, 576–589.

Hemmer, M.C., Wierer, M., Schachtrup, K., Downes, M., Hübner, N., Evans, R.M., and Uhlenhaut, N.H. (2019). E47 modulates hepatic glucocorticoid action. Nat. Commun. *10*, 306.

Hsu, P.L., Shi, H., Leonen, C., Kang, J., Chatterjee, C., and Zheng, N. (2019). Structural Basis of H2B Ubiquitination-Dependent H3K4 Methylation by COMPASS. Mol. Cell *76*, 712–723.e4.

Hua, G., Ganti, K.P., and Chambon, P. (2016). Glucocorticoid-induced tethered transrepression requires SUMOylation of GR and formation of a SUMO-SMRT/NCoR1-HDAC3 repressing complex. Proc. Natl. Acad. Sci. USA *113*, E635–E643.

Ito, K., Barnes, P.J., and Adcock, I.M. (2000). Glucocorticoid receptor recruitment of histone deacetylase 2 inhibits interleukin-1beta-induced histone H4 acetylation on lysines 8 and 12. Mol. Cell. Biol. *20*, 6891–6903.

Jang, Y., Wang, C., Zhuang, L., Liu, C., and Ge, K. (2017). H3K4 Methyltransferase Activity Is Required for MLL4 Protein Stability. J. Mol. Biol. *429*, 2046–2054.

John, S., Sabo, P.J., Thurman, R.E., Sung, M.H., Biddie, S.C., Johnson, T.A., Hager, G.L., and Stamatoyannopoulos, J.A. (2011). Chromatin accessibility pre-determines glucocorticoid receptor binding patterns. Nat. Genet. *43*, 264–268.

Jonat, C., Rahmsdorf, H.J., Park, K.K., Cato, A.C., Gebel, S., Ponta, H., and Herrlich, P. (1990). Antitumor promotion and antiinflammation: down-modulation of AP-1 (Fos/Jun) activity by glucocorticoid hormone. Cell *62*, 1189–1204.

Kaikkonen, M.U., Spann, N.J., Heinz, S., Romanoski, C.E., Allison, K.A., Stender, J.D., Chun, H.B., Tough, D.F., Prinjha, R.K., Benner, C., and Glass, C.K. (2013). Remodeling of the enhancer landscape during macrophage activation is coupled to enhancer transcription. Mol. Cell *51*, 310–325.

Khan, A., Fornes, O., Stigliani, A., Gheorghe, M., Castro-Mondragon, J.A., van der Lee, R., Bessy, A., Chèneby, J., Kulkarni, S.R., Tan, G., et al. (2018). JASPAR 2018: update of the open-access database of transcription factor binding profiles and its web framework. Nucleic Acids Res. *46* (*D1*), D1284.

Kim, J., Kim, J.A., McGinty, R.K., Nguyen, U.T., Muir, T.W., Allis, C.D., and Roeder, R.G. (2013). The n-SET domain of Set1 regulates H2B ubiquitylation-dependent H3K4 methylation. Mol. Cell *49*, 1121–1133.

Kino, T., Nordeen, S.K., and Chrousos, G.P. (1999). Conditional modulation of glucocorticoid receptor activities by CREB-binding protein (CBP) and p300. J. Steroid Biochem. Mol. Biol. *70*, 15–25.

Kulakovskiy, I.V., Vorontsov, I.E., Yevshin, I.S., Sharipov, R.N., Fedorova, A.D., Rumynskiy, E.I., Medvedeva, Y.A., Magana-Mora, A., Bajic, V.B., Papatsenko, D.A., et al. (2018). HOCOMOCO: towards a complete collection of transcription factor binding models for human and mouse via large-scale ChIP-Seq analysis. Nucleic Acids Res. *46* (*D1*), D252–D259.

Lawrence, M., Huber, W., Pagès, H., Aboyoun, P., Carlson, M., Gentleman, R., Morgan, M.T., and Carey, V.J. (2013). Software for computing and annotating genomic ranges. PLoS Comput. Biol. *9*, e1003118.

Lee, J.H., and Skalnik, D.G. (2005). CpG-binding protein (CXXC finger protein 1) is a component of the mammalian Set1 histone H3-Lys4 methyltransferase complex, the analogue of the yeast Set1/COMPASS complex. J. Biol. Chem. *280*, 41725–41731.

Lee, J.H., and Skalnik, D.G. (2008). Wdr82 is a C-terminal domain-binding protein that recruits the Setd1A Histone H3-Lys4 methyltransferase complex to transcription start sites of transcribed human genes. Mol. Cell. Biol. *28*, 609–618.

Li, H. (2013). Aligning sequence reads, clone sequences and assembly contigs with BWA-MEM. arXiv, 13033997. https://arxiv.org/abs/1303.3997.

Li, H., Ilin, S., Wang, W., Duncan, E.M., Wysocka, J., Allis, C.D., and Patel, D.J. (2006). Molecular basis for site-specific read-out of histone H3K4me3 by the BPTF PHD finger of NURF. Nature *442*, 91–95.

Li, H., Handsaker, B., Wysoker, A., Fennell, T., Ruan, J., Homer, N., Marth, G., Abecasis, G., and Durbin, R.; 1000 Genome Project Data Processing Subgroup (2009). The Sequence Alignment/Map format and SAMtools. Bioinformatics *25*, 2078–2079.

Love, M.I., Huber, W., and Anders, S. (2014). Moderated estimation of fold change and dispersion for RNA-seq data with DESeq2. Genome Biol. *15*, 550.

Machanick, P., and Bailey, T.L. (2011). MEME-ChIP: motif analysis of large DNA datasets. Bioinformatics *27*, 1696–1697.

McLean, C.Y., Bristor, D., Hiller, M., Clarke, S.L., Schaar, B.T., Lowe, C.B., Wenger, A.M., and Bejerano, G. (2010). GREAT improves functional interpretation of cis-regulatory regions. Nat. Biotechnol. *28*, 495–501.

Meeks, J.J., and Shilatifard, A. (2017). Multiple Roles for the MLL/COMPASS Family in the Epigenetic Regulation of Gene Expression and in Cancer. Annu. Rev. Cancer Biol. *1*, 425–446.

Mukai, J., Cannavò, E., Crabtree, G.W., Sun, Z., Diamantopoulou, A., Thakur, P., Chang, C.Y., Cai, Y., Lomvardas, S., Takata, A., et al. (2019). Recapitulation and Reversal of Schizophrenia-Related Phenotypes in Setd1a-Deficient Mice. Neuron *104*, 471–487.e12.

Nagy, P.L., Griesenbeck, J., Kornberg, R.D., and Cleary, M.L. (2002). A trithorax-group complex purified from Saccharomyces cerevisiae is required for methylation of histone H3. Proc. Natl. Acad. Sci. USA *99*, 90–94.

Nathan, C., and Ding, A. (2010). Nonresolving inflammation. Cell *140*, 871–882.

Nelson, J.D., Denisenko, O., and Bomsztyk, K. (2006). Protocol for the fast chromatin immunoprecipitation (ChIP) method. Nat. Protoc. *1*, 179–185.

Newburger, D.E., and Bulyk, M.L. (2009). UniPROBE: an online database of protein binding microarray data on protein-DNA interactions. Nucleic Acids Res. *37*, D77–D82.

Ng, H.H., Robert, F., Young, R.A., and Struhl, K. (2003). Targeted recruitment of Set1 histone methylase by elongating Pol II provides a localized mark and memory of recent transcriptional activity. Mol. Cell *11*, 709–719.

Oakley, R.H., and Cidlowski, J.A. (2013). The biology of the glucocorticoid receptor: new signaling mechanisms in health and disease. J. Allergy Clin. Immunol. *132*, 1033–1044.

Pachkov, M., Balwierz, P.J., Arnold, P., Ozonov, E., and van Nimwegen, E. (2013). SwissRegulon, a database of genome-wide annotations of regulatory sites: recent updates. Nucleic Acids Res. *41*, D214–D220.

Patro, R., Duggal, G., Love, M.I., Irizarry, R.A., and Kingsford, C. (2017). Salmon provides fast and bias-aware quantification of transcript expression. Nat. Methods *14*, 417–419.

Pekowska, A., Benoukraf, T., Zacarias-Cabeza, J., Belhocine, M., Koch, F., Holota, H., Imbert, J., Andrau, J.C., Ferrier, P., and Spicuglia, S. (2011). H3K4 tri-methylation provides an epigenetic signature of active enhancers. EMBO J. *30*, 4198–4210.

Postic, C., Shiota, M., Niswender, K.D., Jetton, T.L., Chen, Y., Moates, J.M., Shelton, K.D., and Lindner, J. (1999 Jan 1). A D: "Dual roles for glucokinase in glucose homeostasis as determined by liver and pancreatic beta cell-specific gene knock-outs using Cre recombinase". J. Biol. Chem. *274*, 305-15. https://doi.org/10.1074/jbc.274.1.305.

Quagliarini, F., Mir, A.A., Balazs, K., Wierer, M., Dyar, K.A., Jouffe, C., Makris, K., Hawe, J., Heinig, M., Filipp, F.V., et al. (2019). Cistromic Reprogramming of the Diurnal Glucocorticoid Hormone Response by High-Fat Diet. Mol. Cell *76*, 531–545.e5.

Quinlan, A.R., and Hall, I.M. (2010). BEDTools: a flexible suite of utilities for comparing genomic features. Bioinformatics *26*, 841–842.

Ramírez, F., Ryan, D.P., Grüning, B., Bhardwaj, V., Kilpert, F., Richter, A.S., Heyne, S., Dündar, F., and Manke, T. (2016). deepTools2: a next generation web server for deep-sequencing data analysis. Nucleic Acids Res. *44* (*W1*), W160–W165.

Ray, A., and Prefontaine, K.E. (1994). Physical association and functional antagonism between the p65 subunit of transcription factor NF-kappa B and the glucocorticoid receptor. Proc. Natl. Acad. Sci. USA *91*, 752–756.

R Core Team (2017). R: A Language and Environment for Statistical Computing (R Foundation for Statistical Computing).

Rollins, D.A., Kharlyngdoh, J.B., Coppo, M., Tharmalingam, B., Mimouna, S., Guo, Z., Sacta, M.A., Pufall, M.A., Fisher, R.P., Hu, X., et al. (2017). Glucocorticoid-induced phosphorylation by CDK9 modulates the coactivator functions of transcriptional cofactor GRIP1 in macrophages. Nat. Commun. *8*, 1739.

Sacta, M.A., Tharmalingam, B., Coppo, M., Rollins, D.A., Deochand, D.K., Benjamin, B., Yu, L., Zhang, B., Hu, X., Li, R., et al. (2018). Gene-specific mechanisms direct glucocorticoid-receptor-driven repression of inflammatory response genes in macrophages. eLife *7*, e34864.

Santos-Rosa, H., Schneider, R., Bannister, A.J., Sherriff, J., Bernstein, B.E., Emre, N.C., Schreiber, S.L., Mellor, J., and Kouzarides, T. (2002). Active genes are tri-methylated at K4 of histone H3. Nature *419*, 407–411.

Schneider, J., Wood, A., Lee, J.S., Schuster, R., Dueker, J., Maguire, C., Swanson, S.K., Florens, L., Washburn, M.P., and Shilatifard, A. (2005). Molecular regulation of histone H3 trimethylation by COMPASS and the regulation of gene expression. Mol. Cell *19*, 849–856.

Scrucca, L., Fop, M., Murphy, T.B., and Raftery, A.E. (2016). mclust 5: Clustering, Classification and Density Estimation Using Gaussian Finite Mixture Models. R J. *8*, 289–317.

Shilatifard, A. (2012). The COMPASS family of histone H3K4 methylases: mechanisms of regulation in development and disease pathogenesis. Annu. Rev. Biochem. *81*, 65–95.

Sims, R.J., 3rd, Millhouse, S., Chen, C.F., Lewis, B.A., Erdjument-Bromage, H., Tempst, P., Manley, J.L., and Reinberg, D. (2007). Recognition of trimethylated histone H3 lysine 4 facilitates the recruitment of transcription postinitiation factors and pre-mRNA splicing. Mol. Cell *28*, 665–676.

Soares, L.M., Radman-Livaja, M., Lin, S.G., Rando, O.J., and Buratowski, S. (2014). Feedback control of Set1 protein levels is important for proper H3K4 methylation patterns. Cell Rep. *6*, 961–972.

Soares, L.M., He, P.C., Chun, Y., Suh, H., Kim, T., and Buratowski, S. (2017). Determinants of Histone H3K4 Methylation Patterns. Mol. Cell *68*, 773–785.e6.

Soneson, C., Love, M.I., and Robinson, M.D. (2015). Differential analyses for RNA-seq: transcript-level estimates improve gene-level inferences. F1000Res. *4*, 1521.

Strähle, U., Klock, G., and Schütz, G. (1987). A DNA sequence of 15 base pairs is sufficient to mediate both glucocorticoid and progesterone induction of gene expression. Proc. Natl. Acad. Sci. USA *84*, 7871–7875.

Tang, Z., Chen, W.Y., Shimada, M., Nguyen, U.T., Kim, J., Sun, X.J., Sengoku, T., McGinty, R.K., Fernandez, J.P., Muir, T.W., and Roeder, R.G. (2013). SET1 and p300 act synergistically, through coupled histone modifications, in transcriptional activation by p53. Cell *154*, 297–310.

Tronche, F., Kellendonk, C., Kretz, O., Gass, P., Anlag, K., Orban, P.C., Bock, R., Klein, R., and Schütz, G. (1999 Sep). Disruption of the glucocorticoid receptor gene in the nervous system results in reduced anxiety. Nat Genet *23*, 99–103. https://doi.org/10.1038/12703.

Turvey, S.E., and Broide, D.H. (2010). Innate immunity. J. Allergy Clin. Immunol. *125* (*2, Suppl 2*), S24–S32.

Tusi, B.K., Deng, C., Salz, T., Zeumer, L., Li, Y., So, C.W., Morel, L.M., Qiu, Y., and Huang, S. (2015). Setd1a regulates progenitor B-cell-to-precursor B-cell development through histone H3 lysine 4 trimethylation and Ig heavy-chain rearrangement. FASEB J. *29*, 1505–1515.

Tyanova, S., and Cox, J. (2018). Perseus: A Bioinformatics Platform for Integrative Analysis of Proteomics Data in Cancer Research. Methods Mol. Biol. *1711*, 133–148.

Uhlenhaut, N.H., Barish, G.D., Yu, R.T., Downes, M., Karunasiri, M., Liddle, C., Schwalie, P., Hübner, N., and Evans, R.M. (2013). Insights into negative regulation by the glucocorticoid receptor from genome-wide profiling of inflammatory cistromes. Mol. Cell *49*, 158–171.

van de Lagemaat, L.N., Flenley, M., Lynch, M.D., Garrick, D., Tomlinson, S.R., Kranc, K.R., and Vernimmen, D. (2018). CpG binding protein (CFP1) occupies open chromatin regions of active genes, including enhancers and non-CpG islands. Epigenetics Chromatin *11*, 59.

Vermeulen, M., Mulder, K.W., Denissov, S., Pijnappel, W.W., van Schaik, F.M., Varier, R.A., Baltissen, M.P., Stunnenberg, H.G., Mann, M., and Timmers, H.T. (2007). Selective anchoring of TFIID to nucleosomes by trimethylation of histone H3 lysine 4. Cell *131*, 58–69.

Wang, W., Guo, C., Li, W., Li, J., Wang, W., Myatt, L., and Sun, K. (2012). Involvement of GR and p300 in the induction of H6PD by cortisol in human amnion fibroblasts. Endocrinology *153*, 5993–6002.

Wang, Y., Li, X., and Hu, H. (2014). H3K4me2 reliably defines transcription factor binding regions in different cells. Genomics *103*, 222–228.

Wang, S.P., Tang, Z., Chen, C.W., Shimada, M., Koche, R.P., Wang, L.H., Nakadai, T., Chramiec, A., Krivtsov, A.V., Armstrong, S.A., and Roeder, R.G. (2017). A UTX-MLL4-p300 Transcriptional Regulatory Network Coordinately Shapes Active Enhancer Landscapes for Eliciting Transcription. Mol. Cell *67*, 308–321.e6.

Wickham, H. (2016). Elegant Graphics for Data Analysis (Springer-Verlag).

Wu, M., Wang, P.F., Lee, J.S., Martin-Brown, S., Florens, L., Washburn, M., and Shilatifard, A. (2008). Molecular regulation of H3K4 trimethylation by Wdr82, a component of human Set1/COMPASS. Mol. Cell. Biol. *28*, 7337–7344.

Wysocka, J., Swigut, T., Xiao, H., Milne, T.A., Kwon, S.Y., Landry, J., Kauer, M., Tackett, A.J., Chait, B.T., Badenhorst, P., et al. (2006). A PHD finger of NURF couples histone H3 lysine 4 trimethylation with chromatin remodelling. Nature *442*, 86–90.

Yang, W., and Ernst, P. (2017). SET/MLL family proteins in hematopoiesis and leukemia. Int. J. Hematol. *105*, 7–16.

Yang-Yen, H.F., Chambard, J.C., Sun, Y.L., Smeal, T., Schmidt, T.J., Drouin, J., and Karin, M. (1990). Transcriptional interference between c-Jun and the glucocorticoid receptor: mutual inhibition of DNA binding due to direct protein-protein interaction. Cell *62*, 1205–1215.

Yu, G., Wang, L.G., Han, Y., and He, Q.Y. (2012). clusterProfiler: an R package for comparing biological themes among gene clusters. OMICS *16*, 284–287.

Zhang, Y., Liu, T., Meyer, C.A., Eeckhoute, J., Johnson, D.S., Bernstein, B.E., Nusbaum, C., Myers, R.M., Brown, M., Li, W., and Liu, X.S. (2008). Model-based analysis of ChIP-Seq (MACS). Genome Biol. *9*, R137.

Zhang, T., Zhang, Z., Dong, Q., Xiong, J., and Zhu, B. (2020). Histone H3K27 acetylation is dispensable for enhancer activity in mouse embryonic stem cells. Genome Biol. *21*, 45.

Zhu, L.J., Gazin, C., Lawson, N.D., Pagès, H., Lin, S.M., Lapointe, D.S., and Green, M.R. (2010). ChIPpeakAnno: a Bioconductor package to annotate ChIP-seq and ChIP-chip data. BMC Bioinformatics *11*, 237.

STAR★METHODS

KEY RESOURCES TABLE

REAGENT or RESOURCE	SOURCE	IDENTIFIER
Antibodies		
Rabbit polyclonal anti-betaTubulin	Santa Cruz Biotechnology	Cat.#sc-9104; RRID:AB_2241191
Mouse monoclonal anti-CXXC1	Santa Cruz Biotechnology	Cat.#sc-136419
Mouse monoclonal anti-GR	Santa Cruz Biotechnology	Cat.#sc-393232; RRID:AB_2687823
Rabbit polyclonal anti-H3	Abcam	Cat.#ab1791; RRID:AB_302613
Mouse monoclonal anti-H3K4me1	Diagenode	Cat.#C15200150
Mouse monoclonal anti-H3K4me2	Diagenode	Cat.#C15200151
Mouse monoclonal anti-H3K4me3	Diagenode	Cat.#C15200152
Goat anti-mouse IgG (HRP-conjugated)	Bio-Rad	Cat.#170-6516; RRID:AB_11125547
Donkey anti-mouse IgG (IRDye680LT)	Li-Cor	Cat.#926-68022; RRID:AB_10715072
Goat anti-rabbit IgG (HRP-conjugated)	Dianova	Cat.#111-035-003; RRID:AB_2313567
Donkey anti-rabbit IgG (IRDye800CW)	Li-Cor	Cat.#926-32213; RRID:AB_621848
Mouse monoclonal anti-SETD1A	Thermo Fisher Scientific	Cat.#MA5-26764; RRID:AB_2725334
Rabbit monoclonal anti-WDR82	Cell Signaling Technology	Cat.#99715; RRID:AB_2800319
Rabbit polyclonal anti-CXXC1	Abcam	Cat.#ab198977
Rabbit polyclonal anti-GR	Protein Tech	Cat.#24050-1-AP; RRID:AB_2813890
Rabbit polyclonal anti-H3	Abcam	Cat.#ab1791; RRID:AB_302613
Rabbit polyclonal anti-H3K27Ac	Abcam	Cat.#ab4729; RRID:AB_2118291
Rabbit polyclonal anti-H3K4me1	Diagenode	Cat.#C15410194; RRID:AB_2637078
Rabbit polyclonal anti-H3K4me2	Abcam	Cat.#ab7766; RRID:AB_2560996
Rabbit polyclonal anti-H3K4me3	Millipore/Merck	Cat.#05-745R; RRID:AB_1587134
Normal rabbit IgG	Cell Signaling Technology	Cat.#2729; RRID:AB_1031062
Rabbit polyclonal anti-SET1	Bethyl	Cat.#A300-289A; RRID:AB_263413
WDR82	Cell Signaling Technology	Cat.#99715; RRID:AB_2800319
Bacterial and virus strains		
Biological Samples		
Chemicals, peptides, and recombinant proteins		
cOmplete, Mini, EDTA-free Protease-Inhibitor-Cocktail	Roche	Cat.#11836170001
cOmplete-Ultra, EDTA-free Protease Inhibitor Cocktail	Roche	Cat.#5892953001
Ficoll Paque PLUS	GE Healthcare	Cat.#17144002
DMEM (4.5 g/L glucose)	Sigma	Cat.#D6429-500
Fetal Bovine Serum	Sigma	Cat.#F9665
Fetal Bovine Serum, dyalized	Sigma	Cat.#F0392-100ml
dexamethasone	Sigma	Cat.#D4902
LPS E.COLI O111:B4	Sigma	Cat.#LPS25
Interferon-beta1	R&D Systems	Cat.#8234-MB-010
Dynabeads M-280 Sheep Anti-Rabbit IgG	Life Technologies	Cat.#11204D
Sepharose Protein A/G	Rockland	Cat.#PAG50-00-0002
DSG Crosslinker	Proteochem	Cat.#C1104
16% Formaldehyde (w/v), Methanol-free	Thermo Scientific	Cat.#28906
Power Sybr Green Mastermix	Thermo Scientific	Cat.#4367659

(*Continued on next page*)

Continued

REAGENT or RESOURCE	SOURCE	IDENTIFIER
Gel Cassettes, Pippin Prep, dye-free	Sage Science	Cat.#CDF2010
4-12% Bis-Tris SDS-PAGE gel	Life Technologies	Cat.#NP0323BOX
Agencourt® AMPure® XP	Beckman Coulter GmbH	Cat.#A63881
Critical commercial assays		
RNeasy Mini Kit for RNA extraction	QIAGEN	Cat.#74106
MinElute PCR purification kit	QIAGEN	Cat.#28006
Kapa Hyper Prep	Roche	Cat.#7962363001
Lib Quant Illumina Rox Low	Roche	Cat.#7960336001
RNA 6000 Nano Kit	Agilent Technologies	Cat.#5067-1511
High Sensitivity DNA Kit	Agilent Technologies	Cat.#5067-4626
QuantiTect Reverse Transcription kit	QIAGEN	Cat.#205314
Neon Transfection System 10 μL Kit-25 x	Life Technologies	Cat.# MPK1025
Qubit dsDNA HS Assay Kit	Life Technologies	Cat.#Q32854
Deposited data		
ChIP-MS	This paper	PRIDE:PXD018077
ChIP-Seq in macrophages	This paper	GEO:GSE136070
GR ChIP-Seq in macrophages	This paper	GEO:GSM1446192
GR ChIP-Seq in macrophages	This paper	GEO:GSM788651
ChIP-Seq in RAW264.7	This paper	GEO:GSE138017
RNA-Seq in wildtype macrophages	This paper	GEO:GSE137412
RNA-Seq in RAW264.7 cells (wildtype and *Setd1a*$^{Del/+}$) and *Setd1bKO* macrophages	This paper	GEO:GSE137944
Experimental models: cell lines		
RAW264.7	ATCC	Cat.#TIB-71 ; RRID:CVCL_0493
RAW264.7 *Setd1a*$^{Del/+}$	This paper	
S2 cells (*Drosophila*)	provided by Prof. P. Becker (LMU Munich, Germany)	RRID:CVCL_Z232
Experimental models: organisms/strains		
Speer6-ps1$^{Tg(Alb-cre)21Mgn}$	Postic et al., 1999	
Nr3c1^{tm2Gsc}/*Nr3c1*^{tm2Gsc}	Tronche et al., 1999	RRID:MGI:6257049
Setd1b$^{tm1.3Afst}$/*Setd1b*$^{tm1.3Afst}$	provided by Prof. Dr. K. Anastassiadis (TU Dresden, Germany) Bledau et al., 2014	RRID:MGI:5568956
Setd1a$^{tm1.2Afst}$/*Setd1a*$^{tm1.2Afst}$	provided by Prof. Dr. K. Anastassiadis (TU Dresden, Germany) Bledau et al., 2014	RRID:MGI:5568947
Rosa26-Cre-ERT2 (RC)	provided by Prof. Dr. K. Anastassiadis (TU Dresden, Germany) Bledau et al., 2014	
Oligonucleotides		
See Table S6		
Recombinant DNA		
pU6.chimeric	gift from I. Burtscher, Helmholtz Zentrum Muenchen	
pCAG.Cas9D10A-EGFP	gift from I. Burtscher, Helmholtz Zentrum Muenchen	
pPB-Puro-mPGK-EGFP:3xGGGGS:mSetd1a	This paper, VectorBuilder	

(*Continued on next page*)

Continued

REAGENT or RESOURCE	SOURCE	IDENTIFIER
Software and algorithms		
Perseus v.1.5.1.1	Tyanova and Cox, 2018	RRID:SCR_015753; https://maxquant.net/perseus/
MaxQuant v1.5.1.1	Cox and Mann, 2008	RRID:SCR_014485; https://maxquant.net/maxquant/
GOrilla	Eden et al., 2009	RRID:SCR_006848; http://cbl-gorilla.cs.technion.ac.il/
FastQC	http://www.bioinformatics.babraham.ac.uk/projects/fastqc/	RRID:SCR_014583
Salmon v0.10.2	Patro et al., 2017	RRID:SCR_017036; https://combine-lab.github.io/salmon/
R v3.6.1	R Core Team, 2017	RRID:SCR_001905; https://cran.r-project.org/
DESeq2 v1.22.0	Love et al., 2014	RRID:SCR_015687; https://bioconductor.org/packages/release/bioc/html/DESeq2.html
tximport	Soneson et al., 2015	RRID:SCR_016752; https://bioconductor.org/packages/release/bioc/html/tximport.html
GenomicRanges v1.36.1	Lawrence et al., 2013	RRID:SCR_000025; https://bioconductor.org/packages/release/bioc/html/GenomicRanges.html
ggplot2 v3.2.1	Wickham, 2016	RRID:SCR_014601; https://cran.r-project.org/web/packages/ggplot2/index.html
gplots v3.0.1.1	https://github.com/talgalili/gplots/	
ChIPpeakAnno v3.18.2	Zhu et al., 2010	RRID:SCR_012828; https://bioconductor.org/packages/release/bioc/html/ChIPpeakAnno.html
biomaRt v2.38	Durinck et al., 2009	RRID:SCR_002987; https://bioconductor.org/packages/release/bioc/html/biomaRt.html
Clusterprofiler v3.16.1	Yu et al., 2012	RRID:SCR_016884; https://bioconductor.org/packages/release/bioc/html/clusterProfiler.html
seqLogo v1.5	Bembom, 2019	https://bioconductor.org/packages/release/bioc/html/seqLogo.html
Mclust v5.4.5	Scrucca et al., 2016	https://cran.r-project.org/web/packages/mclust/index.html
GREAT v4.0.4	McLean et al., 2010	RRID:SCR_005807; http://great.stanford.edu/public/html/
MEME suite	Machanick and Bailey, 2011	RRID:SCR_001783; http://meme-suite.org/
HOMER software suite v4.10	Heinz et al., 2010	RRID:SCR_010881; http://homer.ucsd.edu/homer/
BWA-MEM v0.7.13	Li, 2013	RRID:SCR_010910; https://sourceforge.net/projects/bio-bwa/files/
Picard Tools v2.0.1	http://picard.sourceforge.net/	RRID:SCR_006525
Samtools v1.8	Li et al., 2009	RRID:SCR_002105; http://www.htslib.org/
Deeptools v3.0.2-1	Ramírez et al., 2016	RRID:SCR_016366; https://deeptools.readthedocs.io/en/develop/
Integrated genome browser v9.0.2	Freese et al., 2016	RRID:SCR_011792; https://www.bioviz.org/
MACS2 v2.1.1.20160309	Zhang et al., 2008	RRID:SCR_013291; https://github.com/macs3-project/MACS
BEDtools v2.25.0	Quinlan and Hall, 2010	RRID:SCR_006646; https://bedtools.readthedocs.io/en/latest/#

RESOURCE AVAILABILITY

Lead contact

Further information and requests for resources and reagents should be directed to and will be fulfilled by the Lead Contact, N. Henriette Uhlenhaut: *henriette.uhlenhaut@tum.de*

Materials availability

Cell lines generated in this study can be requested without restriction upon completion of a material transfer agreement.

Data and code availability

The NGS datasets supporting the conclusions of this article are available at GEO (https://www.ncbi.nlm.nih.gov/geo/) with the following accession numbers:

RNA-Seq data: Expression in wild-type BMDMs, GSE137412, Expression in RAW264.7 cells (wild-type and *Setd1aDel*/+) and *Setd1b* knockout BMDMs, GSE137944. ChIP-Seq data: GR binding and H3K4me2/me3 in RAW264.7 cells, GSE138017, GR, SETD1A and CXXC1 binding, H3K4me1/me2/me3 and H3K27ac in BMDMs, GSE136070, GSM1446192 and GSM788651.

The mass spec proteomic datasets are available at the ProteomeXchange Consortium via the PRIDE repository with the dataset identifier PXD018077 (https://www.ebi.ac.uk/pride/archive/).

EXPERIMENTAL MODEL AND SUBJECT DETAILS

Animals

C57BL/6 mice were housed in a controlled environment (12h light/12h dark cycle, ~23°C). Mouse experiments were performed according to the rules and guidelines established by the Institutional Animal Committee at Helmholtz Center Munich. Ethical approval was obtained from the local animal welfare authority (LAGeSo Berlin; district government of Upper Bavaria).

GR floxed mice (Nr3c1 tm2Gsc, RRID:MGI:6257049) were crossed with hepatocyte-specific Albumin (Alb)-Cre mice obtained from JAX (B6.Cg-Tg(Alb-cre)21Mgn/J). Alb-Cre negative floxed littermates served as controls (Quagliarini et al., 2019). *R26*$^{creERT2/+}$, *Setd1a*$^{fl/fl}$, *R26*$^{creERT2/+}$, *Setd1b*$^{fl/fl}$ and litter mate control (*R26*$^{creERT2/+}$) bones were kindly provided by Prof. Dr. K. Anastassiadis (TU Dresden, Germany) (Bledau et al., 2014). We exclusively study male mice. BMDMs were derived from 6-12 week old mice. Livers were harvested from 16 week old animals.

Cell lines

RAW264.7 cells (ATCC TIB-71, RRID:CVCL_0493; male, BALB/c-derivd) obtained from ATCC were maintained at sub confluent level in DMEM (10% FBS, including antibiotics) at 37°C and 5% CO2. Cells were regularly screened for mycoplasma.

METHOD DETAILS

Isolation and differentiation of BMDMs

Primary bone marrow-derived macrophages were isolated and differentiated in culture as previously described [10]. Shortly, bone marrow was harvested from 6-12 week old male mice with RPMI. Erythrocytes were lysed using AKC lysis buffer (1M NH4Cl, 1M KHCO3, 0.5M EDTA), and mononucleated cells were purified by Ficoll Paque gradient. Cells were differentiated in DMEM containing 20% FBS, 1% penicillin/streptomycin and 30% supernatant from L929 cells for 6 days on bacterial plates. Macrophages were harvested in Versene and seeded in macrophage serum-free medium.

Cells were treated with vehicle (0.1% EtOH and PBS), 1μM dexamethasone (in EtOH) for 16h or 0.1% ethanol and/or lipopolysaccharide (LPS, 100ng/ml, Sigma-Aldrich) for 3h (ChIP-Seq) or 6h (RNA-Seq, qPCR) unless indicated otherwise.

For deletion of *Setd1a* and *Setd1b* in bone marrow-derived macrophages of *R26*$^{creERT2/+}$, *Setd1a*$^{fl/fl}$ or *R26*$^{creERT2/+}$, *Setd1b*$^{fl/fl}$ mice, cells were treated with 1μM 4-hydroxytamoxifen (Sigma-Aldrich) after 3 days in differentiation medium.

Cell culture

RAW264.7 cells were treated with vehicle (0.1% EtOH and PBS), LPS (100ng/ul in D-PBS, Sigma-Aldrich) or dexamethasone (1μM in EtOH, Sigma-Aldrich) and LPS for the indicated time periods. Unless stated otherwise, treatment times were 16h Dex and 3h LPS for ChIP or 6h LPS for RNA, respectively. 3h IFN-β1 treatment (10ng/ml, R&D Systems) was performed alone or in combination with 100ng/ml LPS. 3h incubation with 0.05% BSA/PBS was used as vehicle control. Spike-in chromatin was generated from *Drosophila* S2 cells (a gift from P. Becker, RRID:CVCL_IZ06) grown in T175 flasks with Schneider's *Drosophila* medium supplemented with 10% FBS and 1% Penicillin/Streptomycin at 28°C under normal atmosphere.

Generation of CRISPR mutant cell lines

GuideRNAs were designed using the e-crisp tool (Heigwer et al., 2014) and cloned into pU6.chimeric via BbsI overhangs (a gift from I. Burtscher, Helmholtz Zentrum Muenchen). For mutation of RAW264.7 cells, pU6.chimeric.gRNA (Table S6), pCAG.Cas9D10A-EGFP (expressing Cas9 nickase, a gift from I. Burtscher) and a single strand DNA repair template (IDT, see Table S6)) were electroporated using the NEON electroporation system, FACS sorted after 24h and seeded as single clones. Positive clones were identified by genotyping PCR (Table S6 for oligo sequences) and PCR products were sequenced. *Setd1a*$^{DelSet/+}$ was generated by introduction of a premature STOP codon after exon 14, leading to a destabilized form of SETD1A (see Figure S5A).

Nuclear extraction and Co-ImmunoPrecipitation

Nuclear extraction was performed using standard protocols. Shortly, cells were harvested by washing in ice-cold PBS and collected by centrifugation (300 g at 4°C). Cell lysis was performed in hygroscopic conditions using V1 buffer (10mM HEPES-KOH pH 7.9; 1.5mM MgCl2; 10mM KCl and 1μM dexamethasone, 0.5mM DTT, 0.15% NP40, protease inhibitors and PhosphoSTOP) while

douncing on ice. Crude nuclei were collected by centrifugation (2,700 g at 4°C) and nuclear lysis was performed in V2 buffer (420mM NaCl; 20mM HEPES-KOH pH 7.9; 20% glycerol; 2mM MgCl2; 0.2mM EDTA and 1μM dexamethasone; 0.5mM DTT; 0.1% NP40; protease inhibitors and PhosphoSTOP) while incubating for 1h at 4°C and subsequent centrifugation at 21,000 g (4°C). Supernatants were directly processed for co-IP. Co-IP was performed by diluting 200 μg 1:1 in AM100 (100mM KCl, 5mM MgCl2, 20mM Tris (pH 8.0), 0.2mM EDTA and 20% glycerol) with EDTA-free proteinase inhibitors and pre-cleared with pre-blocked sheep α-rabbit or sheep α-mouse IgG Dynabeads for 2h at 4°C while agitating. IPs were incubated with 1μg of antibody (Key resources table) for 2h at 4°C. Subsequently, pre-blocked sheep α-rabbit or sheep α-mouse IgG Dynabeads (ThermoFisher Scientific) were collected after 3 washes with buffer AM100 plus 0.5% Triton. Bound proteins were eluted in Laemmli buffer and analyzed by western blots. For Co-IP from whole cell lysates, RAW264.7 cells were lysed in NP40 buffer (25mM Tris pH 7.5, 150mM NaCl, 1mM EDTA, 1% NP40, 5% glycerol, freshly added phosphatase and proteinase inhibitors), sonicated for 15 s and cleared by spinning 10min at 12,000xg. After preclearing samples were diluted 1:5 in Tris IP buffer (20mM Tris pH 7.5, 2mM $MgCl_2$, 100mM NaCl, 0.2mM EDTA, 0.1% Triton X-100, freshly added phosphatase and proteinase inhibitors) for incubation with 1ug of primary antibody (Key resources table) overnight at 4°C. Pre-blocked beads were added for 3h on the next day and proteins eluted from the beads after three washes with Tris-IP buffer, one wash with Tris-IP buffer including 500nM NaCl and 1 wash of Tris-IP buffer including 500nM NaCl and 1% Triton X-100.

Western Blotting

Standard procedures were applied for western blotting using precast Bis-Tris SDS-PAGE 4%–12% gradient gels. Histones were run on 12% Bis-Tris gels. Antibodies are listed in the Key resources table. Specificity of H3K4me1/me2/me3 antibodies was tested in peptide competition western blots (data not shown).

RNA isolation and qRT-PCR

Total RNA from 200,000 (qPCR) or 1 million cells (RNA-Seq) was isolated using the RNeasy Mini kit (QIAGEN) with on-column DNaseI digest, following the manual. RNA was measured with Nanodrop2000. 500ng RNA were reverse transcribed using a Reverse Transcription Kit (QIAGEN) according to manufacturer's instructions. Quantitative PCR was run on Quantstudio 6/7 using SYBR Green in standard curve mode. Primer pairs are listed in Table S6. Gene expression was normalized to the housekeeping gene *Rplp0*. Values from independent experiments were standardized using z-scores. Plots show means with standard deviations as error bars. Individual data points are given as dots.

RNA-Seq

RNA quality was verified using an Agilent2100 Bioanalyzer with RNA 6000Nano Reagents. Library preparation and rRNA depletion was performed using the TruSeq Stranded mRNA Library Prep Kit starting with 500ng total RNA as input for each sample. Libraries were sequenced on the Illumina HiSeq4000. Experiments were performed in triplicates.

ChIP-Seq

For ChIP experiments, 20 million cells (BMDMs, RAW264.7 or S2 cells) were treated as indicated above. Mouse livers were harvested at night (peak of corticosterone levels) and snap frozen in liquid nitrogen. 250mg of liver tissue were thawed on ice and incubated with 1% formaldehyde for 15min while homogenizing (Dounce) at room temperature. Cells were washed in D-PBS and fixed either in 1% formaldehyde (methanol-free) for 10min or in 2mM disuccinimidyl-glutarate for 30min plus 10min 1% FA (see Table S5). Formaldehyde was quenched with 150mM glycine, and cells were washed with D-PBS, pelleted and stored at −80°C or directly processed for ChIP using 2μg (transcription factor/coregulator) or 1μg (histones) of antibody (Key resources table) as previously described (Nelson et al., 2006; Quagliarini et al., 2019).

For ChIP-Seq, 40 million cells per sample were used for GR and COMPASS proteins. For histone marks, 20 million cells per sample were used. ChIP-Seq was performed with the following modifications: Chromatin was sonicated using a Bioruptor pico (Diagenode) with either 8μg (GR, COMPASS) or 3μg antibody (histones): see Key resources table. Purified DNA was quantified using Qubit. Library preparation was performed from 5ng of ChIP DNA using the Kappa Hyperprep and library amplification kits according to the manufacturer's manual (Roche). Libraries were sequenced on an Illumina HiSeq4000. A minimum of two replicates per condition was performed (See Table S5).

NGS Data analysis

RNA-Sequencing

NGS data quality was assessed with FastQC (RRID:SCR_014583, http://www.bioinformatics.babraham.ac.uk/projects/fastqc/). Gene-level quantification was performed with Salmon version 0.10.2 (RRID:SCR_017036 (Patro et al., 2017)). Settings were: -libType A, -gcBias, -biasSpeedSamp 5 using the mm10 (GRCm38.p6) reference transcriptome provided by Ensembl (RRID:SCR_002344 (Cunningham et al., 2019)). Gene count normalization and differential expression analysis was performed with DESeq2 version 1.22.0 (RRID:SCR_015687 (Love et al., 2014)) after import of gene-level estimates with "tximport" (RRID:SCR_016752 (Soneson et al., 2015)) in R (RRID:SCR_001905, R version 3.6.1 (R Core Team, 2017)).

For gene annotation, Ensembl gene Ids were mapped to MGI symbols using the Bioconductor package "biomaRt" version 2.38 (RRID:SCR_002987 (Durinck et al., 2009)) and genome information was provided by Ensembl (GRCm38.p6 (Cunningham et al., 2019)). Genes with a minimal mean count across samples (baseMean) of 50, fold change of 1.5 and Benjamini-Hochberg-adjusted p value < 0.05 were called significantly changed. Significance of the genotype contribution to the treatment effect (Dex versus veh; LPS+Dex versus LPS) was determined by log-likelihood-ratio test comparing the full model ~genotype+treatment+treatment:genotype with the reduced model ~treatment. p values are Benjamini-Hochberg adjusted. The dependency of the Dex response from genotype and treatment time was accessed by likelihood-ratio test between the full model (~genotype + treatment + treatment:genotype) and the reduced model (~genotype + treatment).

Gene Ontology biological process enrichment was performed using GOrilla (RRID:SCR_006848 (Eden et al., 2009)) using the unranked list mode. All genes expressed with a mean expression level over 50 counts were used as the background set for macrophages or RAW264.7 cells respectively. GO terms were significantly enriched with a FDR < 0.01 and a set size smaller than 500 genes per term. Redundant terms were removed manually.

ChIP-Sequencing

ChIP-Seq reads were aligned to the reference genome mm10 (Ensembl GRCm38.p6 (Cunningham et al., 2019)) using BWA-MEM version 0.7.13 (RRID:SCR_010910 (Li, 2013)) and PCR duplicates were removed using Picard Tools version 2.0.1 (RRID:SCR_006525, http://picard.sourceforge.net/). Samples with duplication levels above 80% were excluded from further analysis. For visualization, bam files were filtered for properly paired and mapped reads with Samtools version 1.8 (RRID:SCR_002105 (Li et al., 2009)) and converted to bigwig files merging 10 bp per bin using "bamCoverage" from the Deeptools package version 3.0.2-1 (RRID:SCR_016366 (Ramírez et al., 2016)). Tracks were visualized using the integrated genome browser (IGB, RRID:SCR_011792 (Freese et al., 2016)) version 9.0.2.

Peaks were called using MACS2 version 2.1.1.20160309 (RRID:SCR_013291) with an FDR threshold of 0.1 for reproducible peaks and FDR = 0.05 for the generation of a "peak union" (Zhang et al., 2008). Blacklisted regions (http://mitra.stanford.edu/kundaje/akundaje/release/blacklists/mm10-mouse/mm10.blacklist.bed.gz) were removed from the called peaks. Peaks were termed reproducible when they were called in two independent ChIP-Seq experiments and overlapped for 50% of the mean peak width. We also identified a "peak union" merging any peak called by MACS2 in any of the experiments.

For Venn diagrams, peaks overlapping each other with a minimum of 1bp on either strand were termed overlapping. The overlap was determined using the "GenomicRanges" package version 1.36.1 (RRID:SCR_000025 (Lawrence et al., 2013)).

Heatmaps were generated using HOMER software suite version 4.10 (RRID:SCR_010881 (Heinz et al., 2010)) and visualized with the "ggplot2" package version 3.2.1 (RRID:SCR_014601 (Wickham, 2016)) or the "gplots" package (https://github.com/talgalili/gplots/) version 3.0.1.1 in R 3.6.1 (RRID:SCR_014601 (R Core Team, 2017)). Heatmaps represent the mean the mean and the standard deviation of at least two replicates (Table S5).

Bigwig files were scaled according to DESeq2 scale factors estimated from reads covering the whole peak union ("static peak" normalization), assuming that most of the peaks do not change their coverage in response to dexamethasone. When spike-in ChIP-Seq was performed, the data were normalized by the spike-in ratios in cases where the DESeq2 assumption (Love et al., 2014) might be violated (e.g., *Setd1a*$^{Del/+}$ mutants). All scaling factors are provided in Table S5.

Peaks were annotated to the nearest TSS using the "ChIPpeakAnno" package version 3.18.2 (RRID:SCR_012828 (Zhu et al., 2010)) and called intergenic when more than 1kb away from any gene.

Read counts covering peaks were obtained using BEDtools version 2.25.0 (RRID:SCR_006646 (Quinlan and Hall, 2010)) (Table S5).

Immunoprecipitation (IP) efficiencies were defined as portion of mapped unique read pairs covering the peak union. Samples with an IP efficiency below 15% were excluded from further analysis.

For Volcano plots, correlations, and modeling, reads were counted after adjustment to a unique peak length of 588bp (4 nucleosomes) around the peak center and scaled afterward, as described above.

Differential ChIP-Seq analysis was performed with "DESeq2" (RRID:SCR_015687 (Love et al., 2014)) using the above calculated scaling factors. Log2FoldChanges always refer to the comparison between Dex plus LPS and LPS only treatments, unless stated otherwise.

For spike-in normalization of H3K4me1/me2/me3 ChIP-Seq in *Setd1a*$^{Del/+}$ mutants, reads were mapped to the murine reference genome mm10 and the *Drosophila melanogaster* genome build dm6 (Ensembl BDGP6 release 78 (Cunningham et al., 2019)). Scaling factors for bigwig files were determined as the fly-specific reads-in-peaks ratio between all samples, and adjusted for differences in IP efficiencies between samples for the spiked fly S2 cell chromatin as follows (see Table S5). Variations in the *Drosophila* ChIP were assumed to account for technical variations between samples and therefore applied to the mm10-mapped reads (Egan et al., 2016). Scaling factors for heatmaps and genome-browser tracks were calculated as above.

Statistical analysis and visualization was performed in R 3.6.1 (RRID:SCR_001905 (R Core Team, 2017)).

For KEGG pathway enrichment, the "clusterprofiler" package was used (RRID:SCR_016884 (Yu et al., 2012)). Results are displayed as circles reflecting the gene ratio (number of genes in a given subset covered by the pathway, divided by the number of genes in that pathway) and shades representing the Benjamini-Hochberg adjusted hypergeometrical p value.

For enrichment of Gene Ontology biological processes, peak positions were assigned to the nearest gene, and enrichment analysis was performed with GREAT (RRID:SCR_005807 (McLean et al., 2010)). Bonferroni-adjusted hypergeometrical p values are shown, and terms were significantly enriched and reported when the p value was < 0.01.

Motif enrichment was performed on peaks trimmed to 100bp around the peak center with MEME suite (RRID:SCR_001783 (Machanick and Bailey, 2011)) in enrichment or differential mode as indicated in the figure legends. MEME parameters were set to: "-dna -meme-mod anr -meme-minw 6 -meme-maxw 30 -meme-nmotifs 10 -meme-p 10" using the JASPAR (2018 version, RRID:SCR_003030 (Khan et al., 2018)), Uniprobe (RRID:SCR_005803 (Newburger and Bulyk, 2009)) and SwissRegulon (RRID:SCR_005333 (Pachkov et al., 2013)) databases. Motifs were visualized from position-weight matrices obtained from the HOCOMOCO (version 11 (Kulakovskiy et al., 2018)) or JASPAR databases with the "seqLogo" package version 1.5 in R 3.6.1 (Bembom, 2019). Centrimo motif enrichment was performed to identify centrally enriched motifs, and MEME was used for motif enrichment within a given peak set.

Model-based clustering was performed with the "mclust" package version 5.4.5 in R 3.6.1 (Scrucca et al., 2016). Features were quantified at GBSs extended by 588 bp and scaled to unit length. Bayesian Information Criterion (BIC) was used to determine cluster numbers and the best fitting model. The model selected in this paper is VEE (diagonal distribution with variable volume and ellipsoidal shape).

ChIP-qPCR

For ChIP-qPCR, 20 million cells were used per sample. A minimum of two independent experiments with two biological replicates each were performed.

Cells were fixed and processed as described above with 1μg of antibody against histone marks and 3μg of antibody against other proteins (Key resources table).

qPCRs were run on Quantstudio 6/7 in standard curve mode using SYBR Green and the primers listed in Table S6. Enrichment was calculated as percent of input and ChIPs against histone marks were normalized to total histone H3. To account for inter-experimental variation, ChIP results from independent experiments were standardized using z-scores. Plots show means with standard deviations as error bars. Individual data points are given as dots.

Spike-in ChIP

Spike-in ChIP-Seq/qPCR was performed as indicated above with addition of 5% (ChIP-Seq) or 10% (ChIP-qPCR) *Drosophila* S2 chromatin to all samples before sonication. qPCRs against genomic regions positive for *Drosophila* H3K4me1/me2/me3, H3K27ac and H3 were used for normalization (see Table S5). Ct-values were corrected for PCR efficiency; enrichment over input was calculated and normalized to the *Drosophila* signal (Egan et al., 2016). Histone modifications were additionally normalized to total H3 (see above).

ChIP-MS interactomes

For mass spectrometric analysis of purified co-enriched proteins, GR ChIP was performed as described above, followed by proteomics. Chromatin was sonicated to an average size of 200 bp using the Bioruptor pico (Diagenode). After incubation with primary α-GR antibody (#sc-1004X SantaCruz, RRID:AB_2155786) or rabbit IgG (#2729, Cell Signaling Technology, RRID:AB_1031062), samples were processed as described in (Hemmer et al., 2019; Quagliarini et al., 2019).

In detail, cells were treated and crosslinked as for ChIP-Seq, lysed in IP-buffer (50 mM Tris-HCl, pH 8.0, 100 mM NaCl, 5 mM EDTA, 0.3% SDS, 1.7% Triton X-100) and chromatin sonicated to an average size of 200bp. After overnight immunoprecipitation with α-GR antibody antibody, or rabbit IgG, antibody-bait complexes were captured by ChIP-Grade Protein G Agarose Beads (#9007 Cell Signaling Technology), washed three times with wash buffer A (50mM HEPES pH 7.5, 140mM NaCl, 1% Triton), once with wash buffer B (50mM HEPES pH 7.5, 500mM NaCl, 1% Triton), and twice with TBS. Beads were incubated for 30min with elution buffer 1 (2M Urea, 50mM Tris-HCl pH 7.5, 2mM DTT, 20μg/ml trypsin) followed by a second elution with elution buffer 2 (2M Urea, 5 mM Tris-HCl pH 7.5, 10mM Chloroacetamide) for 5min. Both eluates were combined and further incubated at room temperature overnight. Tryptic peptide mixtures were acidified to 1% TFA and desalted with Stage Tips containing three layers of C18 reverse phase material and analyzed by mass spectrometry.

Peptides were separated on 50cm columns packed with ReproSil-Pur C18-AQ 1.9 μm resin (Dr. Maisch GmbH). Liquid chromatography was performed on an EASY-nLC 1200 ultra-high-pressure system coupled through a nanoelectrospray source to a Q-Exactive HF mass spectrometer (Thermo Fisher Scientific). Peptides were loaded in buffer A (0.1% formic acid) and separated applying a non-linear gradient of 5%–60% buffer B (0.1% formic acid, 80% acetonitrile) at a flow rate of 250nl/min over 120min. Data acquisition switched between a full scan (60K resolution, 20ms max. injection time, AGC target 3e6) and 10 data-dependent MS/MS scans (15K resolution, 60ms max. injection time, AGC target 1e5). Isolation window was set to 1.4 and normalized collision energy to 27. Multiple sequencing of peptides was minimized by excluding the selected peptide candidates for 30 s.

Data analysis

Raw mass spectrometry data were analyzed with MaxQuant (v1.5.1.1, RRID:SCR_014485) (Cox and Mann, 2008). Peak lists were searched against the mouse UniprotFASTA database (2015_08 release) combined with 262 common contaminants by the integrated Andromeda search engine. False discovery rate was set to 1% for both peptides (minimum length of 7 amino acids) and proteins. 'Match between runs' (MBR) with a maximum time difference of 0.7min was enabled. Relative protein amounts were determined by the MaxLFQ algorithm with a minimum ratio count of two.

Statistical analysis of LFQ derived protein expression data was performed using Perseus (v.1.5.1.1, RRID:SCR_015753) (Tyanova and Cox, 2018). Protein entries referring to contaminants, proteins identified via matches to the reverse database, and proteins

identified only via modified sites, were removed, LFQ values log2 transformed and missing values imputed from a normal distribution applying a width of 0.2 and a downshift of 1.8 standard deviations. Significant outliers were defined by permutation-controlled Student's t test (FDR < 0.01, s0 = 1) comparing triplicate ChIP-MS samples for each antibody, requiring at least two valid values in the GR replicates.

Functional annotation of proteins significantly ($p < 0.05$) enriched over IgG, was performed with GOrilla (RRID:SCR_006848 (Eden et al., 2009)) in the "two unranked lists" mode, and all detected proteins used as the background set, using the Gene Ontology (GO) 'Biological Processes'. The most specialized GO terms with significant enrichment (FDR < 0.05) are reported.

QUANTIFICATION AND STATISTICAL ANALYSIS

For all experiments, normal distribution of the data was assessed by Shapiro-Wilk test, and plotting the data distribution as histograms if the Shapiro-Wilk test was slightly significant ($0.001 < p < 0.05$). Log2 transformation of the data was performed to obtain normal distribution as indicated. Equal variance of sample groups was tested by Bartlett test (parametric) or Levene test (non-parametric). Significance was assessed by Student's t test in case of normal distributed homoscedastic data, Welch test in case of normal distributed heteroscedastic data and Wilcoxon-Mann-Whitney test in all other experiments with single factor designs. In multi-factor design experiments, significance was tested by analysis of variance (ANOVA) with post hoc pairwise t test (homoscedastic, normal distributed data) or Kruskal-Wallis test with post hoc Wilcoxon-Mann-Whitney (homoscedastic, non-normal data) or Dunn's test (heteroscedastic, non-normal data), respectively. P values were Benjamini-Hochberg adjusted. Unless stated otherwise, p values are only indicated if significant ($p < 0.05$).

Bar plots display the mean and individual data points are indicated. The standard deviation is given as error bars unless indicated otherwise. Detailed information for each experiment can be found in the figure legends.

Cell Reports, Volume *34*

Supplemental Information

The glucocorticoid receptor recruits the COMPASS complex to regulate inflammatory transcription at macrophage enhancers

Franziska Greulich, Michael Wierer, Aikaterini Mechtidou, Omar Gonzalez-Garcia, and N. Henriette Uhlenhaut

Supplemental figures, legends and tables, Greulich F. *et al.*

Supplemental Figure 1 - GR interactions with the SETD1A/COMPASS complex. (Relates to figure 1)

Supplemental Figure 2 - SETD1A/COMPASS cistromes in primary macrophages. (Relates to figure 2)

Supplemental Figure 3 - GR recruits SETD1A/COMPASS to its enhancers in murine macrophages and livers. (Relates to figure 3)

Supplemental Figure 4 - Locus-specific changes in H3K4 me1, me2 and me3 at GBSs with SETD1A recruitment, and correlations with H3K27ac and mRNA expression. (Relates to figure 4)

Supplemental Figure 5 - H3K4 methylation dynamics upon SETD1A depletion. (Relates to figure 5)

Supplemental Figure 6 - *Setd1a* is required for GR-mediated inflammatory gene regulation. (Relates to figure 6)

Supplemental Figure 7 - Regulation of GR targets in the absence of TLR4 signaling (Relates to figure 7)

Supplemental Table 1 – ChIP-MS data of proteins significantly enriched in α-GR IPs in macrophages (LPS+Dex). (Relates to figure 1)

Supplemental Table 2 – Differential expression of genes in macrophages, in wild type and in *Setd1a*$^{Del/+}$ RAW264.7 cells, under various conditions (±LPS, ±Dex). (Relates to figures 1, 6, 7)

Supplemental Table 3 – GR ChIP peaks in macrophages and RAW264.7 cells (Relates to figures 3, 4, 5)

Supplemental Table 4 – Gene Ontology of various gene sets (Relates to figures 3, 6, 7)

Supplemental Table 5 – List of ChIP-Seq samples, including mapping statistics and scale factors. Scaling factors applied in this study are marked in red. (Relates to STAR methods)

Supplemental Table 6 – List of oligos used for ChIP and mRNA qPCR as well as CRISPR cloning. (Relates to STAR methods)

Supplemental figures and legends

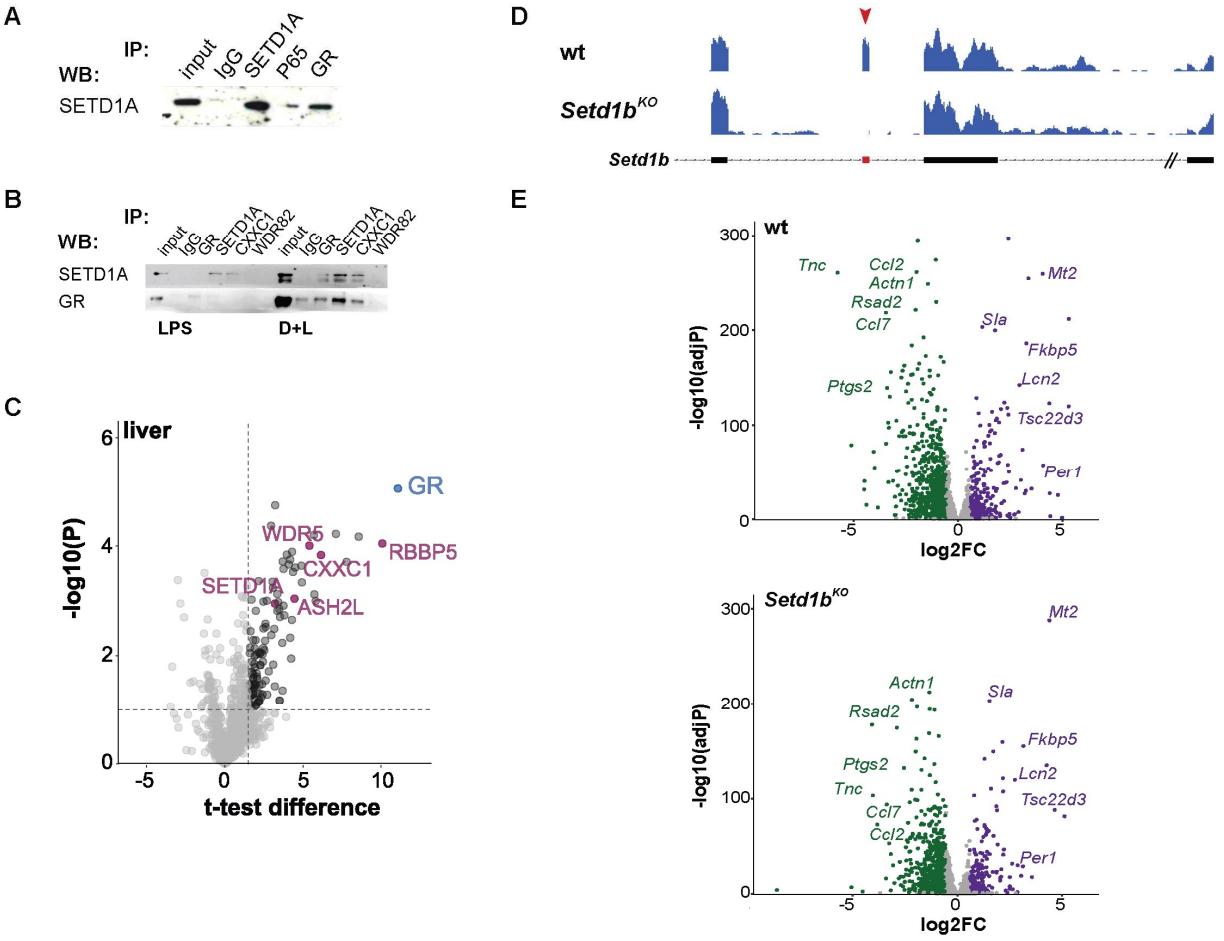

Supplemental Figure 1. ***GR interactions with the SETD1A/COMPASS complex*****.**

This figure relates to figure 1. **(A)** Co-IP of SETD1A with GR and p65 in RAW264.7 cells. WB - Western blot, IP - immunoprecipitation **(B)** Co-IPs of SETD1A, CXXC1 and GR in nuclear extracts from RAW264.7 cells treated either with LPS only or with Dex+LPS (D+L). **(C)** ChIP-MS for GR in murine liver. COMPASS proteins present in the hepatic interactome are colored in purple (Hemmer et al., 2019) **(D)** Genome browser tracks of *Setd1b* mRNA in wild type and *Setd1b* KO macrophages after Dex and LPS treatment. Gray shadow indicates the deletion of exon 5 (orange) in *Setd1b* conditional cells as described in Bledau 2014. **(E)** Volcano plots of RNA-Seq results from wild type and *Setd1b* knockout BMDMs. Displayed is the negative log10-transformed Benjamini-Hochberg adjusted p-value (-log10(adjP)) over the log2FoldChange (log2FC). Green – reduced expression. Purple – increased expression. Selected classical GR target genes are labeled.

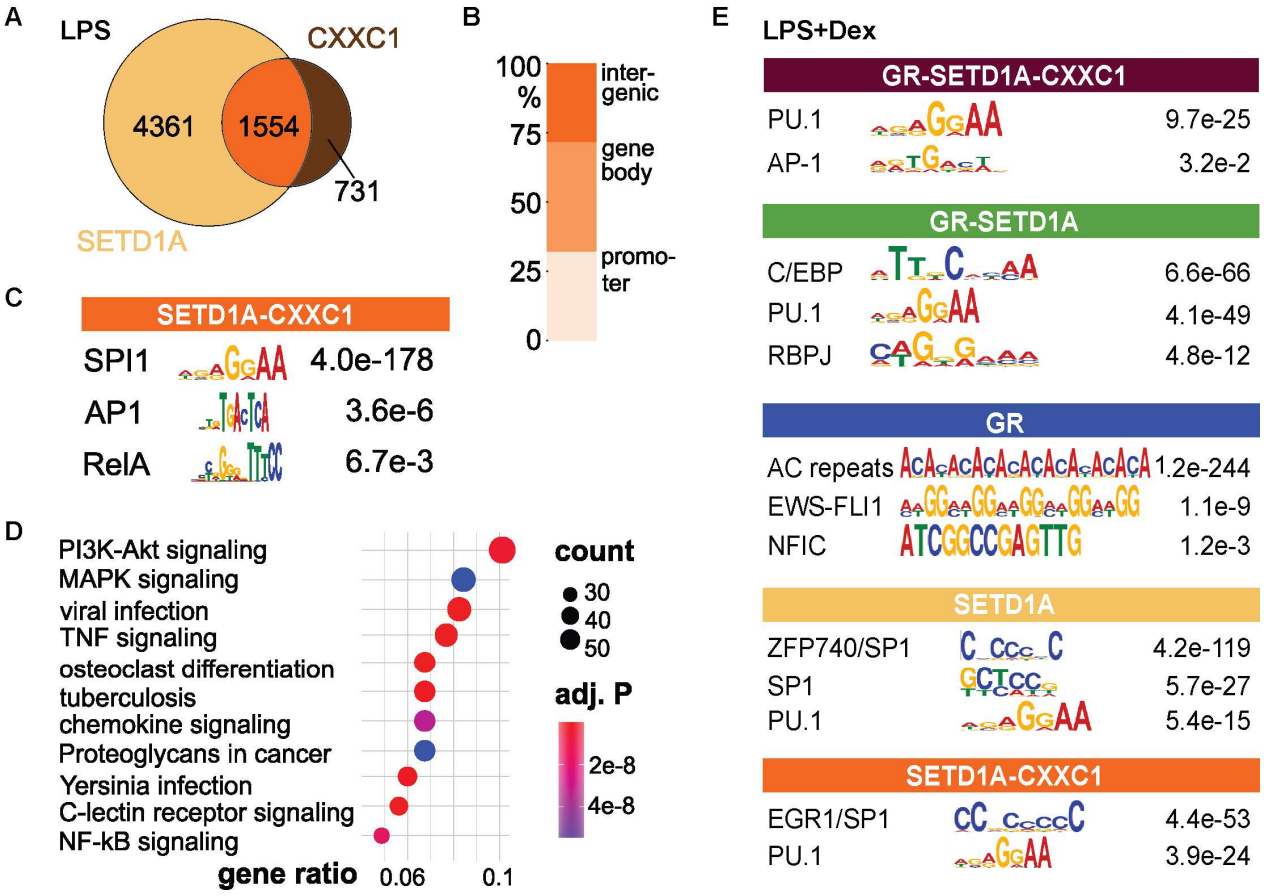

Supplemental Figure 2. SETD1A/COMPASS cistromes in primary macrophages.

This figure relates to figure 2. (**A**) Overlap of SETD1A and CXXC1 binding sites in LPS treated BMDMs. Numbers are called peaks. (**B**) Genomic feature distribution (%) of SETD1A-CXXC1 co-occupied regions in LPS treated BMDMs. (**C**) MEME motif enrichment for the SETD1A-CXXC1 overlap. Consensus sequencea and E-values are displayed (**D**) KEGG pathway enrichment for the SETD1A/CXXC1 peak overlap in LPS- stimulated BMDMs (1554 peaks mapped to the nearest TSSs). (**E**) MEME motif enrichment for indicated peak subsets, as defined in **Fig. 2A**. The union of GR, SETD1A and CXXC1 peaks was used as background. Displayed are the consensus sequences and E-values. Motifs already displayed in Fig. 2A are not shown here.

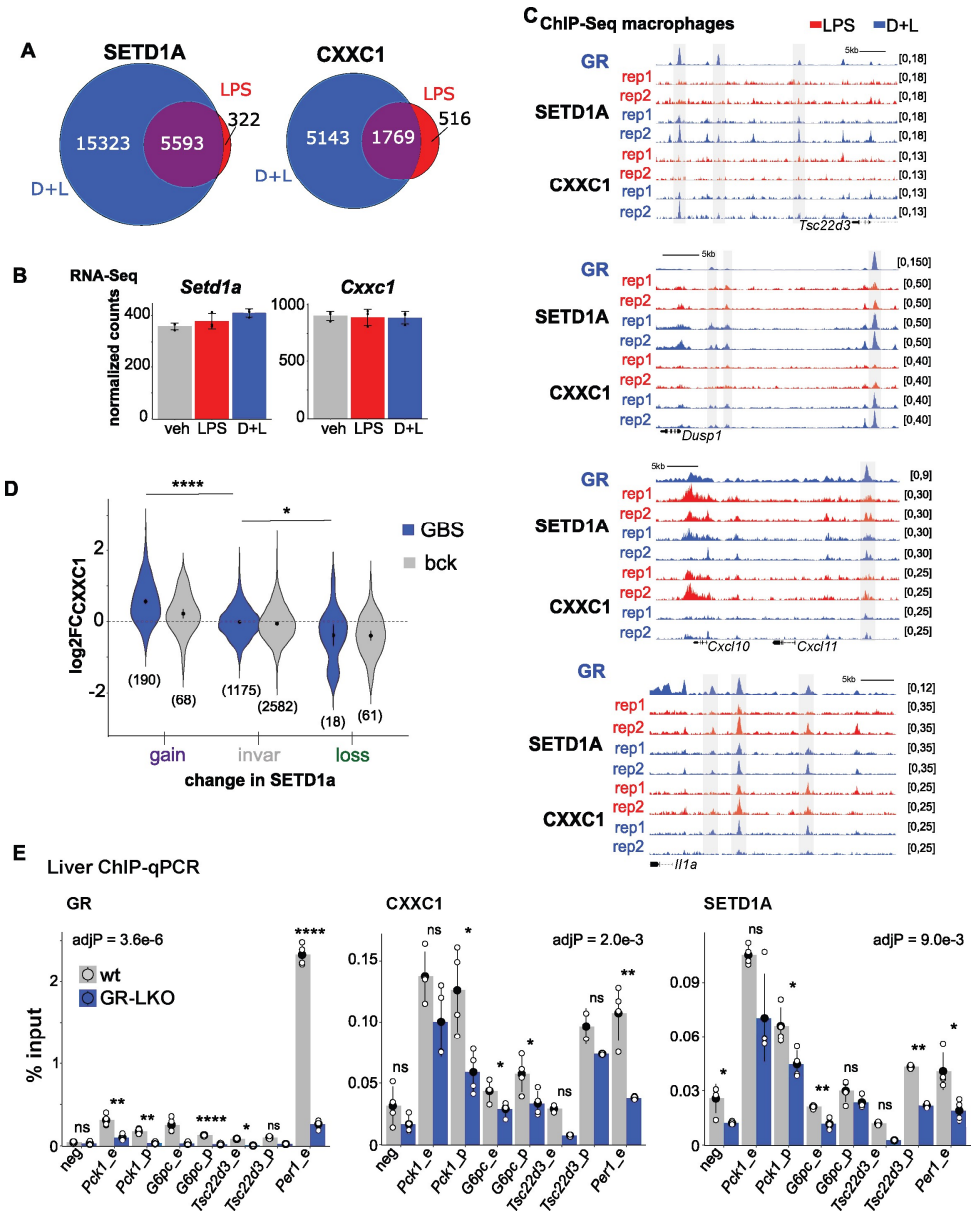

Supplemental Figure 3. GR recruits SETD1A/COMPASS to its enhancers in murine macrophages and livers.

This figure relates to figure 3. **(A)** Venn diagram illustrating the SETD1A and CXXC1 peak union overlap upon Dex+LPS (D+L) and LPS treatment in BMDMs. **(B)** *Setd1a* and *Cxxc1* expression in vehicle (veh), LPS or Dex+LPS (D+L) treated BMDMs, as measured by RNA-Seq. Mean DESeq2-normalized counts from three replicates are shown. Single dots are individual data points. Error bars reflect the standard deviation. **(C)** Example genome browser tracks of ChIP-Seq for GR, SETD1A and CXXC1 in macrophages treated either with LPS (red) or with Dex+LPS (blue). Grey boxes highlight GR-bound enhancers. **(D)** Log2FoldChange (FC) of CXXC1 occupancy at GR-bound sites (blue) or non-GR-bound (grey) intergenic regions (+/-1kb from any gene) summarized as Violin plot. Loci are categorized by gained (p<0.1, FC>1.5), lost (p<0.1, FC<-1.5) or invariant (p>0.1, -1.5<FC<1.5) SETD1A binding upon Dex+LPS treatment compared to LPS alone. Dunn's test shows the significance of CXXC1 dynamics between different SETD1A categories. * p<0.05; **** p<0.0001. Numbers in parentheses are subset sizes. **(E)** ChIP qPCR for GR, CXXC1 and SETD1A in murine livers from wild type (wt) and hepatocyte-specific GR knockout (GR-LKO) mice (pairwise Wilcoxon-Mann-Whitney test, adjP – Benjamini-Hochberg adjusted p-value). Pair-wise comparisons of individual enhancer by two-sided Student's t-test (n=4). ns – non-significant, * p<0.05, ** p<0.01, **** p<0.0001.

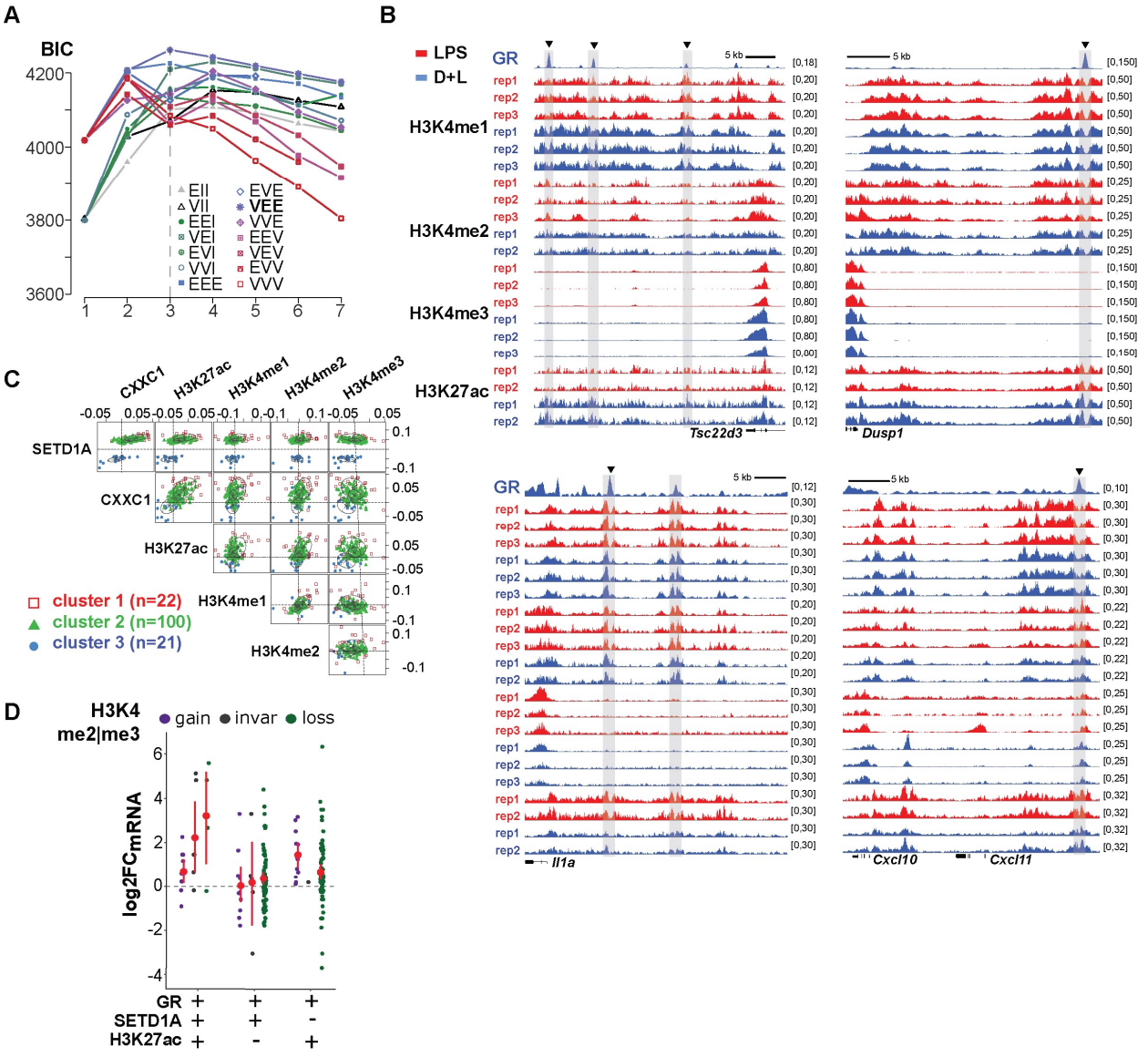

Supplemental Figure 4. Locus-specific changes in H3K4 me1, me2 and me3 at GBSs with SETD1A recruitment, and correlations with H3K27ac and mRNA expression.

This figure relates to figure 4. **(A)** Bayesian Information Criterion (BIC) plot for classification of intergenic GR-bound enhancers with differential SETD1A occupancy (|FC|>1.5, p<0.1) in Fig. S4B. The best model used for enhancer classification is indicated by the dashed line and bold text. **(B)** Representative ChIP-Seq genome browser tracks for LPS- and Dex+LPS- stimulated BMDMs. Individual replicates are shown, corresponding to the mean representation in the main figure. **(C)** Scatter plots of scaled SETD1A, CXXC1, H3K27ac and H3K4me1/me2/me3 log2FoldChanges (FC) at GBSs with significantly changed SETD1A occupancy (p<0.1, -1.5>FC>1.5) upon Dex and LPS treatment. Colors reflect clusters identified by "mclust". The dashed line represents axis centers and circles mark the uncertainty border **(D)** Scatter plot showing log2FC in mRNA expression of indicated groups, separated according to their change in H3K4me2 or me3. Red dots indicate the mean and the red bars the 95% confidence intervals. + gain; - invariant or lost.

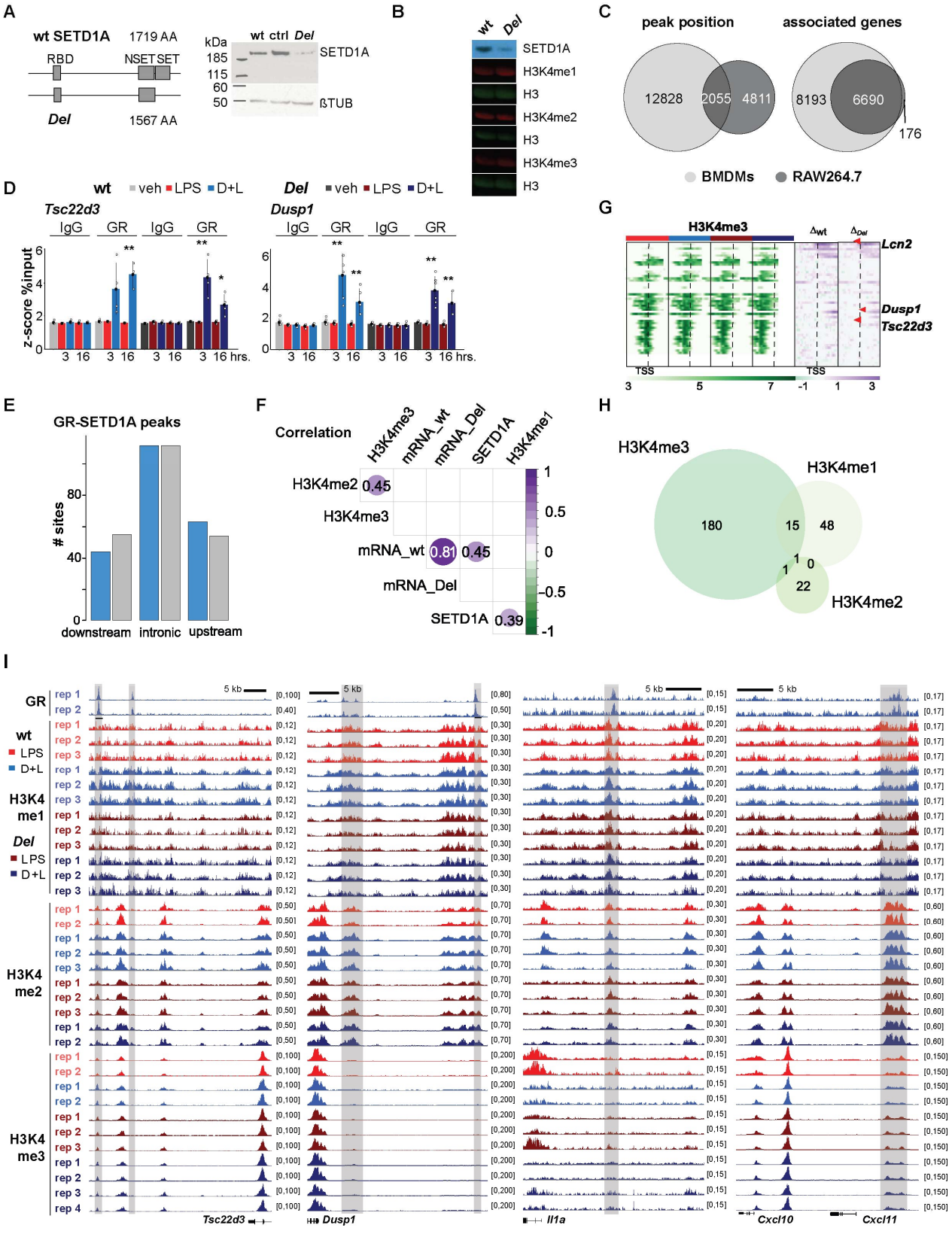

Supplemental Figure 5. H3K4 methylation dynamics upon SETD1A depletion.

This figure relates to figure 5. (**A)** *Setd1a*$^{Del/+}$ (*Del*) RAW264.7 cells, carrying a deletion of the SET domain, show reduced SETD1A expression by Western Blot. Loading control: beta tubulin (ßTUB); RBD: RNA-binding domain. **(B)** Western blot for SETD1A, H3K4me1, H3K4me2, H3K4me3 and total H3 in wild type (wt) and *Setd1a*$^{Del/+}$ (*Del*) RAW264.7 cells. **(C)** Venn diagram comparing GR ChIP-Seq peaks and associated genes in RAW264.7 cells (dark) and primary macrophages (lighter shade) after Dex+LPS treatment. **(D)** ChIP qPCR against IgG and GR for the *Tsc22d3* and *Dusp1* enhancers (indicated by the black line in I) after vehicle (veh), LPS or Dex+LPS (D+L) treatment. Dex treatment time as indicated. (n=4, Kruskal-Wallis with post-hoc Dunn's test. P values are Benjamini-Hochberg adjusted. * $p<0.05$; ** $p<0.01$. Bar plots display the mean z-score of % input and error bars show the standard deviation. **(E)** Genomic localization of GR-SETD1A overlapping sites shown in figure 5. **(F)** Correlation plot of Dex-induced log2FCs for SETD1A, H3K4me1/me2/me3 and mRNA in wild type RAW264.7, as well as mRNA changes in *Setd1a*$^{Del/+}$ (*Del*) cells for the GR subset with significantly gained SETD1A occupancy ($p<0.1$, FC>1.5-fold). **(G)** Spike-in normalized plus differential heatmaps (Δ compares Dex+LPS over LPS) for H3K4me3 ChIP-Seq signals at ±2kb around TSSs in wild type (wt) and *Setd1a*$^{Del/+}$ (*Del*) RAW264.7 cells treated with LPS or Dex+LPS. The mean of 2-4 replicates is displayed. TSSs are sorted by descending order of H3K4me3 fold-changes in response to Dex in wild type cells. Arrows point at loci of interest. **(H)** Venn Diagram of the overlap of GR-SETD1A co-occupied intergenic regions with >1.5-fold difference in H3K4 me1, me2 or me3 ($p<0.05$) in Dex+LPS treated wild type RAW264.7 cells when compared to LPS-treated cells. **(I)** Example genome browser tracks of normalized ChIP-Seq signal for GR and H3K4me1/me2/me3 in RAW264.7 cells. Gray boxes mark GR peaks. Black lines indicate the position of the qPCR primers.

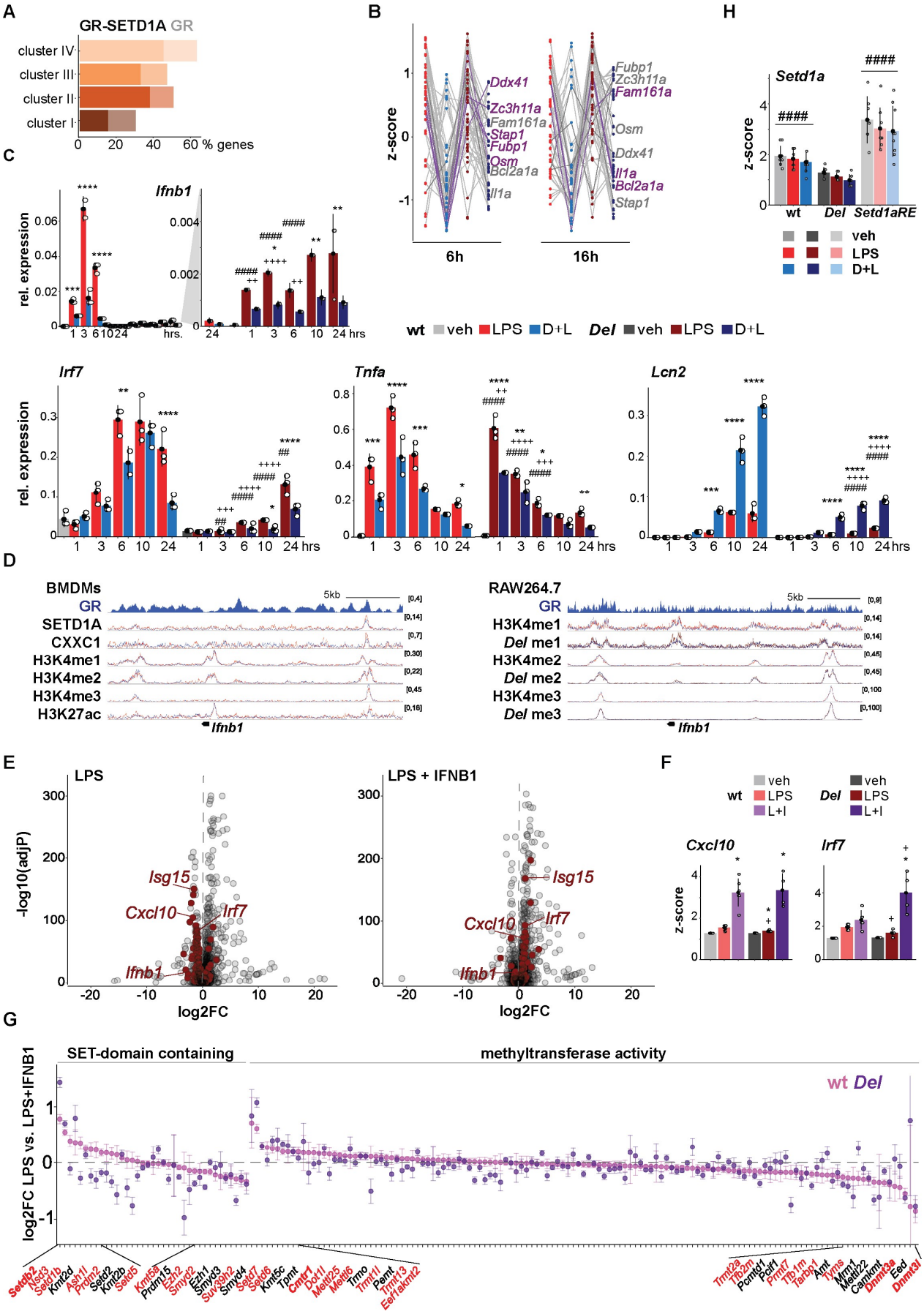
A
GR-SETD1A GR
cluster IV
cluster III
cluster II
cluster I
0 20 40 60 % genes
B
z-score
Ddx41
Zc3h11a
Fam161a
Stap1
Fubp1
Osm
Bcl2a1a
Il1a
6h
16h
H
Setd1a
z-score
wt Del Setd1aRE
veh
LPS
D+L
C
Ifnb1
rel. expression
hrs.
wt veh LPS D+L Del veh LPS D+L
Irf7
Tnfa
Lcn2
rel. expression
1 3 6 10 24 hrs
D
BMDMs
GR
SETD1A
CXXC1
H3K4me1
H3K4me2
H3K4me3
H3K27ac
5kb
Ifnb1
RAW264.7
GR
H3K4me1
Del me1
H3K4me2
Del me2
H3K4me3
Del me3
5kb
Ifnb1
E
LPS
LPS + IFNB1
-log10(adjP)
log2FC
Isg15
Cxcl10
Irf7
Ifnb1
F
wt veh LPS L+I
Del veh LPS L+I
Cxcl10
Irf7
z-score
G
SET-domain containing
methyltransferase activity
wt Del
log2FC LPS vs. LPS+IFNB1
Setdb2 Nsd3 Setd1b Kmt2d Ash1l Prdm2 Setd2 Kmt2b Setd5
Kmt5a Prdm15 Ezh2 Smyd2 Ezh1 Smyd3 Suv39h2 Smyd4
Setd7 Setd6 Kmt5c Tpmt Cmtr1 Dot1l Mettl25 Mettl6 Trmo Trmt1l Trmt13 Eef1akmt2
Trmt2a Tfb2m Pcmtd1 Pcif1 Prmt7 Tfb1m Tarbp1 Aimt Tyms Mrm1 Mettl22 Camkmt Dnmt3a Eed Dnmt3l

Supplemental Figure 6. *Setd1a* is required for GR-mediated inflammatory gene regulation.

This figure relates to figure 6. (**A**) Percent of Dex- and *Setd1a*-dependent genes associated with a GR peak, clustered as in Fig. 6A. (**B**) Slope graph showing the gene expression patterns from cluster III (Fig. 6A). Each gene is shown by one line and one dot per treatment. Purple: genes with lost Dex-dependent repression in Del RAW264.7 cells after 6h or 16h treatment. (**C**) Time series qRT-PCR. (n=3, ANOVA with post-hoc pairwise t-test, Benjamini-Hochberg adjusted; * treatment effect Dex+LPS over LPS; # genotype effect compared to wild type cells treated with LPS; + genotype effect compared to wild type cells (Dex+LPS treatment)). (**D**) Genome browser tracks with ChIP-Seq data for the *Ifnb1* locus from primary macrophages and RAW264.7 cells treated with LPS or Dex+LPS, as described. (**E**) Volcano plots of transcript changes in Setd1a$^{Del/+}$ versus wild type RAW264.7 cells after LPS and LPS+IFNb1 stimulation. The negative log-transformed Benjamini-Hochberg adjusted p-value (adjP) is plotted over the log2FC (fold change). Brown dots represent genes from cluster I (Fig. 6A). Four selected genes are labeled. (**F**) qRT-PCR of wild type and Del cells stimulated with vehicle (veh), LPS or LPS plus IFNb1 (I+L). (n=6, Kruskal-Wallis with post-hoc pairwise Wilcoxon-Mann-Whitney test, Benjamini-Hochberg adjusted; * treatment effect; + genotype effect compared to wild type cells). (**G**) Log2FC of methyltransferase mRNA expression in LPS+IFNb1 and LPS treated wild type (pink) and Setd1a$^{Del/+}$ (purple) cells. Dots represent the mean with the standard deviation as error bars. The top up- and downregulated genes are shown in red when significantly regulated (Benjamini-Hochberg adjusted p-value <0.05) and in bold when regulated >1.5fold in wild type cells. (**H**) *Setd1a* expression (qRT-PCR) in vehicle (veh), LPS or Dex plus LPS (D+L) treated RAW264.7 cells. (n=3, Kruskal-Wallis with post-hoc pairwise Wilcoxon-Mann-Whitney test, Benjamini-Hochberg adjusted; # genotype effect compared to *Del* cells). * # + p<0.05; ** ## ++ p<0.01; *** ### +++ p<0.001; **** #### ++++ p<0.0001.

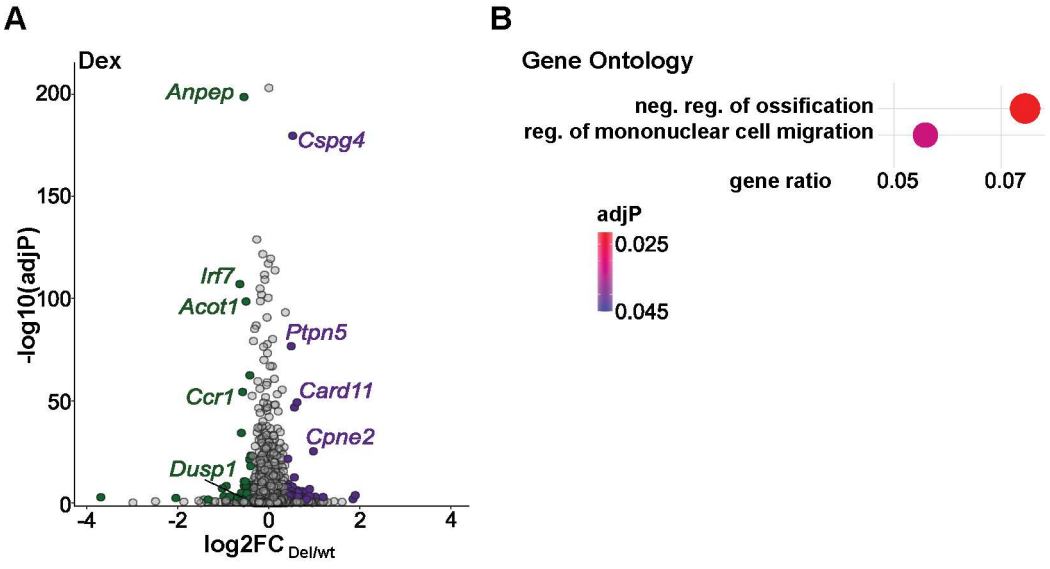

Supplemental Figure 7. Regulation of GR targets in the absence of TLR4 signaling

This figure relates to figure 7. (**A**) Volcano plot of mRNA profiles in Dex-treated (compared to vehicle) wild type and Setd1a$^{Del/+}$ RAW264.7 cells. -log10 Benjamini-Hochberg adjusted p value (Wald test) for the genotype dependence of the gene expression model (full model: ~genotype+treatment +treatment:genotype versus reduced model: ~treatment) is shown over the difference in log2FC between Setd1a$^{Del/+}$ and wild type cells. Purple: genes with lost gene repression (adjP<0.05, FC>1.3); green: genes with impaired activation (adjP<0.05, FC>1.3). Selected transcripts are labelled. (**B**) Gene Ontology enrichment for biological processes, for genes >1.3-fold differentially regulated in Setd1a$^{Del/+}$ RAW264.7 cells in response to Dex (adjP<0.05). Colors are Benjamini-Hochberg adjusted p-values.

3.3 BRG1 defines a genomic subset of inflammatory genes transcriptionally controlled by the glucocorticoid receptor

Contribution

The article ‘’BRG1 defines a genomic subset of inflammatory genes transcriptionally controlled by the glucocorticoid receptor’’ was uploaded as pre-print in BioRxiv in December 2021 and is submitted in EMBO. For this manuscript I generated the NGS data, performed most of the experiments and contributed to the writing of the manuscript.

Summary

ChIP-MS data published in (Greulich et al. 2021) showed that GR interacts with components of the ATP-dependent SWI/SNF chromatin remodeling complex in LPS+Dex treated BMDMs. These interactions were validated in RAW264.7 cells by a co-immunoprecipitation experiment, which additionally revealed an interaction between GR and BRG1 (the catalytic subunit of the SWI/SNF complex). ChIP-seq against GR and BRG1 in LPS+Dex treated macrophages demonstrated that 90% of the GR-bound sites were occupied by BRG1. These sites are near genes related to immune responses, indicating that GR and BRG1 co-bind to inflammatory regulatory sites. ChIP-seq against BRG1 in LPS stimulated macrophages with and without the GR ligand revealed that there is a subset of sites like *Fkbp5* and *Klf9* (two classical target gens activated by GR), where BRG1 is recruited by GR. However, most of the GR binding sites were already occupied by BRG1 before addition of the ligand and are associated with genes involved in inflammatory pathways. This last observation suggests that BRG1 is not evicted by GR in order to repress the expression of pro-inflammatory genes. ATAC-seq in LPS activated macrophages showed that there is a subset of GR binding sites with increased chromatin accessibility upon addition of dexamethasone. These sites displayed also higher BRG1 recruitment in presence of the GR ligand. On the contrary, a large fraction of the GR-bound sites presented constant levels of chromatin openness and BRG1 occupancy independent of GR presence.

Loss of function experiment using small interference RNAs revealed that some genes induced by GR (like *Fkbp5* and *Klf9*) were down-regulated upon *Brg1* knockdown. These genes were related to GBS with increased accessibility and BRG1 recruitment upon addition of the ligand. Most interestingly, silencing of *Brg1* led *to* up-regulation of pro-inflammatory genes negatively regulated by GR (like *Cxcl10, Ccl2, Il1a,* etc.), which are related to GR bound sites with constant BRG1 binding and chromatin openness upon Dex. Pharmacological inhibition of the ATPase domain of BRG1 revealed that its catalytic activity

is crucial for both the transcriptional activation and repression of GR target genes in LPS activated macrophages. Loss of BRG1 activity resulted in reduced GR and MED1 occupancy at the GBS of the activated *Fkbp5* and *Klf9.* Additionally, reduced histone deacetylase recruitment and subsequently increased acetylation of histone 3 was observed at GBS associated with the repressed GR target genes *Cxcl10, Ccl2, Il1a and Il1rn.* Altogether our data suggest that GR interacts with BRG1, and its catalytic activity is important not only for the activation of a subset of GR target genes, but also for GR-mediated repression of inflammatory genes.

BRG1 defines a genomic subset of inflammatory genes transcriptionally controlled by the glucocorticoid receptor

Aikaterini Mechtidou [1,5], Franziska Greulich [1,2,5], Benjamin A. Strickland [2], Céline Jouffe [1,2], Filippo M. Cernilogar [3], Gunnar Schotta [3] & N. Henriette Uhlenhaut [1,2,4] *

[1] Institute for Diabetes and Endocrinology (IDE), Helmholtz Center Munich (HMGU) and German Center for Diabetes Research (DZD), 85764 Neuherberg (Munich), Germany

[2] Metabolic Programming, School of Life Sciences Weihenstephan, ZIEL - Institute for Food & Health, Technische Universitaet Muenchen (TUM), 85354 Freising, Germany

[3] Division of Molecular Biology, Biomedical Center (BMC), Faculty of Medicine, Ludwig-Maximilians-University (LMU) Munich, Großhaderner Straße 9, 82152 Martinsried, Germany

[4] Gene Center, Metabolic Biochemistry and Genetics, Ludwig Maximilians Universitaet (LMU), 81377 Munich, Germany

[5] These authors contributed equally to this work

* corresponding author: henriette.uhlenhaut@tum.de - phone # +49 8161 714322

Running title: BRG1 is required for anti-inflammatory GR actions

Keywords: glucocorticoids, transcription, nuclear receptors, chromatin, SWI/SNF remodelers, innate immunity, repression, inflammation

GRAPHICAL ABSTRACT

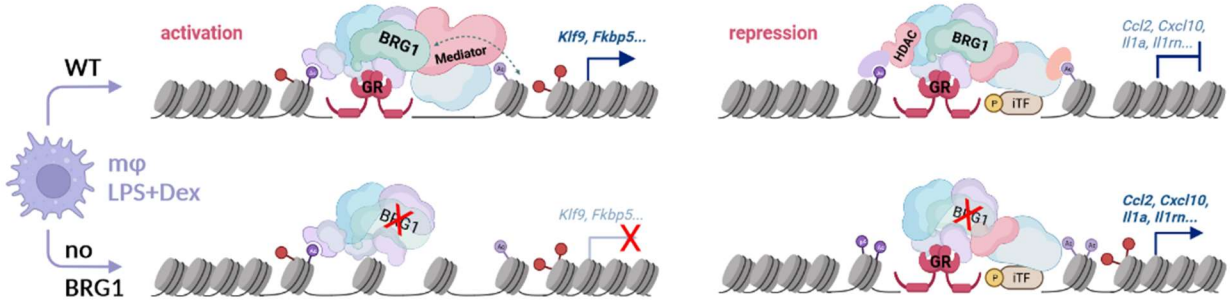

Graphical Abstract. In macrophages (mΦ) responding to bacterial LPS and Dexamethasone, the Glucocorticoid Receptor (GR) activates target genes like *Klf9* or *Fkbp5* via interaction with the BRG1-containing SWI/SNF complex, chromatin remodeling and Mediator recruitment. At the same time, GR represses the expression of inflammatory cytokines and chemokines such as *Ccl2, Cxcl10, Il1a etc*. by assembling a BRG1-containing co-repressor complex and de-acetylating surrounding histone tails. Loss of BRG1 activity affects both the transcriptional activation and repression of a subset of myeloid GR target genes via distinct mechanisms. (iTF: inflammatory transcription factor; Ac: histone acetylation) (Created with BioRender.com.)

ABSTRACT

Glucocorticoids (such as Dexamethasone) are commonly used immunomodulatory drugs with potent anti-inflammatory effects, whose mechanisms of action remain incompletely understood. They bind to the Glucocorticoid Receptor (GR), a nuclear hormone receptor that acts as a transcription factor to directly control the expression of inflammatory genes. To elucidate the complex molecular mechanisms employed by GR during the suppression of innate immune responses, we have performed proteomics, ChIP-seq, ATAC-seq, RNA-seq and bioinformatics together with genetic and pharmacological loss of function studies in primary mouse macrophages. We found that GR interacts with the ATP-dependent SWI/SNF chromatin remodeling complex to regulate a specific subset of target genes. Here we show that the central catalytic subunit BRG1 is required not only for the transcriptional activation of classical GR target genes such as *Fkbp5* or *Klf9*, but also for the transcriptional repression of cytokines and chemokines such as *Ccl2*, *Cxcl10* or *Il1a*. We demonstrate that loss of BRG1 activity leads to reduced histone deacetylase (HDAC) function, and consequently increased histone acetylation, at these repressive GR binding sites. Altogether, our findings suggest that GR interacts with BRG1 to assemble a functional co-repressor complex at a defined fraction of macrophage *cis*-regulatory elements. These results may indicate additional non-classical, remodeling-independent functions of the SWI/SNF complex and may have implications for the development of future immunomodulatory therapies.

INTRODUCTION

The Glucocorticoid Receptor (GR, encoded by the *Nr3c1* gene) is an important immunomodulatory drug target and a prominent physiological regulator. It belongs to the nuclear receptor family of ligand gated transcription factors, whose clinical relevance is underscored by its life-saving effects in COVID-19 patients (Group et al. 2021). Upon binding to its ligands such as Dexamethasone, GR translocates to the nucleus to either activate or repress target gene transcription. The exact mechanisms specifying positive versus negative regulation and the composition of coregulatory complexes assembled on target promoters or enhancers are inherently complex and pose many open questions (Escoter-Torres et al. 2019). Several studies have suggested that *cis*-regulatory element recognition and binding by GR is predetermined by each cell type's specific chromatin landscape, which is established by pioneer factors like PU.1, AP-1 or C/EBP, and which shapes the GR cistrome (Biddie et al. 2011; John et al. 2011; Greulich et al. 2016).

In that respect, chromatin remodeling is both an essential prerequisite as well as a central component of GR-mediated transcriptional regulation. Assembly of the SWI/SNF (SWItch/Sucrose-NonFermentable) remodeling complex and its interaction with GR have been shown to enhance the transcriptional hormone response. BRG1 (SMARCA4), the central ATPase of the SWI/SNF complex, is required for proper and robust GR-regulated gene activation (Fryer and Archer 1998). Both structural models and biochemical experiments indicate that SMARCD1 (BAF60A), SMARCC1 (BAF155), SMARCE1 (BAF57) and ARID1A (BAF250) components engage in protein-protein interactions between GR and the SWI/SNF complex (Hsiao et al. 2003; Muratcioglu et al. 2015). Gene activation of various nuclear receptors, including GR, has been reported to broadly require the cooperation of this well-studied chromatin remodeling complex. In this context, BRG1 both precedes GR chromatin occupancy, by establishing pioneer factor recruitment to create accessible GR DNA binding

sites, and also serves subsequently as a coactivator and remodeler required for GR-induced DNA accessibility and transcription (Trotter and Archer 2004; Trotter et al. 2015; Hoffman et al. 2018).

Regarding its clinical use, the direct transcriptional repression of pro-inflammatory cytokines and chemokines by GR is thought to underlie a major part of its immunomodulatory potency (Escoter-Torres et al. 2019). Indeed, gene repression was partially affected in 3134 cells expressing a dominant negative BRG1, and individual glucocorticoid-induced BRG1-dependent DNAse hypersensitivities were described. *John et al.* suggested an important role of chromatin remodeling in GR-mediated repression, based on the detection of numerous transition events linked to repressed loci (John et al. 2008). Furthermore, BRG1 was found to be required together with HDAC2 for histone de-acetylation and repression of the human *POMC* promoter, a well-known negative GR target (Bilodeau et al. 2006).

Finally, genome wide studies during the past decade have revealed that GR binding sites are not only cell type-, signal- and time point- specific, but that given GR cistromes are far from uniform, and can be divided into distinct subsets or particular classes of target loci. We therefore hypothesized that BRG1-containing remodeling complexes may mediate significant fractions of anti-inflammatory glucocorticoid actions. Here we chose primary bone marrow derived murine macrophages, which are important cellular mediators of the innate immune response, as a model to study the GR-mediated repression of inflammatory genes (Uhlenhaut et al. 2013; Greulich et al. 2021b). We performed ChIP-seq and ATAC-seq in lipopolysaccharide-activated macrophages to functionally characterize the role of BRG1 (SMARCA4) for a subset of GR target genes. Our data suggest that the catalytic activity of the SWI/SNF complex is not only involved in the activation of classical GR target genes (such as *Klf9* or *Fkbp5*), but also in the transcriptional repression of pro-inflammatory cytokines, chemokines and interleukins (such as *Ccl2, Cxcl10* or *Il1a*).

RESULTS

GR and BRG1 co-occupy macrophage *cis*-regulatory loci

In order to chart the composition of the transcriptional complexes assembled by GR during the regulation of innate immune responses, we performed protein-protein interactome mapping by ChIP-MS for GR in primary murine bone marrow derived macrophages activated with the TLR4 ligand lipopolysaccharide (LPS) and treated with the GR ligand Dexamethasone (Dex) (Greulich et al. 2021b). In addition to various known co-regulators and to novel interaction partners such as the COMPASS complex, we found several components of the SWI/SNF complex significantly enriched together with GR (**Fig. 1A**). For example, we detected SMARCD2 (BAF60B), SMARCE1 (BAF57), SMARCC2 (BAF170) and ARID1A (BAF250) peptides in our IP dataset.

To confirm these putative interactions between GR and SWI/SNF subunits in activated macrophages, we then carried out endogenous Co-IPs in the RAW264.7 myeloid cell line, in the presence of LPS and Dex. Indeed, we were able to detect GR together with SMARCD1 (BAF60A), SMARCE1 (BAF57) and SMARCA4 (BRG1) by Western Blotting (**Fig 1B).**

Similarly, when we compared our macrophage interactome with data from livers and Dex-treated mouse embryonic fibroblasts (MEFs, activated by LPS), we also found the SWI/SNF subunits to be enriched (Fig. S1A) (Quagliarini et al. 2019; Escoter-Torres et al. 2020). Therefore, we conclude that GR robustly interacts with the SWI/SNF chromatin remodeling complex across tissues and cell types.

To further investigate potential functional relationships between GR and the SWI/SNF remodeling complex, we next performed ChIP-seq for both GR and the core ATPase subunit BRG1 (SMARCA4) in primary murine macrophages. (Since the other catalytic SWI/SNF component, SMARCA2 (BRM), was transcriptionally downregulated upon Dex stimulation, we focused only on BRG1 (Fig. S1B)). As shown in **Fig. 1C**, almost all GR binding sites mapped in

response to LPS and Dex, also showed co-occupancy of BRG1 (about 90%). As expected, we also detected many additional BRG1 binding sites throughout the genome, not overlapping with GR, which represent the central, essential functions of the SWI/SNF complex within the macrophage chromatin landscape (Chen et al. 2020). Bioinformatic motif analyses of those ~8,000 common GR-BRG1-bound ChIP sequences revealed the GR consensus motif (GRE) as significantly enriched, together with the known macrophage pioneer factor PU.1 and the inflammatory mediators AP-1 and NF-κB (**Fig. 1D**, Fig. S1C), validating our data sets (Uhlenhaut et al. 2013). For instance, we observed BRG1 binding to GR target sites such as the *Fkbp5*, *Klf9*, *Ccl2*, *Cxcl10, Il1a and Il1rn* loci (**Fig. 1E,** Fig. S1D). *Fkbp5* and *Klf9* are two typical examples of positive GR targets *induced* by Dex, while *Cxcl10, Ccl2*, *Il1a, and Il1rn,* are representative cases of negative GR target genes *repressed* in response to ligand (Uhlenhaut et al. 2013; Escoter-Torres et al. 2020; Greulich et al. 2021b). In addition to these exemplary cytokines, the functional annotation of the ~8,000 common GR-BRG1 target sites, based on the nearest gene, include many genes involved in inflammation, immune responses, myeloid migration and inflammatory signaling cascades (**Fig. 1F**).

Altogether, our immunoprecipitation studies in macrophages show that the central SWI/SNF component BRG1 co-localizes together with GR at inflammatory promoters and enhancers in response to TLR4 signaling and glucocorticoids.

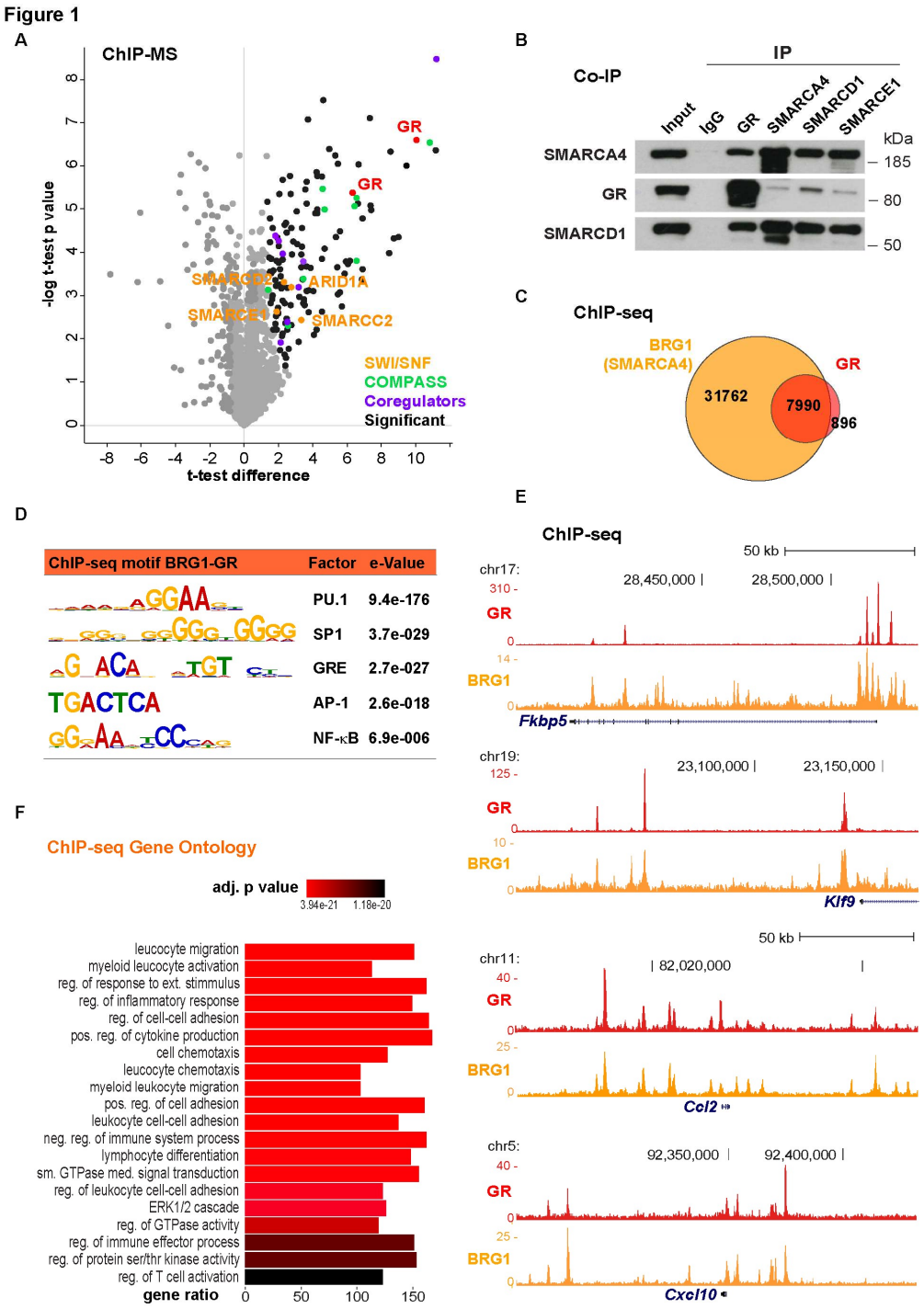

Figure 1: GR interacts with the SWI/SNF complex in activated macrophages. (A) ChIP-MS GR interactome in primary macrophages treated with Dexamethasone (Dex) and lipopolysaccharide (LPS) (Greulich et al. 2021b). Colored dots show interactors significantly enriched in a GR pulldown over non-specific isotype-matched IgG, functionally annotated (1.5fold, $p<0.05$). (B) Western blot of endogenous Co-IPs in RAW 264.7 cells treated with LPS and Dex. (C) Venn diagram of reproducible GR and BRG1 ChIP-seq peaks overlapping in primary macrophages treated with LPS and Dex (n=2). (D) Motif enrichment analysis for the 7,990 common GR and BRG1 ChIP-seq peaks. (E) Representative genome browser tracks of GR and BRG1 ChIP-seq signals, showing means from two replicates. (F) Functional annotation of the 7,990 common GR-BRG1 sites, assigned to the nearest gene.

GR recruits BRG1 to a distinct subset of macrophage binding sites

Since we had found protein-protein interactions and DNA co-occupancy between GR and the SWI/SNF complex, we performed ChIP-seq for the core component BRG1 in activated primary macrophages with and without GR ligand stimulation, to determine whether GR recruits BRG1 to chromatin. When analyzing the ~8,000 GR binding sites shared with BRG1, we found that over 1,300 of them were dependent on GR ligand, meaning that BRG1 occupancy was induced by Dex in LPS-activated primary macrophages (**Fig. 2A**). Similar to previous studies for the GR co-regulators GRIP1 and SETD1A/COMPASS, we observed a ligand-mediated expansion of the BRG1 cistrome in macrophages (Uhlenhaut et al. 2013; Greulich et al. 2021b). Around 15,500 BRG1 binding sites were gained upon Dex stimulation, while ~4,700 LPS-specific BRG1 sites were lost (Fig. S2A). Generally, most BRG1 binding sites were found in intronic or intergenic enhancer regions, under both conditions (Fig. S1B) (Hoffman et al. 2018).

Accordingly, these GR ligand-dependent BRG1 ChIP peaks featured a GRE consensus sequence as significantly enriched in motif analyses. Additional motifs include the ubiquitous, general transcription factor SP1, the master regulator of macrophage cell fate PU.1 and the inflammatory mediator NF-κB (**Fig. 2B**) (Glass and Natoli 2016). Of note, motifs for the inflammatory transcription factor AP-1 were identified in both BRG1 cistromes (LPS and LPS plus Dex), without a significant enrichment for the GR-BRG1 subset (Fig. S2C).

In line with GR's prominent role in the transcriptional control of macrophage function and activity, these Dex-induced BRG1 binding sites mapped near genes involved in chemotaxis and migration, protein phosphorylation, metabolism and T cell activation (**Fig. 2C**) (Escoter-Torres et al. 2019). For example, both ChIP-seq as well as ChIP-qPCR show increased binding of BRG1 to the *Fkbp5* and the *Klf9* *cis*-regulatory regions in response to Dex (**Fig. 2D&E**). These observations are consistent with transcriptional activation of *Fkbp5* and *Klf9*, for example, by

GR, and with BRG1's role in nucleosome remodeling and transcription by nuclear receptors (Trotter and Archer 2008).

Importantly, the majority of GR and BRG1 co-bound loci, which are associated with inflammatory pathways, were pre-bound by BRG1 in the absence of Dex, in line with their known function in LPS-activated macrophages (**Fig. 2C**, Fig. S2D). That means we did not detect changes in BRG1 ChIP-seq signal intensity between the samples treated with LPS only, and those treated with LPS plus Dex. For example, GR binding sites near *Ccl2*, *Cxcl10*, *Il1a* or *Il1rn* displayed robust BRG1 occupancy in both conditions (LPS and LPS+Dex) (**Fig. 2D&E**, Fig. S2E). Since these genes are expressed in LPS-activated macrophages, they may depend on the SWI/SNF complex for their induction upon TLR4 stimulation (McAndrew et al. 2016; Chen et al. 2020). Our observations suggest that GR does not appear to evict BRG1 in order to repress the transcription of chemokines, cytokines, interleukins *etc.*, since we did not observe a significant reduction in global BRG1 occupancy in response to Dex, but rather a gain at specific activated GR target loci.

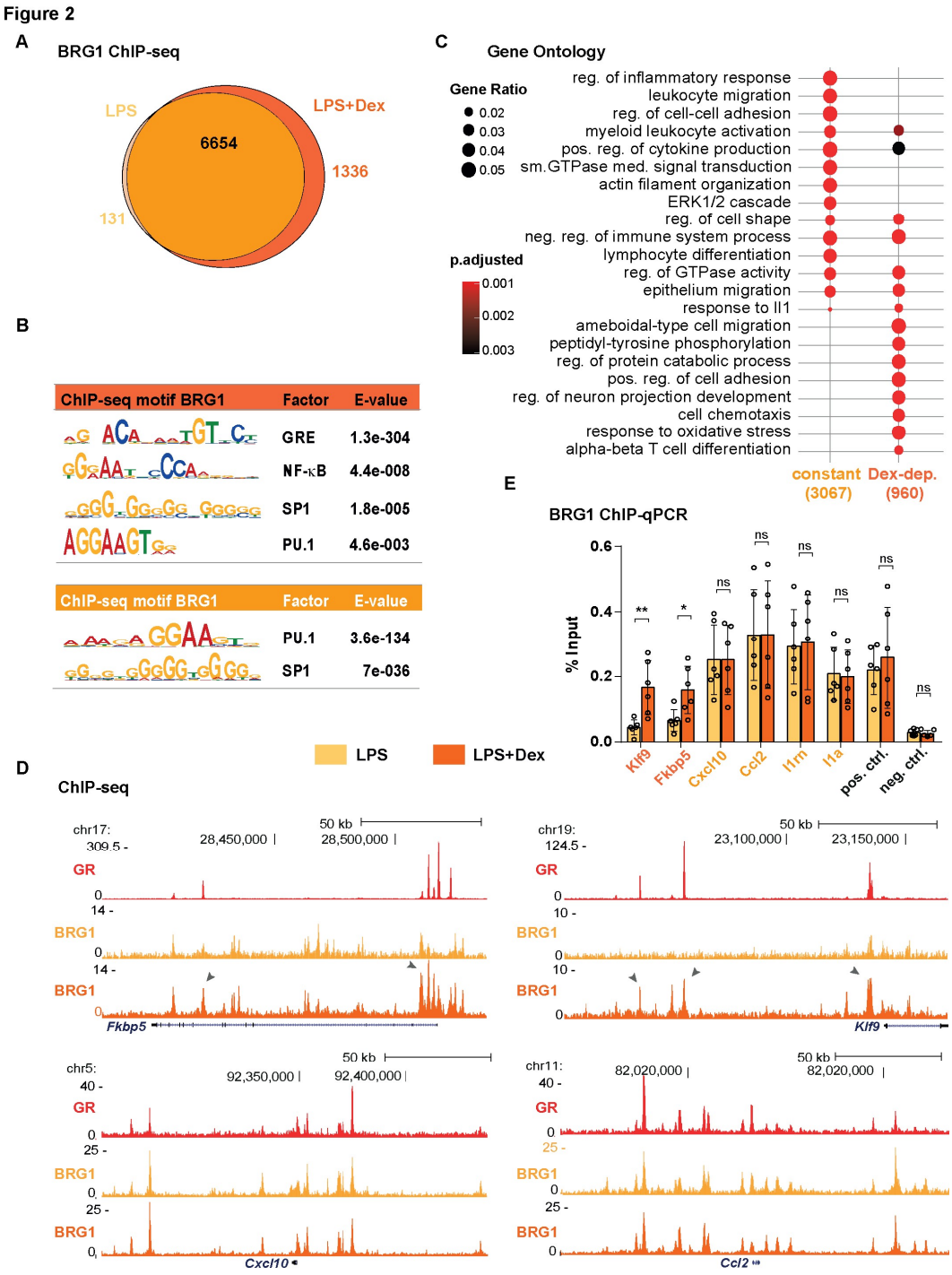

Figure 2: Locus-specific recruitment of BRG1 by GR in macrophages. (A) Venn diagram of BRG1 ChIP-seq peaks overlapping with the GR cistrome (~8,000, see Fig. 1C), in response to LPS alone, or LPS plus Dexamethasone (Dex). (B) Motif enrichment of the 1,336 Dex-induced BRG1 peaks, and the constant BRG1 ChIP peaks (detected in both LPS and in LPS+Dex, 6,654) shown in A. (C) Functional annotation of the two BRG1 ChIP peak classes, Dex-induced and constant, based on the nearest gene. (D) Example genome browser tracks of GR and BRG1 ChIP-seq in macrophages treated with LPS alone (BRG1) or LPS plus Dex (GR, BRG1), means of n=2. Arrows point at sites of GR-induced BRG1 recruitment. (E) BRG1 ChIP-qPCR validation for selected loci shown in D. Error bars show standard deviation, * p<0.05, ** p<0.01, ns= not significant, unpaired two-tailed Student's t-test, n=3.

Chromatin remodeling in response to GR ligand

As we had observed co-occupancy and recruitment of the core SWI/SNF subunit BRG1 at GR-bound *cis*-regulatory sites in murine macrophages, we performed ATAC-seq in LPS and in LPS+Dex treated cells, to measure chromatin accessibility in response to GR ligand. Overall, we identified over 100,000 sites of open chromatin in our primary macrophages, of which 8,860 were only present in macrophages treated with both LPS and Dex (**Fig. 3A**). Amongst those accessible regions, ~27,800 displayed BRG1 occupancy and ~8,200 showed GR co-binding, in LPS and Dex stimulated cells. Conversely, essentially all (99.8%) GR plus BRG1 co-occupied sites mapped to accessible chromatin (Fig. S3A).

When quantifying and comparing the ATAC-seq signal detected at *cis*-regulatory sites occupied by both GR and BRG1, we found that 1,234 loci gained ATAC-seq signals, while only 12 loci lost DNA accessibility. For example, classical GR target genes like *Fkbp5*, *Tsc22d3* (*Gilz*) and *Klf9* gained chromatin accessibility together with BRG1 recruitment upon Dexamethasone exposure (**Fig. 3B**). Consistent with retained BRG1 occupancy, we found only minimal reductions in ATAC-seq signals at GR target loci, on the other hand, indicating that GR does not generally close chromatin to repress transcription.

When performing a differential motif enrichment search among those sequences mapping to loci which gained openness in response to GR ligand, we found the GRE consensus motif over-represented among the ATAC-seq signatures (**Fig. 3C**). These results might point towards GR's role in nucleosome positioning or phasing, possibly via BRG1 recruitment. Our data underscore the broad requirement and central role of the BRG1-containing SWI/SNF remodeling complex for transcriptional activation by GR (Hoffman et al. 2018). Furthermore, general motif enrichment analyses of our ATAC-seq signatures revealed consensus sites for the myeloid lineage factor PU.1 and the architectural factor CTCF, both of which are known to shape the macrophage chromatin landscape (Fig. S3B) (Ghirlando and Felsenfeld 2016).

Fig. 3D compares the BRG1 and the H3K27acetyl ChIP-seq reads with the ATAC-seq signal strength between LPS and LPS plus Dex treated macrophages, for all GR/BRG1 co-bound sites with either gained, reduced or constant (1.5>FC<-1.5, FDR>0.05) ATAC-seq signals (5,519 peaks in total). Generally, chromatin accessibility correlated with BRG1 recruitment and histone H3K27 acetylation induced by GR (**Fig. 3D**). Moreover, GR/BRG1 co-occupied loci with constant DNA accessibility were associated with genes involved in inflammation, such as 'positive regulation of cytokine production', 'ERK1/2 cascade' or 'negative regulation of immune system processes' (Fig. S3C).

For example, the *Klf9* and the *Fkbp5* loci both showed increased BRG1 occupancy, increased ATAC-seq read signals and increased histone H3K27 acetylation in response to Dex (**Fig. 3E**). Negative GR targets such as *Ccl2*, *Cxcl10, Il1a* or *Il1rn*, however, appeared to maintain a rather constant level of BRG1 binding, chromatin accessibility and H3K27 acetylation (**Fig. 3D**, Fig. S3D).

In general, our ATAC-seq profiling in primary macrophages revealed a cluster of distinct GR target loci, which displayed increased chromatin accessibility coinciding with ligand-activated BRG1 recruitment. Furthermore, a large fraction of GR-BRG1 co-bound genomic sites appeared to retain a constant level of BRG1 occupancy and openness not affected by GR ligand. The former subset mainly appears to correspond to activated GR target genes, while the latter seems to represent genes repressed by GR.

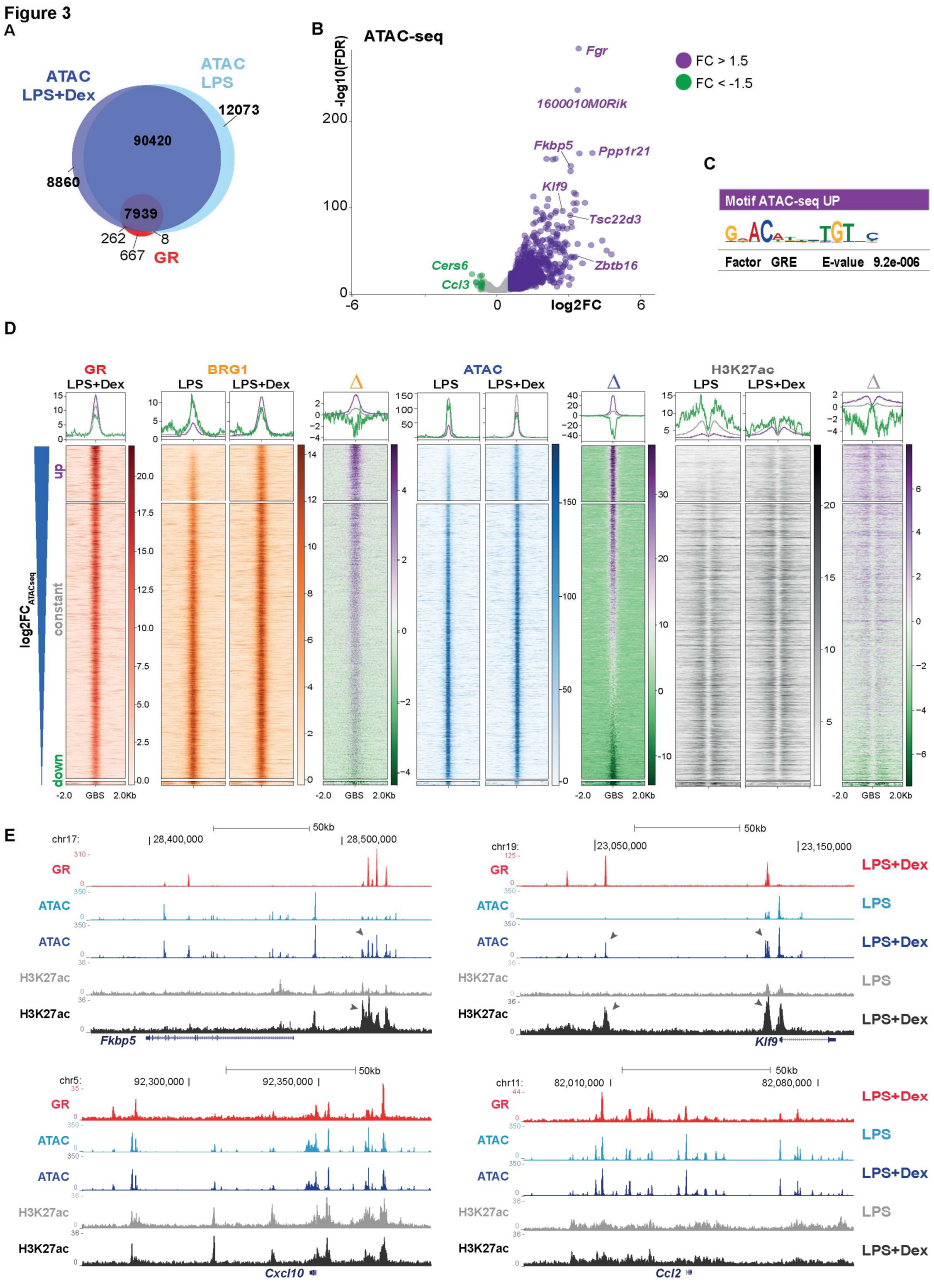

Figure 3: GR-induced macrophage chromatin accessibility changes. (A) Venn diagram with numbers of ATAC-seq peaks called in LPS and in LPS+Dex treated macrophages (n=4) and GR ChIP-seq (n=2). (B) Volcano plot of differential ATAC-seq signals at GR and BRG1 co-occupied regions, fold changes (FC) in LPS+Dex versus LPS treated samples. Dots represent single genomic regions, associated to the nearest gene. 7,351 peaks, n=4, FDR<0.05 (C) Differential motif enrichment analysis of the three categories of ATAC-seq peaks (shown in B), versus the union of all three peak sets (5,519 peaks). No significant enrichment was found for the gray or green sets. (D) Heatmaps of mean GR, BRG1, H3K27ac ChIP- and ATAC-seq signals at +/-2kb of GR-BRG1 co-occupied regions after LPS or LPS+Dex treatment. Sites are sorted by the Dex-induced change in ATAC-seq signal in descending order, and clustered by GR-BRG1 binding sites gaining (FC>1.5, FDR<0.05), maintaining (1.5>FC<-1.5, FDR>0.05) or losing (FC<-1.5, FDR<0.05) accessibility. Differential heatmaps (Δ) compare LPS+Dex versus LPS. Coverage plots on top summarize the median signal per group (GBS: GR binding site). (E) Representative genome browser tracks showing the mean signal of GR (n=2), ATAC-seq (n=4) and H3K27ac ChIP-seq (n=2) for *Fkbp5, Klf9*, *Ccl2* and *Cxcl10* loci. Arrows highlight signal changes.

BRG1 is required for transcriptional activation and repression by GR

Since our ChIP-seq and ATAC-seq profiles had exposed interactions between GR and the SWI/SNF complex at macrophage *cis*-regulatory elements, which manifested as BRG1 recruitment or co-occupancy together with chromatin remodeling or openness, respectively, we next performed loss of function studies. We knocked down *Brg1* expression in primary macrophages by siRNA, and performed RNA-seq to study the effects of *Brg1* inactivation on GR target gene regulation. Indeed, in macrophages treated with LPS and Dex, *Brg1* knockdown resulted in both up- and down-regulation of GR target genes compared to controls. For example, *Fkbp5*, *Klf9* and other positive GR targets were downregulated (induced to a lesser extent) upon transfection with *Brg1* siRNAs (**Fig. 4A,** Fig. S4A). Strikingly, many negative, inflammatory GR targets, such as *Ccl2, Ccl4, Cxcl10, Mmp27, Btg1, Il1a*, *Il1b* and *Il1rn* etc. were upregulated, meaning those were de-repressed. Generally, functional annotation of significantly differentially expressed genes showed an enrichment of genes involved in inflammation, immune responses, cytokines, defense responses and migration among those de-repressed genes (**Fig. 4B**, Fig. S4B).

Importantly, with respect to the LPS response, many of these genes did not appear to depend on BRG1 for their activation by TLR4 signaling (**Fig. 4C**). Compared to quiescent macrophages, several inflammatory mediators were still induced upon LPS stimulation in *Brg1* knockdown samples. These effects were neither due to differential mRNA expression of the *GR* gene itself, nor downregulation of known GR co-regulators such as *GRIP1* or *Setd1a* (Fig. S4C&D).

Our RNA-seq profiles revealed that BRG1 is not only required for the transcriptional activation of nuclear receptor target genes, but also for the transcriptional repression of key inflammatory targets by GR. For example, *Cxcl10* and *Ccl2* were potently upregulated in *Brg1* knockdown and control cells activated by LPS, but showed impaired repression by Dex in the absence of BRG1 (**Fig. 4D**).

Taken together, our *Brg1* loss of function studies demonstrated a functional requirement of this enzymatic subunit not only for transcriptional activation, but also for transcriptional repression by GR, which could conceivably occur independently of its function in chromatin accessibility (**Fig. 4C**).

Figure 4

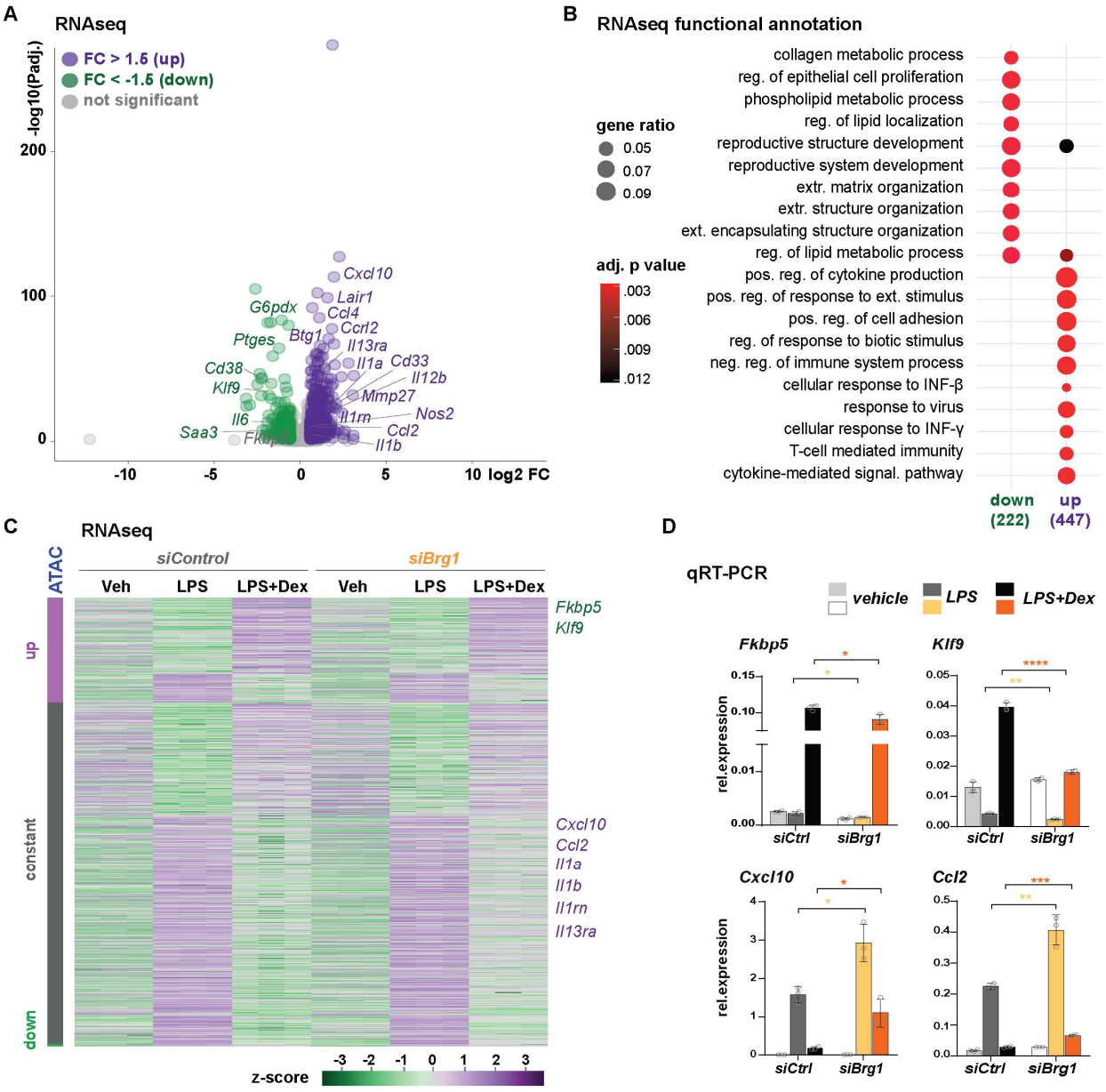

Figure 4: Loss of *Brg1* affects the glucocorticoid response in macrophages. (A) Volcano plot for transcripts harboring a nearby GR/BRG1 ChIP peak, showing RNAseq expression changes between control and *Brg1* knockdown macrophages treated with LPS+Dex (n=3, fold change ±1.5, p adjusted<0.05). (B) Gene Ontology enrichment ('biological process') of the differentially expressed common GR/BRG1 target genes shown in A. (C) Heatmap for GR/BRG1 targets associated with the three ATAC-seq categories (Fig. 3D), in control and *Brg1* knockdown macrophages treated with vehicle (Veh), LPS and LPS+Dex. (D) qRT-PCR validation of two positive and two negative GR/BRG1 targets upon *Brg1* or control siRNA transfection. Error bars show standard deviation, *p<0.05, **p<0.01, ***p<0.001, ****p<0.0001, ns = not significant, unpaired two-tailed Student's t-test, n=3.

BRG1 is required for histone deacetylation by GR

As we had observed impairments in both transcriptional activation and repression of GR target genes after *Brg1* siRNA knockdown in macrophages, we next aimed to validate these observations and to functionally characterize these affected loci. We first treated primary macrophages with a commercially available allosteric dual brahma homolog (BRM)/(BRG1) ATPase activity inhibitor (Papillon et al. 2018): As shown in **Fig. 5A**, inhibiting BRG1 catalytic activity reproducibly impaired the transcriptional activation of *Fkbp5* and *Klf9*, and compromised the transcriptional repression of *Ccl2, Cxcl10, Il1a* and *Il1rn* by GR in LPS-activated cells.

When performing ChIP-qPCR for GR itself, in the presence of the SWI/SNF inhibitor, we found strongly reduced binding of the receptor to the *cis*-regulatory regions of the *Klf9* and *Fkbp5* genes, while the occupancy of the *Ccl2, Cxcl10, Il1a* and *Il1rn* binding sites was not affected (**Fig. 5B**). The diminished GR target gene binding and transcriptional activation was accompanied by weakened recruitment of the Mediator complex, as determined by ChIP-qPCR for the central MED1 subunit, at the *Fkbp5* and *Klf9* loci (Chen and Roeder 2007).

Conversely, *Cxcl10, Ccl2, Il1a* and *Il1rn*, which displayed impaired transcriptional repression by GR despite maintained chromatin interactions, showed increased total histone H3 acetylation correlating with increased mRNA production (**Fig. 5C**). These histone acetylation marks coincided with diminished recruitment of the histone deacetylases HDAC1 and HDAC3 in response to GR ligand. Of note, this observation refers to specific loci, as global HDAC activity was not diminished in primary macrophages treated with the BRG1 inhibitor (Fig. S5A).

To support our hypothesis that BRG1 might be required for the assembly of a functional corepressor complex containing HDACs and affecting the histone acetylation levels of inflammatory genes controlled by GR, we treated macrophages with the histone deacetylase inhibitor ‘Vorinostat’, also known as suberanilohydroxamic acid (SAHA) (Marks and Breslow 2007). Indeed, HDAC inhibition was able to recapitulate the impaired repression of *Ccl2,*

Cxcl10, Il1a and *Il1rn* by GR, in macrophages treated with LPS and Dex (**Fig. 5D**). Importantly, these differential gene expression and chromatin pattern changes were observed despite maintained GR, BRG1, HDAC1, HDAC2 and HDAC3 mRNA and protein expression levels in these cells, and despite comparable BRG1 occupancy of these loci (Fig. S5B-F).

In conclusion, we found that BRG1 activity is essential for both transcriptional activation and repression of macrophage GR target genes. Our data may suggest that the transcriptional repression of inflammatory cytokines, chemokines and interleukins in response to glucocorticoids requires BRG1 for the assembly of a functional, HDAC-containing co-repressor complex. Conceivably, these findings point towards a novel role for the SWI/SNF complex independent of its nucleosome remodeling function.

Figure 5

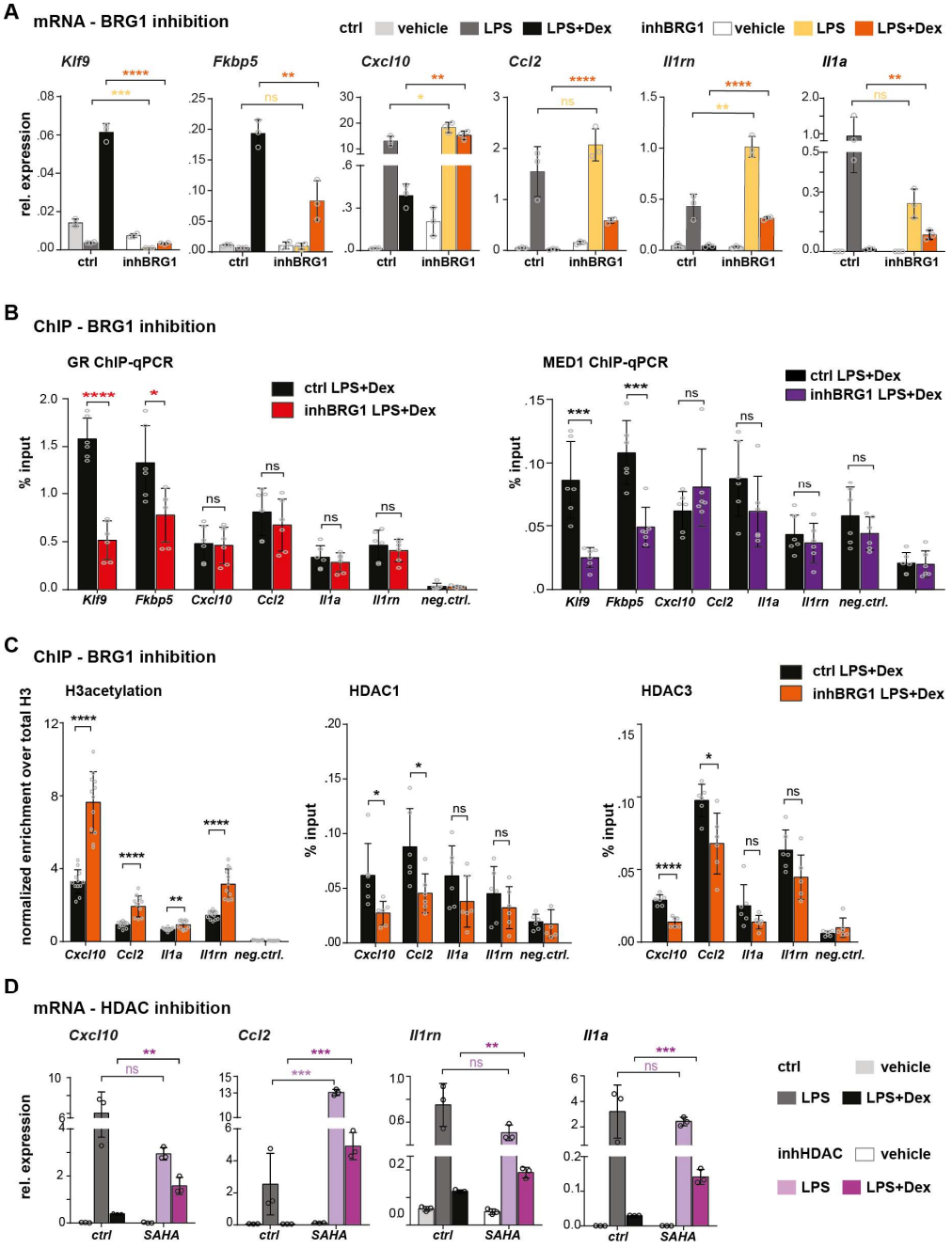

Figure 5: BRG1 catalytic activity is important for macrophage GR target gene regulation. (A) qRT-PCR of GR target genes in vehicle, LPS and LPS+Dex treated primary macrophages upon BRG1 inhibition (compared to DMSO). (B) GR and Mediator (Med1) ChIP-qPCR in control and BRG1 inhibitor treated macrophages (LPS+Dex). (C) Total histone H3 acetylation, HDAC1 and HDAC3 ChIP-qPCR in control and BRG1 inhibitor treated macrophages, upon LPS+Dex stimulation, at repressed GR target sites. For H3 acetylation ChIP, data were spike-in normalized and the values represent the % input over the total histone H3. (D) qRT-PCR of repressed GR target genes in vehicle, LPS and LPS+Dex stimulated macrophages treated with control (DMSO) or SAHA (HDAC inhibitor). For all bar graphs, values are mean ± standard deviation. *p<0.05, **p<0.01, ***p<0.001, ****p<0.0001, ns = not significant, unpaired two-tailed Student's t-test, n=3 biological replicates.

DISCUSSION

Our study revealed a dual role for the BRG1-containing SWI/SNF chromatin remodeling complex in GR-mediated inflammatory gene regulation in murine macrophages. Near activated GR target genes (such as *Klf9* and *Fkbp5*), we found that BRG1 was required for stable GR DNA binding and Mediator recruitment, coincident with increased chromatin accessibility. This continuous requirement of BRG1 for enhancer maintenance, openness and transcriptional activation is in line with previous reports on SWI/SNF complexes in other cell types (Hoffman et al. 2018; Iurlaro et al. 2021; Schick et al. 2021).

However, near negative GR target genes (like *Ccl2, Cxcl10, Il1rn and Il1a*), on the other hand, BRG1's catalytic activity was necessary for transcriptional repression, independently of its chromatin remodeling function. For those loci, we found that the histone H3 acetylation levels were maintained after stimulation with Dexamethasone, rather than decreased, which concurred with increased mRNA expression (i.e., reduced repression). While the DNA accessibility remained constant, the impaired repression could be explained by reduced recruitment of the histone deacetylases HDAC1 and HDAC3 in response to GR ligand, especially since pharmacological HDAC inhibition mirrored this phenotype.

Interestingly, a requirement of BRG1 and HDAC2 for nuclear hormone receptor-mediated transcriptional repression was also shown for the closely related progesterone and estrogen receptors (Jung et al. 2001; Nacht et al. 2016). Furthermore, BRG1 was found to be critical for the formation of stable complexes between GR and HDAC2 on the *POMC* promoter, along with histone H4 de-acetylation and GR-dependent repression (Bilodeau et al., 2006).

SWI/SNF chromatin remodeling complexes have been described as having both co-activator as well as co-repressor functions and thus may provide a molecular hub or platform, switching from transcriptional activation to repression (Zhang et al. 2007; Kim et al. 2021). For example, locus-specific phosphorylation of BRG1 at Ser1382 has been reported to release the HDAC1/2-

containing NURD complex and to favor BRG1's nucleosome remodeling activity (Kim et al. 2021).

Currently, the molecular mechanisms that specify positive versus negative gene regulation by GR, mediated via co-activator or co-repressor complex assembly, respectively, remain elusive. Besides an enrichment for classical, palindromic GRE consensus motifs amongst GR binding sequences associated with *de novo* BRG1 recruitment and increased chromatin accessibility, we have not yet been able to identify discriminatory signatures or sequence motifs. It is conceivable that BRG1 represents a key interaction partner of GR, which might switch between co-activator and co-repressor conformations in a locus-specific manner, depending on the chromatin context.

In summary, our findings show that BRG1 is involved in anti-inflammatory glucocorticoid responses, which might suggest that future therapeutic approaches using SWI/SNF or HDAC inhibitors may have immunomodulatory effects.

METHODS

Cell lines

RAW264.7 cells (ATCC TIB-71, RRID CVCL 0493) were cultured in DMEM supplemented with 10% FBS and 1% penicillin/streptomycin. The cells were grown at 37 °C in the presence of 5% CO_2.

Drosophila S2 cells (donated from P. Becker, RRID: CVCL_IZ06) were cultured in Schneider's *Drosophila* medium supplemented with 10% FBS and 1% penicillin/streptomycin. The cells were grown in T175 flasks at 28 °C in absence of CO_2.

Extraction and differentiation of bone marrow derived macrophages

Leg bones were surgically removed from 6-14 weeks old wild type C57BL6/J male mice. After muscle dissection and clean-up of the bones with ethanol, bone marrow was extracted in RPMI. Erythrocytes were lysed with AKC lysis buffer (1 M NH_4Cl, 1 M $KHCO_3$, 0.5 M EDTA). Afterwards the cells were purified on a Ficoll-Paque gradient and cultured in differentiation medium (DMEM containing 30% supernatant of L929 cells, 20% FBS 1% penicillin/streptomycin) for 7 days on non - cell culture treated plates. Versene was applied to the differentiated macrophages, which were subsequently counted and seeded in macrophage serum free medium.

Cells were treated either with vehicle (0.1% EtOH and PBS), LPS (100 ng/ml, Sigma Aldrich and 0.1% EtOH) or LPS+Dex (100 ng/ml LPS Sigma; 1 µM Dexamethasone in EtOH). For the inhibitor experiments, macrophages were additionally treated either with 500 nM BRG1/BRM inhibitor (MedChemExpress, HY-119374) or with 1 µM SAHA (Sigma, SML0061) or 0.05%-0.1% DMSO, respectively, for 6 hours.

Nuclear extraction and co-IP

RAW264.7 cells were treated with 1μM Dexamethasone overnight, followed by 3 hours treatment with 100ng/mL of LPS. The cells were washed thoroughly with ice-cold PBS and then lysed in V1 lysis buffer (10 mM HEPES-KOH pH 7.9, 1.5 mM $MgCl_2$, 1 0mM KCl and freshly added 1 μM Dexamethasone, 0.5 mM DTT, 0.15% NP40, protease inhibitors and PhosphoSTOP) in a glass douncer on ice. After centrifugation at 2,700g for 20 min, the nuclei were collected and lysed in V2 buffer (420 mM NaCl, 20 mM HEPES-KOH pH 7.9, 20% glycerol, 2 mM $MgCl_2$, 0.2 mM EDTA and freshly added 1 μM Dexamethasone, 0.5 mM DTT, 0.1% NP40, protease inhibitors and PhosphoSTOP) for 1 hour while agitating at 4ºC. The nuclear extracts were collected after 45 min centrifugation at 21,000g at 4ºC and used for co-IPs.

Co-IPs were performed with 200μg of nuclear protein extract that was pre-cleared with α-rabbit Dynabeads (Invitrogen) for 1 hour in IP buffer (20 mM Tris pH 8, 100 mM KCl, 5 mM $MgCl_2$, 0.2 mM EDTA, 20% glycerol and freshly added protease inhibitors) under rotation at 4ºC. The pre-cleared protein extracts were incubated with 3μg rabbit α-BRG1 (Cell Signalling, 49360), rabbit α-GR (Proteintech, 24050-1-AP), rabbit α-Baf57 (Bethyl Labs, A300-810A) and rabbit α-Baf60a (Proteintech, 10998-2-AP) antibody or 3μg of rabbit IgG antibody (Cell Signalling, 2729) for 2 hours under rotation at 4ºC, followed by an overnight incubation with BSA blocked α-rabbit Dynabeads (Invitrogen) at 4ºC. Beads were washed 3 times with IP buffer supplemented with 0.3% Triton X-100. Bound proteins were eluted in Laemmli buffer and DTT for 30 min at 37ºC and analyzed by Western Blot using mouse α-GR (Santa Cruz, sc-393232), mouse α-Brg1 (Cell Signalling, E9O6E) and goat α-Baf60a (Santa Cruz, sc-82778) antibodies.

siRNA mediated gene silencing

Gene silencing in primary macrophages was performed using the RNAimax kit (Invitrogen) in a 12-well plate according to the manufacturer's instructions. Briefly, in each well, 50nM of siRNA diluted in 165μL serum free medium were mixed with 2μl of RNAimax in 165μl serum free

medium. After 20 min of incubation at room temperature, 430.000 BMDMs were added to each well and incubated for 48 hours. Macrophages were treated either with vehicle, LPS or LPS+Dex for 6 hours before collection. We used non-targeted scramble control (D-001206-14) or si*Smarca4*/*Brg1* (M-041135-01-0005) (Dharmacon, siGenome, SMARTpool) siRNAs.

RNA extraction, cDNA synthesis and qRT-PCR

Total RNA was extracted from macrophages using the RNeasy Mini Kit (Qiagen) and 500ng of mRNA were reverse transcribed using the QuantiTect reverse transcription kit (Qiagen) following the manufacturer's instructions. qPCR was performed on Viia 6/7 Real time PCR system using SYBR Green master mix (Life Technologies). The primers used are listed in Supplementary table 1. The expression was normalized to the house keeping gene *Rplp0.*

RNA-sequencing

RNA-seq was performed in BMDMs after siControl and siBRG1 knockdown. The RNA quality was determined on an Agilent 2100 Bioanalyzer with the RNA 6000 Nano kit, following manufacturer's instructions. Library preparation and rRNA depletion were conducted using the TruSeq stranded mRNA Library Prep kit (Illumina) starting with 1µg of total RNA for each sample. The libraries were sequenced on the Illumina HiSeq4000 machine.

ChIP-seq

40 million primary macrophages were used for each ChIP. The cells were treated with 100ng/ml LPS and with 1µM Dexamethasone or 0.1% EtOH for 3 hours and then fixed with 2mM disuccinimidyl glutarate (DSG) for 30 min at 4°C and 1% formaldehyde for 10 min at room temperature. The IP was performed using 8µg of rabbit α-GR (24050-1-AP, Proteintech) and 16µg of rabbit α-BRG1 (Cell Signalling, 49360 and Abcam ab110641, 8µg each) as previously described (Uhlenhaut et al. 2013). The DNA was quantified via Qubit, and the enrichment was

validated by qPCR. Libraries were performed with the Kappa Hyperprep kit (Roche) according to the manufacturer's instructions and sequenced on an Illumina NovaSeq6000 machine. The H3K27ac ChIP-seq dataset was previously published in *Greulich et al. 2021b.*

ChIP-qPCR

For ChIP-qPCR, 2 million BMDMs were used. The cells were treated with DMSO or BRG1/BRM inhibitor and LPS or LPS+Dex for 3 hours. ChIP was performed as described previously (Uhlenhaut et al. 2013). 1µg of antibody was used for H3ac (Active Motif, 61937) and total H3 (Abcam, ab1791) IPs, and 2µg for BRG1 (Cell Signaling 49360 and Abcam ab110641, 1µg each), GR (24050-1-AP, Proteintech), MED1 (Bethyl labs, A300-793A), HDAC1 (Abcam, ab7028) and HDAC3 (Active Motif, ACM-40968) IPs. A spike-in normalization strategy with *Drosophila* chromatin was applied for the H3ac and total H3 IPs (Greulich et al. 2021a). qPCRs were performed with SYBR Green in a ViiA6/7 real time PCR system, and the enrichment was calculated as % input. H3ac samples were additionally normalized to total H3. The primers are listed in Supplementary table 2.

ATAC-sequencing

For ATAC-seq, 50.000 BMDMs were treated either with 100ng/ml LPS or PBS, and 1µM Dexamethasone or 0.1% ethanol for 3 hours. Transposition was performed using the OmniATAC protocol (Corces et al. 2017) and the tagment DNA TDE1 enzyme (Illumina, 20034197). DNA was purified using the MinElute PCR purification kit (Qiagen). Afterwards, the transposed DNA was amplified using custom primers as previously described (Buenrostro et al. 2013). Libraries were purified using the MinElute PCR purification kit (Qiagen) and size selected for fragments 150bp-600bp using the Agencourt AMPure XP beads (Beckman Coulter). The quality of the libraries was determined by the Qubit dsDNA HS kit (Thermo Scientific) and the

Agilent High Sensitivity DNA 2100 Bioanalyzer. The samples were sequenced on an Illumina Novaseq 6000 machine.

Western blot

Nuclear extraction was performed in LPS+Dex primary macrophages treated either with DMSO control or BRG1 inhibitor or SAHA as described above. Western blot was performed using standard procedures with the following antibodies: mouse α-BRG1 (Cell Signalling, 52251), rabbit α-GR (Cell Signalling,12041), rabbit α-SNRP70 (Abcam, ab83306), mouse α-HDAC1 (Cell Signalling, 5356), mouse α-HDAC2 (Cell signalling, 5113) and mouse α-HDAC3 (Cell Signalling, 3949).

HDAC activity assay

HDAC activity assays were performed using the HDAC GLO I/II assay kit (Promega, G6430) in 96 well plates following the manufacturer's instructions. BMDMs were seeded in phenol-red free DMEM (Gibco, 21063-029), stimulated with LPS plus Dex and treated either with DMSO or with BRG1 inhibitors or SAHA as described above.

NGS data analysis

NGS data quality was assessed with FastQC (RRID:SCR 014583, http://www.bioinformatics.babraham.ac.uk/projects/fastqc/).

For RNA Sequencing, gene-level quantification was performed with Salmon version 1.4.0 (RRID:SCR_017036 (Patro et al. 2017)). Settings were: -libType A, -gcBias, -biasSpeedSamp 5 using the mm10 (M25, GRCm38, mm10) reference transcriptome provided by Genecode (Frankish et al. 2019). Gene count normalization and differential expression analysis was

performed with DESeq2 version 1.32.0 (RRID:SCR_015687 (Love et al. 2014)) after import of gene-level estimates with "tximport" version 1.20.0 (RRID:SCR_016752 (Soneson et al. 2015)) in R (RRID:SCR_001905, R version 4.1.0 (Team 2017)).

For gene annotation, Ensembl gene Ids were mapped to MGI symbols using the Bioconductor package "biomaRt" version 2.48.2 (RRID:SCR_002987 (Durinck et al. 2009)) and genome information was provided by Ensembl (GRCm38.p6 (Cunningham et al. 2019)). Genes with at least 1 read count, fold change of 1.5 and Benjamini-Hochberg-adjusted p-value < 0.05 were called significantly changed. We compared BMDMs after *Brg1* and control siRNA knockdown under LPS+Dex conditions (Table S3). Plots were generated with "ggplot2" version 3.3.5 (RRID:SCR_014601, (Wickham 2016)) or "pheatmap" version 1.0.12 (RRID:SCR_016418, https://github.com/raivokolde/pheatmap) packages and GO enrichment performed with "clusterProfiler" version 3.18 (RRID:SCR 016884 (Yu et al. 2012)) (Table S4). Details on the downstream analysis is documented in the R scripts available on github (https://github.com/FranziG/GRandBrg1).

ChIP-seq and ATAC-seq paired-end reads were mapped to the murine reference genome mm10 (Ensembl GRCm38.p6 (Cunningham et al. 2019)) with BWA-MEM version 0.7.13 (RRID:SCR 010910 (Li 2013)) or Bowtie2 version 2.4.2 (RRID: SCR 005476 (Langmead and Salzberg 2012)) respectively, and PCR duplicates were removed using Picard Tools version 2.0.1 (RRID:SCR -006525, http://picard.sourceforge.net/). Samples with duplication levels above 25% (ATAC-seq) or 50% (ChIP-seq) were excluded from further analysis. For visualization, bam files were filtered for properly paired and mapped reads and multimappers were removed with Samtools version 1.11 (RRID:SCR 002105 (Li et al. 2009)). Alignments were converted to bigwig files, merging 10 bp per bin using 'bamCoverage' from the Deeptools package version 3.5.0 (RRID:SCR -016366 (Ramirez et al. 2016)). Tracks were visualized with UCSC genome browser (Kent et al. 2002). Peaks were called with MACS version 3.0.0a5 in

BAMPE mode and an FDR cutoff of 0.05. ChIP-seq peaks were called over matched input controls. Blacklisted regions (http://mitra.stanford.edu/kundaje/akundaje/release/blacklists/mm10-mouse/mm10.blacklist.bed.gz) were removed from analyses. Peak annotation was performed in R version 4.0.3 (RRID:SCR 014601 (Team 2017)) using the ChIPpeakAnno package version 3.24.1 and annotation data from the mouse Ensembl genome GRCm38.p6 (mm10 (Cunningham et al. 2019)).

The peak union of all replicates was used to determine reads in peaks (RiP) ratios and scaling factors to normalize for library size and background-to-noise ratio. Genome browser tracks were normalized by the RiP fraction.

For peak overlaps, reproducible peaks (peak intersection in at least 2 replicates) were used and displayed as Venn diagrams, made in R version 4.0.3 (RRID:SCR 014601 (Team 2017)) using the VennDiagram package version 1.6.20. Peaks regions were defined as overlapping when overlapping by at least 1bp using the GenomicRanges package version 1.42.0 (RRID:SCR 000025 (Lawrence et al. 2013)) in R. Peaks were annotated to the closest gene expressed in macrophages in any of our conditions with the 'ChIPpeakAnno' package version 3.24.1 (RRID:SCR 012828 (Zhu et al. 2010)) (Table S5). Genes were called expressed when passing a mean expression value of the 25th percentile. Enrichment analysis for Gene Ontology (GO) of Biological Processes was performed using the 'clusterProfiler' package 3.18.0 (RRID:SCR 016884 (Yu et al. 2012)) (Table S4). GO terms with more than 60% similarity in gene composition were removed, and only the term with the lowest Benjamini-Hochberg adjusted p-value was reported. Results of GO enrichment analyses are displayed as dot plots showing the top 20 enriched GO terms (by Benjamini-Hochberg adjusted p-value), sorted by gene ratio (proportion of set genes enriched in GO term). Motif enrichment was performed on peaks trimmed to 100 bp or 300 bp around the peak center with MEME suite version 5.3.0 (RRID:SCR 001783 (Machanick and Bailey 2011)) in enrichment or differential mode. MEME parameters were set to: '-dna –mod zoops -minw 5 -maxw 25 -nmotifs 20 -p 10' using the JASPAR (2018

version, RRID:SCR - 003030 (Khan et al. 2018)), Uniprobe (RRID:SCR 005803 (Newburger and Bulyk 2009)) and SwissRegulon (RRID:SCR 005333 (Pachkov et al. 2013)) databases.

Data access

Scripts and analytical details are available on github (https://github.com/ FranziG/GRandBrg1). Previously published data for H3K27ac ChIP-seq in murine macrophages is accessible on GEO with the accession numbers GSM4040445-48.

All next generation sequencing data generated in this study is available on the NCBI Gene Expression Omnibus as a SuperSeries with the accession number GSE186514 (ATAC-seq: GSE186511, ChIP-seq: GSE1865112, RNA-seq: GSE1865113), Reviewer token: avmrmccqfjqnvyh.

COMPETING INTEREST STATEMENT

None of the authors have competing interests to declare.

ACKNOWLEDGMENTS

We would sincerely like to thank T. Horn, S. Regn, I. Guderian, O. Garcia-Gonzalez and A. P. Syed for their contributions to this study. We are grateful for the help of I. de la Rosa Velazquez, B. Haderlein, the HMGU genomics core and the animal facilities (AVM). This project received funding from the Deutsche Forschungsgemeinschaft DFG (SFB 1064 Chromatin Dynamics Project ID 213249687 to NHU and to GS, TRR 205 Adrenal Research to NHU, Entzuendungsprozesse GR 5179/1-1 to FG and SFB 1321 Pancreatic Cancer Project ID 329628492 to GS) and from the ERC (ERC-2014-StG 638573 SILENCE to NHU).

AUTHOR CONTRIBUTIONS

AM designed and performed the majority of the experiments together with NHU and FG. AM and CJ performed NGS experiments in primary macrophages, FG performed bioinformatics analyses, and BAS performed additional experiments. FMC and GS supported the establishment of ATAC-seq protocols. NHU secured funding, supervised the work, and wrote the manuscript together with AM and FG. All the authors participated in writing, reviewing and editing the manuscript.

REFERENCES

Biddie SC, John S, Sabo PJ, Thurman RE, Johnson TA, Schiltz RL, Miranda TB, Sung MH, Trump S, Lightman SL et al. 2011. Transcription factor AP1 potentiates chromatin accessibility and glucocorticoid receptor binding. *Mol Cell* **43**: 145-155.

Bilodeau S, Vallette-Kasic S, Gauthier Y, Figarella-Branger D, Brue T, Berthelet F, Lacroix A, Batista D, Stratakis C, Hanson J et al. 2006. Role of Brg1 and HDAC2 in GR trans-repression of the pituitary POMC gene and misexpression in Cushing disease. *Genes Dev* **20**: 2871-2886.

Buenrostro JD, Giresi PG, Zaba LC, Chang HY, Greenleaf WJ. 2013. Transposition of native chromatin for fast and sensitive epigenomic profiling of open chromatin, DNA-binding proteins and nucleosome position. *Nat Methods* **10**: 1213-1218.

Chen S, Yang J, Wei Y, Wei X. 2020. Epigenetic regulation of macrophages: from homeostasis maintenance to host defense. *Cell Mol Immunol* **17**: 36-49.

Chen W, Roeder RG. 2007. The Mediator subunit MED1/TRAP220 is required for optimal glucocorticoid receptor-mediated transcription activation. *Nucleic Acids Res* **35**: 6161-6169.

Corces MR, Trevino AE, Hamilton EG, Greenside PG, Sinnott-Armstrong NA, Vesuna S, Satpathy AT, Rubin AJ, Montine KS, Wu B et al. 2017. An improved ATAC-seq protocol reduces background and enables interrogation of frozen tissues. *Nat Methods* **14**: 959-962.

Cunningham F, Achuthan P, Akanni W, Allen J, Amode MR, Armean IM, Bennett R, Bhai J, Billis K, Boddu S et al. 2019. Ensembl 2019. *Nucleic Acids Res* **47**: D745-D751.

Durinck S, Spellman PT, Birney E, Huber W. 2009. Mapping identifiers for the integration of genomic datasets with the R/Bioconductor package biomaRt. *Nat Protoc* **4**: 1184-1191.

Escoter-Torres L, Caratti G, Mechtidou A, Tuckermann J, Uhlenhaut NH, Vettorazzi S. 2019. Fighting the Fire: Mechanisms of Inflammatory Gene Regulation by the Glucocorticoid Receptor. *Front Immunol* **10**: 1859.

Escoter-Torres L, Greulich F, Quagliarini F, Wierer M, Uhlenhaut NH. 2020. Anti-inflammatory functions of the glucocorticoid receptor require DNA binding. *Nucleic Acids Res* **48**: 8393-8407.

Frankish A, Diekhans M, Ferreira AM, Johnson R, Jungreis I, Loveland J, Mudge JM, Sisu C, Wright J, Armstrong J et al. 2019. GENCODE reference annotation for the human and mouse genomes. *Nucleic Acids Res* **47**: D766-D773.

Fryer CJ, Archer TK. 1998. Chromatin remodelling by the glucocorticoid receptor requires the BRG1 complex. *Nature* **393**: 88-91.

Ghirlando R, Felsenfeld G. 2016. CTCF: making the right connections. *Genes Dev* **30**: 881-891.

Glass CK, Natoli G. 2016. Molecular control of activation and priming in macrophages. *Nature immunology* **17**: 26-33.

Greulich F, Hemmer MC, Rollins DA, Rogatsky I, Uhlenhaut NH. 2016. There goes the neighborhood: Assembly of transcriptional complexes during the regulation of metabolism and inflammation by the glucocorticoid receptor. *Steroids* **114**: 7-15.

Greulich F, Mechtidou A, Horn T, Uhlenhaut NH. 2021a. Protocol for using heterologous spike-ins to normalize for technical variation in chromatin immunoprecipitation. *STAR Protoc* **2**: 100609.

Greulich F, Wierer M, Mechtidou A, Gonzalez-Garcia O, Uhlenhaut NH. 2021b. The glucocorticoid receptor recruits the COMPASS complex to regulate inflammatory transcription at macrophage enhancers. *Cell Rep* **34**: 108742.

Group RC, Horby P, Lim WS, Emberson JR, Mafham M, Bell JL, Linsell L, Staplin N, Brightling C, Ustianowski A et al. 2021. Dexamethasone in Hospitalized Patients with Covid-19. *N Engl J Med* **384**: 693-704.

Hoffman JA, Trotter KW, Ward JM, Archer TK. 2018. BRG1 governs glucocorticoid receptor interactions with chromatin and pioneer factors across the genome. *Elife* **7**.

Hsiao PW, Fryer CJ, Trotter KW, Wang W, Archer TK. 2003. BAF60a mediates critical interactions between nuclear receptors and the BRG1 chromatin-remodeling complex for transactivation. *Mol Cell Biol* **23**: 6210-6220.

Iurlaro M, Stadler MB, Masoni F, Jagani Z, Galli GG, Schubeler D. 2021. Mammalian SWI/SNF continuously restores local accessibility to chromatin. *Nat Genet* **53**: 279-287.

John S, Sabo PJ, Johnson TA, Sung MH, Biddie SC, Lightman SL, Voss TC, Davis SR, Meltzer PS, Stamatoyannopoulos JA et al. 2008. Interaction of the glucocorticoid receptor with the chromatin landscape. *Mol Cell* **29**: 611-624.

John S, Sabo PJ, Thurman RE, Sung MH, Biddie SC, Johnson TA, Hager GL, Stamatoyannopoulos JA. 2011. Chromatin accessibility pre-determines glucocorticoid receptor binding patterns. *Nat Genet* **43**: 264-268.

Jung DJ, Lee SK, Lee JW. 2001. Agonist-dependent repression mediated by mutant estrogen receptor alpha that lacks the activation function 2 core domain. *J Biol Chem* **276**: 37280-37283.

Kent WJ, Sugnet CW, Furey TS, Roskin KM, Pringle TH, Zahler AM, Haussler D. 2002. The human genome browser at UCSC. *Genome Res* **12**: 996-1006.

Khan A, Fornes O, Stigliani A, Gheorghe M, Castro-Mondragon JA, van der Lee R, Bessy A, Cheneby J, Kulkarni SR, Tan G et al. 2018. JASPAR 2018: update of the open-access database of transcription factor binding profiles and its web framework. *Nucleic Acids Res* **46**: D1284.

Kim B, Luo Y, Zhan X, Zhang Z, Shi X, Yi J, Xuan Z, Wu J. 2021. Neuronal activity-induced BRG1 phosphorylation regulates enhancer activation. *Cell Rep* **36**: 109357.

Langmead B, Salzberg SL. 2012. Fast gapped-read alignment with Bowtie 2. *Nat Methods* **9**: 357-359.

Lawrence M, Huber W, Pages H, Aboyoun P, Carlson M, Gentleman R, Morgan MT, Carey VJ. 2013. Software for computing and annotating genomic ranges. *PLoS Comput Biol* **9**: e1003118.

Li H. 2013. Aligning sequence reads, clone sequences and assembly contigs with BWA-MEM. *arXiv:13033997*.

Li H, Handsaker B, Wysoker A, Fennell T, Ruan J, Homer N, Marth G, Abecasis G, Durbin R, Genome Project Data Processing S. 2009. The Sequence Alignment/Map format and SAMtools. *Bioinformatics* **25**: 2078-2079.

Love MI, Huber W, Anders S. 2014. Moderated estimation of fold change and dispersion for RNA-seq data with DESeq2. *Genome Biol* **15**: 550.

Machanick P, Bailey TL. 2011. MEME-ChIP: motif analysis of large DNA datasets. *Bioinformatics* **27**: 1696-1697.

Marks PA, Breslow R. 2007. Dimethyl sulfoxide to vorinostat: development of this histone deacetylase inhibitor as an anticancer drug. *Nat Biotechnol* **25**: 84-90.

McAndrew MJ, Gjidoda A, Tagore M, Miksanek T, Floer M. 2016. Chromatin Remodeler Recruitment during Macrophage Differentiation Facilitates Transcription Factor Binding to Enhancers in Mature Cells. *J Biol Chem* **291**: 18058-18071.

Muratcioglu S, Presman DM, Pooley JR, Grontved L, Hager GL, Nussinov R, Keskin O, Gursoy A. 2015. Structural Modeling of GR Interactions with the SWI/SNF Chromatin Remodeling Complex and C/EBP. *Biophys J* **109**: 1227-1239.

Nacht AS, Pohl A, Zaurin R, Soronellas D, Quilez J, Sharma P, Wright RH, Beato M, Vicent GP. 2016. Hormone-induced repression of genes requires BRG1-mediated H1.2 deposition at target promoters. *EMBO J* **35**: 1822-1843.

Newburger DE, Bulyk ML. 2009. UniPROBE: an online database of protein binding microarray data on protein-DNA interactions. *Nucleic Acids Res* **37**: D77-82.

Pachkov M, Balwierz PJ, Arnold P, Ozonov E, van Nimwegen E. 2013. SwissRegulon, a database of genome-wide annotations of regulatory sites: recent updates. *Nucleic Acids Res* **41**: D214-220.

Papillon JPN, Nakajima K, Adair CD, Hempel J, Jouk AO, Karki RG, Mathieu S, Mobitz H, Ntaganda R, Smith T et al. 2018. Discovery of Orally Active Inhibitors of Brahma Homolog (BRM)/SMARCA2 ATPase Activity for the Treatment of Brahma Related Gene 1 (BRG1)/SMARCA4-Mutant Cancers. *J Med Chem* **61**: 10155-10172.

Patro R, Duggal G, Love MI, Irizarry RA, Kingsford C. 2017. Salmon provides fast and bias-aware quantification of transcript expression. *Nat Methods* **14**: 417-419.

Quagliarini F, Mir AA, Balazs K, Wierer M, Dyar KA, Jouffe C, Makris K, Hawe J, Heinig M, Filipp FV et al. 2019. Cistromic Reprogramming of the Diurnal Glucocorticoid Hormone Response by High-Fat Diet. *Mol Cell* **76**: 531-545 e535.

Ramirez F, Ryan DP, Gruning B, Bhardwaj V, Kilpert F, Richter AS, Heyne S, Dundar F, Manke T. 2016. deepTools2: a next generation web server for deep-sequencing data analysis. *Nucleic Acids Res* **44**: W160-165.

Schick S, Grosche S, Kohl KE, Drpic D, Jaeger MG, Marella NC, Imrichova H, Lin JG, Hofstatter G, Schuster M et al. 2021. Acute BAF perturbation causes immediate changes in chromatin accessibility. *Nat Genet* **53**: 269-278.

Soneson C, Love MI, Robinson MD. 2015. Differential analyses for RNA-seq: transcript-level estimates improve gene-level inferences. *F1000Res* **4**: 1521.

Team RC. 2017. R: A Language and Environment for Statistical Computing. *R Foundation for Statistical Computing, Vienna, Austria*.

Trotter KW, Archer TK. 2004. Reconstitution of glucocorticoid receptor-dependent transcription in vivo. *Mol Cell Biol* **24**: 3347-3358.

Trotter KW, Archer TK. 2008. The BRG1 transcriptional coregulator. *Nucl Recept Signal* **6**: e004.

Trotter KW, King HA, Archer TK. 2015. Glucocorticoid Receptor Transcriptional Activation via the BRG1-Dependent Recruitment of TOP2beta and Ku70/86. *Mol Cell Biol* **35**: 2799-2817.

Uhlenhaut NH, Barish GD, Yu RT, Downes M, Karunasiri M, Liddle C, Schwalie P, Hubner N, Evans RM. 2013. Insights into negative regulation by the glucocorticoid receptor from genome-wide profiling of inflammatory cistromes. *Mol Cell* **49**: 158-171.

Wickham H. 2016. *Elegant Graphics for Data Analysis*. Springer-Verlag New York.

Yu G, Wang LG, Han Y, He QY. 2012. clusterProfiler: an R package for comparing biological themes among gene clusters. *OMICS* **16**: 284-287.

Zhang B, Chambers KJ, Faller DV, Wang S. 2007. Reprogramming of the SWI/SNF complex for co-activation or co-repression in prohibitin-mediated estrogen receptor regulation. *Oncogene* **26**: 7153-7157.

Zhu LJ, Gazin C, Lawson ND, Pages H, Lin SM, Lapointe DS, Green MR. 2010. ChIPpeakAnno: a Bioconductor package to annotate ChIP-seq and ChIP-chip data. *BMC Bioinformatics* **11**: 237.

Supplementary Data

BRG1 defines a genomic subset of inflammatory genes transcriptionally controlled by the glucocorticoid receptor

Mechtidou A. *et al.,*

Supplementary Figures S1 - S5

Supplementary Tables S1 - S5

Supplementary Figure 1

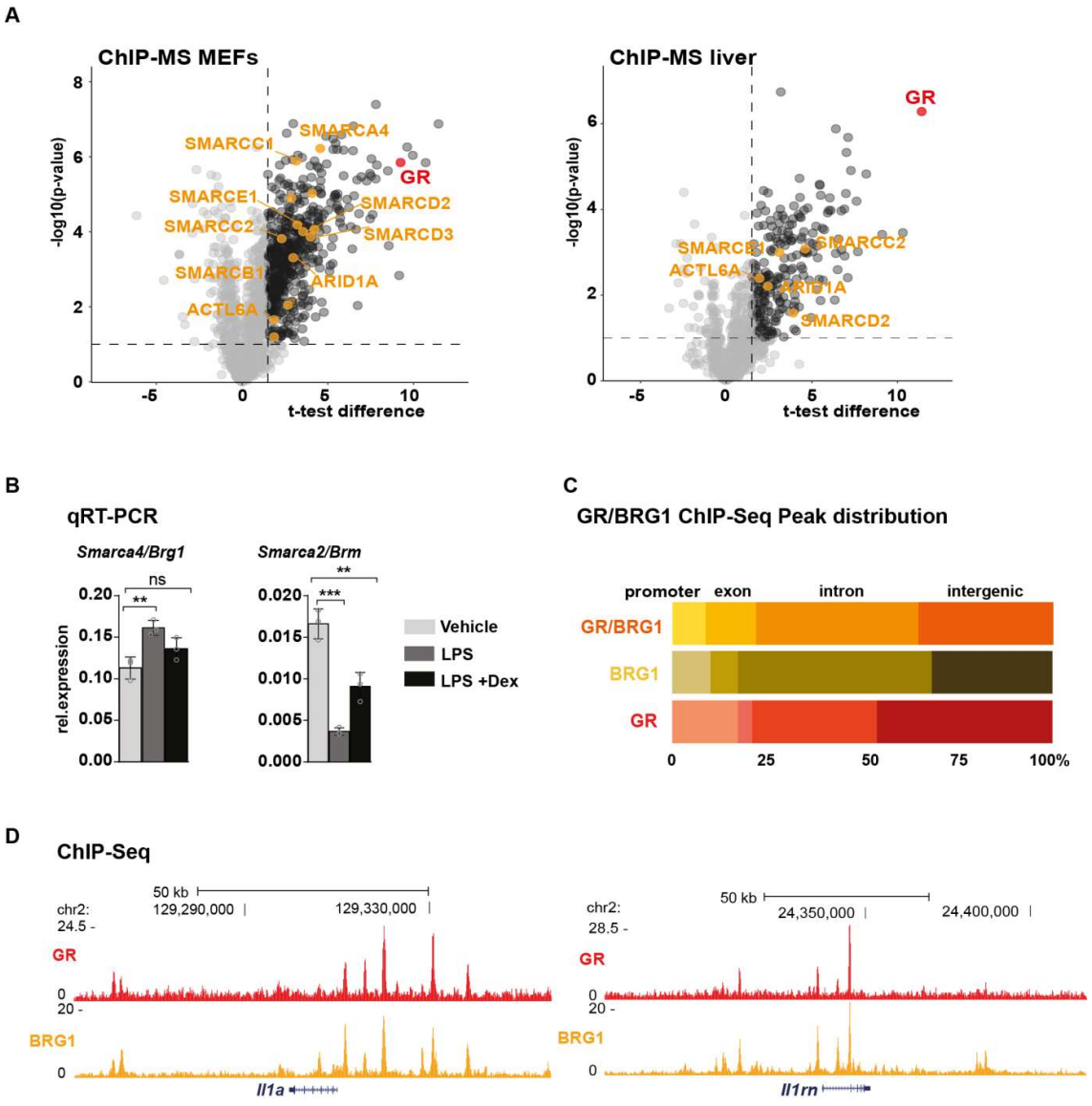

Supplementary Figure 1. GR interacts with SWI/SNF complex. (A) GR ChIP-MS interactomes including subunits of the SWI/SNF chromatin remodeling complex from mouse embryonic fibroblasts (MEFs stimulated with LPS and Dex) and from mouse livers. (Quagliarini et al. 2019; Escoter-Torres et al. 2020) SWI/SNF components are marked in orange. (B) qRT-PCR of *Smarca4/Brg1* and *Smarca2/Brm* in vehicle, LPS and LPS plus Dex stimulated macrophages. Bars = mean ± standard deviation, ns = not significant, unpaired two-tailed Student's t-test, n=3. (C) Genomic feature distribution of GR and BRG1-bound sites and regions specifically occupied by either BRG1 and/or GR. ChIP-seq peak sets as in Fig. 1C. (D) Example genome browser tracks for *Il1a* and *Il1rn* loci showing the mean signal from two GR and BRG1 ChIP-seq replicates in LPS plus Dex treated macrophages (n=2).

Supplementary Figure 2

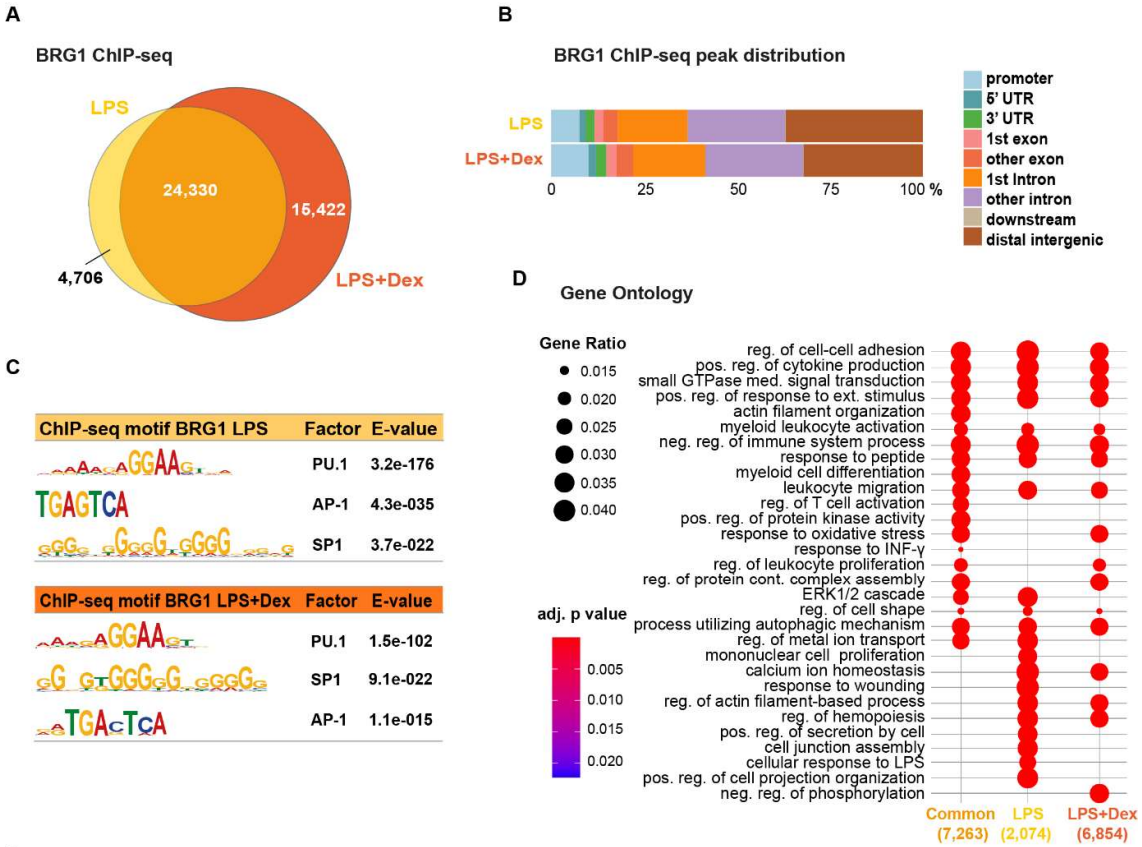

Supplementary Figure 2. BRG1 ChIP-seq in macrophages treated with LPS and with LPS plus Dex. (A) Overlap of BRG1 binding sites in macrophages treated with LPS plus Dex (n=2) or with LPS only (n=2). (B) Genomic feature distribution of BRG1-bound sites for both conditions. (C) MEME motif enrichment of BRG1 ChIP-seq peaks. Motifs were filtered for E<0.01. (D) Enrichment for biological processes of genes associated with nearby BRG1 binding sites, for common (orange) or unique (either LPS or LPS plus Dex) macrophage peaks. neg. = negative, pos. = positive, reg. = regulation (E) Representative genome browser tracks for *Il1a* and *Il1rn* loci showing the mean signal of GR and BRG1 ChIP-seq in macrophages (n=2 each).

Supplementary Figure 3

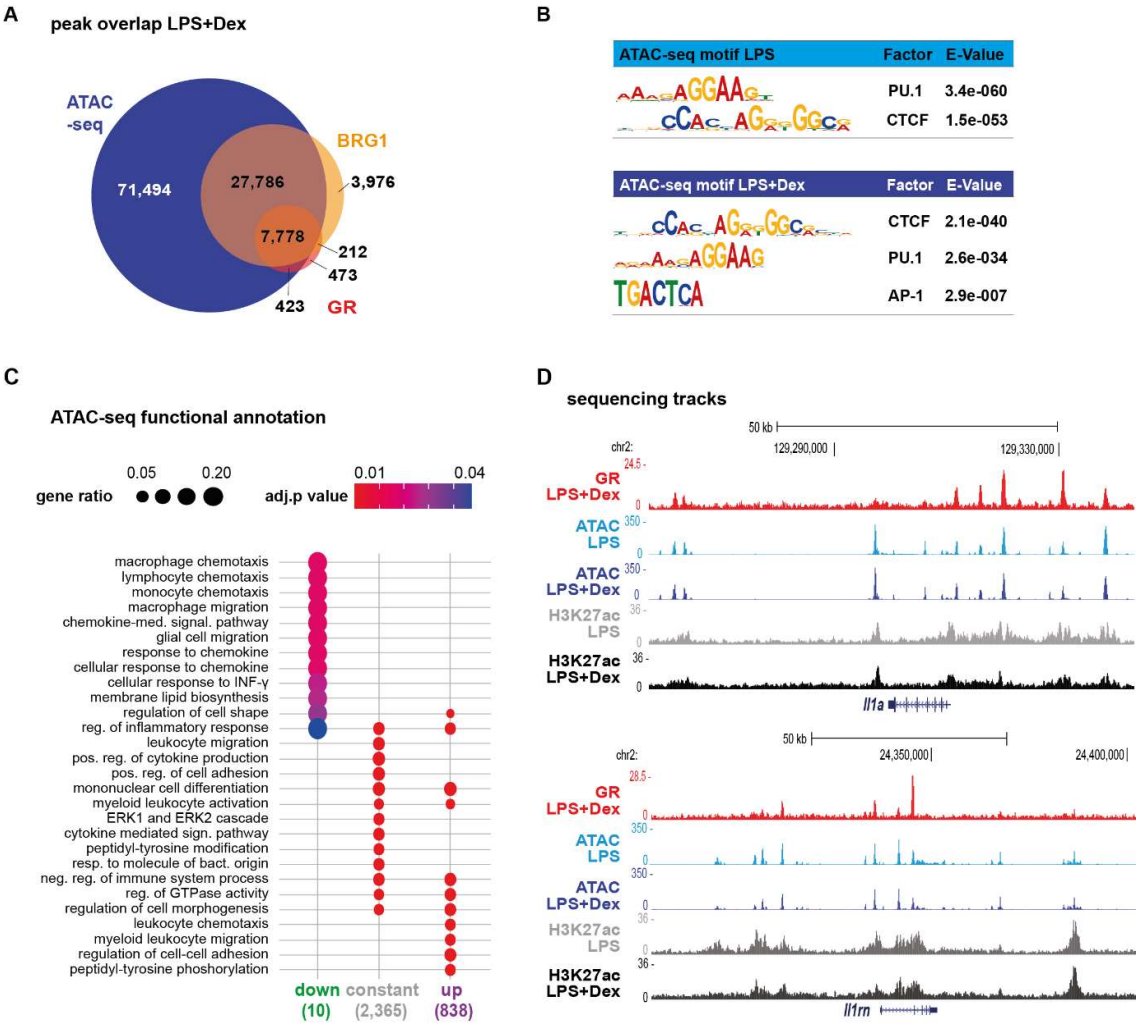

Supplementary Figure 3. ATAC-seq in macrophages responding to LPS or LPS plus Dex. (A) Overlap of accessible regions (ATAC-seq, n=4) with the BRG1 (n=2) and GR (n=2) binding sites, as determined by ChIP-seq in LPS+Dex treated macrophages. (B) MEME motif enrichment for the macrophage ATAC-seq peaks. Motifs were filtered for E<0.01. (C) Gene Ontology enrichment (biological process) of genes associated with the three categories of ATAC-seq peaks shown in Fig. 3B. cell. = cellular, neg. = negative, pos. = positive, reg. = regulation, resp. = response. (D) Representative genome browser tracks for *Il1a* and *Il1rn* loci showing mean ATAC-seq (n=4), GR (n=2) and H3K27ac ChIP-seq (n=2) coverage.

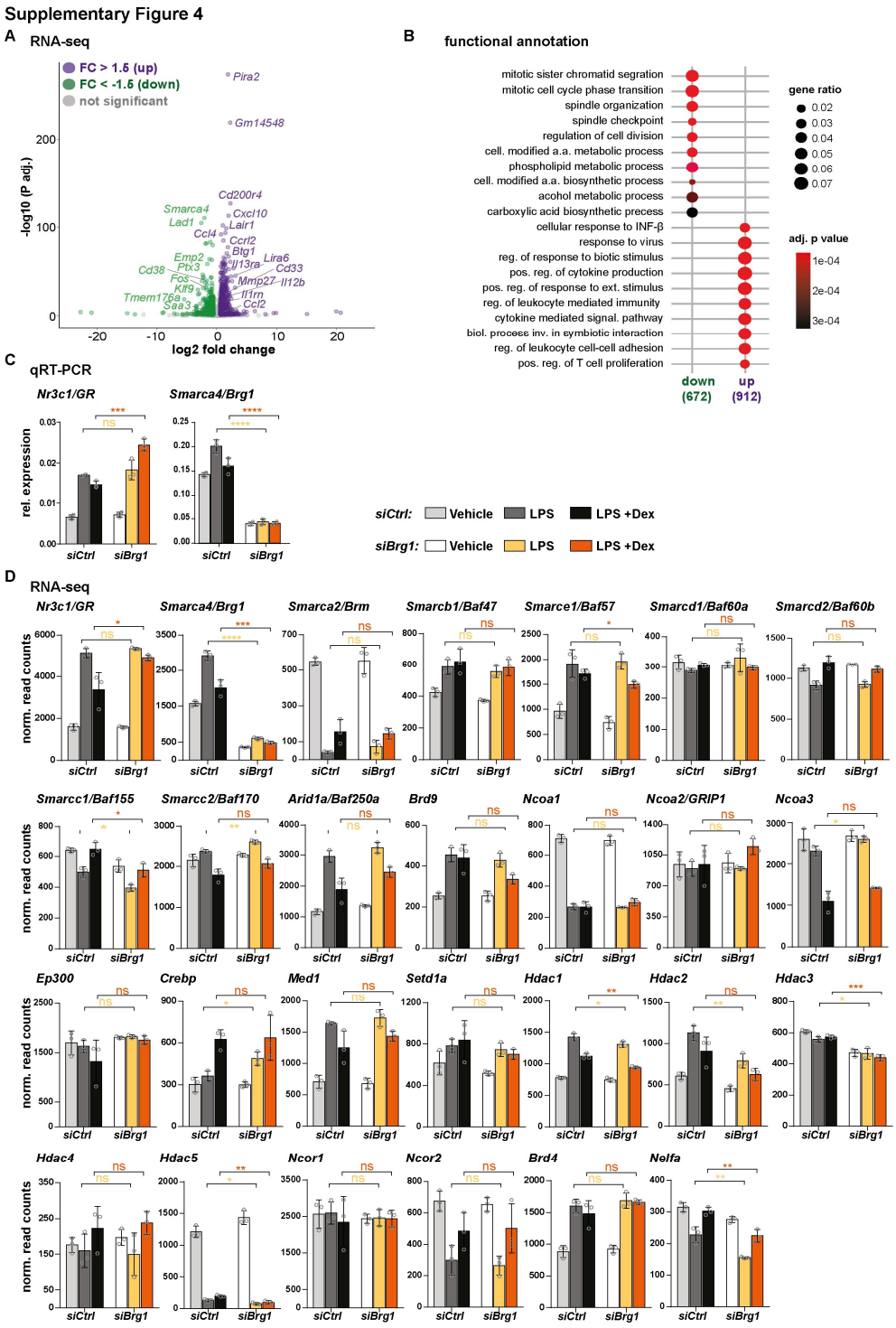

Supplementary Figure 4. *Brg1* knockdown affects macrophage gene expression. (A) Transcripts with differential expression between control and *Brg1* knockdown macrophages upon LPS+Dex treatment. (n=3, fold change ±1.5, p adjusted <0.05). (B) Gene Ontology enrichment for 'biological process' of differentially regulated genes in A. (C) qRT-PCR for *GR* and *Brg1* in control and *Brg1* knockdown macrophages. (D) DESeq-normalized RNAseq read counts for relevant factors in control and *Brg1* knockdown macrophages. For all bar graphs, values are means ± standard deviation. *p<0.05, **p<0.01, ***p<0.001, ****p<0.0001, ns= not significant, unpaired two-tailed Student's t-test, n=3.

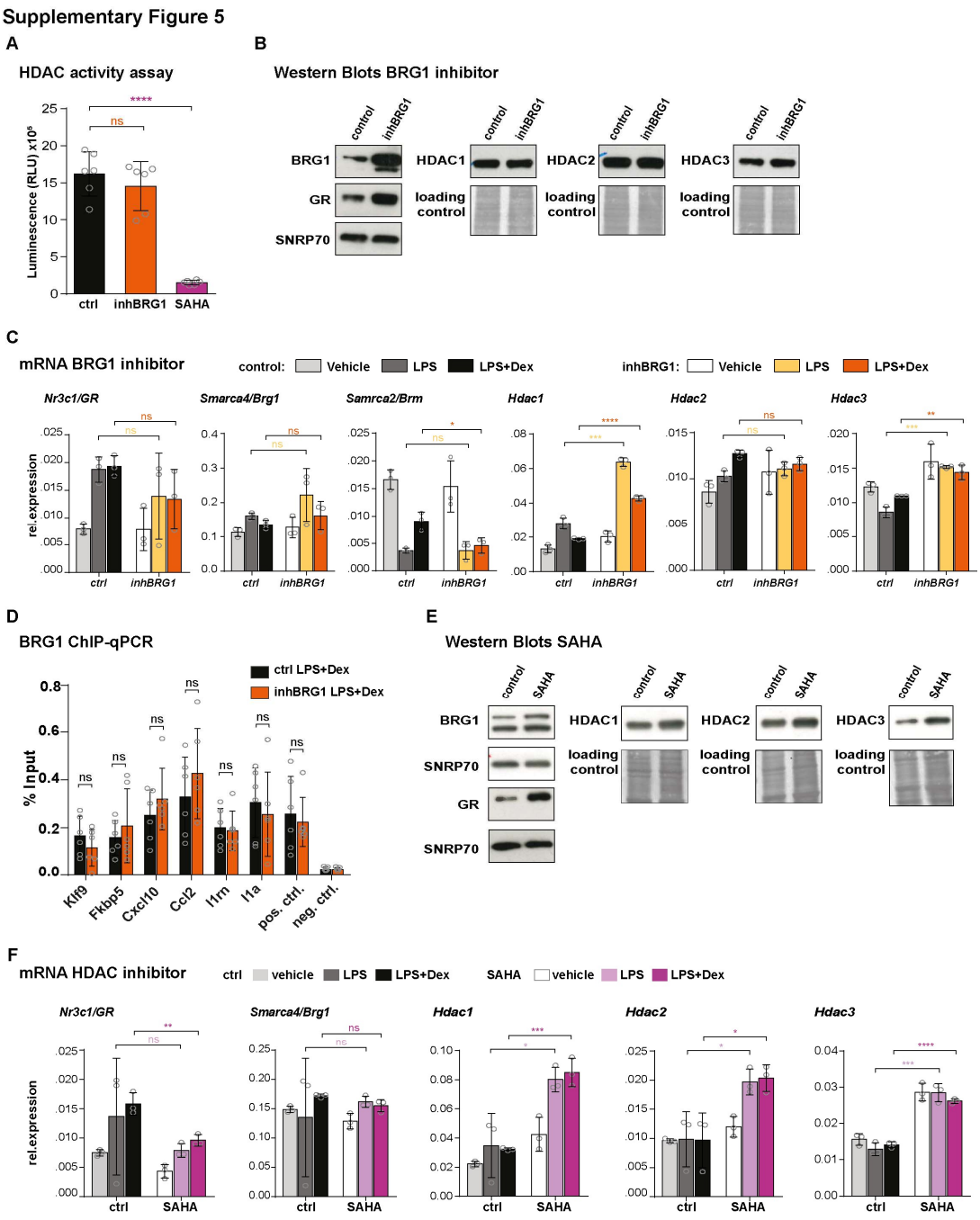

Supplementary Figure 5. BRG1 and HDAC inhibition in primary macrophages (A) HDAC activity assay in LPS+Dex stimulated macrophages treated with control, BRG1 inhibitor or SAHA. (B) Western blot showing nuclear BRG1, GR, HDAC1, HDAC2 and HDAC3 protein levels in control and BRG1 inhibitor treated macrophages (LPS+Dex). SNRP70 blotting and Naphthol Blue Black staining serve as loading control. (C) qRT-PCR of *GR, Brg1, Brm, Hdac1, Hdac2* and *Hdac3* in vehicle, LPS and LPS+Dex stimulated macrophages treated with vehicle (DMSO) or BRG1 inhibitor. (D) BRG1 ChIP-qPCR in LPS+Dex stimulated macrophages treated with vehicle (DMSO) or BRG1 inhibitor. (E) Western blot of nuclear BRG1, GR, HDAC1, HDAC2 and HDAC3 protein levels in control and SAHA treated macrophages (LPS+Dex). Loading controls: same as above. (F) qRT-PCR of *GR, Brg1, Brm, Hdac1, Hdac2* and *Hdac3* in vehicle, LPS and LPS+Dex stimulated macrophages treated with vehicle (DMSO) or SAHA. For all bar plots, values are mean ± standard deviation. *p<0.05, **p<0.01, ***p<0.001, ****p<0.0001, ns= not significant, unpaired two-tailed Student's t-test, n= 3.

4. General discussion

The aim of this thesis was to gain more insights into the mechanisms of transcriptional activation versus transcriptional repression driven by the glucocorticoid receptor in inflamed macrophages. It is known from previous studies that GR requires DNA binding for both induction and suppression of its inflammatory target genes (Uhlenhaut et al. 2013; Escoter-Torres et al. 2020). However, the molecular mechanism by which GR can discriminate between transcriptional activation and repression of inflammatory genes is still unknown. Therefore, it was hypothesized that the action of transcriptional co-regulators might be the key answer to this question.

ChIP-MS against GR in LPS+Dex treated macrophages was performed (Figure 5). Among other proteins, components of the SETD1A/COMPASS complex and the SWI/SNF complex were identified. Both complexes are major epigenetic regulators associated to histone methylation and chromatin remodeling respectively. This study showed that both complexes are involved in the regulation of inflammatory genes by GR, but in a locus-specific manner.

4.1 Locus specific transcriptional regulation by co-regulators

ChIP-sequencing against GR, SETD1A and BRG1 revealed that SETD1A and BRG1 are recruited at GBSs. Overlap of these datasets showed that 17% (1,542/8,886) of the GR binding sites were occupied by both SETD1A and BRG1, 45% (3,787/8,886) only by BRG1 and 8% (746/8,886) only by SETD1A (Figure 7). This observation suggests that there is locus specific requirement of different co-regulators for GR-mediated transcriptional regulation in LPS activated primary macrophages.

For example, higher recruitment of both SETD1A and BRG1 was presented at GBS of the activated genes *Tsc22d3, Klf9* and *Fkbp5* upon addition of the GR ligand, whereas BRG1 was already recruited at the GBS of the activated gene *Dusp1* before addition of dexamethasone (Figure 8). This coincided with changes in chromatin accessibility and H3K27ac, a mark of active enhancers, but differences in H3K4 dynamics were rather locus specific. The *Tsc22d3* enhancer showed increased H3K4me1/me2/me3 in response to Dex, the *Fkbp5* and *Klf9* enhancers presented elevated H3K4me1 levels, whereas no difference was observed inH3K4 levels at GBSs associated to *Dusp1*. Even though the GBS associated with these genes were occupied by SETD1A and BRG1, loss of function experiments revealed that they are important for the regulation of distinct subset of genes.

SETD1A was important for the activation of anti-inflammatory genes like *Tsc22d3* and *Dusp1*, whereas BRG1 was involved in the activation of other GR target genes like *Klf9* and *Fkbp5*.

The GBS associated with the repressed genes like *Cxcl10* and *Ccl2* were already occupied by BRG1 and SETD1A, H3K4 marks and the chromatin was already accessible at these sites prior to addition of the GR ligand (Figure 8). Loss or catalytic inactivation of BRG1 altered the GR-mediated repression of these genes. On the other hand, an unstable SETD1A protein in a mutant RAW264.7 cell line affected the LPS mediated activation of a subset of pro-inflammatory genes like *Cxcl10* and Interferon beta (*Infb)*. Therefore, it is difficult to interpret if SETD1A is involved in the GR-mediated repression of this subset of genes.

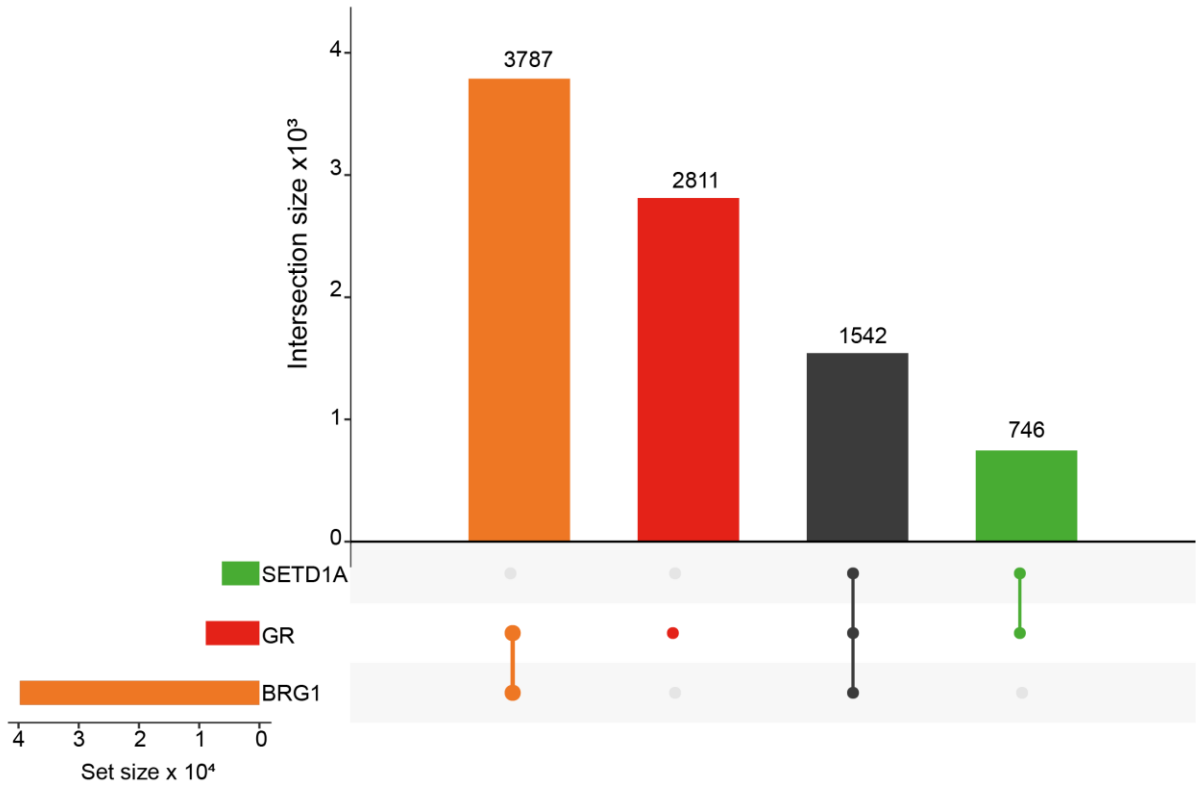

Figure 7. Overlap of GR SETD1A and BRG1 ChIP-seq peaks in LPS+Dex treated BMDMs. Overlap of GR binding sites (red) in LPS+Dex treated primary macrophages with BRG1 occupied sites (orange) and/or SETD1A occupied sites (green) as upsetR plot.

Most interestingly, approximately 31% of the GBS were co-occupied neither by BRG1 nor by SETD1A, indicating that the genes associated with these sites are maybe regulated by a different co-regulator (Figure 7). The ChIP-MS experiment revealed that GR interacts with many co-regulators that act either as co-activators or co-repressors (Figure 4). Among them, are some well described co-regulators like EP300, GRIP-1, NCOA3 and TBLR1XR1, which is a component of the NCoR/SMRT co-repressor complex (Dendoncker et al. 2019). NCOA2 or GRIP1 is a well characterized co-regulator which is shown to be involved not only in the GR-mediated repression of NF-κB target genes, but also in the induction of some anti-inflammatory sites upon phosphorylation by CDK9 (Chinenov et al. 2012; Rollins et al. 2017). Additionally, GR interacts with other histone modifying enzymes like the methyltransferases KMT2A, KMT2B, KMT2D and the histone demethylase KDM1A which is involved in GR-mediated gene activation in A549 lung adenocarcinoma cells (Clark et al. 2019). The C-terminal binding protein 1 and 2 (CtBP1 and CtBP2) are also co-partners of GR in LPS activated macrophages. They are transcriptional regulators that repress several processes by recruiting histone modifying enzymes to regulatory regions (Bergman and Blaydes 2006). Their role in inflammatory gene regulation by GR has not been explored but it might give new mechanistic insights on the repression of inflammatory genes by GR.

4.2 Differential mechanisms of gene activation and gene repression driven by GR in inflamed macrophages

Both studies revealed that there was an increase in SETD1A or BRG1 occupancy at some GR binding sites in LPS treated macrophages upon stimulation with dexamethasone. This coincided with increased H3K27ac. However, changes in H3K4 dynamics were restricted to very few loci, even though SETD1A was involved in the regulation of a subset of inflammatory genes. These data indicate that SETD1A might have an additional role at these sites not related to its H3K4activity. For example, it might be important for the methylation of other non-histone proteins as described previously for other methyltransferases (Carlson and Gozani 2016).

Recently, a phase separation model was proposed for transcriptional regulation. According to this model, specific protein domains of the transcription factors and their co-regulators that are recruited to super enhancers can interact with each other to form more condensed clusters which are named as condensates. These condensates can create interactions with the transcriptional machinery and RNA Pollymerase II and subsequently activate gene expression (Hnisz et al. 2017; Plys and Kingston 2018). The condensates can also form

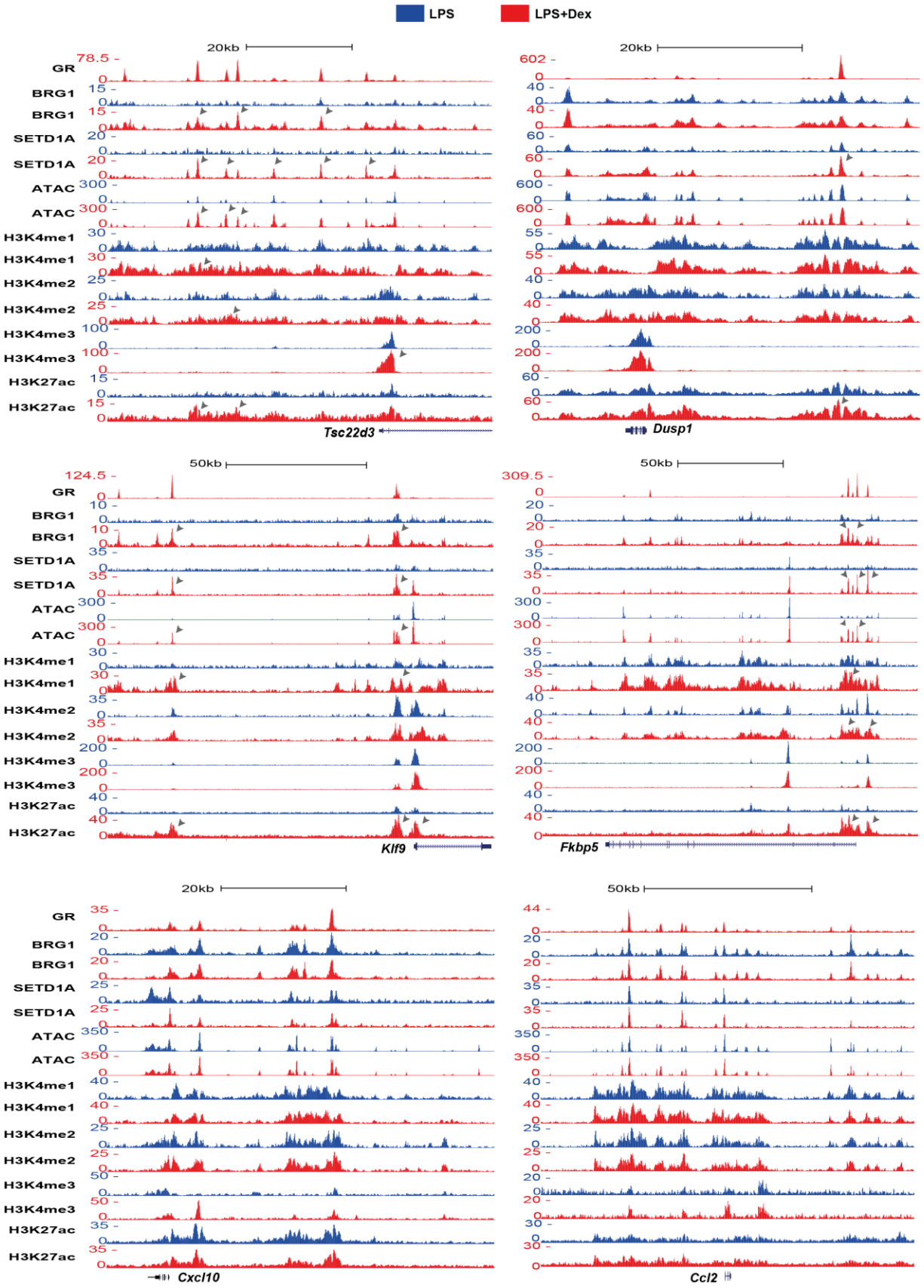

Figure 8. Locus specific recruitment of BRG1 and SETD1A in LPS+Dex treated BMDMs. Example genome browser tracks showing the signal of GR, BRG1, SETD1A, H3K4me1,2,3, H3K27ac and DNA accessibility at selected loci in LPS (blue) and LPS+Dex (red) stimulated macrophages. Arrows indicate signal changes.

liquid droplets which can be separated from the rest of the nucleus. According to Stortz et al., GR forms condensates and Mediator (a well-established co-activator) is included in them (Stortz et al. 2020). This was also documented for estrogen receptor (Boija et al. 2018). Based on this model, our data might indicate that SETD1A and BRG1 are part of the GR condensates and that they are maybe necessary for the creation of more stable interactions with the transcriptional machinery. Destabilization of the SETD1A or catalytic inactivation of BRG1 might lead to structural changes and subsequently to less condensed clusters. Indeed, ChIP-qPCR data in LPS+Dex stimulated macrophages upon BRG1 inhibition revealed less GR and MED1 recruitment at the GBS of the two activated genes *Klf9* and *Fkbp5.* These genes were down-regulated upon BRG1 inhibition. This was also in line with previous studies showing that constant BRG1 is needed for enhancer maintenance and transcriptional activation in other cell types (Iurlaro et al. 2021; Schick et al. 2021). However, the role of the phase separation model in gene repression has not yet been revealed.

The GBS associated with transcriptional repressed genes by GR are occupied by inflammatory transcription factors like NF-κB and AP-1 which can recruit the SWI/SNF complex to open the chromatin and activate transcription (McAndrew et al. 2016; Vierbuchen et al. 2017; Chen et al. 2020). Furthermore, SETD1A was also recruited at these sites. Upon addition of the ligand, GR didn't evict BRG1 from these sites, indicating that constant levels of BRG1 and of chromatin accessibility are important for the repression of these genes. A recent study in mouse embryonic stem cells showed that TF binding and chromatin accessibility were impaired only within minutes after BRG1 inhibition (Iurlaro et al. 2021). Based on this study, it can be hypothesized that BRG1 is needed at the GBS of repressed GR target genes to retain the openness of the chromatin, and subsequently GR recruitment. However, GR was still recruited at these sites upon catalytic inhibition of BRG1even though their associated genes were up-regulated. Our data indicate that the catalytic activity of BRG1 is indeed needed for the repression of these genes but independently of its function to remodel chromatin.

ChIP-qPCR experiments in LPS+Dex primary macrophages upon BRG1 inhibition revealed increased acetylation levels on histone 3 at GBS near *Cxcl10, Ccl2, Il1a* and *Il1rn,* which coincided with less HDAC1 and HDAC3 recruitment. These observations were in line with previous studies, that underlined the role of BRG1 and HDAC1/2 for the transcriptional repression of the progesterone and estrogen nuclear hormone receptors (Jung et al. 2001; Nacht et al. 2016). However, the loss of HDAC1 and HDAC3 recruitment is locus specific, since no differences were observed in the global HDAC activity upon inhibition of BRG1.

Almost ten years ago, it was reported that non-coding RNAs can be transcribed from accessible and active enhancer regions (Kim et al. 2010) and were named as enhancer RNAs (eRNAs) (Sartorelli and Lauberth 2020). Based on our recent study, GR is able to induce or repress the expression of eRNAs in primary macrophages with LPS induced inflammatory responses. GBS with induced eRNA expression corelated with increased chromatin openness, SETD1A occupancy and H3K27ac. Additionally these loci were associated with GR induced inflammatory target genes, whereas decreased eRNA expression was related to repressed GR inflammatory genes (Figure 9) (Greulich et al. 2022).

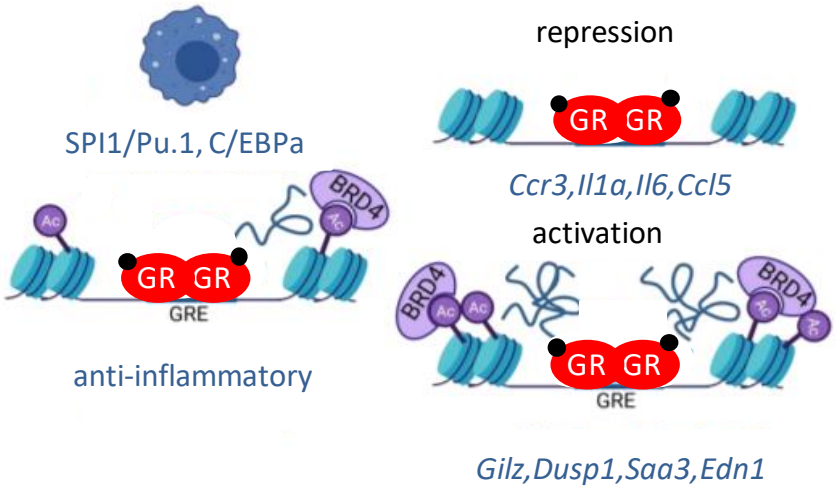

Figure 9. Enhancer RNA expression in response to Dex in murine LPS activated BMDMs. eRNA production at GR enhancers corelates with BRD4 and H3K27ac recruitment and with target gene expression of inflammatory regulated genes in LPS activated primary macrophages treated with dexamethasone. Image adapted from (Greulich et al. 2022).

In summary, our findings indicate that both SETD1A and BRG1 synergize with GR for the transcriptional regulation of GR-mediated inflammatory responses, but in a locus- specific manner (Figure 10). In LPS activated macrophages, GR can recruit BRG1 and/or SETD1A at subsets of GBS near positive regulated genes. However, our data suggest that these co-regulators are involved in the regulation of distinct subset of genes. For example, BRG1 is involved in the regulation of the genes such as *Klf9* and *Fkbp5* potentially by establishing stable GR binding, chromatin openness, H3K27ac and MED1 recruitment. On the other hand, SETD1A is associated with activation of anti-inflammatory genes like *Tsc22d3* and *Dups1,* which does not always corelate with changes in H3K4 dynamics, rather than stable GR binding and enhancer activity. Importantly, enhancers near negative regulated genes were already occupied by BRG1 and SETD1A prior to stimulation with dexamethasone.

Even though both co-regulators are recruited at these enhancers, the catalytic activity of BRG1 is involved in the GR-mediated repression of these genes, but independent of its chromatin remodeling function. Our data suggest, that catalytic active BRG1 might be necessary for the recruitment of some HDAC enzymes and subsequent deacetylation of the surrounding histone tails at GBS near repressed genes. Taken together our findings indicate that GR regulates its target genes in a locus-specific manner, and that different co-regulators can alter the response to glucocorticoids.

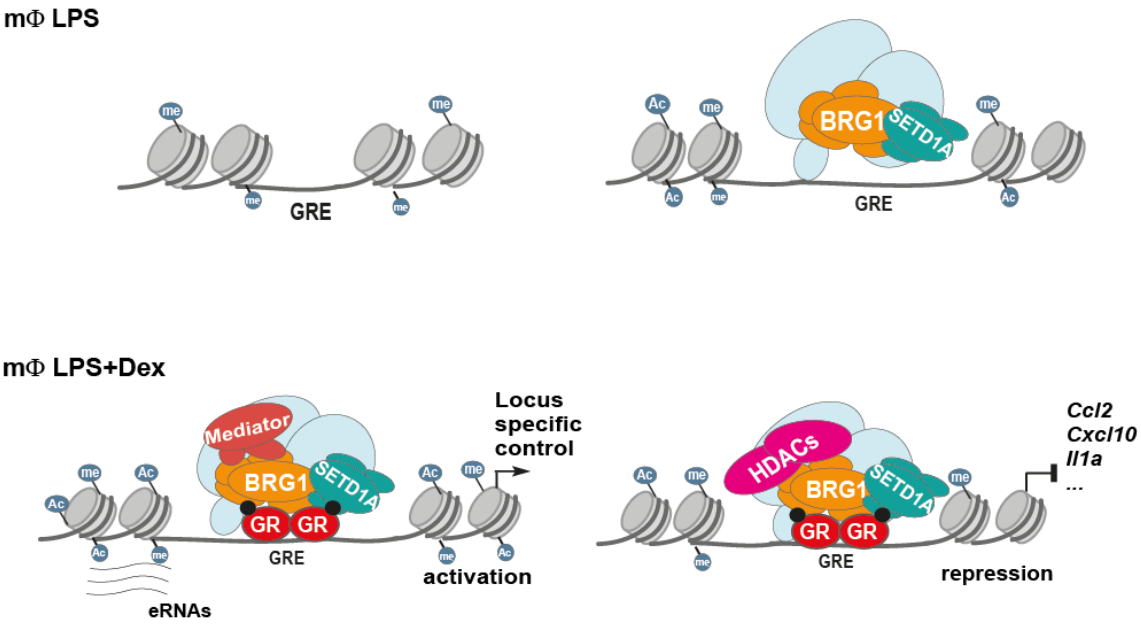

Figure 10. Graphical abstract of proposed mechanism. In LPS activated macrophages GR can bind to enhancers near activated genes (like *Klf9, Fkbp5, Tsc22d3* and *Dusp1*) upon addition of glucocorticoids and recruit SETD1A and/or BRG1 at some subsets. These co-regulators are involved in the activation of distinct subset of genes via different mechanisms that include enhanced GR stability, enhancer activation, Mediator recruitment, increased H3K27ac and chromatin openness. On the contrary, GR enhancers associated with repressed genes (like *Cxcl10, Ccl2, Il1a* etc.) are accessible and occupied by SETD1A and BRG1 prior to glucocorticoid treatment. GR can regulate the repression of these genes via interaction with BRG1 and recruitment of transcriptional repressing HDAC enzymes.

4.3 BRG1 inhibition: an antagonist of Glucocorticoid treatment?

The SWI/SNF is a multi-subunit complex. Mutations on the subunits are reported to be involved in more than 20% of human cancers (Kadoch and Crabtree 2015). Loss or mutations on BRG1are reported to be involved in lung and ovary carcinoma, meduloblastoma and Burkitt's lymphoma (Biegel et al. 2014; Marquez et al. 2014; Kadoch and Crabtree 2015). However, over-expression of BRG1 can lead to the development of breast cancer, melanoma, neuroblastoma, colon cancer as well as pancreatic cancer (Wu et al. 2017). Therefore, inhibition of BRG1 might be an effective therapeutic strategy for the types of cancer where BRG1 is over-expressed. Some inhibitory molecules that target the ATPase domain of BRG1 have reported to reduce tumour growth in breast cancer as well as in a xenograft mouse model of human lung cancer cells subcutaneously implanted into nude mice (Wu et al. 2016; Papillon et al. 2018).

A possible effect of the BRG1 inhibitors in inflammatory responses has not yet been documented. In this study, we applied a BRG1/BRM ATPase inhibitor (Papillon et al. 2018) in LPS and LPS+Dex stimulated macrophages. An up-regulation of inflammatory genes like *Cxcl10, Ccl2, Il1a* and *Il1rn* was observed upon BRG1 inhibition in LPS+Dex treated macrophages. This indicates, that BRG1 is necessary for the repression of pro-inflammatory genes regulated by the glucocorticoid receptor and that inhibition or loss of *Brg1* can potentially affect the suppression of inflammation by glucocorticoids in M1 LPS activated primary macrophages. These findings are of great importance since dexamethasone as well as other glucocorticoids are used in combination with other drugs to treat some forms of cancer. However, this effect was observed in an *in vitro* model system. Therefore, *in vivo* experiments using an inflammation induced mouse model (for example with a sepsis phenotype) administrated with the BRG1 inhibitor and dexamethasone might potentially be more informative.

Glucocorticoids are powerful anti-inflammatory drugs that unfortunately present severe side effects after long term use. Therefore, it is of great importance to develop novel immunomodulatory therapies. The observations reported in this thesis might need to be considered for the development of novel agonists or modulators with less and potentially no severe side effects.

References

Allhoff M, Sere K, J FP, Zenke M, I GC. 2016. Differential peak calling of ChIP-seq signals with replicates with THOR. *Nucleic Acids Res***44**: e153.

Allis CD, Berger SL, Cote J, Dent S, Jenuwien T, Kouzarides T, Pillus L, Reinberg D, Shi Y, Shiekhattar R et al. 2007. New nomenclature for chromatin-modifying enzymes. *Cell***131**: 633-636.

Alnemri ES, Fernandes TF, Haldar S, Croce CM, Litwack G. 1992. Involvement of BCL-2 in glucocorticoid-induced apoptosis of human pre-B-leukemias. *Cancer Res***52**: 491-495.

Ang YS, Tsai SY, Lee DF, Monk J, Su J, Ratnakumar K, Ding J, Ge Y, Darr H, Chang B et al. 2011. Wdr5 mediates self-renewal and reprogramming via the embryonic stem cell core transcriptional network. *Cell***145**: 183-197.

Atsuta J, Plitt J, Bochner BS, Schleimer RP. 1999. Inhibition of VCAM-1 expression in human bronchial epithelial cells by glucocorticoids. *Am J Respir Cell Mol Biol***20**: 643-650.

Auphan N, DiDonato JA, Rosette C, Helmberg A, Karin M. 1995. Immunosuppression by glucocorticoids: inhibition of NF-kappa B activity through induction of I kappa B synthesis. *Science***270**: 286-290.

Bannister AJ, Kouzarides T. 2011. Regulation of chromatin by histone modifications. *Cell Res***21**: 381-395.

Barski A, Cuddapah S, Cui K, Roh TY, Schones DE, Wang Z, Wei G, Chepelev I, Zhao K. 2007. High-resolution profiling of histone methylations in the human genome. *Cell***129**: 823-837.

Bergman LM, Blaydes JP. 2006. C-terminal binding proteins: emerging roles in cell survival and tumorigenesis. *Apoptosis***11**: 879-888.

Berrebi D, Bruscoli S, Cohen N, Foussat A, Migliorati G, Bouchet-Delbos L, Maillot MC, Portier A, Couderc J, Galanaud P et al. 2003. Synthesis of glucocorticoid-induced leucine zipper (GILZ) by macrophages: an anti-inflammatory and immunosuppressive mechanism shared by glucocorticoids and IL-10. *Blood***101**: 729-738.

Biddie SC, Conway-Campbell BL, Lightman SL. 2012. Dynamic regulation of glucocorticoid signalling in health and disease. *Rheumatology (Oxford)***51**: 403-412.

Biegel JA, Busse TM, Weissman BE. 2014. SWI/SNF chromatin remodeling complexes and cancer. *Am J Med Genet C Semin Med Genet***166C**: 350-366.

Bilodeau S, Vallette-Kasic S, Gauthier Y, Figarella-Branger D, Brue T, Berthelet F, Lacroix A, Batista D, Stratakis C, Hanson J et al. 2006. Role of Brg1 and HDAC2 in GR trans-repression of the pituitary POMC gene and misexpression in Cushing disease. *Genes Dev***20**: 2871-2886.

Bochynska A, Luscher-Firzlaff J, Luscher B. 2018. Modes of Interaction of KMT2 Histone H3 Lysine 4 Methyltransferase/COMPASS Complexes with Chromatin. *Cells***7**.

Boija A, Klein IA, Sabari BR, Dall'Agnese A, Coffey EL, Zamudio AV, Li CH, Shrinivas K, Manteiga JC, Hannett NM et al. 2018. Transcription Factors Activate Genes through the Phase-Separation Capacity of Their Activation Domains. *Cell***175**: 1842-1855 e1816.

Cain DW, Cidlowski JA. 2017. Immune regulation by glucocorticoids. *Nat Rev Immunol***17**: 233-247.

Cao K, Collings CK, Marshall SA, Morgan MA, Rendleman EJ, Wang L, Sze CC, Sun T, Bartom ET, Shilatifard A. 2017. SET1A/COMPASS and shadow enhancers in the regulation of homeotic gene expression. *Genes Dev***31**: 787-801.

Cao Y, Bender IK, Konstantinidis AK, Shin SC, Jewell CM, Cidlowski JA, Schleimer RP, Lu NZ. 2013. Glucocorticoid receptor translational isoforms underlie maturational stage-specific glucocorticoid sensitivities of dendritic cells in mice and humans. *Blood***121**: 1553-1562.

Carlson SM, Gozani O. 2016. Nonhistone Lysine Methylation in the Regulation of Cancer Pathways. *Cold Spring Harb Perspect Med***6**.

Cenik BK, Shilatifard A. 2021. COMPASS and SWI/SNF complexes in development and disease. *Nat Rev Genet***22**: 38-58.

Centore RC, Sandoval GJ, Soares LMM, Kadoch C, Chan HM. 2020. Mammalian SWI/SNF Chromatin Remodeling Complexes: Emerging Mechanisms and Therapeutic Strategies. *Trends Genet***36**: 936-950.

Chen L, Deng H, Cui H, Fang J, Zuo Z, Deng J, Li Y, Wang X, Zhao L. 2018. Inflammatory responses and inflammation-associated diseases in organs. *Oncotarget***9**: 7204-7218.

Chen S, Yang J, Wei Y, Wei X. 2020. Epigenetic regulation of macrophages: from homeostasis maintenance to host defense. *Cell Mol Immunol***17**: 36-49.

Chinenov Y, Coppo M, Gupte R, Sacta MA, Rogatsky I. 2014. Glucocorticoid receptor coordinates transcription factor-dominated regulatory network in macrophages. *BMC Genomics***15**: 656.

Chinenov Y, Gupte R, Dobrovolna J, Flammer JR, Liu B, Michelassi FE, Rogatsky I. 2012. Role of transcriptional coregulator GRIP1 in the anti-inflammatory actions of glucocorticoids. *Proc Natl Acad Sci U S A***109**: 11776-11781.

Clapier CR, Iwasa J, Cairns BR, Peterson CL. 2017. Mechanisms of action and regulation of ATP-dependent chromatin-remodelling complexes. *Nat Rev Mol Cell Biol***18**: 407-422.

Clapier CR, Kasten MM, Parnell TJ, Viswanathan R, Szerlong H, Sirinakis G, Zhang Y, Cairns BR. 2016. Regulation of DNA Translocation Efficiency within the Chromatin Remodeler RSC/Sth1 Potentiates Nucleosome Sliding and Ejection. *Mol Cell***62**: 453-461.

Clark EA, Wu F, Chen Y, Kang P, Kaiser UB, Fang R, Shi YG. 2019. GR and LSD1/KDM1A-Targeted Gene Activation Requires Selective H3K4me2 Demethylation at Enhancers. *Cell Rep***27**: 3522-3532 e3523.

Cronstein BN, Kimmel SC, Levin RI, Martiniuk F, Weissmann G. 1992. A mechanism for the antiinflammatory effects of corticosteroids: the glucocorticoid receptor regulates leukocyte adhesion to endothelial cells and expression of endothelial-leukocyte adhesion molecule 1 and intercellular adhesion molecule 1. *Proc Natl Acad Sci U S A***89**: 9991-9995.

Das H, Kumar A, Lin Z, Patino WD, Hwang PM, Feinberg MW, Majumder PK, Jain MK. 2006. Kruppel-like factor 2 (KLF2) regulates proinflammatory activation of monocytes. *Proc Natl Acad Sci U S A***103**: 6653-6658.

Das M, Lu J, Joseph M, Aggarwal R, Kanji S, McMichael BK, Lee BS, Agarwal S, Ray-Chaudhury A, Iwenofu OH et al. 2012. Kruppel-like factor 2 (KLF2) regulates monocyte differentiation and functions in mBSA and IL-1beta-induced arthritis. *Curr Mol Med***12**: 113-125.

De Lucena DD, Rangel EB. 2018. Glucocorticoids use in kidney transplant setting. *Expert Opin Drug Metab Toxicol***14**: 1023-1041.

Debril MB, Gelman L, Fayard E, Annicotte JS, Rocchi S, Auwerx J. 2004. Transcription factors and nuclear receptors interact with the SWI/SNF complex through the BAF60c subunit. *J Biol Chem***279**: 16677-16686.

Dechassa ML, Sabri A, Pondugula S, Kassabov SR, Chatterjee N, Kladde MP, Bartholomew B. 2010. SWI/SNF has intrinsic nucleosome disassembly activity that is dependent on adjacent nucleosomes. *Mol Cell***38**: 590-602.

Dendoncker K, Timmermans S, Vandewalle J, Eggermont M, Lempiainen J, Paakinaho V, Van Hamme E, Dewaele S, Vandevyver S, Ballegeer M et al. 2019. TNF-alpha inhibits glucocorticoid receptor-induced gene expression by reshaping the GR nuclear cofactor profile. *Proc Natl Acad Sci U S A***116**: 12942-12951.

Denissov S, Hofemeister H, Marks H, Kranz A, Ciotta G, Singh S, Anastassiadis K, Stunnenberg HG, Stewart AF. 2014. Mll2 is required for H3K4 trimethylation on bivalent promoters in embryonic stem cells, whereas Mll1 is redundant. *Development***141**: 526-537.

Di Lorenzo A, Bedford MT. 2011. Histone arginine methylation. *FEBS Lett***585**: 2024-2031.

Dorighi KM, Swigut T, Henriques T, Bhanu NV, Scruggs BS, Nady N, Still CD, 2nd, Garcia BA, Adelman K, Wysocka J. 2017. Mll3 and Mll4 Facilitate Enhancer RNA Synthesis and Transcription from Promoters Independently of H3K4 Monomethylation. *Mol Cell***66**: 568-576 e564.

Egan B, Yuan CC, Craske ML, Labhart P, Guler GD, Arnott D, Maile TM, Busby J, Henry C, Kelly TK et al. 2016. An Alternative Approach to ChIP-Seq Normalization Enables Detection of Genome-

Wide Changes in Histone H3 Lysine 27 Trimethylation upon EZH2 Inhibition. *PLoS One***11**: e0166438.

Ehrchen JM, Roth J, Barczyk-Kahlert K. 2019. More Than Suppression: Glucocorticoid Action on Monocytes and Macrophages. *Front Immunol***10**: 2028.

Escoter-Torres L, Caratti G, Mechtidou A, Tuckermann J, Uhlenhaut NH, Vettorazzi S. 2019. Fighting the Fire: Mechanisms of Inflammatory Gene Regulation by the Glucocorticoid Receptor. *Front Immunol***10**: 1859.

Escoter-Torres L, Greulich F, Quagliarini F, Wierer M, Uhlenhaut NH. 2020. Anti-inflammatory functions of the glucocorticoid receptor require DNA binding. *Nucleic Acids Res***48**: 8393-8407.

Fang L, Zhang J, Zhang H, Yang X, Jin X, Zhang L, Skalnik DG, Jin Y, Zhang Y, Huang X et al. 2016. H3K4 Methyltransferase Set1a Is A Key Oct4 Coactivator Essential for Generation of Oct4 Positive Inner Cell Mass. *Stem Cells***34**: 565-580.

Flammer JR, Dobrovolna J, Kennedy MA, Chinenov Y, Glass CK, Ivashkiv LB, Rogatsky I. 2010. The type I interferon signaling pathway is a target for glucocorticoid inhibition. *Mol Cell Biol***30**: 4564-4574.

Franci G, Ciotta A, Altucci L. 2014. The Jumonji family: past, present and future of histone demethylases in cancer. *Biomol Concepts***5**: 209-224.

Fryer CJ, Archer TK. 1998. Chromatin remodelling by the glucocorticoid receptor requires the BRG1 complex. *Nature***393**: 88-91.

Gates LA, Foulds CE, O'Malley BW. 2017. Histone Marks in the 'Driver's Seat': Functional Roles in Steering the Transcription Cycle. *Trends Biochem Sci***42**: 977-989.

Gibney ER, Nolan CM. 2010. Epigenetics and gene expression. *Heredity (Edinb)***105**: 4-13.

Glass CK, Saijo K. 2010. Nuclear receptor transrepression pathways that regulate inflammation in macrophages and T cells. *Nat Rev Immunol***10**: 365-376.

Goossens S, Van Vlierberghe P. 2016. Overcoming Steroid Resistance in T Cell Acute Lymphoblastic Leukemia. *PLoS Med***13**: e1002208.

Gordon S. 2003. Alternative activation of macrophages. *Nat Rev Immunol***3**: 23-35.

Greulich F, Adele Bielefeld K, Scheundel R, Mechtidou A, Strickland B, Uhlenhaut NH. 2022. Enhancer RNA Expression in Response to Glucocorticoid Treatment in Murine Macrophages. *Cells***11**: 28.

Greulich F, Wierer M, Mechtidou A, Gonzalez-Garcia O, Uhlenhaut NH. 2021. The glucocorticoid receptor recruits the COMPASS complex to regulate inflammatory transcription at macrophage enhancers. *Cell Rep***34**: 108742.

Group RC, Horby P, Lim WS, Emberson JR, Mafham M, Bell JL, Linsell L, Staplin N, Brightling C, Ustianowski A et al. 2021. Dexamethasone in Hospitalized Patients with Covid-19. *N Engl J Med***384**: 693-704.

Gupte R, Muse GW, Chinenov Y, Adelman K, Rogatsky I. 2013. Glucocorticoid receptor represses proinflammatory genes at distinct steps of the transcription cycle. *Proc Natl Acad Sci U S A***110**: 14616-14621.

Han D, Huang M, Wang T, Li Z, Chen Y, Liu C, Lei Z, Chu X. 2019. Lysine methylation of transcription factors in cancer. *Cell Death Dis***10**: 290.

Hanaoka BY, Peterson CA, Crofford LJ. 2012. Glucocorticoid effects on skeletal muscle: benefit and risk in patients with autoimmune inflammatory rheumatoid diseases. *Expert Rev Clin Immunol***8**: 695-697.

Harada BT, Hwang WL, Deindl S, Chatterjee N, Bartholomew B, Zhuang X. 2016. Stepwise nucleosome translocation by RSC remodeling complexes. *Elife***5**.

Hardy RS, Raza K, Cooper MS. 2020. Therapeutic glucocorticoids: mechanisms of actions in rheumatic diseases. *Nat Rev Rheumatol***16**: 133-144.

Hartmann K, Koenen M, Schauer S, Wittig-Blaich S, Ahmad M, Baschant U, Tuckermann JP. 2016. Molecular Actions of Glucocorticoids in Cartilage and Bone During Health, Disease, and Steroid Therapy. *Physiol Rev***96**: 409-447.

Hasan N, Ahuja N. 2019. The Emerging Roles of ATP-Dependent Chromatin Remodeling Complexes in Pancreatic Cancer. *Cancers (Basel)***11**.

Hayden MS, Ghosh S. 2004. Signaling to NF-kappaB. *Genes Dev***18**: 2195-2224.

Haynes SR, Dollard C, Winston F, Beck S, Trowsdale J, Dawid IB. 1992. The bromodomain: a conserved sequence found in human, Drosophila and yeast proteins. *Nucleic Acids Res***20**: 2603.

Heitz E. 1928. Das Heterochromatin der Moose. *Jahrbücher für Wissenschaftliche Botanik***69**: 762–818.

Hench PS. 1952. The reversibility of certain rheumatic and nonrheumatic conditions by the use of cortisone or of the pituitary adrenocotropic hormone. *Ann Intern Med***36**: 1-38.

Hench PS, Kendall EC, Slocumb CH, Polley HF. 1949. The effect of a hormone of the adrenal cortex (17-hydroxy-11-dehydrocorticosterone: compound E) and of pituitary adrenocortical hormone in arthritis: preliminary report. *Ann Rheum Dis***8**: 97-104.

Herman JP, McKlveen JM, Ghosal S, Kopp B, Wulsin A, Makinson R, Scheimann J, Myers B. 2016. Regulation of the Hypothalamic-Pituitary-Adrenocortical Stress Response. *Compr Physiol***6**: 603-621.

Hess JL, Yu BD, Li B, Hanson R, Korsmeyer SJ. 1997. Defects in yolk sac hematopoiesis in Mll-null embryos. *Blood***90**: 1799-1806.

Hnisz D, Shrinivas K, Young RA, Chakraborty AK, Sharp PA. 2017. A Phase Separation Model for Transcriptional Control. *Cell***169**: 13-23.

Hoffman JA, Trotter KW, Ward JM, Archer TK. 2018. BRG1 governs glucocorticoid receptor interactions with chromatin and pioneer factors across the genome. *Elife***7**.

Hohmann AF, Vakoc CR. 2014. A rationale to target the SWI/SNF complex for cancer therapy. *Trends Genet***30**: 356-363.

Holland EJ, Fingeret M, Mah FS. 2019. Use of Topical Steroids in Conjunctivitis: A Review of the Evidence. *Cornea***38**: 1062-1067.

Hollenberg SM, Weinberger C, Ong ES, Cerelli G, Oro A, Lebo R, Thompson EB, Rosenfeld MG, Evans RM. 1985. Primary structure and expression of a functional human glucocorticoid receptor cDNA. *Nature***318**: 635-641.

Hsiao PW, Fryer CJ, Trotter KW, Wang W, Archer TK. 2003. BAF60a mediates critical interactions between nuclear receptors and the BRG1 chromatin-remodeling complex for transactivation. *Mol Cell Biol***23**: 6210-6220.

Hyun K, Jeon J, Park K, Kim J. 2017. Writing, erasing and reading histone lysine methylations. *Exp Mol Med***49**: e324.

Ichinose H, Garnier JM, Chambon P, Losson R. 1997. Ligand-dependent interaction between the estrogen receptor and the human homologues of SWI2/SNF2. *Gene***188**: 95-100.

Iurlaro M, Stadler MB, Masoni F, Jagani Z, Galli GG, Schubeler D. 2021. Mammalian SWI/SNF continuously restores local accessibility to chromatin. *Nat Genet***53**: 279-287.

John S, Sabo PJ, Johnson TA, Sung MH, Biddie SC, Lightman SL, Voss TC, Davis SR, Meltzer PS, Stamatoyannopoulos JA et al. 2008. Interaction of the glucocorticoid receptor with the chromatin landscape. *Mol Cell***29**: 611-624.

Johnson TA, Elbi C, Parekh BS, Hager GL, John S. 2008. Chromatin remodeling complexes interact dynamically with a glucocorticoid receptor-regulated promoter. *Mol Biol Cell***19**: 3308-3322.

Jung DJ, Lee SK, Lee JW. 2001. Agonist-dependent repression mediated by mutant estrogen receptor alpha that lacks the activation function 2 core domain. *J Biol Chem***276**: 37280-37283.

Kadmiel M, Cidlowski JA. 2013. Glucocorticoid receptor signaling in health and disease. *Trends Pharmacol Sci***34**: 518-530.

Kadoch C, Crabtree GR. 2015. Mammalian SWI/SNF chromatin remodeling complexes and cancer: Mechanistic insights gained from human genomics. *Sci Adv***1**: e1500447.

Khavari PA, Peterson CL, Tamkun JW, Mendel DB, Crabtree GR. 1993. BRG1 contains a conserved domain of the SWI2/SNF2 family necessary for normal mitotic growth and transcription. *Nature***366**: 170-174.

Kim JH, Choi D, Kende H. 2003. The AtGRF family of putative transcription factors is involved in leaf and cotyledon growth in Arabidopsis. *Plant J***36**: 94-104.

Kim SY, Nair MG. 2019. Macrophages in wound healing: activation and plasticity. *Immunol Cell Biol***97**: 258-267.

Kim TK, Hemberg M, Gray JM, Costa AM, Bear DM, Wu J, Harmin DA, Laptewicz M, Barbara-Haley K, Kuersten S et al. 2010. Widespread transcription at neuronal activity-regulated enhancers. *Nature***465**: 182-187.

Kornberg RD. 1974. Chromatin structure: a repeating unit of histones and DNA. *Science***184**: 868-871.

Kornberg RD, Lorch Y. 1999. Twenty-five years of the nucleosome, fundamental particle of the eukaryote chromosome. *Cell***98**: 285-294.

Kouzarides T. 2007. Chromatin modifications and their function. *Cell***128**: 693-705.

Kumar R, Thompson EB. 2005. Gene regulation by the glucocorticoid receptor: structure:function relationship. *J Steroid Biochem Mol Biol***94**: 383-394.

Kuzmich NN, Sivak KV, Chubarev VN, Porozov YB, Savateeva-Lyubimova TN, Peri F. 2017. TLR4 Signaling Pathway Modulators as Potential Therapeutics in Inflammation and Sepsis. *Vaccines (Basel)***5**.

Lasa M, Abraham SM, Boucheron C, Saklatvala J, Clark AR. 2002. Dexamethasone causes sustained expression of mitogen-activated protein kinase (MAPK) phosphatase 1 and phosphatase-mediated inhibition of MAPK p38. *Mol Cell Biol***22**: 7802-7811.

Lee JH, Skalnik DG. 2005. CpG-binding protein (CXXC finger protein 1) is a component of the mammalian Set1 histone H3-Lys4 methyltransferase complex, the analogue of the yeast Set1/COMPASS complex. *J Biol Chem***280**: 41725-41731.

Lee JH, Skalnik DG. 2008. Wdr82 is a C-terminal domain-binding protein that recruits the Setd1A Histone H3-Lys4 methyltransferase complex to transcription start sites of transcribed human genes. *Mol Cell Biol***28**: 609-618.

Lee JH, Tate CM, You JS, Skalnik DG. 2007. Identification and characterization of the human Set1B histone H3-Lys4 methyltransferase complex. *J Biol Chem***282**: 13419-13428.

Lee KY. 2019. M1 and M2 polarization of macrophages: a mini-review. *Medical Bilogical Science and Engineering***2**: 1-5.

Liao X, Sharma N, Kapadia F, Zhou G, Lu Y, Hong H, Paruchuri K, Mahabeleshwar GH, Dalmas E, Venteclef N et al. 2011. Kruppel-like factor 4 regulates macrophage polarization. *J Clin Invest***121**: 2736-2749.

Lim HW, Uhlenhaut NH, Rauch A, Weiner J, Hubner S, Hubner N, Won KJ, Lazar MA, Tuckermann J, Steger DJ. 2015. Genomic redistribution of GR monomers and dimers mediates transcriptional response to exogenous glucocorticoid in vivo. *Genome Res***25**: 836-844.

Lonard DM, O'Malley B W. 2007. Nuclear receptor coregulators: judges, juries, and executioners of cellular regulation. *Mol Cell***27**: 691-700.

Long HK, Blackledge NP, Klose RJ. 2013. ZF-CxxC domain-containing proteins, CpG islands and the chromatin connection. *Biochem Soc Trans***41**: 727-740.

Lorch Y, Maier-Davis B, Kornberg RD. 2006. Chromatin remodeling by nucleosome disassembly in vitro. *Proc Natl Acad Sci U S A***103**: 3090-3093.

Lu NZ, Cidlowski JA. 2005. Translational regulatory mechanisms generate N-terminal glucocorticoid receptor isoforms with unique transcriptional target genes. *Mol Cell***18**: 331-342.

Lu NZ, Cidlowski JA. 2006. Glucocorticoid receptor isoforms generate transcription specificity. *Trends Cell Biol***16**: 301-307.

Luecke HF, Yamamoto KR. 2005. The glucocorticoid receptor blocks P-TEFb recruitment by NFkappaB to effect promoter-specific transcriptional repression. *Genes Dev***19**: 1116-1127.

Mackaness GB. 1962. Cellular resistance to infection. *J Exp Med***116**: 381-406.

Marquez SB, Thompson KW, Lu L, Reisman D. 2014. Beyond Mutations: Additional Mechanisms and Implications of SWI/SNF Complex Inactivation. *Front Oncol***4**: 372.

Marshall TW, Link KA, Petre-Draviam CE, Knudsen KE. 2003. Differential requirement of SWI/SNF for androgen receptor activity. *J Biol Chem***278**: 30605-30613.

Martinez FO, Gordon S. 2014. The M1 and M2 paradigm of macrophage activation: time for reassessment. *F1000Prime Rep***6**: 13.

McAndrew MJ, Gjidoda A, Tagore M, Miksanek T, Floer M. 2016. Chromatin Remodeler Recruitment during Macrophage Differentiation Facilitates Transcription Factor Binding to Enhancers in Mature Cells. *J Biol Chem***291**: 18058-18071.

Medzhitov R, Horng T. 2009. Transcriptional control of the inflammatory response. *Nat Rev Immunol***9**: 692-703.

Michel BC, D'Avino AR, Cassel SH, Mashtalir N, McKenzie ZM, McBride MJ, Valencia AM, Zhou Q, Bocker M, Soares LMM et al. 2018. A non-canonical SWI/SNF complex is a synthetic lethal target in cancers driven by BAF complex perturbation. *Nat Cell Biol***20**: 1410-1420.

Miller T, Krogan NJ, Dover J, Erdjument-Bromage H, Tempst P, Johnston M, Greenblatt JF, Shilatifard A. 2001. COMPASS: a complex of proteins associated with a trithorax-related SET domain protein. *Proc Natl Acad Sci U S A***98**: 12902-12907.

Miyata M, Lee JY, Susuki-Miyata S, Wang WY, Xu H, Kai H, Kobayashi KS, Flavell RA, Li JD. 2015. Glucocorticoids suppress inflammation via the upregulation of negative regulator IRAK-M. *Nat Commun***6**: 6062.

Mo R, Rao SM, Zhu YJ. 2006. Identification of the MLL2 complex as a coactivator for estrogen receptor alpha. *J Biol Chem***281**: 15714-15720.

Morrison O, Thakur J. 2021. Molecular Complexes at Euchromatin, Heterochromatin and Centromeric Chromatin. *Int J Mol Sci***22**.

Mosser DM, Edwards JP. 2008. Exploring the full spectrum of macrophage activation. *Nat Rev Immunol***8**: 958-969.

Muntean AG, Tan J, Sitwala K, Huang Y, Bronstein J, Connelly JA, Basrur V, Elenitoba-Johnson KS, Hess JL. 2010. The PAF complex synergizes with MLL fusion proteins at HOX loci to promote leukemogenesis. *Cancer Cell***17**: 609-621.

Muratcioglu S, Presman DM, Pooley JR, Grontved L, Hager GL, Nussinov R, Keskin O, Gursoy A. 2015. Structural Modeling of GR Interactions with the SWI/SNF Chromatin Remodeling Complex and C/EBP. *Biophys J***109**: 1227-1239.

Nacht AS, Pohl A, Zaurin R, Soronellas D, Quilez J, Sharma P, Wright RH, Beato M, Vicent GP. 2016. Hormone-induced repression of genes requires BRG1-mediated H1.2 deposition at target promoters. *EMBO J***35**: 1822-1843.

Niewoehner DE, Erbland ML, Deupree RH, Collins D, Gross NJ, Light RW, Anderson P, Morgan NA. 1999. Effect of systemic glucocorticoids on exacerbations of chronic obstructive pulmonary disease. Department of Veterans Affairs Cooperative Study Group. *N Engl J Med***340**: 1941-1947.

Nijland R, Hofland T, van Strijp JA. 2014. Recognition of LPS by TLR4: potential for anti-inflammatory therapies. *Mar Drugs***12**: 4260-4273.

Oakley RH, Cidlowski JA. 2013. The biology of the glucocorticoid receptor: new signaling mechanisms in health and disease. *J Allergy Clin Immunol***132**: 1033-1044.

Oeckinghaus A, Ghosh S. 2009. The NF-kappaB family of transcription factors and its regulation. *Cold Spring Harb Perspect Biol***1**: a000034.

Papillon JPN, Nakajima K, Adair CD, Hempel J, Jouk AO, Karki RG, Mathieu S, Mobitz H, Ntaganda R, Smith T et al. 2018. Discovery of Orally Active Inhibitors of Brahma Homolog

(BRM)/SMARCA2 ATPase Activity for the Treatment of Brahma Related Gene 1 (BRG1)/SMARCA4-Mutant Cancers. *J Med Chem***61**: 10155-10172.

Parihar A, Eubank TD, Doseff AI. 2010. Monocytes and macrophages regulate immunity through dynamic networks of survival and cell death. *J Innate Immun***2**: 204-215.

Piunti A, Shilatifard A. 2016. Epigenetic balance of gene expression by Polycomb and COMPASS families. *Science***352**: aad9780.

Plys AJ, Kingston RE. 2018. Dynamic condensates activate transcription. *Science***361**: 329-330.

Pratt WB, Toft DO. 1997. Steroid receptor interactions with heat shock protein and immunophilin chaperones. *Endocr Rev***18**: 306-360.

Raff H, Carroll T. 2015. Cushing's syndrome: from physiological principles to diagnosis and clinical care. *J Physiol***593**: 493-506.

Ramamoorthy S, Cidlowski JA. 2016. Corticosteroids: Mechanisms of Action in Health and Disease. *Rheum Dis Clin North Am***42**: 15-31, vii.

Rickels R, Hu D, Collings CK, Woodfin AR, Piunti A, Mohan M, Herz HM, Kvon E, Shilatifard A. 2016. An Evolutionary Conserved Epigenetic Mark of Polycomb Response Elements Implemented by Trx/MLL/COMPASS. *Mol Cell***63**: 318-328.

Rollins DA, Kharlyngdoh JB, Coppo M, Tharmalingam B, Mimouna S, Guo Z, Sacta MA, Pufall MA, Fisher RP, Hu X et al. 2017. Glucocorticoid-induced phosphorylation by CDK9 modulates the coactivator functions of transcriptional cofactor GRIP1 in macrophages. *Nat Commun***8**: 1739.

Sarkar SB, Sarkar S, Ghosh S, Bandyopadhyay S. 2012. Addison's disease. *Contemp Clin Dent***3**: 484-486.

Sartorelli V, Lauberth SM. 2020. Enhancer RNAs are an important regulatory layer of the epigenome. *Nat Struct Mol Biol***27**: 521-528.

Scheinman RI, Cogswell PC, Lofquist AK, Baldwin AS, Jr. 1995. Role of transcriptional activation of I kappa B alpha in mediation of immunosuppression by glucocorticoids. *Science***270**: 283-286.

Schick S, Grosche S, Kohl KE, Drpic D, Jaeger MG, Marella NC, Imrichova H, Lin JG, Hofstatter G, Schuster M et al. 2021. Acute BAF perturbation causes immediate changes in chromatin accessibility. *Nat Genet***53**: 269-278.

Schneider R, Grosschedl R. 2007. Dynamics and interplay of nuclear architecture, genome organization, and gene expression. *Genes Dev***21**: 3027-3043.

Schuettengruber B, Bourbon HM, Di Croce L, Cavalli G. 2017. Genome Regulation by Polycomb and Trithorax: 70 Years and Counting. *Cell***171**: 34-57.

Sevilla LM, Perez P. 2018. Roles of the Glucocorticoid and Mineralocorticoid Receptors in Skin Pathophysiology. *Int J Mol Sci***19**.

Sharma ST, Nieman LK, Feelders RA. 2015. Cushing's syndrome: epidemiology and developments in disease management. *Clin Epidemiol***7**: 281-293.

Shilatifard A. 2012. The COMPASS family of histone H3K4 methylases: mechanisms of regulation in development and disease pathogenesis. *Annu Rev Biochem***81**: 65-95.

Silverman MN, Sternberg EM. 2012. Glucocorticoid regulation of inflammation and its functional correlates: from HPA axis to glucocorticoid receptor dysfunction. *Ann N Y Acad Sci***1261**: 55-63.

Sima X, He J, Peng J, Xu Y, Zhang F, Deng L. 2019. The genetic alteration spectrum of the SWI/SNF complex: The oncogenic roles of BRD9 and ACTL6A. *PLoS One***14**: e0222305.

Smith BC, Denu JM. 2009. Chemical mechanisms of histone lysine and arginine modifications. *Biochim Biophys Acta***1789**: 45-57.

Soares LM, He PC, Chun Y, Suh H, Kim T, Buratowski S. 2017. Determinants of Histone H3K4 Methylation Patterns. *Mol Cell***68**: 773-785 e776.

Stortz M, Pecci A, Presman DM, Levi V. 2020. Unraveling the molecular interactions involved in phase separation of glucocorticoid receptor. *BMC Biol***18**: 59.

Sudarsanam P, Winston F. 2000. The Swi/Snf family nucleosome-remodeling complexes and transcriptional control. *Trends Genet***16**: 345-351.

Swygert SG, Peterson CL. 2014. Chromatin dynamics: interplay between remodeling enzymes and histone modifications. *Biochim Biophys Acta***1839**: 728-736.

Sze CC, Cao K, Collings CK, Marshall SA, Rendleman EJ, Ozark PA, Chen FX, Morgan MA, Wang L, Shilatifard A. 2017. Histone H3K4 methylation-dependent and -independent functions of Set1A/COMPASS in embryonic stem cell self-renewal and differentiation. *Genes Dev***31**: 1732-1737.

Szerlong H, Hinata K, Viswanathan R, Erdjument-Bromage H, Tempst P, Cairns BR. 2008. The HSA domain binds nuclear actin-related proteins to regulate chromatin-remodeling ATPases. *Nat Struct Mol Biol***15**: 469-476.

Tang L, Nogales E, Ciferri C. 2010. Structure and function of SWI/SNF chromatin remodeling complexes and mechanistic implications for transcription. *Prog Biophys Mol Biol***102**: 122-128.

Terranova R, Agherbi H, Boned A, Meresse S, Djabali M. 2006. Histone and DNA methylation defects at Hox genes in mice expressing a SET domain-truncated form of Mll. *Proc Natl Acad Sci U S A***103**: 6629-6634.

Trotter KW, Archer TK. 2004. Reconstitution of glucocorticoid receptor-dependent transcription in vivo. *Mol Cell Biol***24**: 3347-3358.

Trotter KW, Archer TK. 2008. The BRG1 transcriptional coregulator. *Nucl Recept Signal***6**: e004.

Trotter KW, King HA, Archer TK. 2015. Glucocorticoid Receptor Transcriptional Activation via the BRG1-Dependent Recruitment of TOP2beta and Ku70/86. *Mol Cell Biol***35**: 2799-2817.

Uhlenhaut NH, Barish GD, Yu RT, Downes M, Karunasiri M, Liddle C, Schwalie P, Hubner N, Evans RM. 2013. Insights into negative regulation by the glucocorticoid receptor from genome-wide profiling of inflammatory cistromes. *Mol Cell***49**: 158-171.

Vastenhouw NL, Schier AF. 2012. Bivalent histone modifications in early embryogenesis. *Curr Opin Cell Biol***24**: 374-386.

Vicent GP, Ballare C, Zaurin R, Saragueta P, Beato M. 2006. Chromatin remodeling and control of cell proliferation by progestins via cross talk of progesterone receptor with the estrogen receptors and kinase signaling pathways. *Ann N Y Acad Sci***1089**: 59-72.

Vierbuchen T, Ling E, Cowley CJ, Couch CH, Wang X, Harmin DA, Roberts CWM, Greenberg ME. 2017. AP-1 Transcription Factors and the BAF Complex Mediate Signal-Dependent Enhancer Selection. *Mol Cell***68**: 1067-1082 e1012.

Voss TC, Hager GL. 2014. Dynamic regulation of transcriptional states by chromatin and transcription factors. *Nat Rev Genet***15**: 69-81.

Wang P, Lin C, Smith ER, Guo H, Sanderson BW, Wu M, Gogol M, Alexander T, Seidel C, Wiedemann LM et al. 2009. Global analysis of H3K4 methylation defines MLL family member targets and points to a role for MLL1-mediated H3K4 methylation in the regulation of transcriptional initiation by RNA polymerase II. *Mol Cell Biol***29**: 6074-6085.

Wang Z, Malone MH, He H, McColl KS, Distelhorst CW. 2003. Microarray analysis uncovers the induction of the proapoptotic BH3-only protein Bim in multiple models of glucocorticoid-induced apoptosis. *J Biol Chem***278**: 23861-23867.

Weissman B, Knudsen KE. 2009. Hijacking the chromatin remodeling machinery: impact of SWI/SNF perturbations in cancer. *Cancer Res***69**: 8223-8230.

Workman JL, Kingston RE. 1998. Alteration of nucleosome structure as a mechanism of transcriptional regulation. *Annu Rev Biochem***67**: 545-579.

Wu M, Wang PF, Lee JS, Martin-Brown S, Florens L, Washburn M, Shilatifard A. 2008. Molecular regulation of H3K4 trimethylation by Wdr82, a component of human Set1/COMPASS. *Mol Cell Biol***28**: 7337-7344.

Wu Q, Lian JB, Stein JL, Stein GS, Nickerson JA, Imbalzano AN. 2017. The BRG1 ATPase of human SWI/SNF chromatin remodeling enzymes as a driver of cancer. *Epigenomics***9**: 919-931.

Wu Q, Sharma S, Cui H, LeBlanc SE, Zhang H, Muthuswami R, Nickerson JA, Imbalzano AN. 2016. Targeting the chromatin remodeling enzyme BRG1 increases the efficacy of chemotherapy drugs in breast cancer cells. *Oncotarget***7**: 27158-27175.

Yang W, Ernst P. 2017. SET/MLL family proteins in hematopoiesis and leukemia. *Int J Hematol***105**: 7-16.

Zenz R, Eferl R, Scheinecker C, Redlich K, Smolen J, Schonthaler HB, Kenner L, Tschachler E, Wagner EF. 2008. Activator protein 1 (Fos/Jun) functions in inflammatory bone and skin disease. *Arthritis Res Ther***10**: 201.

Zhang G, Zhang L, Duff GW. 1997. A negative regulatory region containing a glucocorticosteroid response element (nGRE) in the human interleukin-1beta gene. *DNA Cell Biol***16**: 145-152.

Zielinska KA, Van Moortel L, Opdenakker G, De Bosscher K, Van den Steen PE. 2016. Endothelial Response to Glucocorticoids in Inflammatory Diseases. *Front Immunol***7**: 592.

Conference attendance and poster presentations

1.Identifying coregulatory complexes mediating GR's anti-inflammatory actions
FEBS Advanced lecture course ALC19-046 SPETSE summer school on Epigenomics Nuclear Receptors and disease, Greece, 2019

2. Characterization of H3K4methylation profiles on inflammatory enhancers in macrophages
Chromatin and Epigenetics, EMBL Heidelberg, Germany, 2019

3. Spike-in normalized ChIP-qPCR to profile histone modifications
Transcription and Chromatin, EMBL Heidelberg, Germany,2018

Curriculum Vitae

Aikaterini Mechtidou

Date of birth:	23-11-1990
Place of birth:	Thessaloniki, Greece
Nationality:	Greek

Education

15/11/17- 31/12/21	**PhD in Molecular biology** AG Prof. Dr.rer. nat. N.H. Uhlenhaut, Institute for Diabetes and Cancer Helmholtz Zentrum München &Ludwig MaximillianUniversity,Munich Title of the thesis: „Involvement of chromatin modifying enzymes in the regulation of inflammatory genes by Glucocorticoid Receptor”
09/2014 – 06/2016	**Master of Science (MSc) in Molecular Medicine** 120 credits Department of Immunology Genetics and Pathology, **Uppsala University, Sweden** **Master Thesis** Title: “Applying a tagmentation approach “ChIPmentation” for histone modification profiling in ALL”
10/2008 -03/2013	**BSc in Molecular Biology and Genetics, Democritus University of Thrace**, Alexandroupolis, Greece **Grade average**: 7.38/10 **Bachelor Thesis** Title: “*Molecular Genetics of multifactorial diseases: Study of neuregulin 1 gene polymorfism rs3924999 in Parkinson's disease.”*
2008	Graduation from 2nd General High School of Evosmos, Thessaloniki, Greece. Grade: 17.6/20

Internships

01/07/16 – 31/01/17	**Research Internship** Lab: Molecular Medicine, Department of Medical Sciences, Uppsala University, Sweden Principal Investigator: Prof. Ann-Christine Syvänen